Materials for Bioelectronic Applications

Designing a transducing hydrogel scaffold to function as a bioelectronic device for spinal cord injuries.

Rachel Lee

A thesis presented for the degree of Doctor of Philosophy

School of Engineering

Faculty of Science and Engineering

Newcastle University

July 2024

Abstract

Robust hydrogels, which are biocompatible, transducing, and stable in water for at least 25 days were synthesised with mechanical properties appropriate for the spinal cord. Hyaluronic acid, a naturally occurring polymer, was chemically crosslinked to function as a scaffold and a doping agent in a bioelectronic device. HA is a glycosaminoglycan which provides it with inherent biocompatibility and is therefore an excellent starting material in the production of a bioelectronic device. An organic electrochemical transistor has been designed which mimics the biological communication which occurs in the spinal cord. A key property for this device is its softness, which must be similar to that of the spinal cord. The elastic modulus provides a means of quantifying the softness. Previous studies indicate that the target modulus for the device should be between 5 and 100 kPa. The scaffold presented has a modulus of 20-30 kPa achieved using an indentation method. The aim of the device is to provide information about cellular communication if used *in vivo*, such as how neurons carry a potential through the body to send a message. To carry out this function an active layer must be present, which consists of either poly(3,4-ethylenedioxythiophene), PEDOT, or poly[bis(3,4-ethylenedioxythiophene)-3-thiophene butyric acid, sodium salt], (PETE-S). For PEDOT to function as a semiconductive material a doping agent must also be present. Fortunately, the carboxylic acid group of hyaluronic acid presents as a natural doping agent to PEDOT. Early scaffolds containing both active layers were characterised as transistors, finding they both display good transistor switching ability and output characteristics.

Acknowledgements

I would like to extent a massive thank you to my supervisor Prof. Mark Geoghegan who has been a source of knowledge and expertise throughout my PhD. Throughout my studies, Mark has had a keen interest in my project, my hobbies, and interests. When I started my PhD in 2020 it was incredibly useful to be able to meet with Mark online almost weekly, where he thoughtfully introduced me to many of the topics. I would come to physically study in the lab once the Covid regulations were lifted. These meetings continued throughout my PhD, providing a place for scientific discussion and experimental updates. I would also like to thank my second supervisor, Dr. Marloes Peeters, who was also involved in these meetings from the beginning. Thank you for your expertise and contributions as well as for inviting me into your research group where I was able to meet many fellow students.

I would also like to thank Dr. Fabio Biscarini for his expertise and allowing me to visit Ferrara to use some of his equipment to characterise my samples. Dr. Michele Di Lauro and Federico Rondelli met me in Ferrara and spent the week with me showing me how to carry out experiments and lending me their expertise in the area. Federico and Michele continued to provide information and further experiment results once I had finished my visit and they have been keen to continue to collaborate.

Dr Toby Hallam and Safeyah Alshehri provided some of this electronic characterisation once I arrived back in Newcastle, I would like to provide a special thank you to them for their willingness and adaptability in helping me characterise my devices in Newcastle.

I would also like to thank Dr. Saweta Garg for her knowledge of cell line studies, I am grateful for your ability to perform biocompatibility studies so quickly on my samples. I was given samples of starting materials from Dr. Daniele Mantione and I would like to thank him for providing these, as it gave me the chance engage with new and novel polymers which have been vital to my PhD.

I would also like to thank my family, thank you for being incredibly supportive, motivating and encouraging. Thank you for your silliness, it makes me laugh and keeps me going. I started my PhD during Covid lockdowns and now we try and spend as much time as we can in the countryside, where I mostly write this thesis, what a contrast and something I couldn’t have achieved without you all.

Contents

Part. 1 Background

Chapter 1. Introduction

This thesis concerns a bioelectronic device which is designed to have appropriate physical properties for the spinal cord. Therefore, it is essential to understand the nature of the human spinal cord and how such a device can be tailored to match these properties.

1.1 *Approach and Application Background*

The human nervous system contains a vast number of cells; some 100-200 billion are likely to make up the nerve cells alone. The entire system, including containing the brain, would also feature glial cells.[1]

1.1.1. The Human Nervous System

A large and complicated system, the nervous system is often divided up into categories of similar anatomy or function. Splitting the nervous system anatomically results in two systems, the peripheral nervous system (PNS) and the central nervous system (CNS). A further two categories are created when dividing the nervous system up by function - these are the somatic nervous system and the autonomic nervous system.[2]

The peripheral nervous system is the collection of nerves which emerge from the brain and the spinal cord, making it capable of conveying messages between the sensory receptors and effectors.[2] The central nervous system, however, includes the brain and the spinal cord which process the information delivered to it by the PNS to provide the body with information such as movement or sensation.[3, 4] Parts of the PNS and CNS which involve sensory information, whether conscious or afferent, are referred to as the somatic nervous system, providing the body with sensations such as vision, touch, or pain. Areas of the human nervous system which concern visceral motor activities are referred to as the autonomic nervous system, providing control of cardiac muscle.[2]

1.1.2. Neurons

Neural stem cells differentiate into a diversity of nerve cells of varying lengths and sizes which make up the nervous system. The neuron is the most basic unit of these cells, containing dendrites, presynaptic terminals, and a soma (the cell body).[1, 5] The long projection extending from the soma, known as an axon, carries singular electrical impulses to the presynaptic terminals where it can be delivered to other neurons via a synapse.[1] The cell body and the cytoplasmic functions within it can be described as

being part of the neurons receptive region, whereas the axon and presynaptic terminals which carry the current are part of the conductive region.[1, 6] Neurons have many extensions called dendrites which increase the ability of the cells to detect the surrounding environment.[6]

The number of dendrites correlates to the number of synapses. If the neuron has more dendrites, there is potential for the cell to have more synapses, meaning it could process information from multiple pathways.[5]

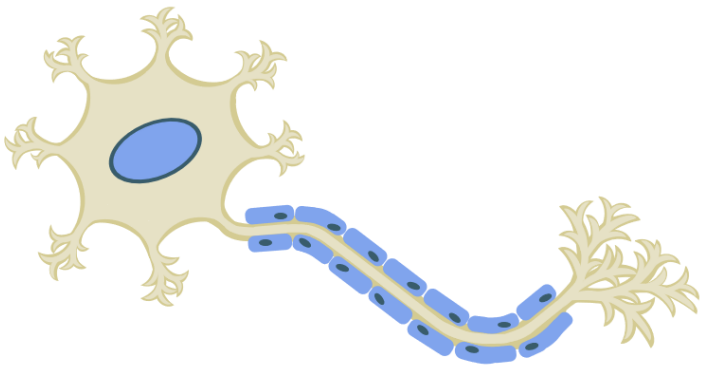

Figure 1. A diagram showing an example neuron.

Glial cells produce a layer of insulating material which surrounds the axon, speeding up the transmission of the action potential. This means the size of the axon can be relatively small in comparison to the scale of the action potential it can conduct. [7-9] Within the CNS, the glial cells responsible for producing myelin are oligodendrocytes and the cells in the PNS are Schwann cells. Although the myelin is deposited around the axon, there are regular intervals where no myelin is present, and these gaps are the nodes of Ranvier.[8, 10] The action potential continues to move along the axon at speed due to a depolarisation at each node of Ranvier. This depolarisation appears to jump from node to node causing the action potential to follow.[10]

The PNS is made up of sensory and motor neurons, with the former carrying signals toward the CNS and the latter carrying signals towards an effector such as a muscle or gland.[6]

1.1.3. The Action Potential

An excited neuron is one which is capable of transmitting information in the form of an electrical signal resulting from the rapid change in the potential within the cell. Ion channels within the membrane control the flow of ions into and out of the cell and it is this build up or removal of charge which provides control of the current flow.[1]

The rapid change in potential across the cell is known as the action potential and associated voltage is determined by the ratios of ions internally and externally. When the neuron is at rest, most of the ion and gated channels are closed, but open in response to a stimulus. When this occurs, the cell experiences a rise in potential which is initiated by the opening of sodium ion channels in the plasma membrane, causing a reversible polarization of the cell known as depolarisation. Another type of ion channel present in the cell membrane is a potassium ion channel. The opening of these channels results in restoration of the resting potential, known as repolarisation. Depolarisation and repolarisation make up two of the three main events which take place during an action potential, the remaining event is hyperpolarisation.[1, 11]

A cell's threshold voltage drives depolarisation; the presence of sodium ions induces a change in potential, which in turn causes more sodium ions to be pumped into the cell via voltage-gated sodium channels, creating a positive-feedback loop. An action potential is 'fired' when a potential threshold has been achieved, the potential then passes along the neuron in what is referred to as an 'all or nothing' type of response.[11, 12]

Repolarisation occurs when potassium ions are pumped out of the cell via voltage-gated potassium channels, the kinetics of which are slower than those of sodium channels. Therefore, the time taken for the potassium channel to open is enough so that the potential in the cell can build from the presence of sodium ions. Once open, the potassium channels put out potassium ions, lowering the potential of the cell towards its resting potential. Once the potential becomes negative, both the sodium and potassium channels close. Since it takes longer for the potassium channels to close, the potential continues to fall until closed. This dip below resting potential is known as hyperpolarisation.[11]

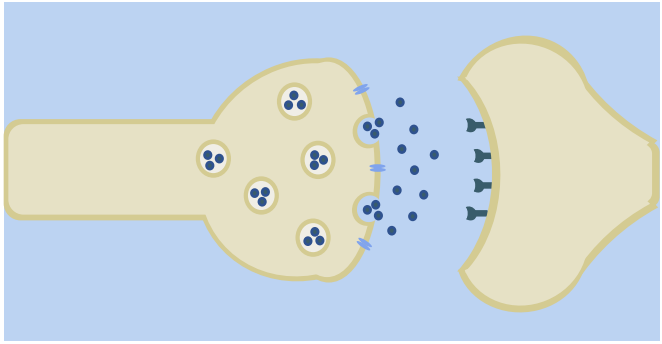

Figure 2. A diagram showing an example of a synapse between two neurons.

The threshold voltage, at which an action potential will occur, is constant and therefore if the stimulus provides a large response, multiple equivalently sized action potentials will be transmitted instead of one large action potential. Once triggered the action potential passes through a neuron from on synapse to another. The means of transport is a neurotransmitter which travels along the neuron before being passed onto another. To do so, the vesicle, in which the neurotransmitter is incorporated, binds to the presynaptic membrane allowing the neurotransmitter to enter the synapse. The neurotransmitter then travels across the synapse between the neurons, ultimately binding with the receptors on the other neurons membrane (postsynaptic membrane) where it generates a response.[1]

1.1.4. Impact of a Myelin Sheath

The myelin sheath contains many layers of plasma membrane which act as an electrical insulator.[1, 13] An axon which is insulated by myelin enables a potential to pass much faster than it would in an unmyelinated axon of the same size. A series of small gaps in the myelin sheath, known as Nodes of Ranvier, enable this increase in speed. The potential generated cannot pass through the gaps in the myelin sheath so instead it moves back into the axon, causing the following node to depolarise. Depolarisation of the myelin sheath requires a relatively small amount of energy, which means that the remaining membrane between the nodes is depolarised. At this point, the potential can spread along to the next node. This apparent jump from node to node is given the name saltatory conduction.[9, 13]

Although the myelin sheath appears to have an overwhelmingly favourable effect on the human spinal cord, caution should be taken when simplifying it, as there is in fact a vast array of myelin which exists within the human spinal cord. It may consist of different lengths, thicknesses, or the sheath may contain no myelin at all. Humans are born with very little myelin but develop it over many years, which may even stretch into adulthood. Myelin is produced by oligodendrocytes which can provide myelin for around 30-60 axons per cell. If the ability of the cell is interrupted demyelination of axons may occur and may result in symptoms of disease.[9, 14] Multiple Sclerosis (MS) is the most common inflammatory disease of the spinal cord, it occurs when the immune system attacks both oligodendrocytes and myelin leading to axons which are more easily injured.[15]

1.1.5. Spinal Cord Injury

The immune system cells which are present in the spinal cord are called microglia and originate from white blood cells which were trapped into the CNS during its development. During an immune response, the cells become more active and begin to

proliferate, therefore the extent of damage can be monitored by the number of activated microglia cells. Response to an injury varies in the PNS and the CNS. In the PNS, it is assumed communications lost by the injury can be recovered by regeneration of the associated neurons,[14, 16] whereas in the CNS both physical and chemical factors prevent axon regrowth.[14]

MS, among other diseases such as infection, tumours, and other chronic or acute diseases, can result in spinal cord injury (SCI). This type of SCI is categorised as a non-traumatic SCI as it does not involve external impact, which would be classified as a traumatic SCI. The impact which causes a traumatic SCI often results in a secondary injury which includes the death of both neurons and glia cells, and causing inflammation, followed by a reorganisation of spinal cord and generation of a glial scar. A combination of these events and the lack of axonal regrowth means that SCIs can result in permanent damage.[17]

A SCI is a serious condition with a life-changing and huge socioeconomic impact on the individual it affects and their family.[17, 18] In the UK there are anticipated to be around 16 new traumatic SCI cases and a further 2 or 3 cases of non-traumatic SCI per million of the population, meaning statistically there could be more than 1200 SCI cases per year.[19] There are also around 12,500 new cases of SCI each year in North America.[20] The majority of SCI cases are a result of traumatic injury of which the cases appear to occur more commonly with males; in the years 2010 to 2014 the US reported that 79.8% of traumatic SCI cases occurred in males.[17, 21] Motor vehicles accidents are the major cause of traumatic SCIs resulting up to 48% of SCI cases in the US. Violence, falls, and recreational activities such as sports make up the other major risk factors. The modal age of these injuries is between 15 and 25 years.[22] In the UK around 40,000 people are estimated to be living with a long-term disability resulting from an SCI.[23]

Over the last 20 years, the nature of SCI injuries has changed. There are more injuries which occur in the cervical level of the spinal cord and there is an increasing number of injuries which occur in the population aged over 50. An increase in injuries in the neck is linked with an increase in the need for tracheostomies and ventilation, and an increased risk of pneumonia and malnutrition.[24-26] Several countries prioritise SCI patients being admitted to specialist spinal injury facilities. In the UK the pathway of care may involve being admitted to a major trauma centre with a high likelihood of surgery. Following surgical recovery, the patient would be transferred to a Spinal Injury Unit (SIU). These units are prompt to identify and treat complications, giving improved

outcomes for SCI patients.[24, 27] It should be noted that the UK has limited SIU capacity due to a reduction in the number of beds available, meaning early access to SIU can be compromised.[24, 28] Approximately 25% of traumatic SCIs occur after the primary impact has occurred, which may be during transport or handling.[23]

1.1.6. Treatment of Spinal Cord Injuries

A spinal cord fracture can cause a spinal cord injury, which occurs in roughly 14% of cases, of which half of these patients may be able to walk when discharged if their care is managed appropriately.[23]

In immediate treatment the spinal cord is immobilised using a collar, blocks, and a spinal board. This treatment should be monitored in case pressure sores occur. All patients with a spinal cord injury must be assessed by an Advanced Trauma and Life Support protocol to prevent missing life-threatening conditions. Following this the spinal cord must be imaged to inform the medical team as to whether decompression surgery is needed.[23]

The patients care then focuses on rehabilitation, with a focus on minimising complications and preventing a need for readmittance to hospital.[22] Rehabilitation requires a combination of many different medical experts, this is not limited to physical assistance but also support for a patient's mental wellbeing, addressing the change in patient's life, loss of independence, and practical needs.[17] Kennedy *et. al.* summarised the data obtained from a Needs Assessment Checklist (NAC) taken patients admitted to the National Spinal Injuries Centre (Stoke Mandeville Hospital, UK) between February 2008 and October 2014.[29] Two assessments are conducted as part of the article, the first is four weeks post-mobilisation and the second when the patient is moved to a pre-discharge ward. They report that in a population of 362 patients 77% were employed at the time of their injury, 22.4% reported having plans to return to work during their first assessment, which increased to 34.3% on the second assessment.[29] An SCI is a life-changing event which affects an individual's ability to work, and therefore it is key that rehabilitation is not limited to medical care but also addresses and understands concerns patients have regarding with finance and vocation.[17]

1.1.7. Understanding Treatments for an SCI

Patients work on strength training by carrying out both cardiovascular and respiratory exercise in order to prevent muscle contractures, which has become common practise after noticing the influence physical exercise has on the body. Such reports originate from animal models.[17, 30] Barbeau *et. al.* reports that cats can recover some function in

the rear limbs when aided by weight supports following a full spinal laceration.[31] Not only was this noted in young animals, similar results were also observed in adult cats.[31] Barbeau *et. al.* were not alone in studying cats. A series of experiments in the 1980s looked to model the effect of exercise training has on the ability to stand or step when a cat has a SCI.[31, 32] Studies also looked at animals ability to regain weight-bearing stepping, concluding that while some load bearing stepping function was regained, it was dependent on the training of the animal and the authors speculated whether this was related to changes in the neural networks that normally generate stepping, but were unlikely to function in the same way as before the spinal laceration.[33, 34]

Reports of a recovery of standing ability are not limited to those following training. In fact, Giuliani *et. al.* noted animals standing following an SCI and Goldberger *et.al* found reflex responses associated with supporting standing.[35, 36] The comparison of practising an exercise to recover from an SCI compared to spontaneous recovery was compared in an experiment by de Leon e*t. al.* finding that the recovery generated from specific standing training was significantly improved in comparison to spontaneous recovery.[37] Animal models, such as the experiments carried out on cats have provided a foundation to understanding the pathophysiology of an SCI.[17] Animal models have also been useful for testing new therapies. Bunge *et. al.* reported how the body develops cysts in response to an injury and how this response is similar to those seen in rats, making them a good candidate for animal models.[38, 39] Rats have also found to be robust enough for their brain and spinal cord to be studied and imaged.[39-41]

Rats have become a staple in animal modelling and research on them which pertains to SCIs is well established, and they are also relatively inexpensive to keep. Although there are several advantages to their use, there are also disadvantages: their size, for example, makes translation to humans difficult. [39, 42] This however is not simply solved by using larger animals which are more expensive to keep and still do not provide exact translation to humans. They can, however, provide a means of confirming the results found in smaller animals such as rats.[43, 44] Testing multiple species of animal has become fairly standard procedure in screening novel treatments such as implants.[17] Stimulating the spinal cord and the brain *in vitro* can also provide an injury model for an individual with an SCI without using animals as models. Once a model has been gathered, a plan for treatment can then be discussed.[14]

In animal models, recovery is often estimated based on an observable improvement in motion and exercise tests are another means of assessing recovery. Based on these tests,

the Basso, Beattie, and Bresnahan (BBB) rating scale was created. For sensory tests, reflexes are monitored, and reaction times recorded and scored. Quantifying and understanding the recovery made by those with an SCI has led to further advances in novel treatment approaches.[14, 45, 46]

1.1.8. From Model to Tissue Engineering

New therapeutic approaches for the treatment of an SCI appear to focus on regeneration of affected tissue within the nervous system, improvements in biomolecules, biomaterials and cell-based therapies have been a driving factor. It should be noted that while there are many promising treatment ideas, no regenerative agent is currently approved for use.[46]

Cell-based therapies have been targeted in part because of their multiple benefits, they have been linked to angiogenesis (formation of new blood vessels), neuroprotection, and tissue regeneration.[46] Early cell-based therapies proposed using embryonic stem cells but due to ethical concerns and limited supplies, attention was turned to pluripotent stem cells which can be delivered from any somatic cell.[47] Neural precursor cells are an example of these cells which can differentiate into neurons specific to the central nervous system. Animal trials confirmed that such cells improve recovery following integration with the test subjects' cells.[48] Alternative approaches are also proposed such as, mesenchymal stem cells which can differentiate into the cells involved in the connective tissues, allowing them to repair said tissues. Another advantage of these cells is that they are able to control inflammation which is key in the treatment of SCIs.[47]

Spinal cord injuries often cause a cavity in the tissue which make it hard for cell-therapies to remain in place. Biomaterials offer a solution. Biomaterials can be designed to fill the cavity while offering the opportunity to capture stem cells and deliver them to the correct position.[47]

1.1.9. Future Treatment Options

Not only can a cavity be filled by a biocompatible material, but this material can also be specially designed and fine-tuned to have beneficial properties. A potential application includes biodegradable hydrogels which can have material dispersed throughout their network, such as medicine in a drug delivery system. These gels degrade as the extracellular matrix grows, providing tissue specific treatment.[49, 50] Another potential application would be to disperse a bioelectronic material into the cavity to provide the potential for nerve stimulation.[51]

Chapter 2. Experimental Background

This section covers the theory and experimental approaches which will be applied to the aims outlined for this project. The information in the following section will be a broad overview of the techniques and theory behind them. More detailed descriptions of the experiments, theory, and information they provide is provided in their relevant chapters.

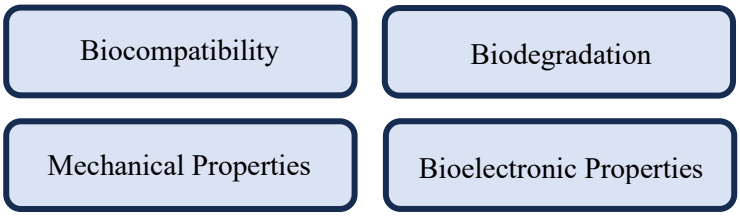

Figure 3. An image detailing the key areas to consider when characterising a bioelectronic device.

2.1 Biocompatibility

As a starting point, inherent biocompatibility can be found in naturally occurring materials, particularly those which occur in the human body. Therefore, materials such as hyaluronic acid and chondroitin sulfate are of note. Gelatin is also of interest due to its proposed biocompatibility, but it should be noted that it is derived from collagen, and it is collagen which is the material which occurs in the body not gelatin itself.

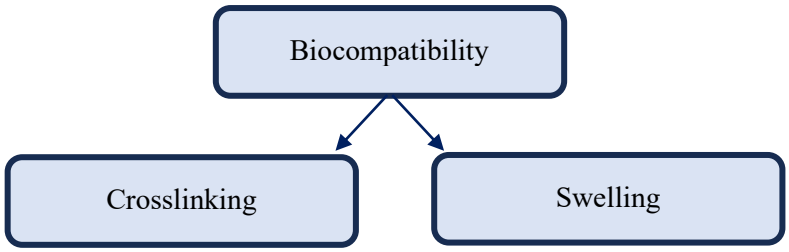

Figure 4. A breakdown of possible biocompatibility characterisation methods.

A 3D hydrogel network would provide the most appropriate geometry for a device, which can be used to fill a cavity formed when an induvial suffers an SCI and provides a workable structure which can be physically handled. To provide such a network, the hydrogel polymers require crosslinking. The crosslinking agent should not drastically change the polymer backbone, to minimise the effect on its inherent biocompatibility. Therefore, zero-length crosslinking agents, which form covalent bonds between the

polymer chains without inserting their chemical formula into the network are ideal. An example of which is 1-ethyl-3-(3-dimethylaminopropyl)carbodiimide (EDC).

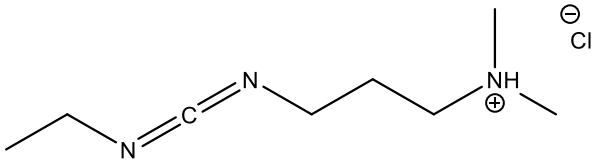

Figure 5. Chemical structure of EDC.HCl

2.1.1. Crosslinking Hydrogel Networks

EDC promotes the crosslinking between carboxylic acid and amino acid groups, and it is typically used to crosslink proteins or polysaccharides.[52] EDC is a zero-length crosslinking agent, one which does not incorporate itself into the backbone, but simply enables the formation between two existing functional groups in the hydrogel network. Therefore, zero-length crosslinking agents are powerful for their ability to improve the properties of a network, by forming covalent bonds, while causing minimal changes to the polymer backbone.[53, 54] The by-product of the reaction is a specific urea which can be removed from the network by rinsing with water.[55] EDC crosslinking has been linked to decreased degradation rates, which was demonstrated in the work of J. S. Pieper *et. al.* who prepared crosslinked collagen matrices containing chondroitin sulfate.[56]

EDC crosslinking is typically used to crosslink biological molecules containing an amine functional group, producing an amide, useful in the formation of amino acids or peptides.

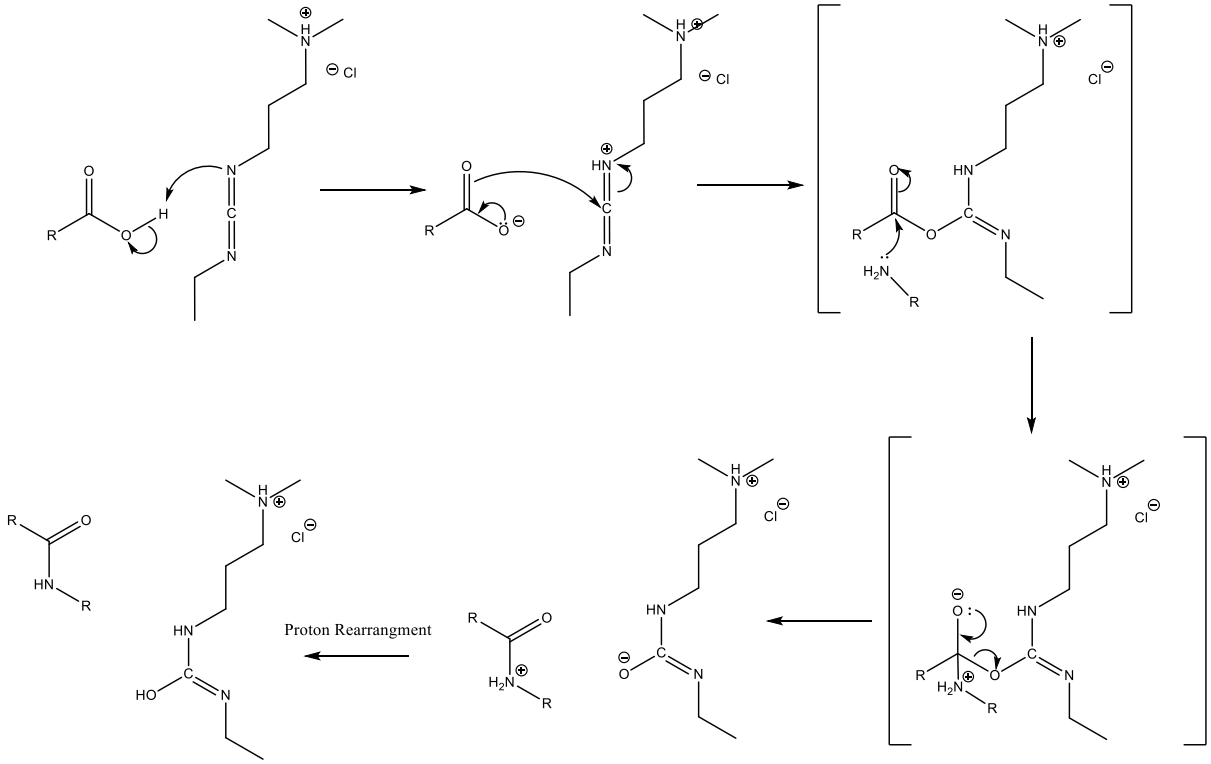

Figure 6. Mechanism for EDC crosslinking for form an amide.

To form an amide functional group, EDC couples with the existing carboxylic acid containing functional group to form an unstable intermediate. It is assumed here that due to the instability of the intermediate the reaction here is very quick. The intermediate compound undergoes nucleophilic attack from an amine functional group to form the desired amide bond. On formation of a good leaving group, the next step in the reaction is elimination to remove said leaving group, increasing the stability of the resultant compounds. The final step in the reaction is a proton rearrangement to form the target amide group and a urea by-product.

EDC has also been used to demonstrate the formation of ester bonds, from a carboxylic acid and hydroxyl group. The mechanism by which this occurs has been studied using infrared spectroscopy finding that an ester is formed as the product of the reaction, which provides both inter- and intra-molecular crosslinking.[57] It should be noted that reactions of EDC occur most optimally in acidic conditions. This is important in the crosslinking reaction of carboxylic acid and hydroxyl as the initial electrophilic addition to form a charged oxygen in the double bond is necessary so that the double bond is unstable and can be attacked by COOH, with is a very weak nucleophile.[58]

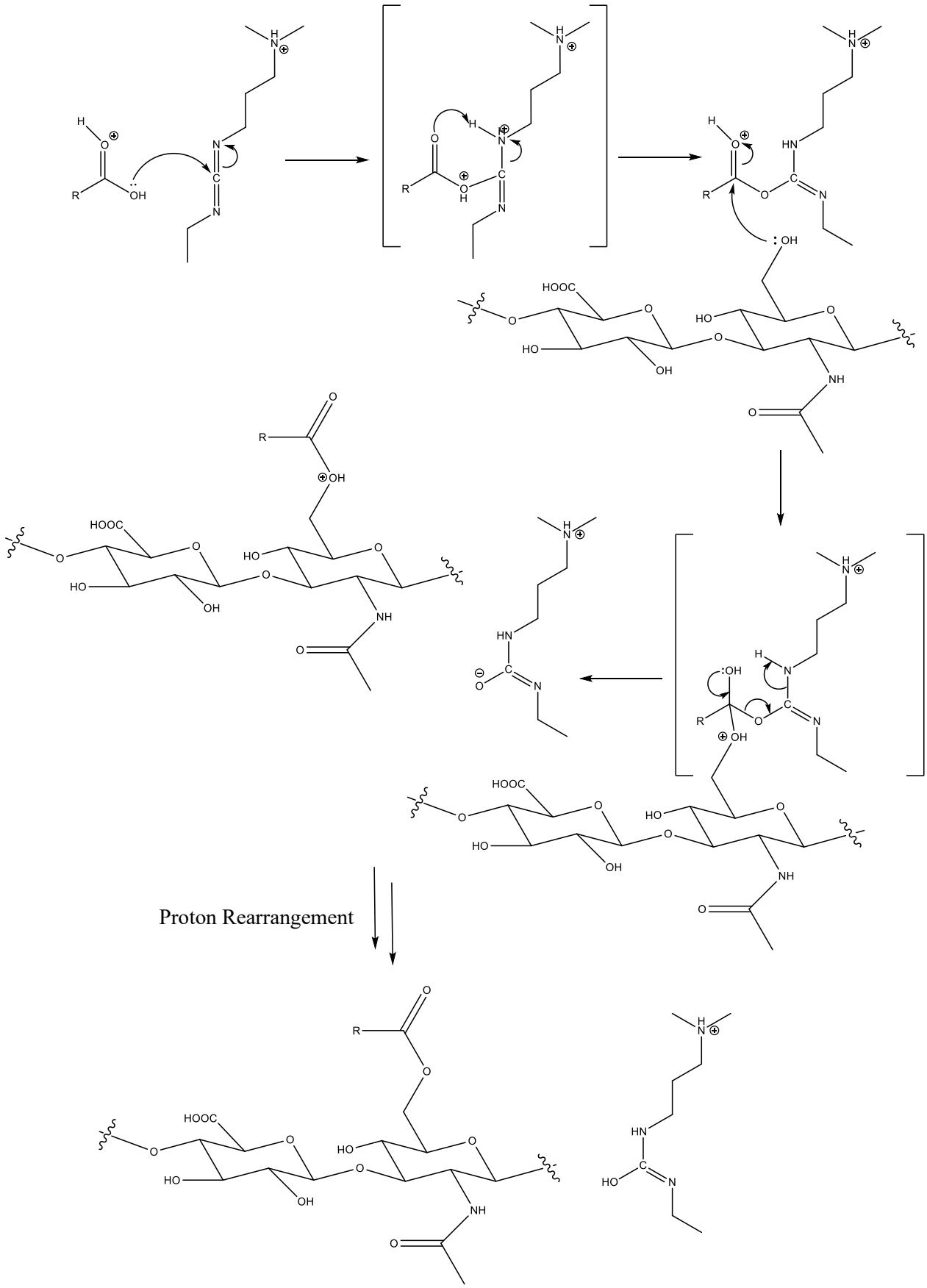

Figure 7. EDC crosslinking starting with a carboxylic acid function group. In the presence of HA the more nucleophilic hydroxyl group attacks the activated carbonyl resulting in an ester bond formation.

An activated carboxyl is formed in the initial stages of the reaction, this could be attacked by a subsequent carboxyl acid group to from an acid anhydride. However acid anhydrides undergo hydrolysis and therefore it is more likely that the activated carbonyl is attacked by the more nucleophilic hydroxyl group from a neighbouring HA molecule to from an ester. Again, a water-soluble urea by-product is formed.

N-hydroxysuccinimide (NHS) has been used in reactions with EDC to provide an intermediate with more stability than those detailed in Figure 6 and Figure 7. The use of NHS is believed to improve the efficiency of the reaction.

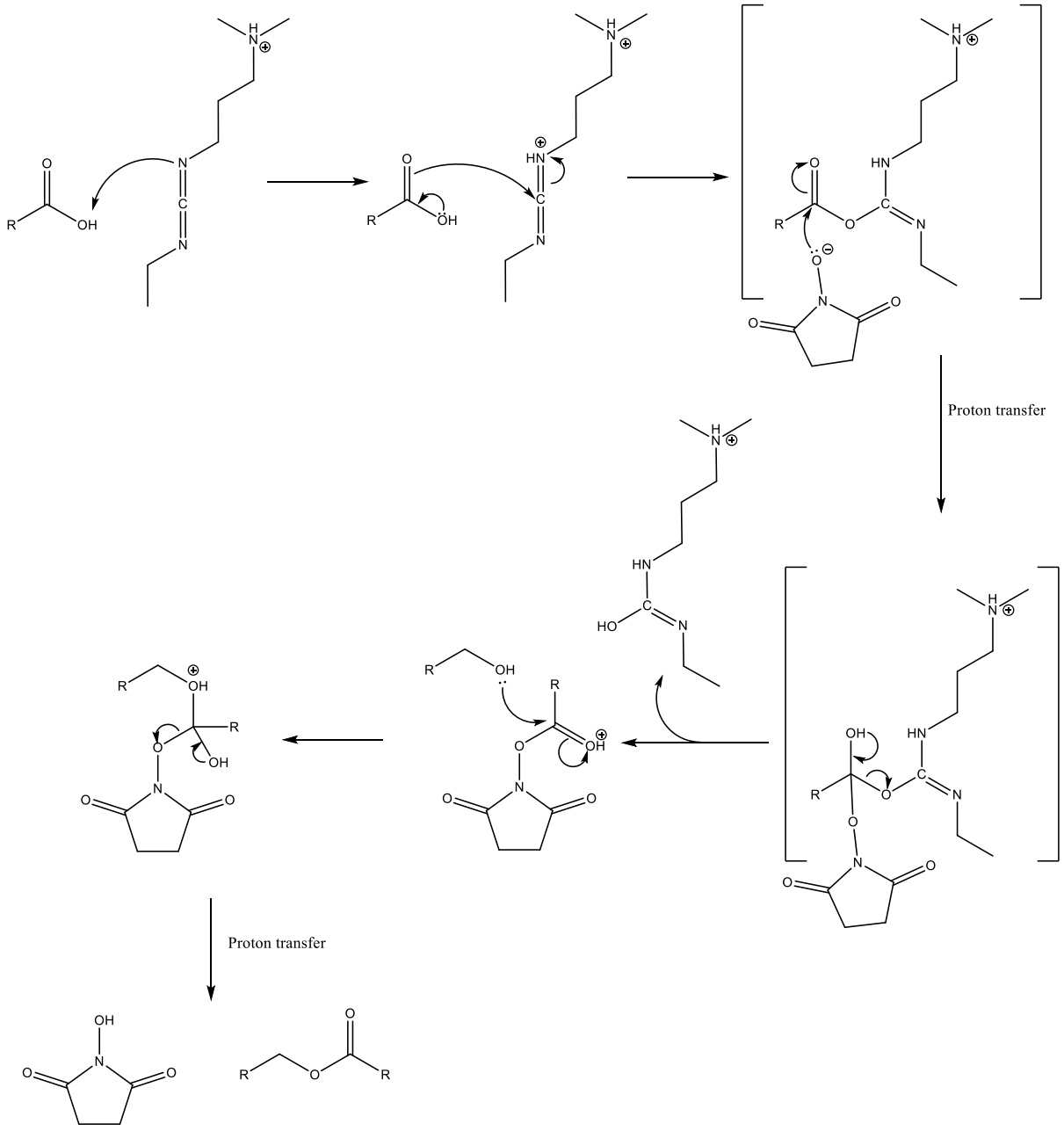

Figure 8. EDC/NHS crosslinking mechanism with a hydroxyl containing functional group.

Following the coupling of NHS to EDC, NHS is regenerated in the reaction, meaning it functions as a catalyst which can be easily removed from the reaction by rinsing with water. Both NHS and EDC are soluble in water but are considered toxic, therefore any excess material should be removed with careful rinsing of the hydrogel. Again, a water-soluble urea by-product is formed in this reaction which can also be removed in the presence of water.

EDC has been used in biomaterial applications for a number of years and across a broad variety of applications. There are a number of examples of EDC crosslinking being used in a hydrogel setting, such as to produce artificial skin by crosslinking chondroitin sulfate and collagen, forming an amide bond. As well as the crosslinking of a pectin based system to from ester bonds via the reaction of two carboxylic acid groups.[59] Hyaluronic acid has also been successfully crosslinked with EDC also producing an ester bond.[57] More recently, a system of collagen, hyaluronic acid, and chondroitin sulfate was formed by crosslinking the polymer stands using EDC for the use in tissue engineered therapies, in particular traumatic brain injury.[60]

Any hydrogel produced must be able to swell in water and maintain stability in its swollen state. The hydrogel will be used in the body, where there is an abundance of water, therefore it is vital that the hydrogel maintains its desirable properties throughout swelling. The swollen hydrogel will also need display similar mechanical properties to that of the surrounding tissue in its target application, here, the spinal cord.

2.1.2. Swelling Hydrogel Networks

Swelling is directly affected by the crosslink density throughout the network, when there are more crosslinks present the number of pores throughout the network is reduced and therefore there is less space to which water can enter the network and bind via hydrogen bonding. The higher the degree of crosslinking the less the network is expected to swell. Therefore, when designing a hydrogel to have finely tuned properties it is important to consider not only the mechanical properties which are affected by the degree of crosslinking but also the swelling.

Here, ratio of the mass of the swollen hydrogel network to that of the dehydrated network,

$$Swelling\ Ratio = \frac{Mass\ of\ the\ Swollen\ Sample}{Mass\ of\ the\ Dry\ Sample}. \qquad \text{Eq. 1}$$

The relationship increased crosslinking density and the reduction in swelling can be described by the Flory-Rehner equation.

The Flory-Rehner theory requires three assumptions to be made of the swollen network, these are: (1) the contributions from the polymer, solvent and elastic deformation of the network strands sum to equal the change in free energy; (2) Flory-Huggins theory descries the mixing term; (3) the affine-deformation model describes the elastic deformation in the network.[61] When applied according to the assumptions the network structure and the equilibrium saturation swelling can be related.[61] Whether or not a polymer will dissolve in or separate out of solvent can be predicted by the energy of the system.[62]

When a small piece of the dehydrated hydrogel is placed into solvent the network deforms and decreases the entropy of the system, this in turn is counterbalanced by an increase in entropy caused by the dispersion of the hydrogel in the solvent. The volume ratio of the network when swelling, V, or when dry, V_d, is the swelling, Q, and can be denoted,

$$Q = \frac{V}{V_d}, \qquad \text{Eq. 2}$$

at any given time during swelling.[61] In a system which involves both polymer and solvent each component will feel an interaction with another, therefore the network can be visualised as a lattice. Here, mean-field theory is needed, with the assumption that individual interactions, such as monomer-monomer, need not be individually counted because a monomer is assumed to be a field containing both monomers and solvent molecules. At this point it is important to note that for mean-field theory to apply the networks are homogeneous.[62]

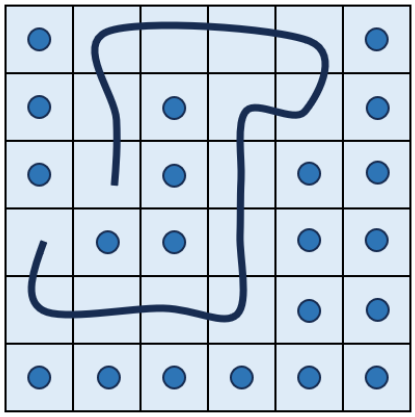

Figure 9. Diagram detailing lattice theory with a polymer and solvent molecules.

The entropy of a molecule in mean-field theory is directly related to the size of its lattice, and so it is better to consider the entropy of individual lattice sites, n, which can be configured, n. Therefore, entropy,

$$S = k_{\mathrm{B}} \ln n, \qquad \text{Eq. 3}$$

can be calculated for the overall molecule.[62] The degree to which the polymer appears in the swollen network can be defined as the volume fraction, Φ,

$$\phi = \frac{V_{\mathrm{d}}}{V}, \qquad \text{Eq. 4}$$

and if the concentration of the solvent changes, then the solvent molecules change and so does the volume fraction, this can be written as $1 - \Phi$.[61-63] Eq 4 can then be modified to,

$$k_{\mathrm{B}} = \ln(n(1-\phi)), \qquad \text{Eq.5}$$

this reflects the change in the volume fraction.[62] There is also a volume fraction associated with the polymer and because of this the entropy, S, for each lattice site can be calculated,

$$n\Delta \mathrm{S_s} = k_{\mathrm{B}}(\ln n\phi) - \ln n) = -k_{\mathrm{B}} \ln \phi.^{62} \qquad \text{Eq. 6}$$

The concentration can be changed by mixing and therefore an equation for the entropy of mixing can be assembled,

$$n\Delta \mathrm{S} = -\mathrm{n}k_{\mathrm{B}}(\frac{\Phi}{\mathrm{N}} \ln \phi + (1-\phi)\ln(1-\phi)), \qquad \text{Eq. 7}$$

and is based on the previous equations.[62] The lattice can also be used to determine the enthalpy, H, of mixing, where the polymer has $\Phi n/N$ molecules, with z neighbours. A concentrated (unmixed) network will have enthalpy,

$$H_{unmixed} = H_{pure} = \frac{nz}{2}(\phi\varepsilon_{mm} + (1-\phi)\varepsilon_{ss}), \qquad \text{Eq. 8}$$

the polymer will have an interaction energy with monomers (ε_{mm}), and the solvent has an interaction energy, ε_{ss}.[62] The interaction between monomer and solvent also needs to be taken into account, and this can be considered in the enthalpy of mixing equation,

$$H_{mixed} = \frac{\mathrm{nz}}{2}(\phi^2\varepsilon_{mm} + (1-\phi)^2\varepsilon_{ss}) + \mathrm{nz}\Phi(1-\phi)\varepsilon_{ms}, \qquad \text{Eq. 9}$$

where the squared terms take into account both the position of a monomer in the lattice as well as the probability of its neighbours to be at the same position.[62] With these two terms defined the energy of mixing can be defined as,

$$\Delta H = H_{mixed} - H_{unmixed} = k_{\mathrm{B}}\mathrm{T}n\chi\phi(1-\phi), \qquad \text{Eq. 10}$$

and introduces the Flory-Huggins interaction parameter, χ. The parameter describes solvent-monomer interactions and is temperature dependent. The Flory-huggins relationship provides a means of quantifying the entropy and enthalpy of the system. It is also a useful way of determining the ability of a gel to be stable in solution.

The Gibbs free energy of mixing can be written,

$$\frac{G}{nk_{\mathrm{B}}\mathrm{T}} = \chi\Phi(1-\phi) + (1-\phi)\ln(1-\phi) + \frac{3\Gamma\phi_s^{\frac{2}{3}}}{2N}\left(\phi^{\frac{1}{2}} - \frac{\phi}{\phi_s^{\frac{2}{3}}}\right), \qquad \text{Eq. 11}$$

and this equation can be differentiated with respect to ϕ to obtain the Flory-huggins parameter. This parameter provides an indication of the state of mixing of a material in solution. Therefore, when it is applied to a gel it can indicate the gels ability to swell in solution.

Typically, the interaction parameter is determined to be between 0 and 1, when the value is greater than 0.5 it is assumed that phase separation would occur, whereas a value of 0 would be classed as an ideal system, one where the solvent is classed as ideal for the polymer it interacts with. Therefore, the higher the interaction parameter the more likely it is to form stable opaque gels.[64-66]

In terms of the biocompatibility of the device, it is important to understand how the device performs in its swollen state and how this effects the mechanical properties. Both of these properties require some understanding of the degree of crosslinking in the system which can be obtained from the interaction of the polymer and solvent – the Flory-Huggins interaction parameter.[62, 67, 68]

2.2 Biodegradation

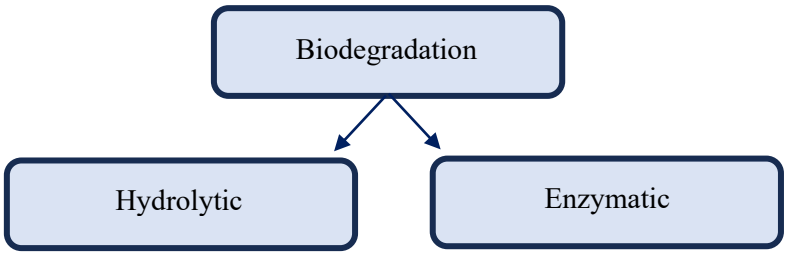

Figure 10. Breakdown of the routes to biodegradation.

The IUPAC definition of a biodegradation is the degradation caused by enzymatic processes. When biodegradation relates to a biorelated polymer, the definition is modified to include degradation which occurs due to cell-mediated phenomena. It should also be noted that a biodegradable polymer is a macromolecule substance which is susceptible to degradation by biological activity, this results in a lowered molar mass.[69]

EDC can crosslink amines and acids to produce either an amide functional group. Another means of degradation which would occur in the body is enzymatic degradation. It is believed that enzymatic degradation would be the primary means of degradation in the body.

Hyaluronidase enzymes degrade hyaluronic acid in the body, where there are six different types of hyaluronidase enzymes with slightly differing properties. Type 1 and 2 are considered the most abundant. Type 1 is found in the major organs of the body such as the liver, heart, spleen, serum and urine.[70, 71] It is active in the bodies plasma and is activated by acidic pH. Hyaluronidase 2 is also found in most tissues where it is an active enzyme but with weaker activity on hyaluronic acid than hyaluronidase type 1. Therefore, type 2 degrades only high-molecular weight HA to oligosaccharides of approximately 20 kDa.[70, 71]

2.2.1. How long should the Scaffold Remain in the Body?

The mammalian response to injury can be categorised into three stages, these stages may occur in the same time periods, or have some overlap, but have distinct enough activities to be individually definable. These stages are inflammation, new tissue formation, and remodelling. Inflammation involves a response by the immune system to prevent blood and fluid loss through coagulation immediately after tissue damage occurs.[72-75] Part of this process is also to remove dead or dying tissue and foreign objects as well as by fitting a temporary plug to seal the wound. This plug is made of platelets and is formed

via haemostasis. Neutrophils (white blood cells) then enter the area to prevent infection occurring. This is followed by the appearance of monocytes 2-3 days post-injury, here the monocytes differentiate into macrophages (key in late-stage healing).[72-75]

The second stage of healing is new tissue formation, typically thought to begin 2-10 days after the tissue damage occurred. The main characteristic of this stage is proliferation and migration of different cells. During this stage new blood vessels are formed, from which capillaries begin to branch out and replace the fibrin and granulation tissue which formed in stage one.[72,76-78] From the edges of the wound fibroblasts begin to differentiate into myofibroblasts and these are responsible for closing the wound. The interaction of the fibroblasts and myofibroblasts lead to the production of the ECM, mostly by producing collagen to form the majority of the scar tissue.[72, 76-78]

The last stage is remodelling, and this can occur for a year or longer the ultimate time taken varies person to person or by the nature of the tissue damage. During this stage fibroblasts and myofibroblasts either leave the area or undergo apoptosis. Any other remaining processes which had been occurring in the earlier stages of healing are mostly stopped, leaving scar tissue.[72, 79]

The extent of injury and medical care will also need to be factored into this consideration. Spinal cord injuries are very serious medical conditions and therefore surgery to implant a device must be considered with caution, the benefits of the device must outweigh the risks of the procedure to implant it and so the devices must function for long enough to be considered advantageous. The extent of degradation on the device's performance requires consideration.

2.3 Mechanical Properties

Quantifying the mechanical properties of a material provides a way to gain an understanding of its stability when experiencing a force.[80] The mechanical properties are contingent upon the flexibility and forces occurring within the material and the extent of their effect on the mechanical properties is significant when trying to characterise a material.[81] There have been several studies making great advances in determining a method for analysing the mechanical properties of a material.[81-83]

Table 1. Literature study on the elastic modulus of humans and animals.

Tissue	Animal	Elastic Modulus (kPa)	Test Method	Condition
Brain	Human	3-10	Mesh, Model	
Spinal Cord	Human	2000	Tensile	Intact, Cadaver [84]
Spinal Cord	Human	1400	Tensile	Intact, Cadaver [85]
Spinal Cord	Human	40.12 ± 6.9	Indentation	Intact, Cadaver [86]
Spinal Cord	Human	1020-1037	Uniaxial Tension	Intact, Cadaver [87]
Spinal Cord	Cow	1190	Uniaxial Tension	Intact, Cadaver [88]
Spinal Cord without Pia Mater	Human	68	Tensile	Incised, Cadaver [85]
Spinal Cord	Sheep	25	Indentation	Intact, Cadaver [89]
Spinal Cord without Pia Mater	Rabbit	5	Indentation	Intact, Cadaver [90]
Spinal Cord	Rat	9.5	Indentation	Intact, Cadaver [91]
Dura Mater	Sheep	5	Indentation	Incised, Cadaver [89]
Pia Mater	Rabbit	2300	Tensile	Incised, Cadaver [90]
Grey Mater	Rabbit	3	Pipette Aspiration	Incised, Cadaver [90]
White Mater	Rabbit	5	Pipette Aspiration	Incised, Cadaver [90]
Grey Mater (axial)	Rabbit	3.4 ± 1.4	Pipette Aspiration	Incised, Cadaver [92]
White Mater (axial)	Rabbit	3.4 ± 0.9	Pipette Aspiration	Incised, Cadaver [92]
Dura Mater	Dog	399	Indentation	Incised, Living [93]
Dura Mater	Dog	463	Indentation	Incised, Living [93]
Brain	Pig	3.24	Indentation	Incised, Living [94]
Spinal Cord	Sheep	22 ± 14	Indentation	Intact, Living [89]
Spinal Cord	Dog	265	Uniaxial Tension	Intact, Living [95]
Spinal Cord	Cat	252	Uniaxial Tension	Intact, Living [96]
Spinal Cord	Dog	16.8	Tensile	Intact, Living [93]
Spinal Cord	Dog	11.9	Tensile	Intact, Living [93]

There is an unfortunately large range in the available data related to the biomechanical properties of the central nervous system and this could be due to environmental factors, sex or species. Therefore, there is no universal value for the modulus of the human spinal cord.[97]

Materials which are designed to have properties very similar to the tissues in the spinal cord are known as surrogate spinal cord materials. It is easier and less controversial to test the elastic moduli of these synthetic materials than it is to test the elastic moduli of living or decreased animals. Therefore, there are more publications on the matter, leading to a much broader scope of potential elastic modulus information. So, there is a large range in the moduli of available surrogate materials, such as 52-614 kPa with the majority of the materials falling into the 5-100 kPa range.[91, 98, 99] However, in a conference publication by T. L. E. Mazuchowski *et. al.* reported an elastic modulus of 89 kPa which they found to be in good agreement with the moduli of the of the human brain (66 kPa) published by J. H. McElhaney *et. al.*[85, 100] In fact the value of 89 kPa has been used as a target elastic modulus, such as in the work by C. Cheng *et. al.*[91]

The elastic modulus is usually measured using the methods listed in Table 1, these are uniaxial tension and indentation testing, more infrequently other methods such as pipette aspiration are used. For soft materials which require somewhat gentle handling an indentation test, where the material can be placed on a surface, is the most appropriate of the methods. During the indentation method a probe is used to define the load-displacement relationship of the material, this method is also useful for small samples where it can detect micro- or even nano-scale sized deviations.[101, 102]

2.3.1. Load-displacement Relationship

The relationship between load and displacement described by Sneddon can be described as:

$$P = ah^m \qquad \text{Eq. 12}$$

Where m is a constant specific to the geometry of the indenter, $m = 1$ when the indenter is a flat cylindrical shape, $m = 2$ for cones and $m = 1.5$ for paraboloids or spheres. [101, 103] This relationship can model the contact between the sample and the indenter when the sample behaves elastically, such behaviour is when the material returns to its original shape after being subjected to stress. Although deformation occurs during this process it is non-permanent, however this is not the case for a material displaying plastic behaviour.[101, 104] The elastic behaviour of a material can also be defined as the region where the relationship between stress and strain is linear, therefore the elastic behaviour of a material should be referred to as the elastic region.[104] Hooke's law applies to a

material in the elastic region. It should be noted that plastic deformation is irreversible and is beyond the scope of this project.

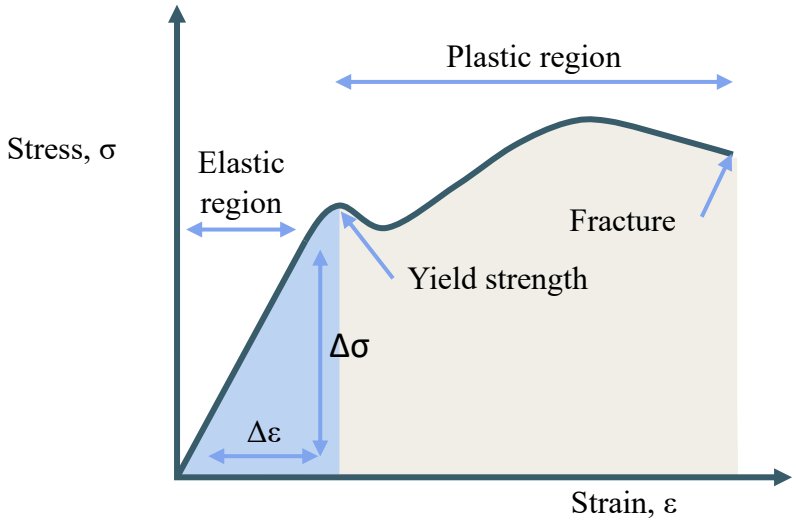

Figure 11. A diagram detailing the elastic and plastic regions which occur in a stress/strain relationship.

Hooke's law relates the length a spring can be extended with the load deforming it. When a force (F) is applied in one dimension the spring changes in length. However, Hooke's law only applies when a spring returns to its original length after being stretched, the equation can be denoted,

$$F = kx, \qquad \text{Eq. 13}$$

where F no longer refers to the applied force but to the force acting to restore the spring to its original length.[105, 106] Hooke's law can be applied to materials other than a spring, in this case it is often more useful to express the law in terms of stress and strain,

Figure 12. A diagram showing the action of tensile force.

$$\sigma = E\varepsilon.^{106} \qquad \text{Eq. 14}$$

There are two fundamental types of stress (σ), shear and normal stress, the first of which is in relation to stress parallel to the plane of the object being tested, the latter regards stress as being at a tangent to the plane of the test object. [80, 107] When a force acts on an object, the object will also experience counterbalancing forces at a tangent,

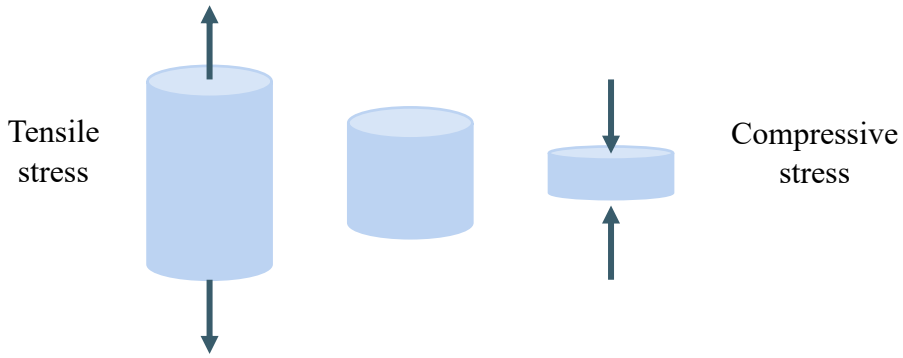

Figure 13. A diagram comparing tensile and compressive stress.

$$\sigma = \lim_{A \to 0} \frac{\Delta P}{\Delta A} = \frac{dP}{dA}, \quad \text{Eq. 15}$$

$$P = \sigma \int dA = \sigma A, \quad \text{Eq. 16}$$

$$\sigma = \frac{P}{A}. \quad \text{Eq. 17}$$ [80, 106, 107]

Eq 17 is the mathematically definition of normal stress and is applied when a material is subjected to a tensile stress. However, in indentation testing the load is compressive. Compressive stress can be given by the negative value of tensile stress. But when it is applied to a material the deformation of the material itself is also required. [80, 106]

Strain can be defined in two ways, the first is

$$e = \int \frac{dl}{l_0} = \frac{l - l_0}{l_0}, \quad \text{Eq. 18}$$

where strain is a ratio of the change in length compared to the original length – known as the deformation and is expressed in terms of e.[80] A second and sometimes a more practical understanding is to express strain as the changes in linear dimension at each instant of the test,

$$\varepsilon = \ln(e + 1). \quad \text{Eq. 19}$$ [80]

In cases where strains are relatively small, such is the case for this project, it can be assumed that the exponent will be larger than one and therefore can be neglected. [80]

$$\varepsilon \cong e \quad \text{Eq. 20}$$

2.3.2. Poisson's Ratio

When the probe compresses the material not all the deformation occurring will be uniform and therefore additional strain must be taken into consideration. As the material deforms strain is expected to occur in the plane of the load but will also occur laterally due to deformation. The comparison between the strains is

$$\nu = -\frac{lateral\ strain}{axial\ strain} = -\frac{\varepsilon_y}{\varepsilon_x} = -\frac{\varepsilon_z}{\varepsilon_x} \qquad \text{Eq. 21}$$

where v is Poisson's ratio.[80]

2.4 Bioelectronics

The term bioelectronics refers to the interface of biological tissue and electronic components and its aims are in developing devices which can enable electronic communication between living tissue. This includes being able to respond to biological signals and stimuli as well as acting as a therapeutic agent. The biological tissues which are targeted range in size and function, from a single cell or a protein to a complex organ. The electronic component may be devised of a circuit, transistor, electrode, or electronic material.[108] Therefore, bioelectronics cover a broad range of disciplines such as medicine, biology, chemistry, engineering, and physics.

2.4.1. Bioelectronic Devices

The first recognised examples of understanding the electronic signals which occur in the body were both carried out in Italy circa. 1780. One of which was carried out by Galvani, who reported twitching in a frog's leg when the exposed sciatic nerve was touched with a steel scalpel.[108] The other was by Volta, who had invented the first battery made of copper disks and zinc. Using himself as a test subject, Volta connected his ear to his battery feeling a shock and hearing noises when the circuit was closed. Volta, although unwilling to repeat his experiment on himself was able to prove that the stimulation reported by Galvani was the electrical stimulation created when Galvani inserted steel and brass into the sciatic nerve creating a different in voltage.[108]

Further study into electrical stimulation of the ear was then picked up again in the 1930s by S. Stevens which later led to the development of the cochlear implant.[109] Although the initial experiment by Galvani on electrical stimulation is considered the foundations of bioelectronics, major interest in the field did not come until after the discovery of the action potential by A. Huxley and A. Hodgkin.[110, 111] Today, bioelectronics is frequently

applied to medicine, where it is seen as an exciting and innovative direction for diagnosis and treatment options.

Table 2. Detailing bioelectronic devices and their applications.

Bioelectronic Device	Application
Deep Brain Stimulator	Parkinson's Disease [112]
	Obsessive Compulsive Disorder [113]
Responsive Epilepsy Stimulator	Epilepsy [114]
Visual Protheses	Vison Loss [115]
Cochlear Implant	Deafness [116]
Prosthesis controllers	Control of Prosthetic Limbs [117]
Electrocardiogram	Detection of Arrhythmia [118]
Cardiac Pacemaker	Treatment of Arrhythmia [119]
Artificial Pancreases	Insulin control [120]
Spinal Cord Implant	Paralysis [121]

Table 2 summarises some of the common applications of bioelectronic devices in medical fields. One of the most important examples of applications to the bioelectronic field surrounds cardiac function - the development of an electrocardiogram (ECG) and the ability to restore normal heart rhythm through fibrillation and the electrical stimulation via a pacemaker. Here, there is both stimulation and transduction occurring. The heart is electrically stimulated back into normal rhythm by a pacemaker after an abnormal rhythm is detected using an ECG.[119, 122] The combination of ECG and pacemaker is important to bioelectronics because it was the first product to display interpretation of biological communication and to transduce the signal into an electrical signal used to stimulate biological tissue.[123]

The patch clamp technique was a pivotal discovery in the detection of a potential across a membrane. The technique creates a seal between the membrane and a pipette allowing a signal to be detected and earned Neher and Sakamnn a Nobel prize in physiology and medicine.[124-126]

Bioelectronic devices face a physical issue in the sense that biological tissue is made up largely of water, which is typically a detriment to many electronic components.[127] Another problem which requires addressing is that biological signals are often masked by other bodily functions and are more localised and less intense. The body sends a signal using a variety of molecules (of ranging size) whereas, electronic components carry a signal via electronics.[127-129]

Organic electronics offer more compatible physical properties which can be tailored to form a biocompatible device. The active material in organic electronics is often a conductive or semi-conductive polymer or molecule. The most common example of an organic electronic are the organic light emitting diodes (OLEDs) which make up a large proportion of the organic electronic market.[130] The history of organic electronics can be traced back to the first descriptions of polyaniline.[131] However, most would consider the field to have truly began in the 1960s when polymers, such as polyacetylene and polythiophene, were found to be conductive.[132]

For their use as a bioelectronic device, the polymers must have an appropriate architecture. One of the most famous examples of which is the first proposed field-effect transistor (FET), published by J. E. Lilienfeld in 1930. Transistors being a device where current flows between two electrodes (the source and drain) which is controlled by a third electrode known as the gate.[133] By 1947 transistors in microelectronics began to flourish. These transistors comprise metals (electrodes) dielectrics (gate), and semiconductors (active layer), the most common example of which is a metal-oxide-semiconductor field-effect transistor (MOSFET). Success also came in the form of being able to produce small scale transistors which led to the development of circuits and the basis for all modern-day electronics. A MOSFET controls the flow of electrons through a circuit to provide switch-like behaviour. A MOSFET can achieve this by field-effect doping, which occurs when a potential is applied across a dielectric metal gate and modulates the charges inside a semiconductive layer. Here, the charges are either mobile electrons, resulting in an n-type transistor, or the charges are holes giving a p-type transistor.[133, 134]

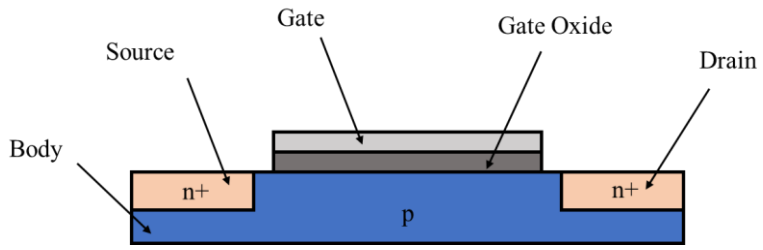

Figure 14. A diagram of a FET.

Many field-effect transistors use one mode of charge carrier, either holes or electrons, and so they are either n- or p-type. There is a small number of FET which can carry

charges using both carriers and these are known as ambient FETs. It is the density of these carriers which determines the strength of the signal passed between source and drain. FETs can either function in 'depletion' or 'enhancement' mode, the first of which involves a current being applied to the gate, resulting in a reduction in the available change carriers, hence the current flow between source and drain decreases until it is ultimately zero. At this point the transistor would be considered 'off'. Enhancement mode does the opposite; when a voltage is applied to the gate, the current begins to flow between source and drain, causing the transistor to be 'on'.[130, 135]

Interest in developing transistors which cover larger areas but are cheaper to manufacture led to the interest in organic field-effect transistors (OFETs). The advantage of using an organic active layer means the properties of the transistor can be finely tuned by changing the chemistry of the semiconducting molecule or polymer which makes up the active layer.[134] OFETs have demonstrated good mobility and mechanical stability in various applications, such as bionic skin and stretchable transistors.[134, 136, 137]

2.4.2. Organic Electrolyte Gated Transistors

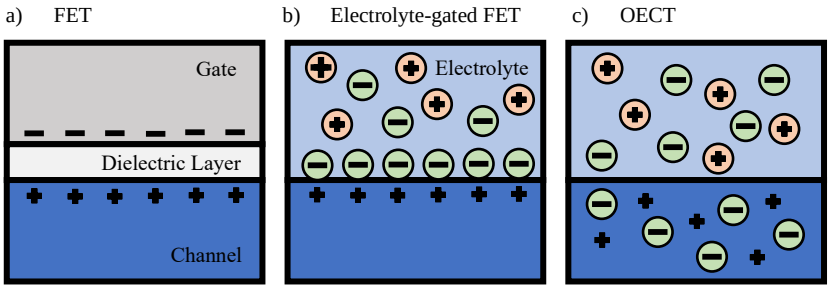

Figure 15. Diagram comparing a FET, an electrolyte-gated FET and an OECT.

In OFETs a crucial dielectric layer is generated when the source, drain, and conductive material are isolated from the gate by an insulating layer. When the gate is separated from the source, drain, and conductive layer via an electrolyte there is no need for an insulting layer. This is because both the gate and the active layer are in contact with the electrolyte creating double layers - one between the gate and electrolyte, the other between the electrolyte and active layer. This architecture is known as an organic electrolyte gated field effect transistor (EGOFET).[138, 139]

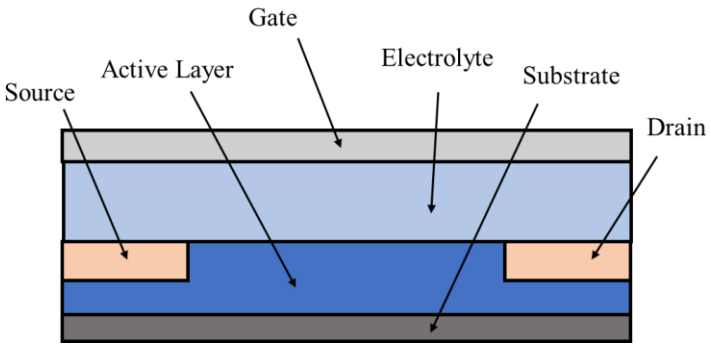

Figure 16. A diagram of an EGOFET.

When a potential is applied to the gate, the double layers form at the interface between the gate and electrolyte. If a negative voltage was applied to the gate, a layer of cations forms in the electrolyte neighbouring the gate. This layer is known as the Helmholtz layer. The layer of cations at the interface is more concentrated than the cations in the rest of the solution, essentially forming a concentration gradient where the number of cations decreases with distance from the gate-electrolyte interface. The cations are drawn away from the bulk of the electrolyte, leaving the negatively charged ions. These ions form a bulk layer at the interface between the electrolyte and active layer.[133,138] The layer of negative charges attracts an oppositely charged layer in the active layer; hence a second double layer is formed. When both double layers are in place, a field effect is generated which is effectively insulating, preventing the flow of a current between the two layers. Since the double layers consist of charges, the effect of the double layer ultimately generates a capacitor, a component which can store energy in the form of charged particles.[133, 138, 140, 141]

To produce printable, flexible, and large area transistors, semiconducting organic polymers are often used as the active layer, hence the name electrolyte gated organic field effect transistors can be applied. EGOFETs have been frequently studied in the hope of creating a biosensor with good compatibility to the human body. EGOFETs make promising devices for the body due to their ability and reliability on electrolytes, meaning they not only function in liquid, they are also capable of sensing in it. Therefore, the device would be able to function in bodily fluids such as saliva, blood, and mucus. Such EGOFETs would be able to detect biomarkers if the necessary recognition element was grafted to the device.[133] An example of such is the creation of a EGOFET modified with an Au gate-aqueous solution interface for the detection of dopamine *in vitro* .[142] A further example is a ‘lab-on-a-chip’ device comprised of

multiple EGOFETs. For proof of concept the device was tested to monitor tumour necrosis.[143]

Interfacing a biomaterial with an electronic device is challenging and there are aspects which need to be addressed in the design process. One of the first attempts to overcome some of these challenges was by F. Buth *et. al.* who functionalised a semiconductor with a biomaterial creating an EGOFET architecture.[144] One of the challenges faced by the team is that many semiconducting materials are hydrophobic but are required to function in a hydrophilic biological tissue. EGOFET devices require proper functionalisation of the gate electrode or electrolyte.[142, 145]

Often in transistor architecture the gate electrode is placed as the 'top' contact and the source and drain are placed towards the bottom of the device. This top-gate, bottom-contact configuration involves the gate being submersed in the electrolyte. It should be noted that the architecture of an EGOFET looks like that of an organic electrochemical transistor (OECT).[145] A key difference is that in an OECT the transistor's ability to have both and 'on' and an 'off' phase is created by the diffusion of electrons into the active layer changing the doping (or redox) state of the semiconductive material. Whereas, in EGOFETs, there is no transfer of charge, and the means of current flows occur by capacitive processes.[142, 145]

OFET is not the only architecture to demonstrate properties which could be taken advantage of in a variety of different applications. Organic electrochemical transistors (OECTs) were developed by M. S. Wrighton *et. al.* in 1984 and since then they have become a major focus in bioelectronics.[146] Part of their interest is because like OFETs they can also be produced at low-cost and can be large enough to cover a surface. Beyond this they also can be designed to have good mechanical compatibility with various environments, such as with plastic, paper, and fibres.[147-149] OECTs are also compatible with aqueous environments and have been successfully demonstrated as amplifying transducers.[134, 150, 151]

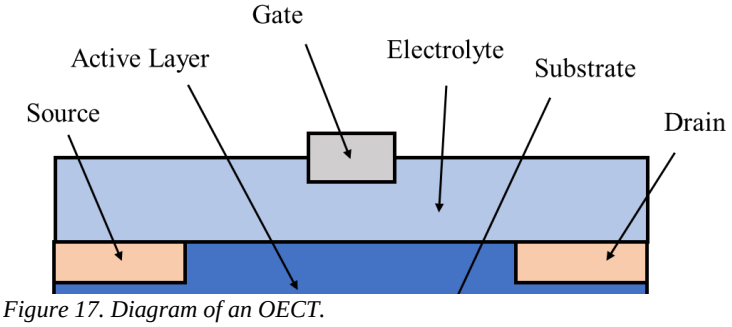

Figure 17. Diagram of an OECT.

In an OECT architecture, metal electrodes are placed in contact with a semiconducting film creating a source and drain as well as a channel through which a current flows from the source to the drain. The OECT itself is formed of an active semiconductive layer which is in contact with an electrolyte. The gate electrode is present, contacting the electrolyte but not in contact with the active layer itself. The current flow through the active layer of the OECT is dependent on the influx of ions from the electrolyte into the active layer. The presence of ions in the active layer causes the doping state of the layer to change, hence changing the ability of the film to carry a current. The doping state of the polymer is known as the redox state amongst electrochemists.[130, 135, 152]

Current flow in an OECT is controlled by changing the potential applied to the gate electrode (V_G). When a current flows between the source and the drain, the voltage at the drain dictates the number of holes or electrons carrying a current through the active layer.[130, 135, 152]

Poly(3,4-ethylenedioxythiophene) (PEDOT) is commonly used as the active layer in OECTs. On its own it does not display the necessary semiconducting properties appropriate for producing a bioelectronic device and requires a doping to achieve this. Poly(styrene sulfonate) (PSS) is the most commonly used doping agent for PEDOT. PEDOT:PSS can be used in a p-type transistor where, when there is no potential to the gate, the flow of current is carried by mobile holes in the polymers which can jump from chain to chain.[134] The holes generated in the presence of a potential are counter-balanced by the negatively charged sulfonate anions on PSS in a process known as hopping. The current flows through the channel between the source and drain when there is no voltage applied, and so the transistor is considered ‘on’. This is an example of a depletion mode transistor. When a potential is applied to the gate, ions from the electrolyte diffuse into the channel, changing the doping state and reducing the flow of current. The transistor is considered to be in an ‘off’ state when the polymer has been dedoped and no current can flow through the channel.[134]

Doping agents such as PSS are added to the semiconductor to improve the conductive abilities of the film. Therefore, when the channel is ‘dedoped’, this implies complete loss of the performance enhancement qualities provided by the doping agent.[153] In an OECT, dedoping occurs throughout the entire channel, this is unlike other architectures where the area impacted by a change to the channel is likely to be small, such as in FETs.[134] This coincides with the fact that OECTs typically have a larger drain-source voltage response when a small change in gate voltage occurs, making them good

amplifiers with a sensitivity which would make them ideal for biological application where signals are often weak. Since dedoping occurs through the volume of the active layer where ionic interactions are at play, the response time to potential changes can be delayed. However, it should be noted that the channel displays capacitance and resistance which are typically more of a limiting factor than the rate of diffusion of ions.[134, 135, 154]

2.4.3. OECT Characteristics

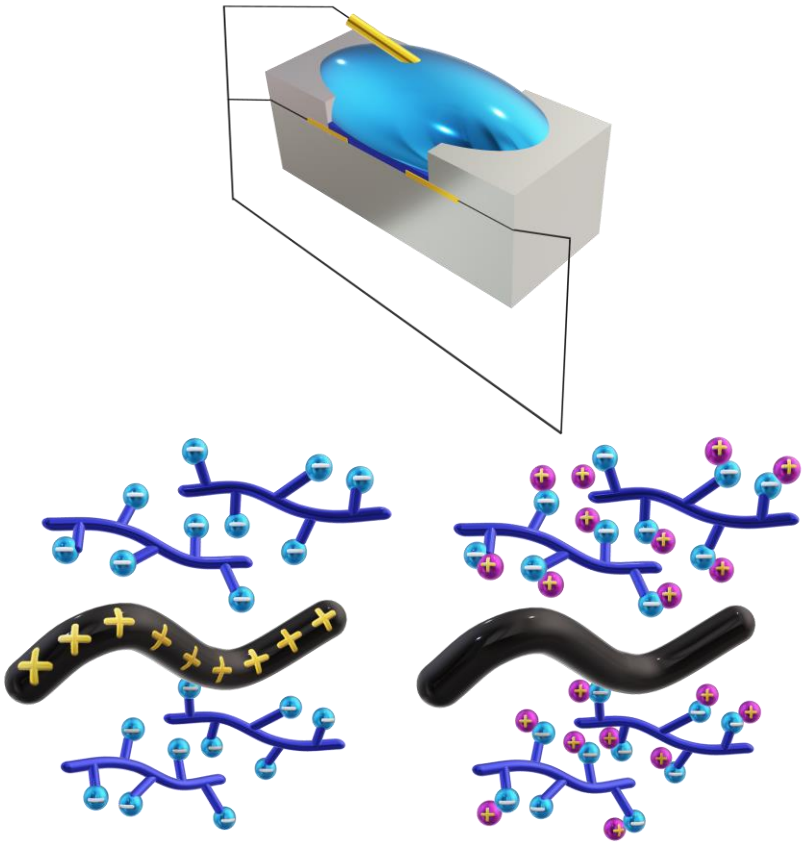

Figure 18. A diagram showing the device set-up and the mode of charge transport in an OECT.

OECTs transduce a small voltage change at the gate (ΔV_G) into a larger current across the channel to the drain (ΔI_D). This process, known as transconductance, is the efficiency of the transduction process and can be thought of simply as the amplification which occurs in the device.[134, 154] Transconductance is denoted,

$$g_m = \frac{\Delta I_D}{\Delta V_G},^{154} \qquad \text{Eq. 22}$$

where g_m is transconductance and is an important transistor parameter.[134, 154] The transduction occurring in a device can be measured from the curve for the drain current against gate voltage, which is known as the transfer curve. Transfer curves are crucial for understanding the characteristics of an OECT device.[134]

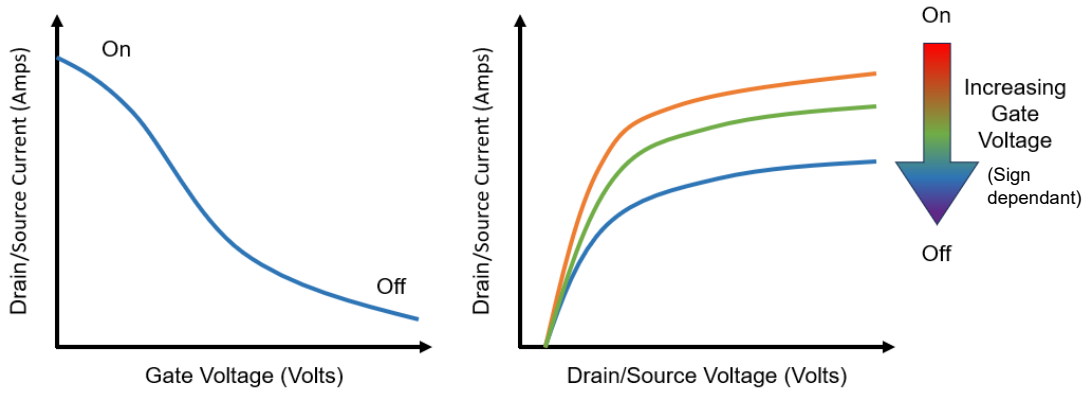

Figure 19. A diagram describing transistor characteristics. A transfer curve and an output curve.

The transconductance of an OECT can be tuned to match that of its target application by scaling the size of the active layer. The transconductance is dependent on the thickness of this layer and therefore by changing the thickness the transconductance of the device can also be scaled. In the case for both the transfer and output characteristic of an OECT, as the gate voltage increases the drain-source current decreases.[135]

The ability of the OECT to transduce both ionic and electronic signals makes them ideal for biological devices. Having the ability to function in electrolyte and hence in a biological tissue, composed mostly of water, OECTs are promising for many bioelectronic applications and sensors.[155]

Chapter 3. Biomaterials

3.1 What is a biomaterial?

The IUPAC definition of a biomaterial is a material which is expected to be used in contact with living biological systems. This definition was derived from a version which specifically states that a biomaterial is a non-viable material for use in medical device.[69] When the word medical is removed from the original definition, the potential scope for biomaterial applications is broadened. Similarly, removing 'non-viable' extends the definition to those who refer to materials of natural origin.[69] In a much broader sense

the biomaterials are part of biomaterials science, a field in which most of the developments have been towards biomaterial synthesis, characterisation, optimization and the interaction between the material and the host tissue.[69] However, there are also significant advancements on the development of surfaces which can interact with surrounding cells and proteins. Ultimately, the aim of biomaterial science is to produce a biocompatible material. 'Biocompatibility' here, is used to compliment the term biomaterial and refers to the ability of a material to be in contact with living tissue without causing adverse effects.[69, 156]

The earliest records of biomaterial products can be traced back to ancient civilisations. Dental implants have been used by humans to stabilise and repair teeth since the earliest parts of known history, such repairs are thought to date back to the ancient Egyptians in approximately 2500 BC. Similar dentistry repairs with gold products have been recorded by the Etruscans and Phoenicians as late as 300 AD. The first known implant was suspected to be of the Mayan population in 600 AD and consisted of an ivory replacement tooth with a gold wire fixture.[157] A Mayan skull was investigated due to having implanted teeth which were originally believed to have been placed as part of a burial ritual but were found to have bone regrowth around them proving the teeth had been implanted while the individual was alive.[157, 158]

There is also evidence of ancient sutures from as far back as 32000 years ago. Wounds have been dressed with materials such as linen, metallic materials and Catgut, however they did not involve the same methods of sterilisation and biodegradation that they do today.[156] The Roman-Greek physician Galen described his use of gold sutures and proposed that arteries in the body connected the liver and heart in order for the circulation of vital spirits. This was later replaced by William Harvey who proposed that the heart drives blood around the entire body by a series of arteries and so the idea of the heart as a pump arose, leading to a series of artificial heart pump theories by C. Lindbergh and A. Carrel, P. Winchell and ultimately to a team lead by W. Kolff who first tested artificial hearts in animals.[132, 159, 160]

The history of biomaterials is rich with examples and these are not limited to dental implants, sutures and heart pumps. One further and notable example is the development of contact lenses, of which the first successful glass lens was believed to be made by A. Fick in around 1860.[161] However, it wasn't until around the time of the second world war that plastic contact lenses were developed, using polymers such as poly(methyl methacrylate).[156]

The second world war necessitated the rapid advancements of many medical techniques, including the field of biomaterials. After the end of the war, materials of particular interest were those which were manufactured in mass for the war, such as silicones, polyurethanes, Teflon, nylon, methacrylates, titanium, and stainless steel.[156]

Evidence of biocompatibility was detected in individuals who suffered eye implantation from projectiles such as shrapnel. At the time it was common belief that the body would reject a foreign object however evidence of regrowth around the object was seen in some, without signs of further irritation or inflammation.[156] This discovery lead to the development of an implant to replace lenses affected by cataracts, however implantation was considered faux pas and so this idea did not pick up until the 1980s when artificial lenses became more common.[156]

3.1.1. Different types of biomaterials

Biomaterials themselves should not alter the normal functioning of the living tissue in which it was applied. There are many common applications such as dental implants, joint replacements and artificial heart values, pacemakers, and stents. However, biomaterials are not solely limited to implantable devices and are of large interest to the field of biomedical engineering, for applications such as surgical instruments, artificial organs, and drug delivery. Therefore, the scope for the type of material which a biomaterial could be is broad, however the most common types are often ceramics, composites, metals, and polymers, and these material groups can be narrowed down according to the target environment.[50]

The 1960s saw a change in the approach to biomaterials, when materials started being specifically developed for medical devices, rather than using mass-produced 'off-the-shelf' materials left from the second world war.[156] The main materials of interest in this era were silicones, polyurethanes, Teflon, poly(lactic-glycolic acid), titanium, and various hydrogels. Though silicones and polyurethanes were used prior to the 1960s, it wasn't until this point when the manufacture of them was scaled up and the introduced to medical applications showing good biocompatibility.[156]

A first generation of biomaterials, known as protheses were developed in the 1960s and 1970s with a particular focus on developing devices considered to have biological inertness. A device which was considered is one which minimises the bodies immunological response to a foreign object.[50, 162] The goal of these early biomaterials was summarised in 1980 by L. Hench as the requirement of a biomaterial to match the

properties of the tissue it was designed to replace and with minimal toxic response.[162, 163] By the time of this publication there were over 50 different implantable protheses made of 40 different biomaterials. There are tens of millions of people who experience the implants of a biomaterial device in their bodies. One such example of these was the total hip replacement where a damaged ball joint was replaced with a stainless steel ball and high density polyethylene (HDPE) socket.[164]

A series of bioactive and resorbable materials made up the second generation of biomaterials which came as a method of improving the flaws in the existing designs. In first-generation biomaterials the interactions at the interface of the host tissue and the biomaterial were minimal or non-existent. Therefore, a need to develop biomaterials which can more closely match the host tissue were required. The mechanical properties of the biomaterial should be similar enough to the target tissue so that a reliable skeletal prothesis can be developed.[50, 162, 165] When there is a mismatch in modulus the matter with the higher elastic modulus carries almost all the load. In the cases where the biomaterial is the one which the higher modulus it carries the load in the place of the host tissue leading to a deterioration in strength, bone resorption and lead to failure of the device.[162, 165]

Hapex, the first biocomposite material, designed specifically for medical devices, was used as an early bone graft material.[162, 165, 166] Various bioactive materials were in use in orthopaedic and dental settings by the mid-1980s, with many more bioactive materials based on glasses, ceramics and composites undergoing clinical trials.[162]

Another phase in second-generation biomaterials focused primarily on resorbable materials, which is where the biomaterial is expected to gradually break down and be replaced by regenerating host tissue. This was demonstrated in the 1980s by L. Hench *et. al.* who demonstrated the hydrolytic degradation of polylactic and polyglycolic acids to carbon dioxide and water which can be metabolised by the body.[162, 163] By the turn of the twenty-first century studies in bioactive materials and resorbable materials had begun to merge and become as the third-generation biomaterials. These materials are often modified to promote cell proliferation and differentiation.[162]

Biomaterials have a long history, and it is relativity late into it when hydrogels are first investigated, however they have existed on earth since life first began. Many of these hydrogels exist as films, living tissues and extracellular matrices, and most exist in their swollen state.[156, 167] Many scientists have made an attempt to define exactly what a

hydrogel is, with most concluding that it is a crosslinked polymer system formed by one or more monomers which swells in water. Another commonly used definition concerns how the hydrogel can swell and retain its swollen state without dissolving in water.[168]

It should also be noted that biomaterial sciences can be separated into two pathways, tissue engineering and *in situ* tissue regeneration. In the former cells are adhered to a resorbable biomaterial acting as a scaffold. These cells are given time to grow *in vitro* before being planted in the body. As the scaffold degrades living tissue resulting from the original cells is left behind. The second pathway involves the use of micro- or nanoparticles which can release products and growth factors to stimulate the assembly of cells into tissues.[162]

3.1.2. Hydrogels as Biomaterials

Hydrogels make promising biomaterials in part because of their ability to have high water contents, like the tissues in the human body. These hydrated hydrogels can mimic the extra cellular matrix environments; therefore, they can encourage cell proliferation and can host cells which multiply before being secreted into the surrounding tissue helping to repair it and reinstate the extra-cellular matrix.[169]

Hydrogels have a relatively modern history in terms of being classified as a material for medical applications, which started with poly(2-hydroxyethyl methacrylate) (pHEMA). HEMA was first described in 1936 as a relatively trivial, brittle molecule and was largely forgotten about.[156] However, in a paper published by Wichterle and Lim, the monomer had been polymerised and crosslinked resulting in a soft, elastic, clear gel which swells in water – a hydrogel. This particular hydrogel is now a mainstay of the soft contact lens industry and modern field of biomedical hydrogels.[156, 170]

Since their discovery hydrogels have frequently been used for the controlled delivery of active agents. Hydrogels provide a means of drug delivery which is direct, requires fewer administrations of the drug, protects the drug from damage and allows for a lower dosage to be delivered. In the decades following the publication of pHEMA, the application of hydrogels became focused on drug delivery and also ophthalmic research. Many of these first-generation hydrogels were prepared from either water-soluble monomers or polymers which are then crosslinked. Water-soluble monomers were typically polymerised by chain addition reactions, where a free radical species adds to a π-bond in a vinyl monomer initiating a chain reaction. The polymerisation also occurs in solution with a multifunctional crosslinking agent, providing the advantage that the

hydrogels can be produced to be a specific shape due to their liquid form, and occur under relatively mild conditions.[49]

The second category of hydrogels which make up the first generation are those which are water-soluble synthetic polymers which have been crosslinked either by a reaction between functional groups or by free radicals. Most notably there are two polymers from this category which have been extensively studied, these are poly(vinyl alcohol) (PVA) and poly(ethylene glycol) (PEG).[49]

PVA has been chemically crosslinked to form gels which include aldehydes, anhydrides, and isocyanates. It also was used to model how to determine the molecular weight between crosslinks as proposed by N. A. Peppas *et. al*.[49, 171] Peppas carried out swelling and dynamic mechanical analysis on glutaraldehyde crosslinked hydrogels to determine such molecular weights.[49, 171] However, there was concern that a residual crosslinking agent may remain in the network leading to incompatibility with biological tissue. An alternative method for polymerising PVA was to irradiate vinyl acetate with gamma radiation producing free radicals capable of forming a crosslinked polymer. Using radiation for these hydrogels was regarded as producing cleaner and safer hydrogels, but unfortunately results in poor mechanical properties.[49] PVA has been studied as a drug delivery system, such as in the work by R. W. Korsmeyer *et. al*.[172] In which glutaraldehyde crosslinks help build a system which can deliver theophylline at kinetics which can be controlled by the crosslink density throughout the network.[49, 172]

PEG was thoroughly studied, particularly in the 1960s and 1970s, due to biocompatibility and resistance to adhesion to proteins. Early studies, such as by P. A. King *et. al.,* on PEG also report successful PEG hydrogel formation after irradiation from gamma rays.[173] Formation of a PEG hydrogel can also be achieved by end-to-end reaction of the PVA chains or by use of low molecular weight crosslinkers. This has more recently expanded to include other known chemistries, such as Michael addition, click chemistry, ligation, and enzymatic reactions.[49, 174-177] Such PVA hydrogels have typically be applied to anti-adhesive biomaterials or used as drug delivery systems.[49]

Blends of PVA and PEG have been successfully developed, by R. W. Korsmeyer *et. al.* to provide drug delivery systems which can release drugs under controlled kinetics based on the crosslink density throughout the network.[178] PVA has also been used in other copolymer system, one which is particularly relevant here is the early use of PVA with glycosaminoglycan (GAG) , heparin. The system designed by M. F. A. Goosen *et. al.*

has demonstrated anticoagulant properties by inactivating coagulants such as thrombin.[49, 179]

The second generation of hydrogels shifted towards developing hydrogel networks which can respond to changes in environmental conditions. Where such changes can trigger events to occur in the gel, such as drug release. To be considered a third-generation hydrogel the gel requires crosslinking via hydrophobic or ionic interactions, with a focus on ensuring the type of crosslinking used being particularly focused on producing hydrogels *in situ*. As a result, smart hydrogels have become of particular interest to modern day scientists. Smart hydrogels can be tailored to have desirable mechanical properties, stability and if used in applications such as drug release they can have tuneable kinetics.[49]

To obtain hydrogels which have good mechanical properties, scientists looked at natural materials, and combinations of both synthetic and naturally occurring polymers. Some of the hydrogels which have been frequently studied include, collagen, chitosan, fibrin, alginate, hyaluronic acid, cellulose and gelatin. Initially, these polymers were used without chemical crosslinking and demonstrated good biocompatibility. However, more recently it has become more common practise to use chemical crosslinking agents to improve the properties of the hydrogels making them tuneable to specific applications.[49]

Glycosaminoglycans (GAGs) are naturally occurring polymers which exist in the body to carry out a variety of important functions with living tissue. GAGs have a disaccharide repeat unit typically containing uronic acid in either its sulfonated or non-sulfonated form, as well as amino sugars. It is the combination of uronic acid and amino sugars which allow for definition between the different GAGs. Common GAGs are heparin and heparan sulfates, chondroitin sulfate, keratan sulfate and hyaluronic acid, where hyaluronic acid (HA) is the only non-sulfonated GAG.[180, 181] The function of each GAG is believed to change with changing molar mass, such as for high molar mass HA the polymer is believed to have anti-inflammatory properties, whereas when the polymer has a low molar mass it is believed to have pro-inflammation properties.[180, 182, 183] A particular interest of GAGs is their application to the extracellular matrix (ECM) and hence involvement in the fields of tissue engineering and regenerative medicine.

GAGs have been proposed as biomaterials for several application, one of which is with neural tissue. More specifically chondroitin sulfate and hyaluronic acid have been proposed as biomaterials on their own or as part of a crosslinked network, where

crosslinking is used to improve their stability.[180] For example a network consisting of crosslinked hyaluronic acid and transglutaminase activity (from coagulation factor) displayed improved stability and no cytotoxicity. [184] Hyaluronic acid was also proposed for use in neural tissues by J. Karvinen *et. al.*, where it was crosslinked forming hydrazone linkages to be used for 3D cell cultures.[185]

3.1.3. Preparing Hydrogels

Hydrogels can be categorised as reversible or permanent depending on the bonds which form the network. If supramolecular forces are at play, such as hydrogen bonds or hydrophobic interactions, the physical state of the gel can often be changed by changing the environmental conditions. Hydrogels which are classified as permanent are those which have been chemically crosslinked to form a covalent bond between individual polymer chains.[186]

Crosslinking a hydrogel network allows the properties of the hydrogel to be changed without significantly changing the polymer backbone. When GAGs are crosslinked, they are often done so with irreversible crosslinks, however they can also be crosslinked using reversible crosslinks. An example of a reversible crosslinking method is light or temperature induced crosslinks, where photosensitive functional groups are included which initiate crosslinking or crosslinks breaking based on changes in wavelength, intensity or exposure time of the light.[180] Q. Li *et. al.* successfully implemented methacrylate groups into chondroitin sulfate demonstrating the formation of a photocrosslinkable biopolymer.[187] Enzymes have also been used to catalyse reversible crosslinking. An advantage of using enzymes is that milder reaction conditions can be used.[180] Broguiere *et. al.* produced an injectable material, formed from transglutaminase substrate peptide modified HA, and the extent to which crosslinking occurred can be controlled by the amount of enzymatic trigger added.[184] Alternatively, dynamic crosslinking can be introduced to the system, which typically involves the interaction of hydrazides and aldehydes which associate or dissociate depending on their location in the structure.[180, 185]

Chemically crosslinked hydrogels can be prepared by polymerising a hydrophilic monomer in the presence of a crosslinking agent. There may also be a need for an initiator which could be another chemical agent, such as a free radical generator, or by using beam-radiation. Once crosslinked the sample must undergo a purification process to remove any remaining monomer, this is a particularly important when the monomer used is toxic. Removing excess monomer from the hydrogel system is a relatively

difficult step, which can be made easier by using water-soluble monomers, crosslinking water-soluble polymers, and using non-toxic monomers. Typical water soluble polymers are poly(acrylic acid), polysaccharides or poly(ethylene glycol).[186] GAGs belong in the family of polysaccharides which are of particular interest here.

A traditional and commonly implemented method of crosslinking in hydrogels is using formaldehyde or glutaldehyde crosslinking agents. However, these agents produce networks which have been found to be cytotoxic and also induce inflammation.[52] Therefore, agents such as genipin or (*N*-(3-dimethylaminopropyl)-*N*'-ethylcarbodiimide hydrochloride (EDC) have been turned to due to their ability to form networks with improved biocompatibility.[52, 135] Genipin, from the gardenia fruit, is a naturally occurring compound which is capable of crosslinking amino acid groups such as those found in collagen. Genipin forms crosslinks with lysine derivative residues found on neighbouring polymers. These networks have been used in whole-liver grafts, myocardial matrices and decellularised spinal cords.[52, 188-190] It is intriguing to scientists because Genipin appears to have therapeutic properties towards the CNS which include being anti-inflammatory and neurogenic.[52, 191]

3.1.4. Requirements of biomaterials

The bioactive, resorbable, and bioinert materials from the first and second-generation of biomaterials science results in a clinical success which was a crucial response to the aging population.[162] However, approximately a third to half of the skeletal protheses and artificial heart values undergo failure within 10-25 years.[192, 193] For patients this means further surgery which has its own risks and results in a costly practice. Continuing to use biomaterials developed during the first and second generations of biomaterials results in only marginal improvement in failure rates and the trial-and-error practice of such materials is expensive. The lifetime of such synthetic biomaterials is limited due to the inability of these materials to respond the changes in the surrounding environment in the same way living tissue can. Therefore, the first notable requirement of a biomaterials is the need to form biological repair, the biomaterial should promote regeneration of tissue.[162]

If a requirement of a biomaterial is to promote regeneration of tissues, then it must also be considered biocompatible. A biocompatible material must not elicit an inappropriate response from a host, therefore it should not result in blood clotting, infection, and complicated healing. This can be achieved by careful selection of materials and experimental testing, which include in vitro and in vivo tests. The biomaterial should

not only prevent infection but should also be non-toxic, unless it is specifically engineered to be so. Toxicology is an evolved branch of science itself, which includes the study of the effect of the material on the surrounding cells and tissues, as well as looking at the materials which migrate into and leach from the biomaterial. Implanting a device into the body will result in a foreign-body reaction. Although a response is expected due to the normal healing of the body is shifted by the presence of a new device and therefore the reaction may have difference a different duration and intensity. This may require identifying for individual biomaterial types but care should be taken in choosing and designing the material in the first place in order to minimise the response of the body.[194]

The target application determines the physical property requirements of the biomaterial. The biomaterial must have a similar mechanical strength to that of the tissue in which it is being implanted. Not only should it have a matching mechanical strength this mechanical strength should last for the period of time in which the device is expected to work, it must have good mechanical durability. There are other physical properties which may require specific engineering, but these are dependent on the target tissue in question, for example a device may need to have specified permeability.[50, 162, 194]

The purpose of a biomaterial should be to improve the life for patients, it should alleviate suffering and prevent death. There may need a need to consider the risks and benefits of a device. There are devices such as heart defibrillators which have more risks associated which them than devices which reduce pain such as a hip joint replacement. The risks to each device need to be considered on an individual basis and cannot be considered without taking into account the ethical concerns involved. If a biomaterial makes it through experiments and trials it must also be subject to regulation and approval before being deemed as a safe medical device.[194]

Figure 20. Areas to consider when characterising a biomaterial.

In the initial stages of designing a biomaterial, the biocompatibility of the material must be considered. The starting materials used should be selected from those known be biocompatible and any changes to their chemistry should be minimal. The biocompatibility of the device should also be assessed based on its ability to swell and

have a water content similar to that over the extracellular matrix. It should also undergo assays to ensure the device is not cytotoxic. The products of any degradation should also be considered in the biocompatibility of the device, and these products should themselves be biocompatible and have appropriate routes of excretion from the body. The device should have appropriate mechanical properties to match that of the tissues in the affected area, this it to ensure that excessive mechanical friction does not occur, avoiding a scenario where the device damages the surrounding tissue by wearing. Lastly, the device needs to perform an appropriate function, so that the risks of having it implanted, possibily by surgery, are outweighed by the benefits which the device provides. Therefore, the device needs to be able to transduce in a means similar to the communications which occur in the body. It should have the correct mechanical properties to form a structure which can successfully remain stable in its target tissue.

3.2 Biocompatible Hydrogels

Hydrogels are networks which are capable of swelling when they are placed into water, which is absorbed by the network, causing it to expand by many times its original weight. Most hydrogels require some form of crosslinking in order to be able to swell in this manner. The crosslinking used in the network may be physical or chemical. Physical crosslinks involve the use of intermolecular bonds such as Van der Waals, π-stacking or hydrogen bonds, whereas chemical crosslinking requires a crosslinking agent, grafting or radiation.

Hydrogels which are commonly used in biomaterials are often made from biocompatible building blocks. There is a large interest in using hydrogels which are naturally occurring such as gelatin, chondroitin sulfate, and hyaluronic acid.

3.2.1. Gelatin

The use of gelatin in some form can be traced back to early human history. Gelatin is formed from the denaturing and partial recovery of collagen. Due to the methods for the recovery of gelatin, the resultant molecules are fragments of varying weight and chemical structure. The fragments contain different amino acids connected by peptide bonds.[195] Both collagen and gelatin have high tensile strengths which aren't observed in typical hydrogel systems. However, collagen does not form hydrogels and therefore, gelatin is favoured as a biomaterial when hydrogels are required. There are, however, some disadvantages to gelatin, such as differing chemical composition throughout the gelatin and its solubility above 37 °C which make it more challenging when designing a scaffold for use in the body. One other important chemical property which makes gelatin

particularly interesting is that it has amphoteric ability, due to the main differing functional groups in its structure there are groups which can act as acid or base respectively. This larger number of functional groups also opens the door to a range of different crosslinking options.[196]

By altering the crosslink density throughout a gelatin scaffold the mechanical properties can be finely tuned to match with a desired application.[196] More densely connected networks of gelatin have been demonstrated with and without hyaluronic acid by altering the crosslinking agents to achieve target densities.[196, 197] Altering the density of the gelatin scaffold by changing the crosslinking in the system was also observed by Ratanavaraporn *et. al.*[198] The group compared the relatively low density achieved using physical crosslinks to the improved densities achieved using chemical crosslinking, via (EDC) and glutaraldehyde. They also note that the chemical crosslinking agents provide crosslinks which spread throughout the entire scaffold rather than those than remain on the surface such as in physically crosslinked scaffolds.[198]

Gelatin has relatively low levels of immunogenicity and cytotoxicity which make it of interest for drug delivery systems.[196, 199]. However, its applications in tissue engineering as a soft material have been limited due to its relatively large stiffness and therefore to improve this feature gelatin is more often used alongside another polymer.[199]

Hydrogel wound dressings have properties which traditional dressings do not offer, such as: being absorbent to keep the wound moist but not too wet; permeable to smaller molecules such as water vapour but preventing the passage of bacteria; and being biodegradable. A hydrogel wound dressing with appropriate properties would be one which has good water absorption and water vapour transmission. Such dressings have been made successfully designed using gelatin and alginate and have been found to promote the healing of wounds on rats.[196, 200]

Mesenchymal stem cells (MSCs) are vital to repairing the skeletal tissues and so there has been significant interest designing biomedical devices that take advantage of their properties. They have been incorporated into scaffold containing polystyrene or polycarbonate which have a limited ability to swell and take up water. Gelatin, however, outperforms other polymers when it comes to swelling, it also provides better adhesion for the cells and a better environment for them to proliferate.[196] Pierce et. al. crosslinked gelatin with various concentrations of ethyl lysine diisocyanate in PBS to see how the viability of MSCs were affected by system. They found promising results which include

low levels of cytotoxicity and long term MSC differentiation on the gelatin-based device.[201]

Hyaluronic acid has also been used as a co-polymer with gelatin to produce scaffolds with more desirable properties.[196] An example of these is the tailoring of the scaffold to promote chondritic differentiation of MSCs, where it was noted that systems which contain only gelatin outperformed those which contained hyaluronic acid alone.[202]

3.2.2. Chondroitin Sulfate

Chondroitin sulfate (CS) is a naturally occurring polymer which has been used both on its own and in networks as a co-polymer. CS is a polysaccharide found in the human body, where it lines the extracellular matric of cartilages. CS is responsible for several beneficial properties due to its ability to ensure that cartilage retains its integrity. Because of this it is beneficial for restoring function in arthritic joints and has anti-inflammatory properties. Hydrogels made of CS have been found to mimic the natural cortical environment but typically have limited stability in water and degrade rapidly.[203] Often a second polymer is introduced to the CS scaffolds to improve the stability of the network and to improve the time the scaffold remains before degrading. Such hydrogels have successfully been used in cartilage, tendons, and bone.[203-205]

One of the most studied materials in tissue engineering is in fact a synthetic material, (PEG).[203] PEG is a known antifouling agent, it is non-toxic and it has anti-inflammatory properties which make it of interest for application to the body, where it has been used in cartilage, the bladder and in neural regeneration applications.[203, 206, 207] Li et. al. used a hyperbranched variation of PEG in combination with CS to develop hydrogels which can promote cartilage repair. Such gels were made using thiol-ene reaction chemistry to promote rapid gelation and results in gels with appropriate mechanical properties.[203]

CS is a promising material, especially in terms of its therapeutic properties, however its poor degradation kinetics and stability are not the only properties which limit its use. CS also has poor mechanical properties, and it does not mix well with naturally occurring cartilage. However, the issues surrounding the mechanical properties of CS can be improved by altering the chemistry of the scaffold. For example, Kang et. al. used catechol chemistry to produce catechol-functionalised CS gels with improved mechanical properties.[208]

Some scaffolds containing CS have been developed using click chemistry, which is an efficient, selective and reliable synthetic route.[209, 210] The reaction can be carried out

rapidly in physiological conditions meaning it is not only relevant but also interesting to the biomedical fields. A gelatinous scaffold, containing modified CS and hyaluronic acid was produced by Hu *et. al.* via click chemistry, finding that the gels produced this way are capable off hosting cells for proliferation. These hydrogels however, lose up to 45% of their mass within 4 weeks of synthesis, and it is estimated that 20% of the gelatin and 10% of CS was lost within 2 weeks.[209]

An application which is close to that of this thesis was target by Covovaloff *et. al.* who looked into preparing a hydrogel scaffold for brachial plexus injuries, which affect the nervous system in the body. The aim was to improve communication throughout the nerves by providing a point in which nerves can regenerate. The authors used CS and HA as possible scaffold materials and found that although the nerve growth has a stronger affinity to HA, the gels they produced which contained CS were more robust and hence were preferred.[211]

3.2.3. Hyaluronic Acid

Another GAG which is found naturally in the body is HA. HA however, does not contain any sulfonate groups like those found in other GAGs. Within the extra cellular matric HA is found in abundance, this is because it is moved there to provide lubrication and structural integrity after having been produced in the plasma membrane. HA has a relatively short lifetime in the body because it is degraded by reactive oxygen species and by hyaluronidase enzymes. Typically, in the blood HA has a half-life of just minutes, whereas in the skin and joints HA this is extended to hours or days.[212, 213]

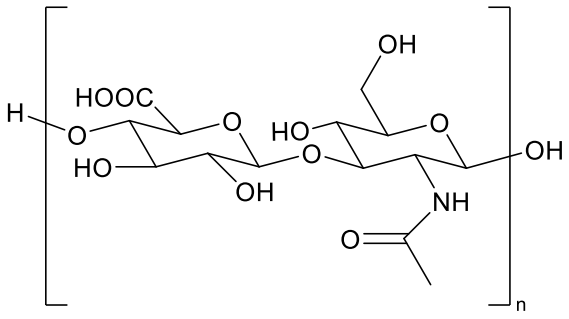

Figure 21. Chemical structure of hyaluronic acid (HA).

The repeat unit of HA is made up of D-glucuronic acid and N-acetyl-D-glucosamine connect by a glycosidic β(1-3) bond. The linear chains of HA then coil up to form a random coil where submerged in solution, where it can absorb large amounts of water. This tertiary structure is affected by various factors including, salt concentration, size

and pH. In the body, GAGs are typically found alongside or attached to a protein core, however HA is independent of these. Combined, these properties make HA of interest because it is considered biocompatible, biodegradable and non-immunogenic, all of which are key in biomaterial applications.[212, 214, 215]

The polymer strands become entangled in each other when random coil structures are formed, and this leads to poor mechanical stability. However, as with the examples previously discussed, HA can also be crosslinked to improve its physical properties.[212] Segura *et. al.* used PEG diepoxide crosslinking agent to form a bond between the alcohol groups on HA polymer chains. The scaffold was crosslinked with the intention of improving the mechanical integrity and collagen was also added to the scaffold to improve its cell adhesion properties. If the scaffold is left in a solution of 100 U/mL hyaluronidase complete degradation occurs, the same occurs in 3 days when submerged in collagenase (66 U/mL).[216]

Glutaraldehyde has also been used to crosslink HA scaffolds, Tomihata *et. al.* reported that the crosslinks formed by glutaraldehyde provided the system with more stability in solution than with crosslinking agents such as diepoxides and carboiimides. However, the swelling of the scaffold appears to be limited; when swollen in PBS the scaffold increases by a maximum of 60% (by weight in water content) which is unusually low when compared to other HA scaffolds. In fact, the authors believed this to be the smallest HA swelling reported at the time of publication (1997). The authors reported how there are optimal reaction conditions for crosslinking the scaffold which include using HCl and a water-acetone mixture.[212, 217]

Carbodiimides are also widely used as crosslinking agents, in the form of biscarbodiimides or EDC.[212, 217] Kuo *et. al.* aimed to produce a crosslinked HA scaffold with a free amino group which via carbodiimide chemistry in the presence of difunctional amides with minimal degradation of HA occurs, however such a polymer was not observed. Instead, the authors report that EDC couples directly to HA, from here they could use the coupled carbodiimide to produce links between HA chains. Alternatively, the coupled carbodiimide can be used to tether other functional groups to the HA chain.[55]

Part. 2 Designing a Hydrogel Scaffold which can host bioelectronic material and is suitable for Spinal Cord Applications

Chapter 4. Biocompatible Hydrogel Scaffolds

4.1 Hydrogels in the Body

Biomaterials have been responsible for many modern medical advancements which are responsible for saving and changing millions of lives.[218] Such advancements can be traced back to or are direct products from the biomaterials field. Prosthetic devices, sutures, bio-adhesives, and controlled drug release systems are amongst these many medical applications. Biomaterials have not only been used for therapeutic use but have also been incorporated into diagnostics.[218]

The polymers which have been used, or are of interest in biomaterials include collagen, chitosan, gelatin, hyaluronic acid, heparin, and alginates. These polymers are of particular interest because they are naturally occurring providing an inherently biocompatible starting point.[218, 219] According to Ratner *et. al.* one of the most important concerns when designing a biomaterial is that is does not leach additives that may cause inflammation when used *in vivo*. The authors express concern about biomaterials which have misaligned physical properties to their target tissues, for example biomaterial in soft tissue should be sufficiently soft to the point where there is minimal mechanical friction between the material and the surrounding tissues and cells.[220]

Chitosan is a popular polymer for use in biomaterials due to its relative stability and because it is considered non-toxic. Chemically, chitosan consists of a repeating unit containing *N*-acetylglucosamine and glucosamine which form long linear polysaccharide chains. At a neutral pH, such as those found in the tissues in the body, unmodified chitosan is insoluble and this limits the possible applications that it could be used in.[221, 222] Another polymer which is used frequently in biomaterial studies is alginate. Alginate is also a linear polysaccharide formed of repeating units which contain β-(1-4')-linked D-mannuronic acid and α-L-guluronic acid, and it can be extracted for use from bacteria and seaweed. Alginate is of interest in controlled release and encapsulation systems, particularly those which involve cells and proteins, due to its ability to form gels when ionic bridges are formed. Therefore, the gelation of alginate can be controlled by the concentration and binding of ions.[221, 223, 224]

Collagen is found throughout the human body, not only is it found in multiple areas it also has a higher prevalence than any other protein in the body.[221,225] It has a high mechanical strength in part due to its 3D structure, which is a triple-helix structure made up by three polypeptide chains wrapping around each other. When collagen is heated the 3D structure begins to degrade, the three strands forming the triple helix begin to unwind and eventually become individual strands. If these strands are recovered, or partially recovered, they are considered gelatin. More simply gelatin is formed by the partial hydrolysis and recovery of collagen. Both collagen and gelatin exhibit high mechanical strength, good biocompatibility, and biodegradability and because of these advantages they have been extensively studied. There have also been several possible crosslinking methods developed, notably using either genipin or water-soluble carboiimides.[221, 225]

Polymers which occur in the extracellular matrix (ECM) are of recent interest due to their ability to retain some of the biological activity which occurs in the ECM. Such polymers are GAGs, proteoglycans and proteins. It is believed these polymers would allow for closer mimicry of the ECM than which has previously been achieved using polymers not native to the ECM. Some glycosaminoglycans, such as hyaluronic acid and chondroitin sulfate, form hydrogels which convey interesting and potentially useful properties.[221]

4.1.1. Summary of Biomaterial Requirements

When designing a biomaterial device, more specifically a hydrogel scaffold, it is important to choose materials which will be biocompatible.[194] This includes choosing a crosslinking agent which will produce crosslinks which do not import cytotoxicity to the polymer. Common crosslinking agents such as formaldehyde and glutaraldehyde have been considered as cytotoxic and are likely to trigger an inflammatory response in the body.[52] Alternative crosslinking agents, such as EDC or genipin, are considered having a less toxic impact on the polymer.[52, 135, 226]

The device must be biodegradable, the products of the degradation must not be toxic and should not leach into inappropriate areas. The degradation products should be compatible not only with the implant site but also broadly across the pathways the body uses to excrete the products.[227, 228] The in vitro rate of degradation can be studied by attributed to hydrolysis, however in vivo enzymes and other oxidative species affect the degradation of the hydrogel scaffold.[229] Another reason for biodegradation to occur is that the extra cellular matrix requires room to grow, and should ultimately be able to replace the hydrogel scaffold.[230]

The device should also have appropriate mechanical integrity and durability consistent with the anatomy of the implant site. Many of these areas may be soft and therefore the device should be designed to be appropriate for the tissue but also needs to be robust enough to be handled by those who implant it.[230] It is believed that mismatched mechanical properties can trigger an immune response and may lead to rejection of the device. A large abnormal immune response can cause the formation of scar tissue which can affect the normal function of the tissues surrounding it. For example in the spinal cord, an action potential is not able to pass through scar tissue, which renders the implant site useless and may lead to cell death.[230, 231]

More advanced cell studies, toxicology and ethical concerns are beyond the scope of this thesis, the aim of the thesis is to study the material science and engineering behind what it takes to design a hydrogel scaffold tailored to spinal cord applications.

Chapter 5. Formulating Gelatin Hydrogels

5.1 Initial Gelatin Gels

In order to find out how gelatin can be dispersed into solution and to gain an idea of the concentration at which gelatin forms gels, some samples containing only gelatin and water were made. A series of samples with varying amounts of gelatin (from 0.5% to 10% (w/w)) were produced. At each concentration the gelatin was able to be dispersed and a gel was formed.

Since gelatin is formed from the denaturing and recovery of collagen, strands of gelatin are formed which have different collagen fragments. Therefore, it is not certain what the exact chemical structure of each gelatin molecule is. However, the ratio of functional groups, in particular the amino acid groups can be compared to give a rough idea of the protein structure.[195] It is assumed that due to the range of amino acids in collagen, there is a range of functional groups for which a range of crosslinkers could be used. Fourier transformer infared (FTIR) spectroscopy can help to understand which functional groups appear in abundance in gelatin and hence help to narrow down the search for a viable crosslinking agent.

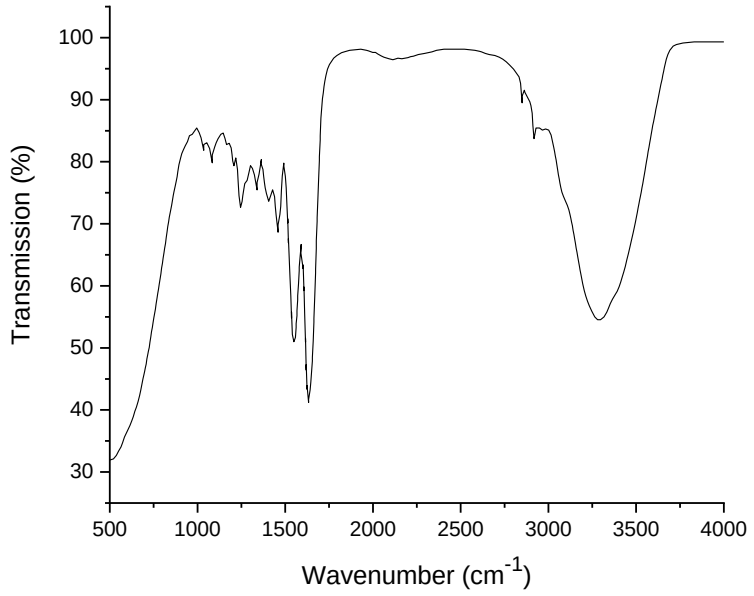

Figure 22. FTIR of gelatin.

The bond observed around 1600 cm^{-1} is associated with a stretching vibration on a C=O, this stretch is formally known as an amide I stretch. This stretch links directly to the secondary structure of gelatin and is typically shown as a doublet, with the other peak in the region of 1500-1700 cm^{-1}. Both bands can be seen in the gelatin spectrum in

Figure 22. The second band is the result of a combination of a C-N bond both bending and stretching and is formally known as amide II stretching.[232-234] The broad band between 2800-3500 cm^{-1} is associated with an O-H stretch, this could be caused by acid groups or independent hydroxyl groups in the structure. If water is present in the sample the O-H bond from water can overshadow other functional groups present in the spectrum, and so it is essential that the gelatin is dry. However, in the spectrum in Figure 22, the sample was dried out so any water remaining should be minimal. It should also be noted that gelatin is hygroscopic and can absorb water from the air, therefore it should not be assumed there would be zero water content in the sample. The FTIR spectrum can be measured quickly and it is reasonable to assume water absorption from the air would be minimal in this time.[235]

Gelatin's ability to swell and take up large amounts of water makes it very versatile in the food and biomaterial industries. The swelling of gelatin is affected by many factors which include charge distribution, temperature and pH.[195,236] Increasing crosslinking can also change the swelling and other physical properties of the gel. Typically adding crosslinks reduces gelatins ability to swell.[196,236]

Gelatin undergoes a sol-gel transformation around 40-50 °C, above which the gel begins to dissolve into the surrounding solution. As the gel dissolves, the gelatin network is denatured and forms a colloidal solution known as a sol state.[236] Reducing the temperature below 40 °C allows for the partial recovery of the gelatin network that existed before heating. While the effect seen by heating and cooling is reversible, there are factors which can affect the recovery of the network and these include, gelatin concentration, humidity, temperature and crosslink density.[196,236]

The gelatin used throughout this project has a bloom strength of 164 G. Since the granules of gelatin do not have a uniform size, assumptions about the average molecular weight must be made. The methodology and machinery to test the bloom strength of a gel was first patented by O. T. Bloom who was the first to propose a machine which would be capable of carrying out tests on the strength of gel like substances.[237] There are some standard requirements necessary for a sample undergoing a bloom test, which include using 112 g of a 6.67% (w/v) gelatin solution in water, and the sample should be probed to a depth of 12.5 mm with a 4 mm diameter probe at 10 °C.[238] Therefore, the surface of a gel which was prepared this way should rupture at 164 grammes of force. A

gel which ruptures at this force is considered to have a low-medium bloom strength and would have a molecular weight of 25,000-40,000 daltons (or $gmol^{-1}$).[237, 239]

The experimental procedure for testing bloom strength can be modified to identify the load-displacement relationship of a gelatin gel, by plotting the stress-strain curve the first linear region of the graph can be used to find the elastic modulus of the gel.[101]

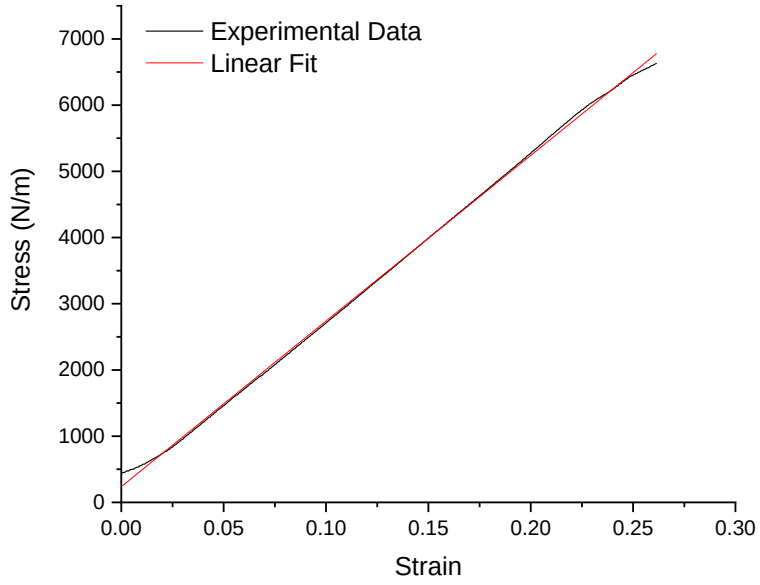

Figure 23. Stress-strain relationship of gelatin.

The elastic modulus of the sample can be taken from the gradient of the first linear region of the slope. The relationship obtained in Figure 23 was repeated totalling a set of 10 measurements. The elastic modulus was extracted from each of the data sets finding that for an uncrosslinked, unaltered gelatin hydrogel the elastic modulus was 21.1 ± 3.3 kPa. It should be noted the sample in Figure 23 has a thickness of 8.2 mm.

An incised human cadaver spinal cord has an elastic modulus of ~ 40 kPa when tested with indentation testing.[86] More indentation studies of the individual tissues and on the spinal cords of other living and cadaver animals suggests that an elastic modulus in the region of 5-100 kPa could be considered appropriate for the spinal cord.[89-91, 94] This range is also supported by the numerous papers which look at developing a surrogate material for the spinal cord. Including the data for surrogate materials is important since there is a relatively small number of papers which study the elastic modulus of the spinal cord of living animals, which is due to ethical concerns. However, surrogate materials aim to replicate the spinal cord without experimenting on living animals and so the data is relevant here. Several surrogate materials point to the work of E. Mazuchowski *et. al*

that suggests 89 kPa to be an appropriate aim for the elastic modulus of the spinal cord.[85, 91]

Since the average elastic modulus of the uncrosslinked gelatin was 21.1 kPa it is within the region of 5-100 kPa and could be considered appropriate for the spinal cord. However, uncrosslinked gelatin degrades rapidly in water and hence requires crosslinking. Fortunately, since the elastic modulus for uncrosslinked gelatin is in the lower end of the 5-100 kPa region there is scope to crosslink the gelatin without making it too rigid for the spinal cord.

Crosslinking gelatin will not only increase the mechanical integrity of the gel but will also affect its swelling. Therefore, before crosslinking the hydrogel the swelling properties of unmodified gelatin should be identified to provide a point of comparison.

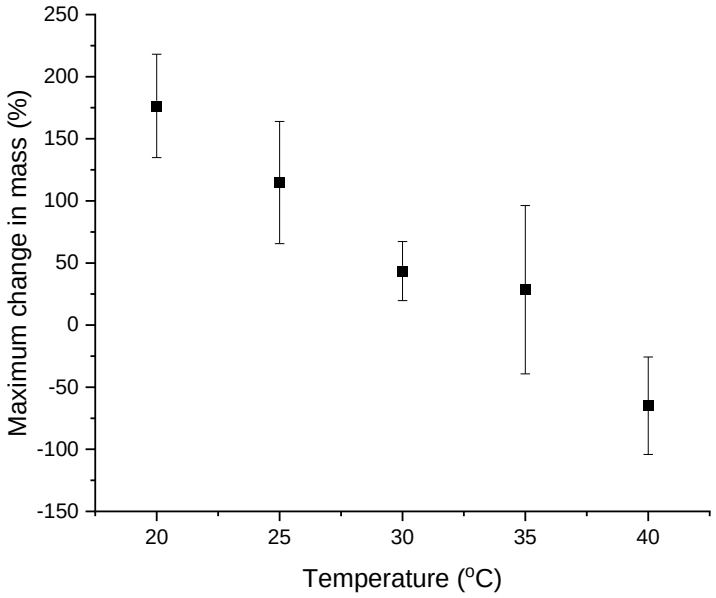

Figure 24. Swelling of uncrosslinked gelatin across different temperatures after a known amount of time. The number of repeats for each temperature was three.

Water enters the gelatin network where it can form bonds which causes the gelatin network to swell and increase in weight. Areas of each gelatin molecule which have more exposed surface area, such as the outer surfaces, are able to swell more rapidly since there is more exposure and places for water to enter and bind than there is in the inner network.[236, 240]. Uncrosslinked gelatin samples increased in weight by the most significant margin at 20 °C, where the gels increased by a maximum of 175% of their original weight. As the temperature of the solution in which the gels are swollen increases the weight of the gel decreases. The samples swollen at 40 °C dissolved in

solution. The dissolution of samples at warmer temperatures is due to the tertiary structure transitioning to a sol state. When the uncrosslinked gels dissolve in the solution it is assumed, they revert to linear chains, in the solution, instead of a random coil and these linear chains may undergo hydrolysis to smaller fragments. The addition of crosslinks would prevent the network 'unravelling' into linear chains and helps to maintain the 3D nature of the system in solution. This 3D structure is responsible for the swelling of the gel in solution.

Gelatin which is obtained from the thermal denaturing of collagen and so it has similar properties and hence understanding the way in which collagen changes thermally can provide a means for understanding what happens to gelatin. Since gelatin is formed from the partial recovery of collagen, the chemistry of collagen alone cannot describe the chemistry of gelatin, however since gelatin is not fully understood, assumptions from the structure of collagen are necessary. In a hot solution collagen adopts a random coil conformation, but on cooling it recovers its helical structure. This conformational change is expected to occur in gelatin too.[241, 242]

The transition from a collagen-fold to a random coil in solution appears to happen between 35 and 40 °C and it is at this point that the gel no longer swells in water but dissolves in it. This would not be appropriate for a biomaterial which would need to retain its mechanical integrity in the body at 37.5 °C. If the gelatin concentration is high enough the transition from a helical structure to random coil is reversible upon cooling. Gelation occurs when gelatin crystalises into helical collagen folds, not when collagen denatures and therefore, the formation of a gel happens sufficiently below the helix-random coil transition.[243]

A series of gels of varying gelatin content (by weight) were made and then heated to 90 °C to see if gelation occurred after heating or if the gels were lost. The gelatin contents used were from 0.01-10% (w/w). The sample with 0.01% gelatin was not able to form a gel. However, from 0.1% through to 10% gelatin gelation occurred on cooling, and so it is believed that the helical structure was recovered.

5.2 Crosslinking Gelatin Hydrogels

Crosslinking polymer chains affects how they can move and change, this can force the polymer chains closer together and increase the mechanical integrity of the overall structure. A zero-length crosslinking agent such as EDC, provides a bond between the polymer chains without appearing in the network, the crosslinker does not insert itself

into the network. Instead, EDC forms urea as a by-product of the crosslinking reaction and this can be easily removed from the network by aqueous rinsing.[54] Introducing a small amount of crosslinking agent not only affects the maximum swelling ability of the samples, meaning each sample can absorb more water, but also changes how the network responds to increasing temperatures.

5.2.1. Swelling Characterisation of Crosslinked Gelatin

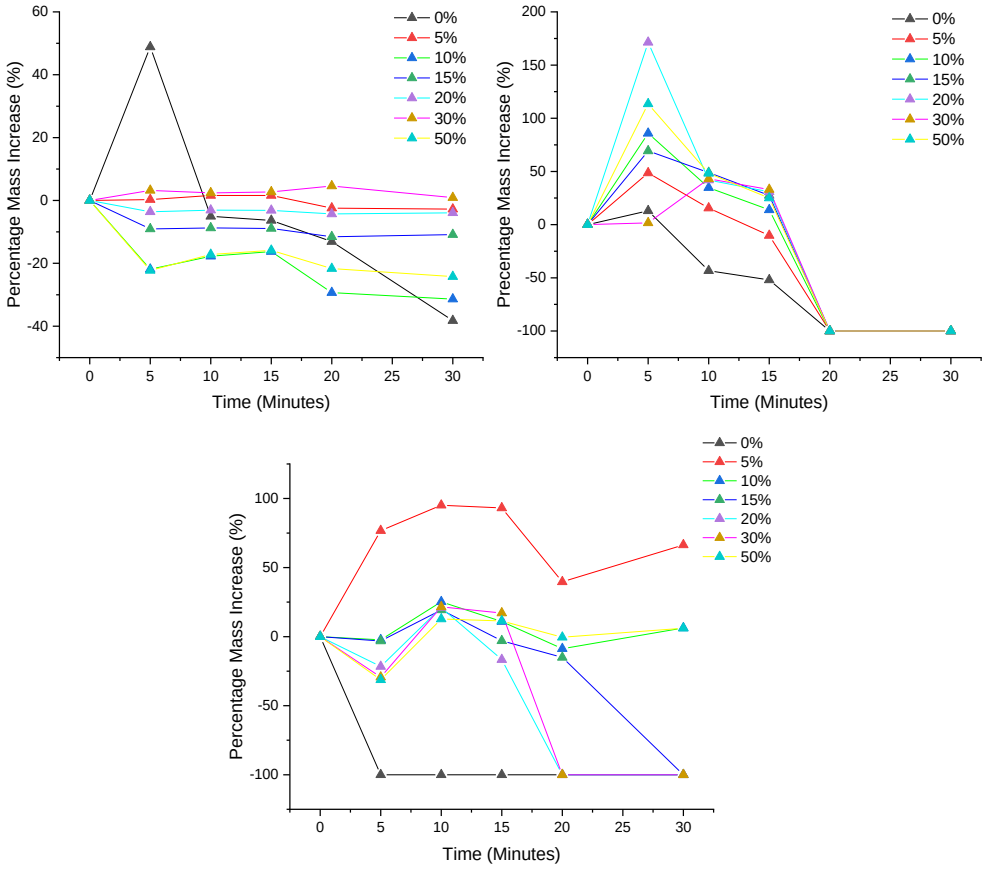

Figure 25. Swelling of gelatin using different experimental methods. Samples of gelatin contained varying amounts of crosslinking from 0 to 50%. The experiment in the top left graph was carried out at 20°C, the top right image at 30°C and the bottom graph at 60°C.

A series of gelatin-based hydrogels were produced with varying crosslinker concentrations, ranging from 5% to 50%. The only gel to be produced which usually appeared homogenous throughout was the gel which contained 5% EDC. At 10 and 20% crosslinker concentration, by mass, some hard solid lumps formed when the crosslinker was added to the solubilised gelatin. Such lumps were difficult to disperse, and remained when the mixture cooled to a gel. Above 20% crosslinker concentration, heterogeneity was evident from the lumps of undispersed crosslinker in the gel and a layer of liquid

which formed over the gel during cooling. At this point it was clear that of the concentrations tested 5% was the best for forming homogenous gels. However, to see if this concentration produced stable gels a brief study of how each hydrogel responded to different temperatures was carried out. At 20 °C uncrosslinked gelatin (0% EDC) initially swells before then losing mass throughout the remainder of the experiment. None of the other gels appear to swell by any significant margin, and some of the gels also begin to degrade in the solution. At 30 °C uncrosslinked gelatin has a small period of swelling before degrading in the solution, whereas the other gels appear to swell significantly more in the initial 5 minutes when compared to 20 °C, before beginning to degrade. At 60 °C results differ across all the samples; the sample at 5% concentration appears to swell and stay relatively stable throughout its time in solution, whereas the other sample have appeared not to swell and to degrade in the solution. The issue of the crosslinking agent crashing out of solution can be attributed to the unusual results observed in this experiment. Except for the sample containing 5% EDC, it is unclear how much crosslinker was dispersed throughout each sample due to the presence of lumps in the final sample. It is clear there was no constant homogeneity throughout the samples.

The sample which contained 5% EDC was the only one of the samples where the crosslinker could be effectively dispersed, and lower concentrations of crosslinker were needed. This would also ensure that the network contained crosslinks between the polymer chains rather than becoming overly dense with crosslinks or contain EDC polymers, EDC can degrade at higher temperatures.

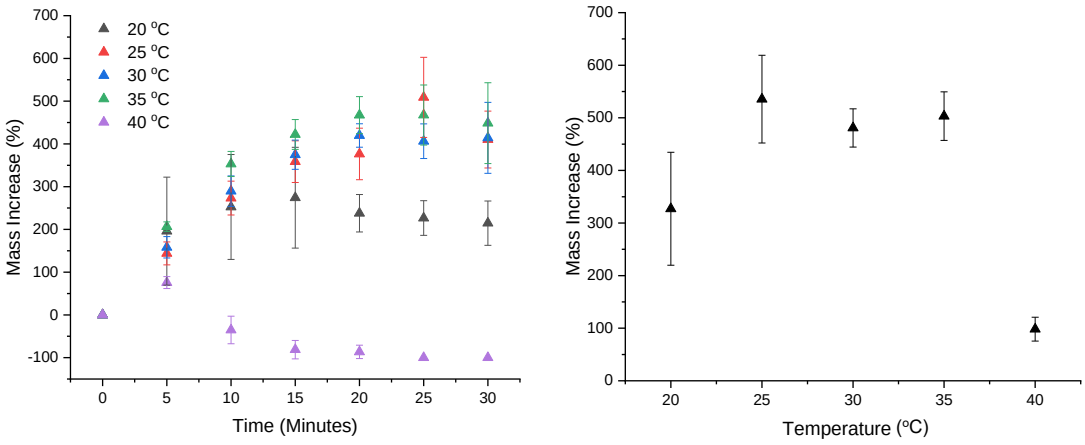

Figure 26. Swelling of gelatin over 30 minutes at varying temperatures.

0.01% EDC (w/v) was introduced to gelatin to form crosslinked samples. This was the smallest amount of crosslinker which was used and should yield samples with the lowest crosslinker density in the rest of this section (except for uncrosslinked samples). The samples swollen at 20 °C reach a maximum extent of swelling before stabilising. Over 30 minutes the swelling appears to have a slight decreasing trend. However, there is no difference between the error bars, the standard deviation of the results overlaps and therefore the results are similar and can be considered stabilised. The same happens with the samples swollen at 25, 30 and 35 °C although it takes less time to reach the point at which the samples do not continue to rapidly swell. Samples measured at 40 °C also decrease in mass in a similar way to the gelatin samples which had not been crosslinked. The samples briefly swell and become a globular mass before breaking apart and dissolving into the solution over the rest of the experiment. With the exception of the samples swollen at 40 °C the average maximum mass, shown in the right-hand-side of figure 26, increased when compared to the uncrosslinked samples. At 25, 30 and 35 °C the average increased in mass during swelling was around 500 % whereas for uncrosslinked gelatin samples at 20 and 30 °C the average increase in mass was between 100-175 %. At 30 °C uncrosslinked gelatin was only able to swell by up 50%. It is assumed that the crosslinks in the system slow down the rate at which the helical structure of gelatin opens to a globular random coil during heating, therefore the system continues to swell at 30 °C because there is not enough kinetic energy to overcome the crosslinks and cause the 3D structure to change. At 35 °C the network begins to change and at 40 °C it the structure loses its helical shape and dissolves into the surrounding solution. To use the gelatin gels in the body, they would need to function at body temperature, although the gels that have been tested these systems would begin to dissolve, if not completely dissolved, at this temperature. Increasing the crosslink

density could once again cause the temperature at which the system begins to coil to increase.

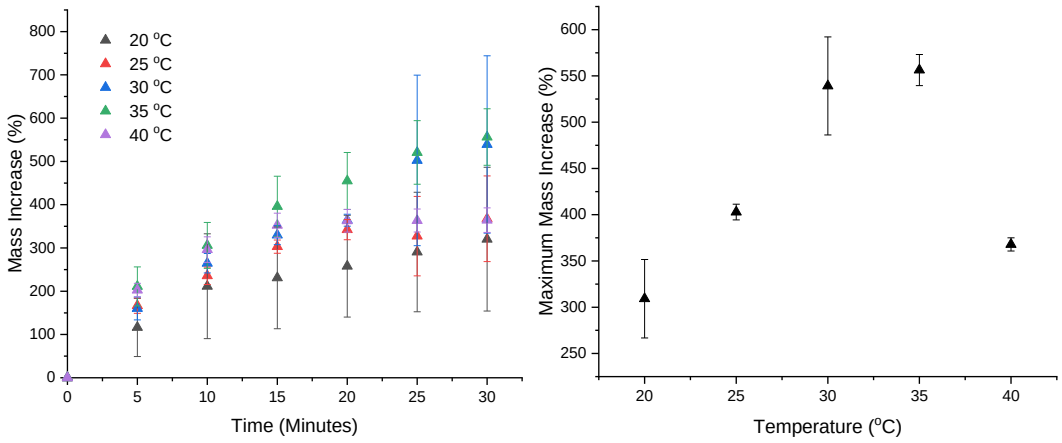

Figure 27. Swelling of gelatin gels containing 0.05% crosslinker over a series of temperatures.

Gelatin gels were then made-up using EDC at a concentration of 0.05% (w/v). Increasing the concentration of the crosslinker from 0.01% to 0.05% appears to have little effect on the maximum swelling shown on the left hand side on fig 27. The main difference was now at 0.05% the sample swollen at 35 °C did not dissolve into the surrounding solution whereas the sample with 0.01% EDC dissolved. The sample at 40 °C was also able to briefly swell before dissolving, which was not observed in samples with 0.01% EDC. Increasing the crosslinker density appears to have had minimal impact on the maximum amount of swelling, however it has enabled the samples to be swollen to their

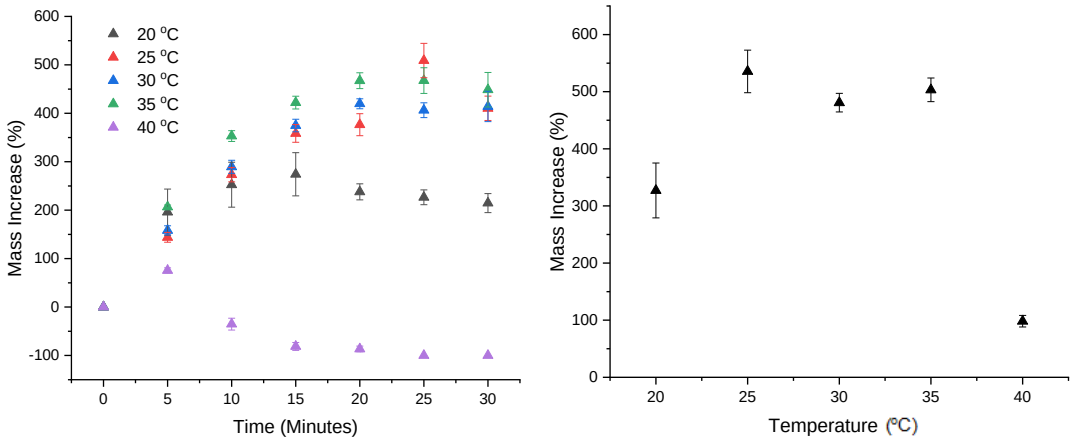

Figure 28. Swelling of gelatin (containing 0.01% crosslinker) over 30 minutes at varying temperatures.

maximum at a higher temperature. Again, an issue with the results from these samples is that the sample at 40 °C has completely dissolved within 30 minutes and so is stable at a temperature significantly beyond body temperature. Therefore, the concentration of

EDC was increased once more to try and produce gels which do not dissolve in solution at 40 °C.

With the concentration increased to 0.1% EDC (w/v) all the samples could be swollen at temperatures from 20 to 40 °C, without dissolving into solution over a 30-minute period, as shown in fig 28. While the maximum swelling for 40 °C is smaller than the value for 30 and 35 °C the sample did not degrade, and the error bars continue to overlap with the other samples and therefore are considered similar. Producing gels which are stable at 40 °C is crucial for an application which is in vivo. The gels need to be stable at body temperature, so they don't degrade into the surrounding tissue immediately and instead provide time for the extracellular matrix to behind to regrow around the biomaterial. The gels also need to be stable at room temperature, the temperatures surrounding it and at body temperature so that it remains robust enough to be handled.

It should be noted that these experiments used very small concentrations of EDC (0.05 and 0.1%) which require weighing out small amounts of crosslinker. Discrepancies in the data can therefore be attributed to a lack of accuracy when handling such small amounts on a balance. Weighing out small amounts of material on a 4-figure balance provides data which lack confidence.

5.2.2. Swelling Gelatin Hydrogels

Various swelling methodologies are discussed in section 2.1.2. Briefly, 3 methods can be considered, the first is using a Buchner funnel to filter out the gelatin samples from the solution to ensure all the gel is caught and unbound water is removed before weighing. The second is removing the sample by hand using tweezers and blotting to

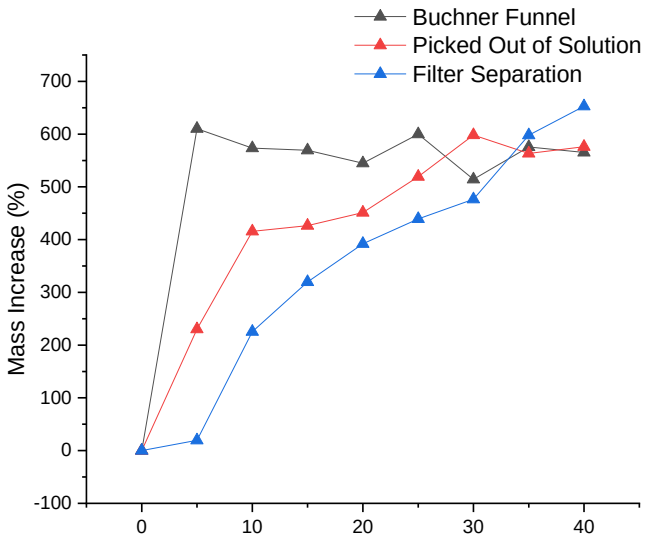

Figure 29. Maximum increase in mass during swelling, three methods were used to separate the sample from the solution, and each is displayed in this graph.

remove the free water before weighing, lastly the solution can be filtered to remove the gel from the solution.

The results suggest that using a Buchner funnel appears to help measure the extent to swelling more rapidly than the other samples allow for, where the results plateau out much quicker than they do in the other methodologies. This plateau suggests the gel is saturated and is considered to be fully swollen. However, the other two methods also achieve similar results in a slightly longer time frame, therefore measuring the extent of swelling can be achieved with each of the methods. Although the Buchner funnel method appears best the number of samples which can be tested at once is limited to the number of Buchner funnels available and therefore since the other methods yield similar results the method where the sample was picked out of the solution, with tweezers, will be used to allow for batch testing to occur.

To gain more of an understanding of the crosslink density and therefore the homogeneity of the samples the swelling of the polymer can be studied using a theory developed by Flory and Rehner.[244, 245] Understanding the crosslink density allows insight into the enthalpic polymer-solvent interaction of the swollen polymers with the surrounding solution Flory-Huggins theory can be applied.[246] The sample in question is assumed to be homogenous to apply mean-field theory.[61]

A quick, and somewhat inaccurate, way to determine the homogeneity of the gels is to take an FTIR spectrum at several different places on the dehydrated hydrogel. Overlapping the spectra will highlight any shifts in peak where the material in question does not have the same functional group as another area of the material.

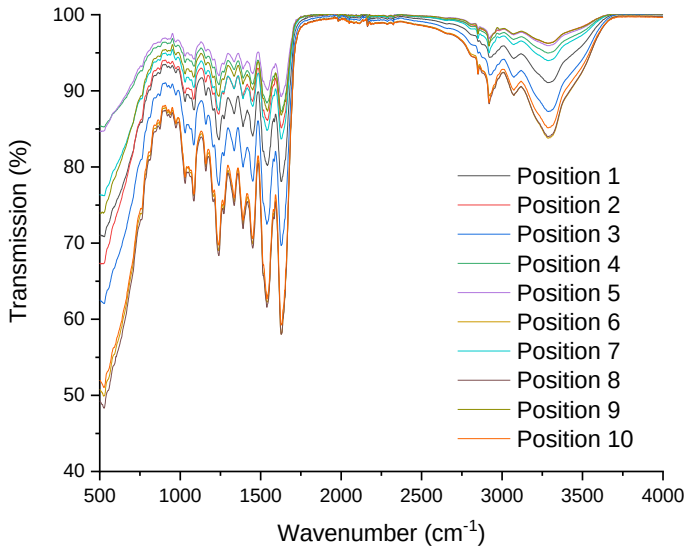

Figure 30. FTIR spectra of a dehydrated gelatin film, each spectrum taken in a different location across the film.

Since all the spectra overlap and there appears to be no shifts or changes in peaks throughout each one it can be assumed that the gelatin gels are relatively homogenous. An FTIR spectrum of a sample provides insight into the functional groups with are present throughout the entire gel. However, these groups may produce a broad band in the trace which can overlap with others, so more complex analytical techniques such as NMR spectroscopy are needed to adequately assess the chemical structure throughout. Here, however, the results from FTIR provide enough of a basis to be able to assume homogeneity for mean-field theory.

Here, eq 23 (section 2.1.2) is needed which defines the Gibbs free energy of mixing in the system,

$$\frac{G}{nk_{\mathrm{B}}\mathrm{T}} = \chi\Phi(1-\phi) + (1-\phi)\ln(1-\phi) + \frac{3\Gamma\phi_s^{\frac{2}{3}}}{2N}\left(\phi^{\frac{1}{2}} - \frac{\phi}{\phi_s^{\frac{2}{3}}}\right), \qquad \text{Eq. 23}$$

which when differentiated with respect to ϕ results in the equation for the Flory-Huggins interaction parameter,

$$\chi = \frac{1}{\phi} - \frac{1}{\phi^2}\ln(1-\phi) - \frac{\phi_s^{2/3}\Gamma}{\phi^{5/3}N}.^{62,\,63} \qquad \text{Eq. 24}$$

Equation 24 can be used to calculate the amount of water molecules which are absorbed into the network when the gelatin hydrogel is swollen. The Flory-Huggins parameter provides a quantifiable understanding of whether the hydrogel has favourable swelling in solvent. However, to use this equation the molecular mass of gelatin is required. The gelatin in use has a bloom strength of 164 G which would be considered in the upper end of low-medium strength gels. A common data set for comparing gelatin bloom is shown in Table 3.[247]

Table 3. Detailing the relationship of bloom strength to average molecular weight for gelatin

Bloom Class	Bloom Strength (G)	Average Molecular Weight (kg/mol)
Low	50-125	20-25
Medium	175-225	40-50
High	225-325	50-100

The bloom strength for the gelatin in use falls between the categories and therefore if an average was taken then based on the data in Table 3 then the average molecular weight would be around 30 kg mol^{-1} however a way to obtain the average molecular mass experimentally is to use a light scattering experiment performed on a Zetasizer to determine the average molecular weight of particles in a sample.

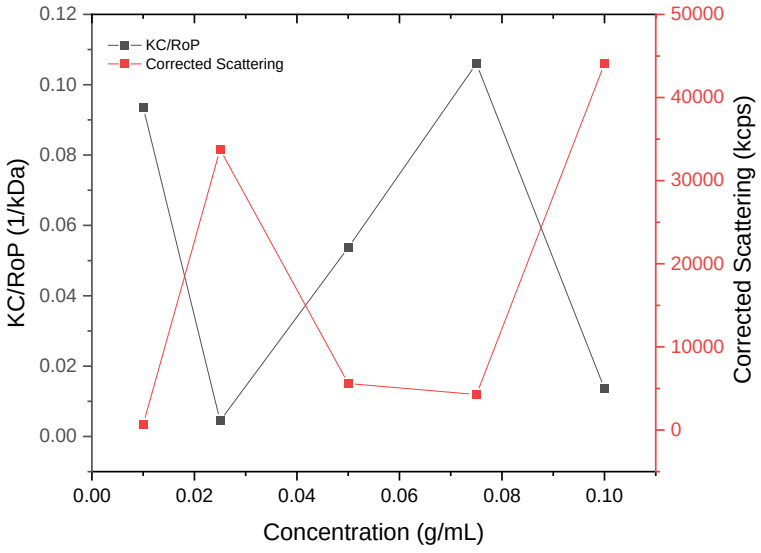

Figure 31. Debye plot for gelatin, created through the results from light scattering experiments.

While the Debye plot can be used to measure molecular weight, the data should form a straight line, which is not the case here, and so this datum cannot be used for this purpose. Particles of multiple sizes can be responsible for causing poor data in light

scattering experiments; however, this was somewhat expected when using gelatin. The average molecular weight reported from the Zetasizer is 15.5 kDa. According to the bloom count the average molecular weight was expected to be between 25-40 kDa. The experimental value of 15.5 kDa will be used as a lower estimate of the average molecular weight, and 40 kDa will be used as an upper estimate to ensure the real molecular weight is covered.

The data in fig 31 do not form a uniform pattern which is usually seen when the sample is too low in quality or very heterogenous to be used on a Zetasizer. Therefore, dynamic light scattering experiments are not appropriate here, the results of these experiments are not reliable.

The Flory-Huggi ns parameter can be calculated at each temperature interval based on the maximum amount of swelling at that corresponding temperature. The maximum swelling from section 2.3.2 is consolidated into Figure 32.

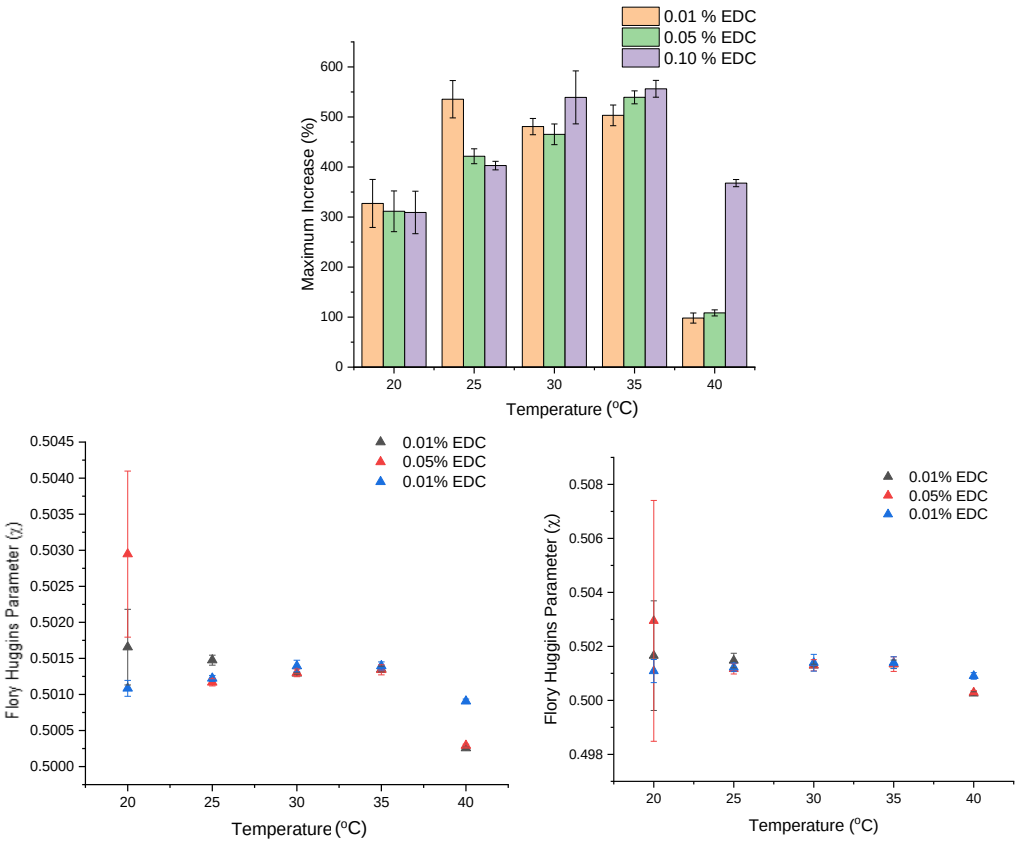

Figure 32. The graph at the top displays the maximum percentage weight increase which occurs when the gels were swollen. The bottom two graphs show the Flory Huggins parameter at each temperature. The bottom left graph uses a mass of 15 kDa for gelatin while the right-hand-side graph uses 32 kDa.

Due to the success of the hydrogels with 0.01% EDC by weight at 40 °C the following gels were tested using this concentration of crosslinking agent. With assortment of

amino acid groups present in gelatin there are a range of different functional groups which are available for chemical reactions. And because of this, gelatin is believed to exist as a zwitterion in solution.[195]

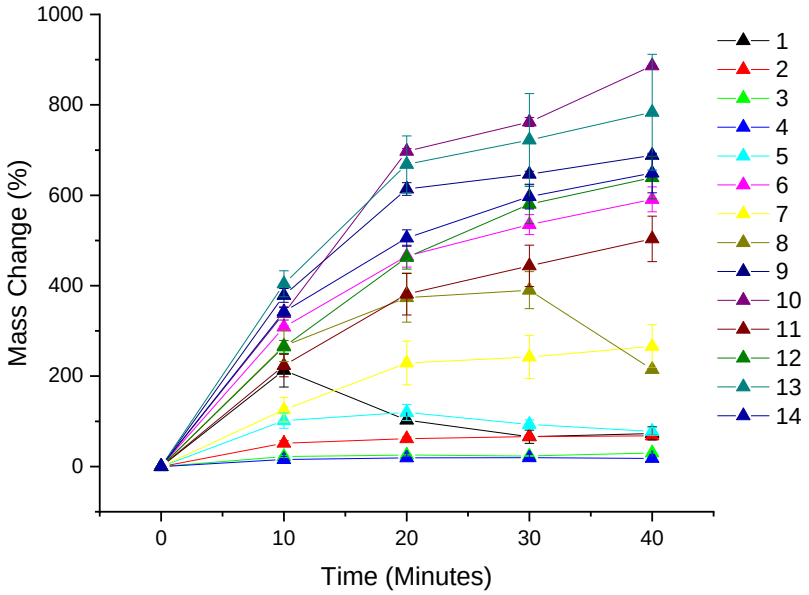

Figure 33. Maximum mass increase in percent when gelatin was swollen in different pH environments.

After examining the maximum swelling at every pH it appears that the gelatin gels take up more water from pH 6-14 and don't swell to the same extent in acidic conditions. However, there are some overlaps in the error bars suggesting there is not true separation in the data.

5.3 Degradation Studies on Gelatin Hydrogels

During the swelling experiments gelatin appears to become a large globular shape just when fully swollen, in this form the gels are unstable and begin to break apart and this leads to rapid degradation. To test for the degradation of the gels the sample is placed into solution which is at body temperature and is left for fixed periods of time before measuring the weight of the sample which remains. However, even though the samples with 0.1% EDC displayed improved temperature resistance properties the samples were found to have degraded within 3 h of beginning the test. This was determined to be too short to meet the aims of this project.

5.4 Mechanical Properties of Gelatin Hydrogels

A hydrogel is required to have similar mechanical properties to the target tissue in order to reduce the possibility of the device being incompatible. Therefore, the mechanical properties of the hydrogels were investigated using compression testing as described in

section 2.3. Again, based on known elastic modulus values of the spinal cord and the target result proposed by E Mazuchowski et. al the aim for this device is to have an elastic modulus between 5-100 kPa.[85, 89-91, 94]

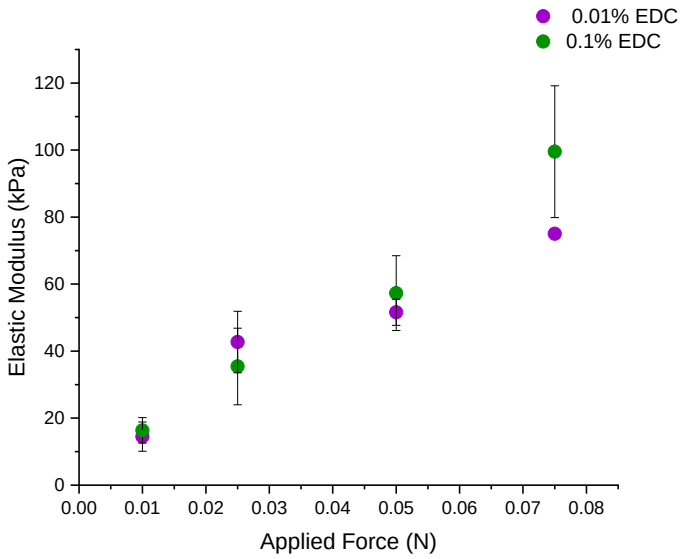

Figure 34. Elastic modulus of some gelatin hydrogels crosslinked at 0.1 and 0.01%

During this experiment a specified force is applied to the sample and the depth of the indentation created is measured. Using this data, the elastic modulus can be calculated from eq 31. There is an increase in the elastic modulus at every interval of applied force. Except for the data recorded at 0.08 N the data for the other points largely overlap suggesting no real difference between the elastic modulus for the samples containing 0.01% and 0.1% EDC. The aim is for the elastic modulus to be between 5-100 kPa, but that recorded for 0.1% EDC at 0.08 N exceeds this limit. If the sample has an elastic modulus which is greater than that of the tissue surrounding it, this mismatch in properties is likely to lead to incompatibility and rejection by the body.

5.5 Summary of Gelatin Hydrogel Formulations

The formulations where there was a 10% gelatin content, and 0.1% EDC gave the most promising results. These samples appeared to be the most homogenous in terms of the crosslinker distribution throughout the sample during synthesis when explored using FTIR. These samples also appeared to be more stable at increased temperatures, when compared to the samples made with less crosslinker content. However, all the samples, including the ones containing 0.1% EDC do not appear to have long term stability in

water, since they break apart within a few hours of submersion. The mechanical strength of the gels is appropriate for applications where tissue compatibility is required but, if they are tested at higher applied forces then the elastic modulus of the samples is greater than the range required in this project, therefore gels which are softer and have better long-term stability at body temperature are required.

Chapter 6. Chondroitin Sulfate Hydrogels

6.1 Formulating and Swelling of Chondrotin Sulfate Films

The methodology using in Part 2, Chapter 3, was repeated substituting gelatin for chondroitin sulfate however after drying a layer of powder made up of crosslinker and CS remained. This suggested that the crosslinking reaction was not occurring and therefore, *N*-Hydroxysuccinimide (NHS), which is often paired with EDC was introduced. NHS was used to promote the crosslinking reaction in the hope of producing more robust films.

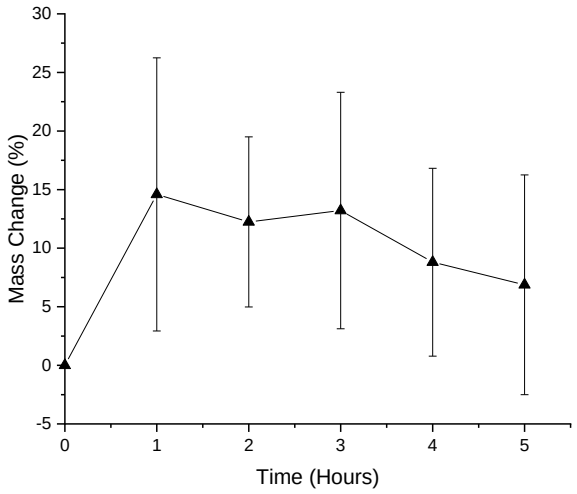

Figure 35. Maximum swelling of CS over 5 hours

By introducing NHS films of CS could be produced which could then be swollen. The extent of swelling is minimal in comparison with gelatin, where the average gel increased by ~300% of their original mass. Here, the CS gels swells only by an average of 15% increase on its dry mass at 20 °C. At 5 h the samples were losing mass, and some had even begun to d egrade meaning less mass was present than at the start of the experiment. It was deemed that although a gel has been formed it is not robust enough for this project.

Instead using a combination of polymers may be more useful to this project. Such as combining gelatin and chondroitin sulfate to produce gels more robust gels which are of an appropriate softness so as to be considered compatible with the spinal cord.

6.2 Gelatin-CS Hydrogels

Chondroitin sulfate and gelatin combinations in hydrogels have been reported in several different studies, some of which are discussed in section 3.2.2. Gelatin provides mechanical strength where chondroitin sulfate is lacking, it was also hoped that gelatin would improve the properties of CS films in water. A series of hydrogels were made using gelatin and chondroitin sulfate, one sample contained equal amounts of gelatin and CS by mass however the remaining samples contained increasing amounts of CS. Therefore, chondroitin sulfate can be considered the majority polymer (by mass) in all the samples with the expecption of the sample with 1:1 ratio.

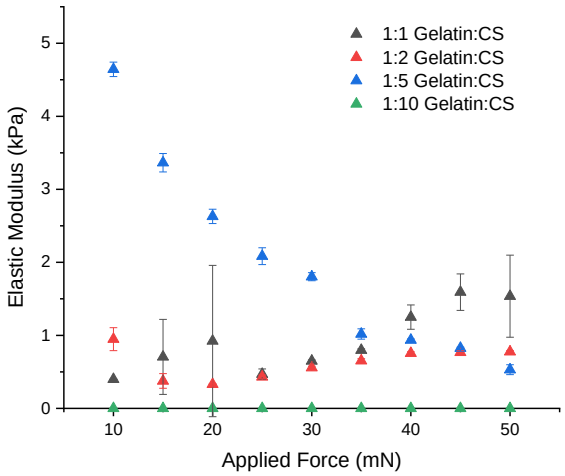

Figure 36. Elastic modulus of hydrogels containing both CS and gelatin at different ratios.

The samples have a significantly lower elastic modulus than the samples which contained only gelatin (which had moduli in the region of 20-100 kPa). The samples which had a gelatin to CS ratio of 1:10 did not form gels and remained at liquids therefore they registered as having no elastic modulus when tested by indentation testing because the parameters for the device could not be met. All of the samples had elastic moduli lower than 5 kPa which was outside the proposed aim of 5-100 kPa. Having a modulus of less than 5 kPa may still be appropriate for the spinal cord because it would not cause too much mechanical friction on the biological tissues which would be expected if the device had an elastic modulus which was significantly more than the tissues in the spinal cord. However, materials which an elastic modulus of less than 5

kPa are very fragile and difficult to handle, therefore they would make devices which are very hard to physically implant.

It appears that CS could be used to provide gels with softer mechanical properties, therefore it was hypothesised that the original gelatin gels could made softer by introducing small amounts of CS.

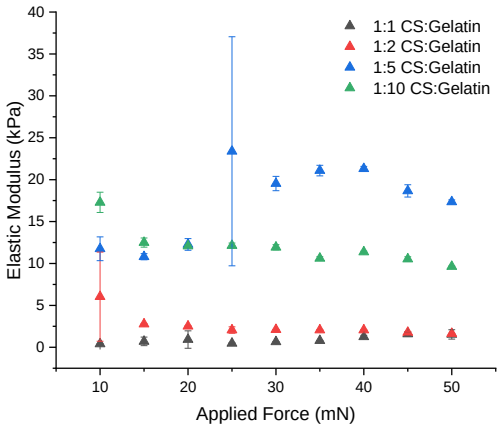

Figure 37. A second series of hydrogels containing both CS and Gelatin but at different ratios to each other and at different ratios to Figure 35.

Here, a consistent amount of chondroitin sulfate was used and the amounts of gelatin were changed. It should be noted the data with a ratio of 1:1 is the same as seen in the last figure (figure 36) due to the amounts of gelatin and CS being equal. The samples with more CS (ratios 1:1 and 1:2) have an elastic modulus below 5 kPa and are considered too soft. However, the samples where the mass of gelatin increased further by a factor of 5 or 10 times the amount of CS (ratios 1:5 and 1:10) had a more realistic elastic modulus for the target application. A device with elastic modulus of between 10 and 25 kPa as seen in figure 34 would have a similar elastic modulus to the tissues in the spinal cord. It would also be somewhat more robust so that it could be delicately handled however it would still be considered difficult to physically manipulate.

The CS films rapidly degrade on their own (figure 35) and so it was hoped that the combination of polymers to form a co-polymer network would slow down the degradation of the network. However, the films continue break apart within hours of being placed into solution and therefore are not to have long term stability.

6.3 Summary of Gelatin-CS Hydrogels

A number of methods to produce chondroitin sulfate gels were attempted however no successful dehydrated film of CS was formed. The methodology used in chapter 6, was repeated substituting gelatin for chondroitin sulfate however after drying a layer of powder made up of crosslinker and CS remained. The powder was soluble in water and did not appear to have any swelling ability. The methodology was changed, and the reaction conditions were altered several ways, including using acidic conditions, alkaline conditions, altering the temperature and changing the crosslinker, throughout minimal improvement was found.

An alternative method and one which would be considered for future work would be to look into studying the effects of an alternative crosslinking agent with CS. (3-glycidyloxypropyl)trimethoxysilane (GOPS), sometimes used in bioelectronics, could also be used here.

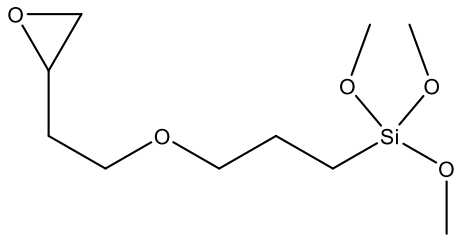

Figure 38. Chemical structure of GOPS

The silane group in present in the crosslinking agent self-polymerises forming a polysilane. Typically, silanes form interpenetrating networks which have high mechanical strengths.

Chapter 7. Formulating a Hyaluronic Acid Hydrogel

7.1 Formulating HA Gels Based on Characterisation

Hyaluronic acid (HA) forms a powder in its dehydrated state, rather than forming shapes which would be considered suitable for a scaffold, such as a film or 3D shape. HA is found naturally in the body providing inherent biocompatibility.[212, 213] Uncrosslinked hyaluronic acid is miscible with water and cannot be easily lifted out of a solution without the aid of a purification or separation process, such as by dehydrating thermally. However, when the system is crosslinked, the resultant network should be able to be manipulated and handled without it breaking apart or dissolving into the surrounding solution.

A series of samples containing varying amounts of polymer were made in order to determine to see which would be considered to have the most appropriate amount of polymer, these were 0.5, 1.0, 1.5, 2.0, 2.5, 3.% (w/w). Samples with 0.5 and 1.0 % polymer dissolved fully in water and when dehydrated they form constant films. At concentrations higher than 1 % the HA became more difficult to dissolve and the dehydrated films frequently had lumps of undispersed HA powder in them which became more apparent when increasing the concentration further. To be able to form a film rather than a powder EDC was used throughout this experiment using a concentration of 0.1% (w/v) EDC (the concentration used in the work with gelatin). Films of this formulation were dehydrated and then reswollen, with the time-dependent swelling recorded as a function of time.

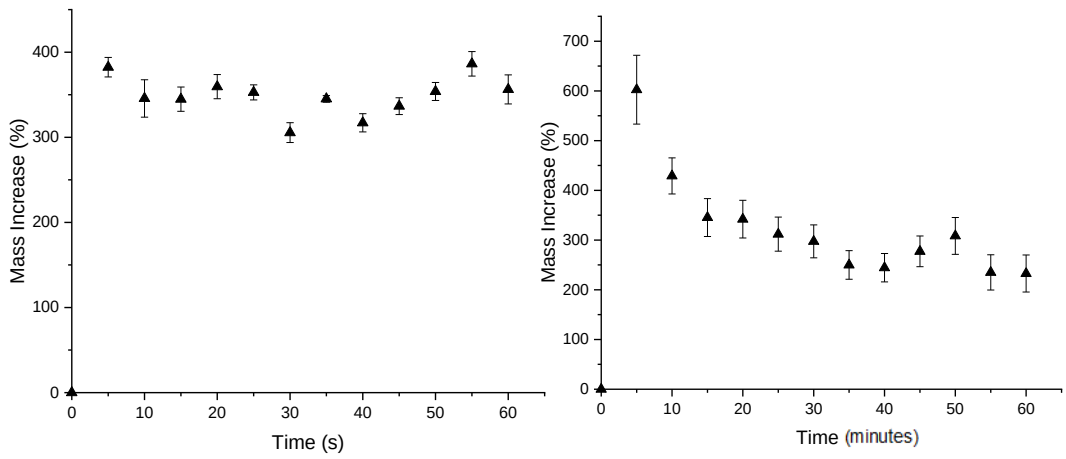

Figure 39. Maximum swelling of HA over varying amounts of time. Number of repeats is four. The experiment for the graph on the left was carried out over 60 seconds, whereas the graph on the right was over 60 minutes.

The gels swell rapidly to have >300% more mass within 60 s of being immersed in water. Over the course of an hour there is a slow decrease in the average mass of the samples, going from 602% to 232%. This decrease in mass can be visually observed when some of the samples break into smaller pieces which in turn begin to degrade into the surrounding solution. However, this does not occur in every sample. It should also be noted that while the average result appears to decrease, the error bars overlap suggesting there is no true trend. The time in which the samples were submerged was extended to the point at which the gelatin and gelatin-CS gels had begun to degrade to compare the robustness of the samples.

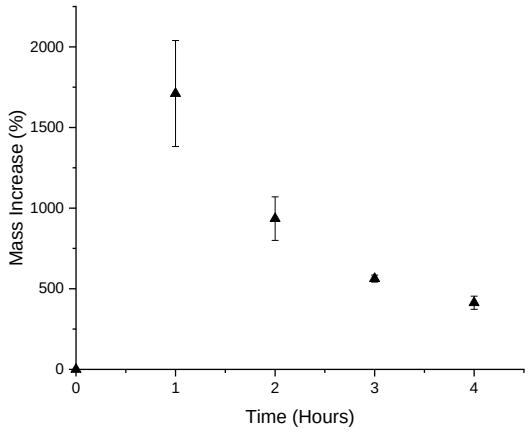

Figure 40. Maximum swelling of HA with minimum disruption over the course of the experiment.

Without being disturbed for 60 minutes the samples are significantly more stable than those for shorter experiments. A decreasing trend is seen in this data suggesting the rapid swelling observed in the first hour is not sustainable. It is likely that the significant amount of swelling which occurs in the first hour causes the network to expand to the point of rupture leading to some gels breaking into smaller fragments, this was also observed in some of the samples from the hour-long experiment. After 4 h the samples have an average mass increase of 413%, similar to the results seen in the samples in figure 39 where the samples were measured more frequently. The gelatin and gelatin-CS samples at 4 h were rapidly degrading and could not be handled without causing further breakage and degradation. The HA samples could be delicately handled and continued to have measurable mass at this point. Beyond the 5 h the samples were very fragile and handling them caused them to break apart, at this point they were classed as ‘degraded’.

To produce gels which are more robust in solution the crosslinking of the network required work. An initiator, *N*-Hydroxysuccinimide (NHS), was introduced to the crosslinking reaction to drive the reaction in the direction of forming successful crosslinks.

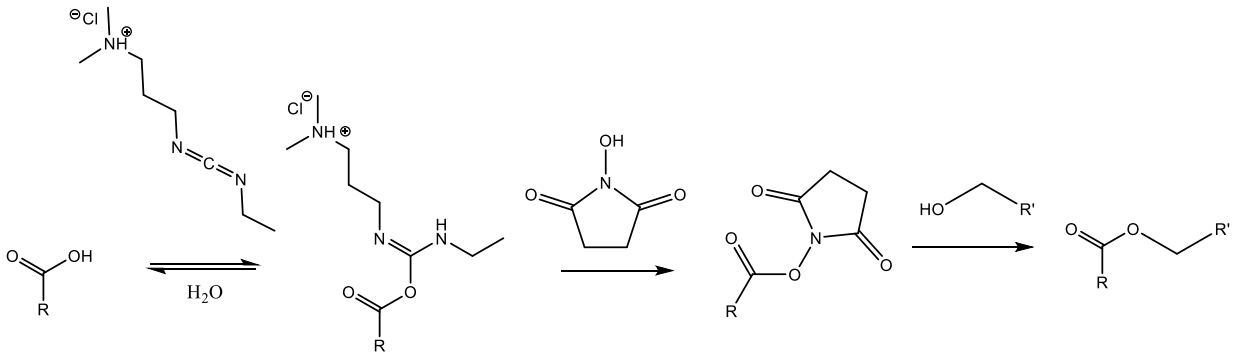

Figure 41. Mechanism for the crosslinking reaction of HA in the presence of EDC and NHS.

It was also vital to confirm that the concentration of EDC (w/v) used in the samples is appropriate. EDC at 0.1% was used for the initial samples because some success was seen using this concentration with gelatin, however, it does not necessarily translate directly to another polymer.

Table 4. Formulations for crosslinking HA

Material	Percentage Material by Mass (%)						
	Formulation 1	**Formulation 2**	**Formulation 3**	**Formulation 4**	**Formulation 5**	**Formulation 6**	**Formulation 7**
HA	1.000	1.000	1.000	1.000	1.000	1.000	1.000
EDC	0.010	0.020	0.040	0.080	0.100	0.200	0.400
NHS	0.040	0.080	0.160	0.320	0.640	1.280	2.560
Ethanol	24.475	24.450	24.395	24.300	24.130	23.760	23.020
Water	74.475	74.450	74.395	74.300	74.130	73.760	73.020

The crosslinks form between acid units on the HA backbone, of which there is one acid functional group per monomer. An estimate of the maximum number of possible crosslinks which can occur can be calculated based on the crosslinker monomer units (or equivalents) in the starting materials assuming one crosslink occurs per monomer.

$$Mr\ eq = \frac{molecular\ weight\ of\ polymer}{molecular\ weight\ of\ monomer} = \frac{16500000}{379.33} = 43497.75 = \sim 43500 \qquad \text{Eq. 25}$$

$$Mol\ equivalents\ of\ repeat\ unit = \frac{Mass\ of\ hyaluronic\ acid}{Molecular\ weight\ of\ repeat\ unit} = 5.27 \times 10^{-5} \qquad \text{Eq. 26}$$

The moles of the crosslinking agent can then be qualitatively compared to the moles of the repeat unit in the polymer, detailed in Table 5.

Table 5. Ratios for the crosslinker and monomer content in each formulation.

	Formulation 1	Formulation 2	Formulation 3	Formulation 4	Formulation 5	Formulation 6	Formulation 7
Mass of EDC (mg)	0.20	0.40	0.80	1.60	2.00	4.00	8.00
Mol EDC $x10^{-6}$	1.29	2.58	5.15	10.31	12.88	25.77	51.53
Mol HA $x10^{-9}$	1.21	1.21	1.21	1.21	1.21	1.21	1.21
mEDC : mHA	1100	2100	4300	8500	10600	21300	42500
mEq Repeat Unit : mEDC	0.02	0.05	0.10	0.20	0.24	0.49	0.98

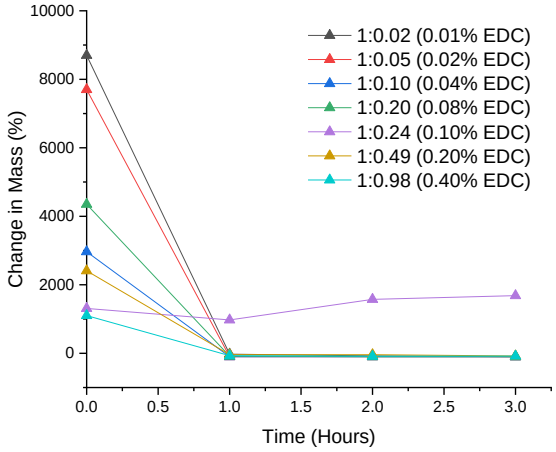

Figure 42. Change in the mass of HA samples when placed in solution for specified amounts of time. Data at 0.1% appears different to other trends in the graph and could be considered an outlier.

Using the crosslinker to polymer ratio a determination of the crosslink density can be carried out, using swelling as a means of comparison with earlier tests. As shown in Figure 42 a majority of samples swelled rapidly in the initial stages of being submerged however all but one of these samples degraded during the experiment. The only sample which did not degrade is the sample with a crosslinker to polymer ratio of 1:4 (or 0.1% EDC). Fortunately, this was same mass which has been used in the previous 2 chapters, involving gelatin and gelatin-CS hydrogels. It should be noted that since such small quantities of material are handled in the experience it could be argued that the results for 0.1% are an outlier due to being difficult to measure out.

Table 6. Detailing the gelatin and chondroitin sulfate ratios. Visible observations about gels crosslinked with different amounts of crosslinking agent.

Formulation 1	50:1	87.0	Lumpy can't be handled
Formulation 2	20:1	77.0	Can't be handled
Formulation 3	10:1	29.7	Can't be handled
Formulation 4	5:1	43.5	Handled
Formulation 5	4:1	14.0	Handled
Formulation 6	2:1	24.1	Stretchy when dry, stringy when wet
Formulation 7	1:1	11.0	V. stretchy when dry, string when wet

The samples with smaller crosslink densities (Formulations 1-3) were very delicate and broke apart very easily, both, while being handled and rapidly while immersed in water. The samples with a higher crosslink density (Formulations 6 and 7) are saturated with crosslinker and become very stretchy when swollen, this apparent elasticity suggests the samples are relatively soft and as seen previously the soft samples tend to dissolve more rapidly. A 'sweet spot' in which the polymer and crosslinker concentration provides desirable properties was found at a ratio of 1:4 (EDC:HA). EDC is known to degrade at room temperature and should be kept cool. As the samples dehydrate at room temperature the crosslinker may also degrade, this is more of a concern the higher the initial concentration of EDC is, therefore formulations 6 and 7 would be a risk of containing more polymerised EDC than in other samples. The polymerisation of EDC may be linked to the remarkable change in the elasticity of the films for formulations 6 and 7; their stretchiness did not occur in the other formulations and may result from excessive degradation of EDC. It appears that Formulation 5 is the most appropriate for the desired application, this is where EDC and HA are in a 1:4 ratio.

It should be noted that again very small quantities of EDC were required in this experiment. Although the balance can measure in microgrammes, the error on the balance will affect the reading and therefore these quantities cannot be accurately weighed out. Overlap in the results and unusual results (such as experiments 6 and 7) could be attributed to attempting to weight out such small amounts of EDC.

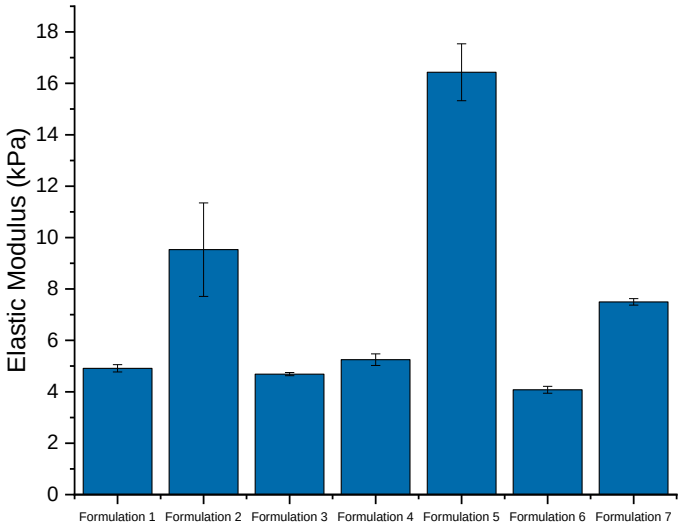

Figure 43. Elastic modulus of HA for each of the formulations containing differing crosslinker densities.

To verify that the softness is indeed related to the poor performance of the films around formulation 5, the mechanical properties of the films were measured (fig 44). The elastic modulus of Formulation 5 is greater than on the other samples, in fact it is the only sample where the average fits into target range of 5-100 kPa. The other samples are quite a bit softer, and as noted previously the softer samples seem to break apart quicker after submersion in water. There is an exception here, where the standard deviation for formulation 2 is significantly larger than the others and overlaps with the bar for formulation 5.

The above calculated crosslinker ratios helped narrow down a useful concentration of EDC, but the reaction conditions still required tweaking to ensure that the reaction produced the maximum amount of crosslinks possible. Such conditions include temperature, ratio of crosslinker to initiator and solvent content. To begin to build a picture of how the reaction conditions affect the polymer and crosslinking reaction, an FTIR spectrum of the unaltered hyaluronic acid powder was first taken.

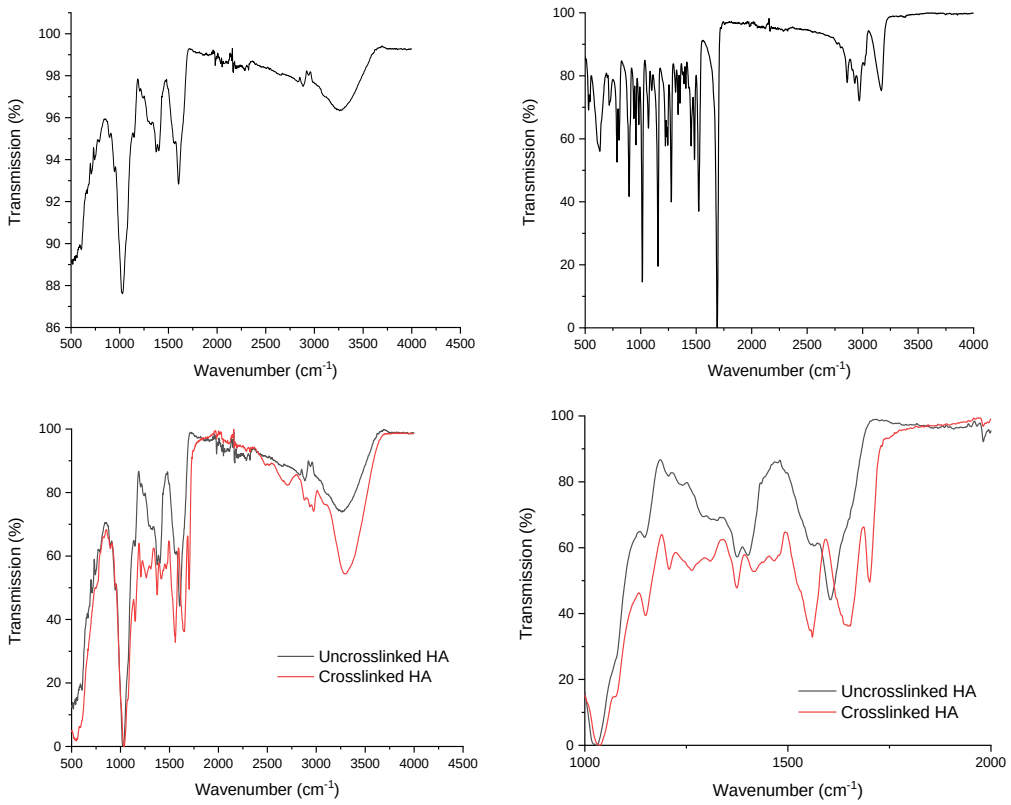

Figure 43. FTIR spectra for HA (top right) and EDC (top left). A comparison of uncrosslinked and crosslinked HA (bottom left) and a zoomed in version of the comparison (bottom right).

The characteristics seen in the FTIR are: a broad hydroxyl stretch around 3300 cm^{-1} representing a hydroxyl stretch; stretches around the 1600 and 1560 cm^{-1} representing a carbonyl and an amine group, and band representing an ether stretch at 1100 cm^{-1}.[248, 249] Taking an FTIR of the unaltered polymer allows for easier identification of any bonds formed during the reaction due to the presence of a new bond or shifting of bonds in the FTIR spectra. The chemical reaction targeted here aims to produce an ester group, as shown in Figure 41. The formation of a new bond or functional group will influence the peaks causing either a new peak or a shift in the peaks which were already present.

Shown in Figure 44, there are various peaks present in the spectra for the crosslinked samples. The peaks which are of interest are at 1028, 1560, 1648, and 1700 cm^{-1} as these regions appear to have changed after crosslinking has occurred. The peak at 1028 cm^{-1} is likely due to a C-O which makes up part of an ester functional group. Esters typically present with multiple C=O stretching peaks in the region 1760-1870 cm^{-1}, two of which are symmetric stretching and the other two are asymmetric. The stretches relating to the carbonyl group occur at a higher wavenumber than in most, and the symmetrical stretch occurs at a higher wavenumber than the asymmetric stretch. The peaks, in this spectrum

seem, to be shifted to lower wavenumber but do however, appear to have the correct shape for an ester.

The most notable feature in the FTIR spectra of crosslinked samples is the appearance of the bond at 1700 cm^{-1} which is not present in the spectra of uncrosslinked HA powder. The peak represents the bond formed during the crosslinking reaction.

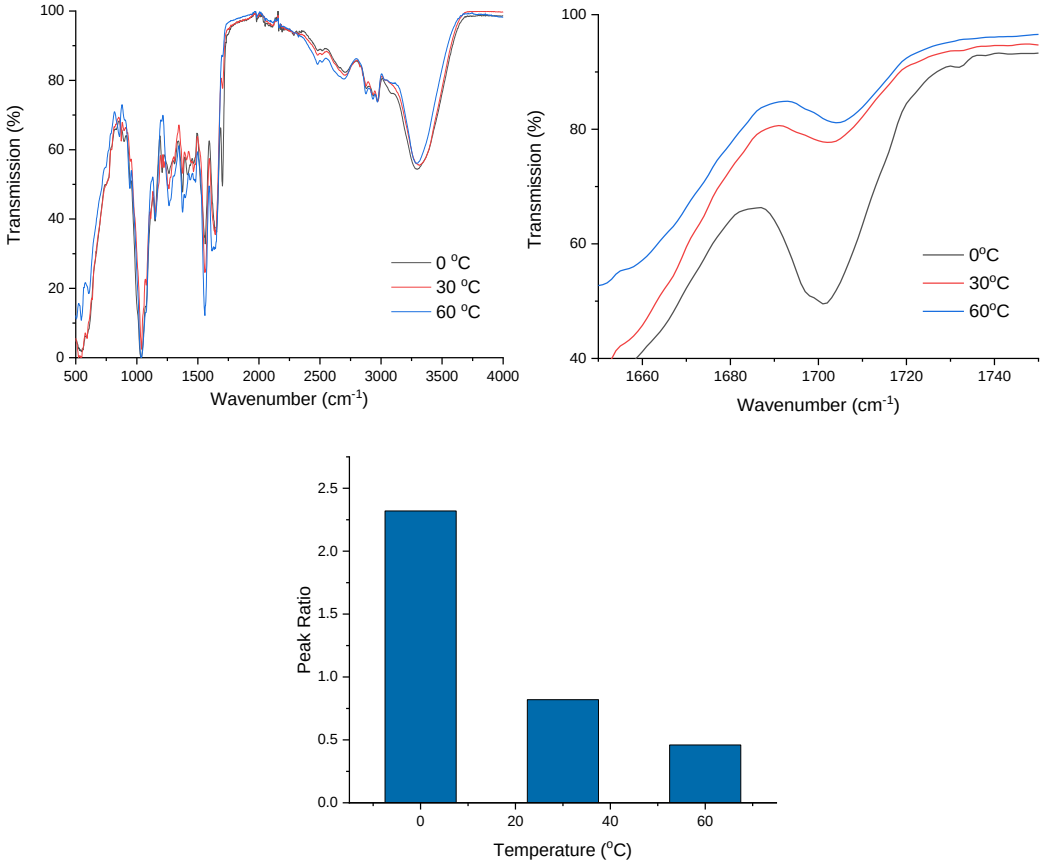

Figure 44. FTIR spectra of crosslinked HA (top images) and the effects of the temperature at which the crosslinking reaction has on the corresponding FTIR peak.

Reactions involving EDC are commonly carried out at low temperature, to minimise its self-polymerisation and to drive the reaction in the direction of forming crosslinks. The reaction was carried out at 0, 30 and 60 °C and FTIR spectra of each of the crosslinked samples was taken. There were varying background transmissions across the samples due to normal noise in room and the setup of the device, therefore the data were normalised. The peak at 2970 cm^{-1} was chosen as the point at which to normalise the data to because the bond which is represented here related to a C-H stretch, and since C-H is unaffected in the crosslinking reaction this bond should remain the same and so its peak should not be changed by crosslinking.

To show the extent to which the temperature effects the crosslinking reaction, a ratio of the peaks (C-H at 2970 cm^{-1} and the peak at 1700 cm^{-1}) were compared using,

$$Intensity\ Peak\ Ratio = \frac{Intensity\ of\ Peak\ at\ 1700\ cm^{-1}}{Intensity\ of\ Peak\ at\ 2970\ cm^{-1}}, \qquad \text{Eq. 27}$$

to calculate the intensity ratio of the peaks to provide a quantitative comparison between the two. The peak for the reaction which occurred at 0 °C is larger and suggests that there is a higher crosslinking density occurring in the throughout the sample. A higher crosslinking density correlates with more successful bond formation. The peak intensity decreases as temperature increases, suggesting that at lower temperatures bond formation is favoured and therefore the crosslinking reaction should be carried out at lower temperatures.

It is well documented that EDC crosslinking occurs most efficiently in acidic conditions, around pH 4.5, without any extraneous amines or carbonyl groups present. It is thought that MES (2-(*N*-morpholino)ethanesulfonic acid) which provides a mildly acidic environment is the most suitable solvent in which to carry out the reaction, although other buffer solutions such as PBS are suitable to the reaction chemistry, albeit with lower efficiency. The lower efficiency of different buffer solutions can be connected by using a greater amount of EDC.[250] A series of solutions were and the efficiency of the reaction was compared to see if the amount of EDC used is enough prevent inefficient reaction conditions. The solutions used were, PBS (pH 7), MES (pH 6), deionised water, and HCl in PBS (0.1M).

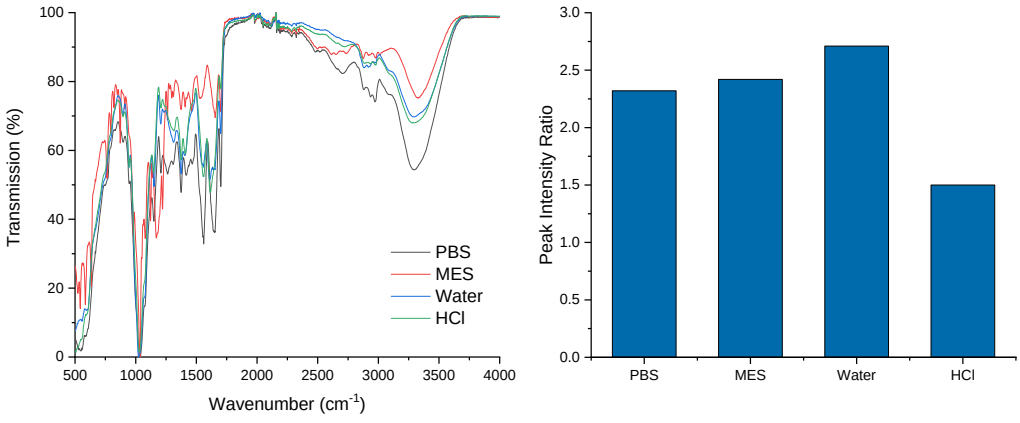

Figure 46. FTIR of crosslinked HA where the crosslinking reaction was carried out in different solutions with pHs.

The peak at 1700 cm^{-1}, related to the formation of crosslinks, was again compared to the peak at 2970 cm^{-1} finding that the ratio for samples made using PBS, MES and water are similar, 2.32-2.71 and suggests that using MES has no real advantage here. However,

there is a lower peak ratio observed using HCl in PBS and therefore it is suspected that the crosslink density in these samples is lower. Water was therefore chosen as the primary solvent.

Again, a similar experiment was carried out to check the quantity of solvent used in the samples. Tomihata *et. al.* state that carrying out the crosslinking reaction in a mixture of 80% ethanol in water produced samples which were able to swell more than the samples which are prepared at other concentrations, such as 90% in water where the resultant samples were brittle and difficult to handle.[57] Samples were made up in 0, 25, 50, 75 and 100% ethanol in water by volume to see how the alterations in the conditions affect the crosslinking reactions. The sample made using 0% ethanol became lumpy as it was difficult to disperse the HA powder in the water, leading to inadequate films which broke apart easily and couldn't be used. Ethanol is useful for providing more homogenous dispersions of both HA and the powders of EDC and NHS. The sample made using 100% ethanol did not form a film since HA does not dissolve in ethanol, therefore, some water is required. The samples containing 25, 50 and 75% ethanol formed films which could be compared using FTIR.

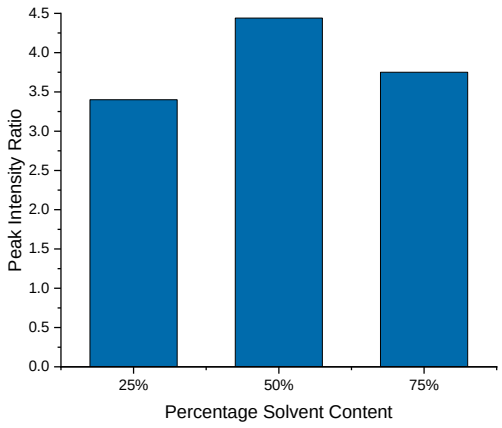

Figure 47. Effect of changing the solvent content has on the crosslinking of HA.

It should be noted that the samples described by Tomihata *et. al.* were prepared via a multi-step synthesis. This involved casting from solutions of HA into a petri dish, which once dry, were submerged into solutions of ethanol and EDC to allow crosslinking to occur.[57] Here ethanol is used as a medium in which HA does not dissolve but EDC does, and so ethanol provides a medium in which the crosslinker can be dispersed without losing the integrity of the HA film.

The ratios for the peak at 1700 cm^{-1} appear similar for all the concentrations of ethanol used, therefore in these samples it is believed the ratio of ethanol to water does not affect the samples in the same way as in the article by Tomihata *et. al.*[57] There appears to be more efficient crosslinking occurring when 50% ethanol in water is used however, the samples at all concentrations could be handled and appear robust so no trend was drawn from the data. Ethanol (25%) in water was used for the samples in the remainder of this section.

The data reported by Tomihata *et. al.* appears to suggest that even a difference as small as a 10% volume change in ethanol could cause large physical difference in the resultant HA sample.[57] However, this was not observed in the data presented in Figure 47. There may be little difference between these samples as the reaction is carried out via one-pot synthesis. Here, EDC and NHS are stirred into ethanol before a small amount of acid is added to produce optimal conditions for the first stage of the EDC/NHS coupling reaction. The samples in the article are placed into a solution containing crosslinking agent, however only the surface is exposed to crosslinking agent therefore, crosslinking may only occur at a surface level, not throughout the sample. In a one-pot synthesis, HA powder is dissolved in water during the crosslinking process ensuring maximum dispersion of the crosslinking agents throughout the sample. Less ethanol may be required in a one-pot synthesis because the HA is dissolved in the water/ethanol whereas Tomihata *et. al.* do not wish to dissolve their HA film and so higher volumes of ethanol are used to prevent loss of HA integrity.[57]

E. Hall verified that the alcohol groups present in the solvent do not affect the crosslinking reaction by carrying out a reaction where HA is crosslinked by submersion in a solution of acetone and comparing the results to those obtained when the acetone is substituted for ethanol. This confirmed that the presence of EDC was required for crosslinking to occur, and that submersion in ethanol or acetone alone does not cause crosslinking to occur. Also, crosslinked films which were submerged in either solution remained as crosslinked films after 24 hours with no notable differences between the samples from either ethanol or acetone mixtures.[251]

HA films which are robust enough to be handled, appear to have no obvious surface defects and are homogenous throughout. The formulation for such a gel contains 0.1% EDC, an NHS initiator, 1% HA powder, and, 25% ethanol in water. These films were made by a one-pot synthesis, where EDC and NHS were dissolved in ethanol followed by the addition of HA and then water is added dropwise. This formulation was chosen

were based on the collective results from: visual inspection of the films, both wet and dehydrated; FTIR; swelling properties, and on how the gels can be handled. This formulation then needs to be characterised in terms of how it would behave in conditions which relate to or are similar to the spinal cord environment.

7.1.1. Characterising the Swelling Properties of HA Hydrogels

Swollen hydrogels display similar abilities to the extracellular matrix has and so it is important to be able to produce a hydrogel which is robust in its swollen state. The samples produced from the new formulation require characterisation.

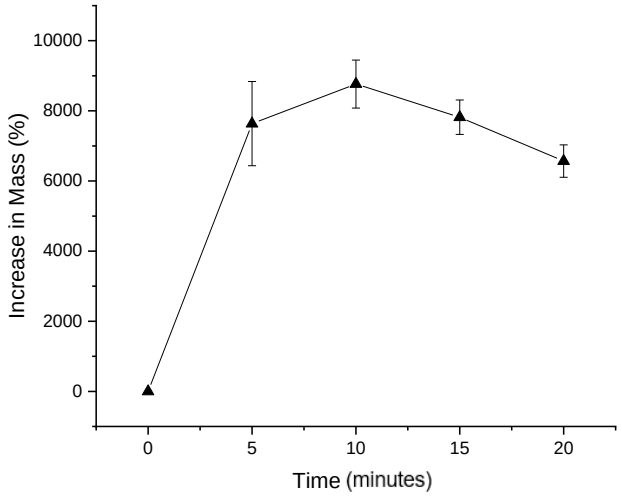

Figure 458. Maximum swelling of the scaffold in solution over 20 minutes.

Initially the gels swell rapidly in water, reaching a maximum swelling around 10 minutes before beginning to stabilise around a constant mass. A further 30 samples were swollen and monitored until the rate of swelling slowed and the mass of the samples stabilised. Once stabilised these samples have an average mass increase of $955 \pm 52\%$ which corresponds to a swelling ratio of 10.6 ± 0.5. The swollen samples are robust enough to be handled and do not fragment in solution over the course of the experiment.

7.1.2. Characterising the Hydrolytic Degradation of HA Hydrogels

In vivo the hydrogel scaffold would need to degrade and must do so without damaging the surrounding tissue and tissues involved in excretion. Therefore, the products of polymer degradation must be biocompatible and should have known routes of excretion from the body.

It is suspected that the crosslinks, which are covalent bonds formed between available carboxylic acid groups on hyaluronic acid chains, may be susceptible to hydrolytic degradation.[251] This is because the acyl anhydride functional group which makes up the crosslink is susceptible to reduction to two carboxylic acid groups through the addition of water. This would reverse the crosslinking reaction and would cause the physical properties of hyaluronic acid to revert to how it was before the reaction occurred. This means that the gels would be weak and would break apart rapidly in solution causing complete degradation.

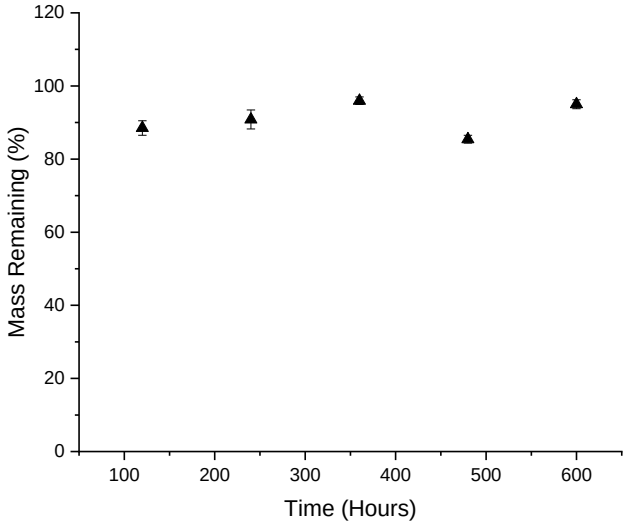

Figure 49. Hydrolytic degradation of the scaffold over 600 hours

The hydrogels were submerged in deionised water (at 37 °C) and were removed at 120-hour intervals over the course of 25 days. When a sample was removed from the solution it was not returned, therefore samples were submerged for either 120, 240, 360, 480 or 600 hours. Any effects caused by handling the samples are minimised by only interacting with the sample once rather than keeping the same samples and monitoring them multiple times throughout the 25 days of testing.

Over the course of the 25 days there was little change in the weight of the samples. The samples lost approximately 10% of their mass over the course of the experiment, however there was no real difference between the results and the raw data largely overlap suggesting the effects of hydrolytic degradation are minor. It can be assumed that there is a small amount of degradation, although significantly less had occurred than expected. The acyl anhydride functional group formed from the crosslinking appeared to be stable in water, and it is likely that more energy is need for hydrolytic degradation to occur than is available at 37 °C.

HA hydrogel samples which had been submerged in deionised water for 25 days had an average of 95 ± 1% mass remaining compared with the mass of the samples prior to testing. The samples are robust enough to be handled both before and after the experiment. Therefore, the samples are considered stable and robust after 25 days of submersion in water.

In vivo a hydrogel scaffold would be surrounded by bodily fluids, such as blood, plasma or interstitial fluid. What is key here is that the environment in the body is around pH 7.4, whereas the pH of deionised water in a container is likely to decrease and become slightly acidic as molecules like ambient CO_2 dissolve into it to form carbonic acid.[252, 253] Buffer systems are better than water alone at maintaining a constant pH over a period of time. A buffer which is commonly used to mimic the biological pH of 7.4 is phosphate buffer solution (PBS). The experiment investigating the hydrolytic degradation was repeated but this time using PBS.

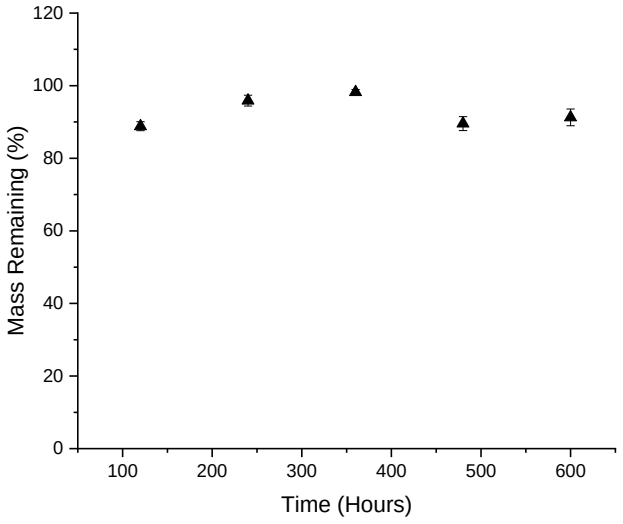

Figure 50. Degradation experiment where the scaffold was submerged in PBS for 600 hours.

The results, shown in Figure 50, were very similar to those of the experiment carried out in water, suggesting that the constant environment provided by the PBS buffer does not affect the degradation or hydrogel. After 600 h 91 ± 2 % of the samples remain, suggesting little to no degradation is occurring. It also suggests the salts and slightly altered pH do not have adverse effects on the hydrogel itself, and the results are consistent with those observed when the solution was deionised water alone.

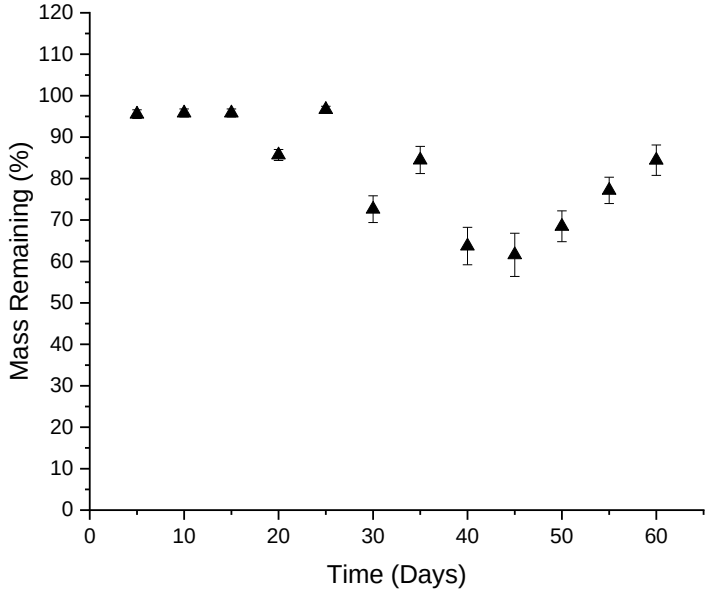

Figure 51. Hydrolytic degradation extended to 60 days

It appears that the hydrogel does not rapidly degrade via hydrolytic degradation, and this is a promising result for producing stable scaffold. For application to SCIs the scaffold would be required to remain in place long enough for the extracellular matric to grow around the scaffold as it degrades. The ECM is complicated and there is no one specific time frame for its regrowth, although it is generally assumed that one month post injury the skin over the wound is fragile but strengthens and forms scar tissue over the next 12 months. The scar tissue often lacks in proteoglycans and may contain elevated levels of collagen, and it may never have the same strength as the skin prior to injury.[254] From 2 to 10 days post-injury the ECM begins to regenerate and reduce the injured site, but the total time it will take for the injury to be entirely replaced is dependent on the overall size of the injured tissue.[255] The hydrogel should be able to remain intact until the ECM regenerates around the wound ensuring the integrity of the cavity remains constant. Therefore, a reasonable time frame for the lifetime of the hydrogel could be 10 days to 1 year with any bioelectronic material implanted within the scaffold remaining in place and functional beyond this period.

The degradation study was extended to see how the hydrogel would handle longer term submersion in water. When the experiment was extended to 60 days some variation in the results began to occur, with some of the samples continuing to have relatively constant masses, while others were losing mass. While the error bars still overlap suggesting there isn't a significant difference between the results, the frequency of the samples which begin to lose mass does increases with time passing.

When the length of time the samples are submerged in water is extended to 5 months there are frequently samples which degrade either during the experiment or once disturbed. In some cases, the samples can be seen in the solution before it is agitated but when the container was moved, and an attempt made to remove the sample, it disintegrated. There are some samples which continue to have almost all their mass remaining after 5 months ($91 \pm 2\%$) although this occurs much less frequently, and the samples are more likely to dissolve when disturbed after being left in solution for 5 months. The samples which do degrade perhaps have more heterogeneity to the samples, or less efficient crosslinking throughout the sample and therefore excess water can enter the structure causing it to rupture when it is disturbed. If the samples which remain intact after 5 months are more homogenous than others, more of them could be created by ensuring the methodology is consistent during sample preparation.

7.1.3. Characterising the Enzymatic Degradation of HA Hydrogels

In vivo the hydrogel will be subjected to an immune response, in which the body will influx enzymes to the site of the implant to identify and remove foreign matter.[72-75] Therefore, the implant will undergo enzymatic degradation, where the amount of enzyme present may be significantly more in the early stages after implantation compared to longer term.

Initially an enzyme named lysozyme was chosen as a starting point for examining potential enzymatic degradation routes of the hyaluronic acid polymer. Lysozyme breaks down peptidoglycan backbones by hydrolysing the β-1,4-glycisidic bonds in the polymer chain. Specifically, it degrades the bond between *N*-acetylglucosamine and *N*-acetylmuramic acid but has been proven to interact with hyaluronic acid.[256-258] Lysozyme is found in the organs, tissues and secretions of the human body, as well as is in tears, saliva, and mucus. Not only is it abundant in the human body, but it is also present in many other species, including both vertebrates and invertebrates, as well as bacteria, and plants. It is abundant and can be easily obtained for use in the laboratory, making it a good candidate for early enzymatic degradation studies.[256]

Samples were submerged in a solution containing lysozyme in PBS for 5 days finding that little degradation occurred and so the test was extended to 25 days, matching the

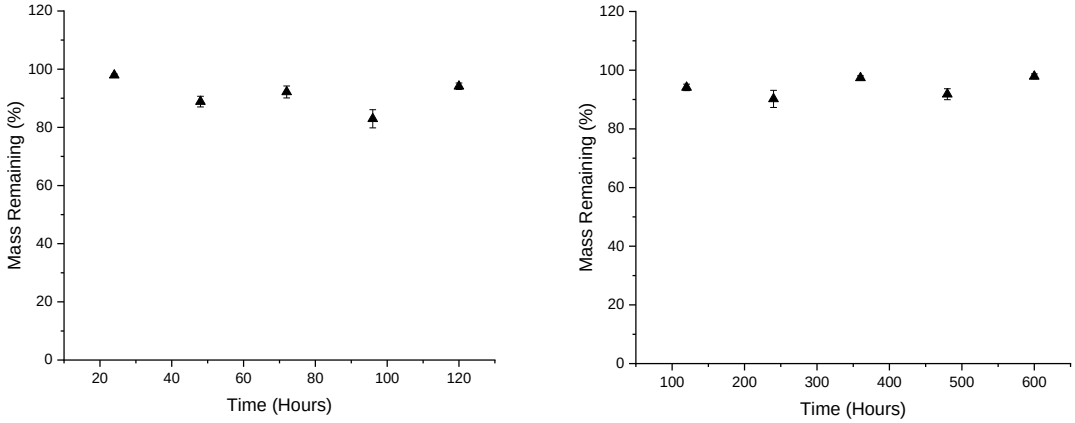

Figure 52. Enzymatic degradation of HA samples using lysozyme. Degradation for 5 days (left graph) and over 25 days (right graph).

methodology used for previous studies in water and PBS. Over 25 days there was only a small amount of degradation which occurred similar to when the samples were submerged in water or in PBS. In fact, the similarity of the results allows the conclusion that no enzymatic degradation occurred, and that only a small amount of hydrolytic degradation occurred. This would suggest the lysozyme is not enzymatically active with the crosslinked hyaluronic acid used here, and therefore it was not tested further. It should also be noted that lysozyme is not present in the spinal cord fluid, however if this material was to be used in a different area in the body lysozyme studies may be essential.[259]

Hyaluronidase enzymes in the body are responsible for breaking down hyaluronic acid and therefore it is essential to characterise the effects of this enzyme on the scaffold. In the body high molecular weight HA is typically processed by hyaluronidase type 2 which breaks the polymer into smaller pieces of different sizes. It is the function of hyaluronidase type 1 to degrade these pieces further.[260] The hyaluronic acid used in this project has a molecular mass of 1.5-1.8 MDa therefore hyaluronidase type 2 was chosen to be the starting point for hyaluronidase-based degradation, since it is used to break down higher molecular weight HA polymers. Hyaluronidase type 1 was then used following this.

To establish the concentration of enzyme required for the *in vitro* tests a study based on the enzyme activity was first carried out. During this UV/Vis adsorbance spectroscopy was used to identify the activity of the enzyme at 600 nm, where one unit of enzyme is

believed to cause a 0.33 change in the absorbance per minute, in a 2 mL mixture at pH 5.35. Therefore, the enzyme has known and quantifiable activity at this wavelength.

$$E + S \rightarrow [ES] \rightarrow E + P$$

A generic equation for enzymatic reactions begins with an enzyme (E) and a substrate (S), which make an intermediate, an enzyme-substrate complex (ES), before separating into a product and recovery of the enzymes initial structure. The enzyme is not used up in the reaction, nor is it changed, but it displays catalytic activity. The rate of the reaction can be labelled k, and typically if the concentration of the substrate (denoted [S]) is sufficiently low relative to the concentration of the enzyme then the V-S relationship is linear. However, when the concentration of the substrate is relatively large compared to the concentration of the enzyme then the rate of the reaction becomes independent of the substrate concentration. At sufficiently large concentrations of substrate, $[S]>K_m$ the enzyme is assumed to be bound to the substrate forming the ES complex and therefore the limiting rate step (v_o) is equal to the velocity achieved by the enzyme when the substrate reaches saturating concentrations, V_{max}. K_m is the Michaelis constant which represents the point at which the rate of the enzymatic reaction is at half the maximum rate.[261-263]

The Michaelis-Menten relationship is,

$$v_o = \frac{V_{max} \cdot [S]}{[S] \cdot K_m} \qquad \text{Eq. 28}$$

which forms a hyperbolic relationship and has been linearised using a series of method, the most common of which is Lineweaver-Burk (Eq. 29).

$$\frac{1}{v_o} = \frac{1}{v_{max}} + \frac{K_m}{v_{max}} \frac{1}{[s]} \qquad \text{Eq. 29}$$

Therefore, having a quantifiable V_{max} is important for knowing the point at which the rate of reaction is no longer influenced by the concentration of the substrate. This helps to decide the concentration of enzyme to use in further enzymatic degradation studies.

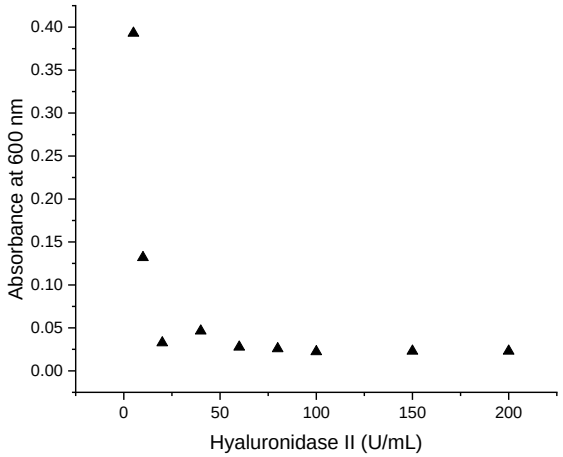

Figure 53. Absorbance/concentration relationship for hyaluronidase type II following a turbidimetric analysis.

Turbidimetric analysis of hyaluronidase type II can be performed by looking at changes in absorbance occurring at 600 nm. Following this a standard enzyme curve can be plotted (figure 53).

During a turbidimetric analysis the turbidity of the solution is proportional to the concentration of the polymer and therefore as the polymer is degraded by the enzyme the turbidity of the solution is reduced.[264] This property can be seen in the standard curve for hyaluronidase type II (figure 53). To make the data simpler to quantify in terms of V_{max} and K_m a Lineweaver-Burk plot is used which shows the data as a linear relationship.

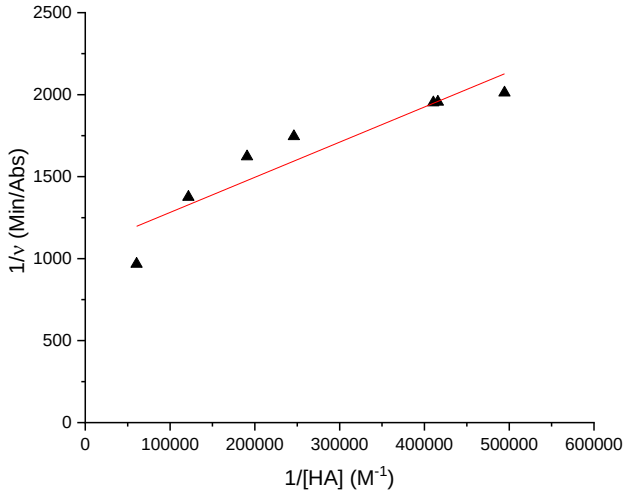

Figure 54. Lineweaver-Burk plot for hyaluronidase type II.

The plot is expected to be linear and therefore small deviations away from a perfectly linear relationship are expected to be due to experimental error, such as small deviations

in pH or salt presence which affects the activity of the enzyme. However, since the overall relationship is linear the data can be used to calculate V_{max} and K_m.

$$V_{max} = \frac{1}{b} = \frac{1}{1067.4} = 0.937 \text{ mmol/minute}, \quad \text{Eq. 30}$$

$$K_m = a \cdot V_{max} = 0.0021 \times 0.937 = 0.002 \text{ mM}, \quad \text{Eq. 31}$$

Assuming that K_m is related to half the reaction rate, then at the concentration corresponding V_{max} would be the point at which saturation occurs. Using the Michaelis-Menten relationship this value can be estimated by solving eq 28. When V_{max} is 0.937 mmol/minute the corresponding x-value is 0.014 mM and this is the concentration at which the rate of reaction is no-longer related to the concentration of the starting material. It should be noted that the Michaelis-Menten relationship is hyperbolic and therefore approaches such as the Lineweaver-Burk method are preferred since they produce graphs with linear trends, and this can be better modelled than a hyperbola.[265, 266]

The results from the enzyme kinetic study suggest that using concentrations of HA above 0.014 mM will best examine the activity of the enzyme where the rate of the reaction is not affected by the concentration of HA. At this concentration there will be ~10mg of HA present in a 1 mL solution. Therefore, samples should be cut into pieces weighing at least 10 mg to be used in the enzymatic degradation experiments so that the rate of the reaction is not affected by the concentration of the substrate, HA.

M. R. Natowicz *et. al.* carried out a study of the concentration of hyaluronidase enzyme in human serum and human umbilical cord, the components of blood which do not involve blood clotting, finding a V_{max} of 5.1 U/I, and the normal reference range of hyaluronidase activity across 100 apparently healthy individuals was 4.5 $\pm$ 1.1 U/I.[267] This correlates to ~ 0.004 mmol/min and therefore, using HA at a mass of 10 mg in a 1 mL solution the concentration of HA should not affect the rate of the reaction. Natowicz *et. al.* also noted that no reaction occurred at pH >5 and that the average human serum containing hyaluronidase has an optimal pH range of 3.7-4.2.[267] A similar observation was made by S. Fang *et. al.* who reported that the optimal pH for a reaction containing hyaluronidases was 4.5-5.5.[268] They also report K_m and V_{max} values of 0.87-0.91 mg/mL and 1.66-1.74 nM/s for solutions containing HA with molecular weights varying from 215-752 kDa.[268] A. Kaul *et. al.* report that the active pH of hyaluronidase type II is around pH 4 or pH 7.[269] The pH of the degradation may need to be monitored to ensure than the enzyme is active and not hindered by the environment.

It would be inappropriate to have varying amounts of enzyme concentrations across the experiments therefore a fixed amount of enzyme, in U/mg, was required. The hyaluronidase II enzyme supplied has an activity of 300 U/mg and therefore the concentration of enzyme used in the degradation tests would need to have an activity less than 300 U/mg. Solutions containing 5-200 U/mL were produced for the experiment to determine the K_m and V_{max}, finding that the UV/Vis experiments for samples containing 150-200 U/mL were not reproducible. This may have been due to increasing turbidity as the amount of enzyme concentration increased or due to reasons unrelated to the enzyme itself, such as salts crashing out of solution while these samples waited to be tested. However, it was decided to continue with the solutions containing 5-100 U/mL to minimise errors in the data. This helped to narrow down the concentration used in the degradation studies.

The enzyme concentration was further narrow down by comparing studies reported in different publications. T. Segura *et. al.* found that a poly(ethylene glycol) diepoxide crosslinked HA scaffold was completely degraded in 14 days by hyaluronidase at 100 U/mL.[270] A scaffold of poly(ethylene glycol) with HA-binding capabilities was degraded in the presence of hyaluronidase at 50 U/ml.[271] A review by J. A. Burdick *et. al.* suggesting that using a concentration of 100 U/mL hyaluronidase would be appropriate.[272] In another study, by J. Patterson *et. al.* a hyaluronic acid gel, designed to have controlled degradation for bone regeneration applications, were degraded in 1 mL of 500 U/mL of hyaluronidase at 37 °C. A common application of hyaluronidase is to break down HA filler. B. A. Buhren *et. al*. looked at the interaction between HA-fillers and hyaluronidase using a concentration of 10 U/mL.[273] Lee *et. al.* also investigated the effectiveness of hyaluronidase for HA-fillers and found that an activity of 30-50 UI was effective when applied by injection to animals, although they report that activities of 100 UI can also be recommended.[70, 274] There appears to be no widely accepted consensus for what is an appropriate concentration of hyaluronidase because the concentration to use appears to be specific to the polymer, crosslinking and any potential application. However, from these reports a consensus can be proposed of equal to or less than 100 U/mL. The amount of hyaluronidase should be in this region but required considering the commercial availability of hyaluronidase II and the number of samples to be tested. Therefore, to be able to perform a suitable number of repeats of the degradation experiment a concentration of 80 U/mL was chosen.

The methodology which was used while studying the hydrolytic degradation of the samples was employed again, but this time the fluid was a solution containing hyaluronidase type II. The solution is PBS to ensure that the pH of the reaction is stable throughout since DI water on storage tends to become more acidic as carbon dioxide dissolves into it from the air forming carbonic acid.

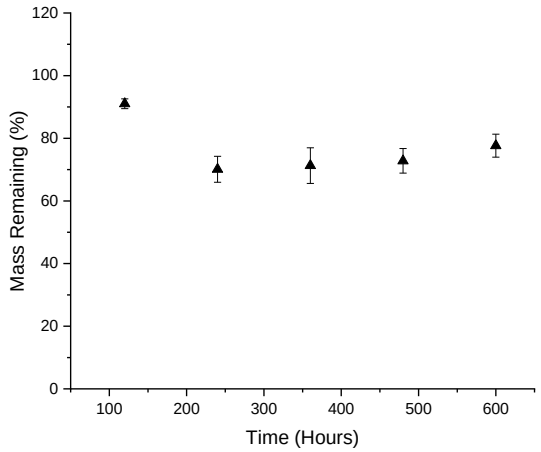

Figure 55. Enzymatic degradation of HA using hyaluronidase type II over 25 days.

Over 25 days of storage around 30% of the mass is lost from the original hydrogel sample, suggesting that there is in fact enzymatic degradation occurring which was not seen when lysozyme was used in the previous degradation experiment. The mass loss which occurred appears to have occurred in the first 240 hours of the experiment, following this the average result appears relatively stable throughout the remainder of the experiment. This remaining mass, of ~70%, appears stable in this solution. The reason for the decrease in the rate of degradation could be due to the enzyme no-longer being effective for the weight of HA. Hyaluronidase type II is effective for breaking down high molecular weight HA and from these results, most degradation is seen to occur in the first 200 hours, after which there is no longer any HA left at a molecular weight that can be degraded by hyaluronidase type II, so another hyaluronidase enzyme would be more appropriate.

The experiment was then repeated this time using Hyaluronidase type I. This is a more potent enzyme than hyaluronidase II, and displays more activity towards HA and therefore more degradation was expected.[70]

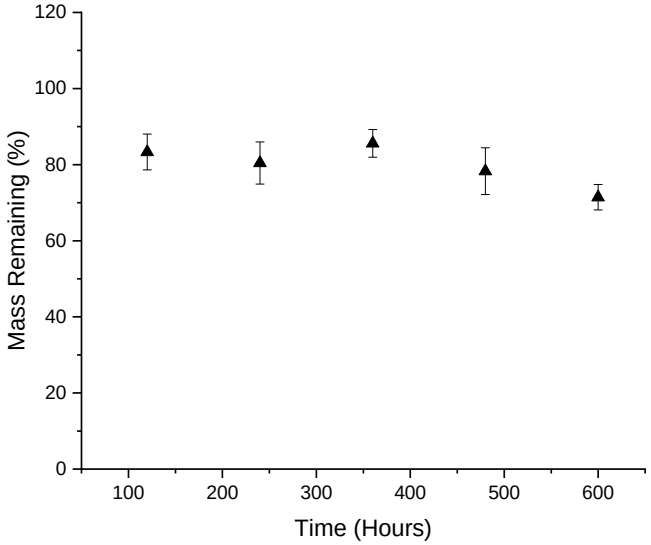

Figure 56. Enzymatic degradation of HA using hyaluronidase type I over 25 days.

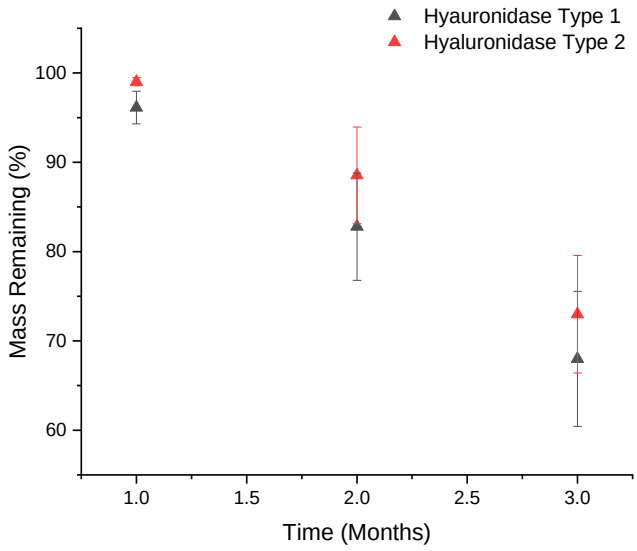

Figure 57. Comparison of the results for the enzymatic degradation of HA using type 1 and 2 hyaluronidase.

The results were unexpected, in that the degradation was relatively similar to that observed when using hyaluronidase type II, where after 600 hours (25 days) there was ~70% of the mass remaining. One difference is that mass loss appears to occur within the first 120 hours of the experiment, whereas when hyaluronidase II was used, the mass lost appeared to extent over the first 240 hours. After 120 hours the mass appears to be constant suggesting any further enzymatic degradation was limited.

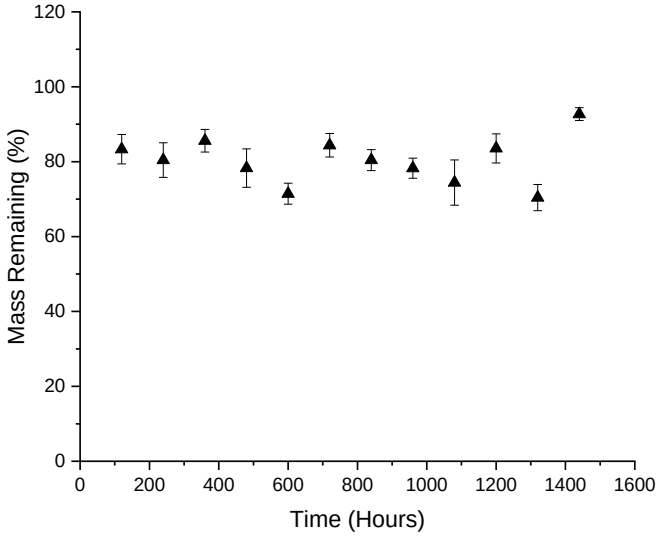

Figure 58. Enzymatic degradation of HA extended to 1440 hours.

When the test was extended to 60 days (1440 hours) a similar trend was observed, where ~30% of the original mass was lost in the early stages of the experiment however, following this the mass remained relatively constant, with approximately 70% mass remaining through the remainder of the experiment.

It was postulated that the enzyme does not remain in conditions in which it would be considered active, therefore the solution was changed from water to an enzyme diluent, based on an assay for the enzyme from the supplier, Merck.[275]

The enzymatic diluent formulation in the methodology requires the solution to be adjusted to pH 7, this appears to be appropriate for the hyaluronidase II enzyme obtained from Merck, however, it should be noted this is extracted from sheep testes and may have a different specific activity requirement to human hyaluronidases.[275] Kaul *et. al.* propose pH 7.5 and 4 as active pH's for hyaluronidase II, and pH 3-4 for hyaluronidase I, although the degradation experiments here, were carried out at pH 7.[269] While pH 7 may be appropriate for hyaluronidase II it is expected not to be the case for hyaluronidase type I. However, since the results from the experiments for each enzyme are similar, they appear to contradict summary. Nevertheless, if a more acidic pH was used for hyaluronidase I it is possible more degradation may have been observed. In future work the degradation reaction for hyaluronidase I could be repeated at a pH of 3-4.

Importantly, the crosslinker plays an important role here, without having chemical crosslinks throughout the network the hydrogel would rapidly dissolve and be lost to the solution. Not only does crosslinking prevent degradation in water it has also provided a system which does not completely dissolve in the presence of hyaluronidase enzymes.

7.1.4. Characterising the Mechanical Properties of the Scaffold

The mechanical properties of the scaffold must match with that of the target tissue. It is essential for minimising mechanical sheering between matter with mismatched properties. When the tissue and scaffold have different harnesses, the harder material will damage and wear the softer of the two. This could be dangerous if the device is significantly harder than the spinal cord tissues. There is also a failure risk if the tissue wears the device.[220]

S. Cheng *et. al.* published a comprehensive review summarising the experimental methodologies and moduli of the brain and spinal cord. The spinal cord is comprised of nerve cell bodies, themselves made of grey matter, surrounded by axons of white matter. This system is wrapped in meningeal layers and blood vessels. Outside of this is the pia matter and dura matter, each of which are significantly harder than the white and grey matter which makes up the spinal cord. Several of the studies for the spinal cord have

the Dura matter removed but continue to keep the Pia matter instated. Therefore, the properties of the grey and white matter themselves should also be investigated.[97]

In studies by T. K. Hung and Chang relatively small amounts of strain were considered in the *in vivo* investigation of the elastic moduli for the spinal cords of puppies and cats, resulting in apparent agreement between the results.[96, 97] T. K. Hung reported an elastic moduli of 0.252, 0.295 and 0.400 MPa for the elastic modulus of differing regions of the cats spinal column.[96] While T. K. Hung and C. L. Chang together report a value of 0.265 MPa for the elastic modulus of a puppies spinal cord.[276] In further articles by the authors they report a pseudo-increase in the elastic moduli as strain increases, however the strains used here could be considered small in comparison to studies by L. E. Bilson *et. al.* and R. J. Fiford *et. al*., with L. E. Bilston *et. al.* reporting human spinal cord elastic moduli of 1.02, 1.17 and 1.37 MPa and R. J. Fiford *et. al.* finding a modulus ~1.14-1.98 MPa for a rat's spinal cord.[87, 277] This finding is supported by the study of R. J. Oakland *et. al.* who reported an elastic modulus of 1.19 MPa for a bovine spinal cord when it was tested using a similar strain used in the work by L. E. Bilston *et. al.*[87, 88]

The above studies are carried out using an axial tension study whereas the study used in this project is an indentation method which involves compression. Compressive and indentation testing is carried out more commonly on the brain than on the spinal cord. Unrestricted compressions of the brain are carried out *in vitro* because compressive measurements are technically difficult to carry out. Indentation specifically looks at applying a load to a specific portion of the tissue rather than across the entirety of a surface such as those carried out in compressive testing.[97] At the time of publication there were two known studies of indentation testing carried out on a brain *in vivo.*[97, 278] The first of which, by S. Cheng *et. al.,* reports an elastic modulus of 350 Pa for white matter.[278]

The tissues surrounding the spinal cord such as the pia matter through to the dura matter are significantly harder than the other tissues in the spinal cord and when they are discounted the tissue remaining can be examined for its elastic properties. The study previously mentioned by L. E. Bilston *et. al.* found intact spinal cords with an elastic modulus of 1.01 MPa.[87] Whereas a series of studies have reported smaller elastic moduli for incised spinal cord, where the pia matter, dura matter and other tissue have been removed. T. L. E. Mazuchowski *et. al.* reported an elastic modulus of 89 kPa for a spinal cord where the pia matter has been removed.[85] A study by H. Zhang *et. al.* found that the elastic modulus of the dura matter from a sheep has an elastic modulus of 5 kPa,

while H. Ozawa *et. al.* found that the elastic modulus of a rabbit's spinal cord with the pia matter removed has an elastic modulus of 5 kPa.[279] Both of these methods use an indentation method of testing the elastic properties of the tissues. Whereas A. R. Tunturi *et. al.* used an uniaxial tension method to determine the elastic modulus of the dura matter from a dog, finding it to be 399 kPa.[93] Therefore, looking specifically at the much softer white and grey matter is important as this is where the bioelectronic device would reside.

There are very few studies which have looked at the grey and white matter, however once such study was carried out by K. Ichihara *et. al.*[97, 280] In the study a uniaxial tension method was implemented finding the elastic moduli of the grey and white matter were 25 and 166 kPa respectively.[280] Whereas pipette aspiration was used in a study by H. Ozawa *et. al.* finding an smaller moduli for the white and grey matter of ~3 kPa.[281] T. L. E. Mazuchowski *et. al.* reported that the pia matter provides the spinal cord with extra tensile strength when it is stretched in an axial direction, which may account for inflated moduli values when axial tension is used to test samples where the pia matter is intact.[85]

The known values of the spinal cord tissues are ~ 5-1500 kPa, and tissues such as the pia matter increase the tensile strength of the matter giving larger elastic moduli. Taking this into account a range for an appropriate spinal cord can begin to be formed, when the pia matter is excluded, and surrogate materials are also considered. The average elastic moduli in the papers included here appears to be in the region of 50-100 kPa however the white and grey matter appear softer than 50 kPa and so the target range was extended to 5-100 kPa. In the hope that if the material is in the lower region of this range, then it would be considered soft but would not cause enough mechanical friction to damage the living tissue. If the elastic modulus was beyond this range it would be more likely to cause such friction.

The standard bloom test for gelatin samples, described in chapter 5, can be used to measure the stress-strain relationship of gels under a compressive load. The slope of the stress-strain relationship is elastic modulus. In the standard operating procedure for a bloom strength test a 112 g sample is used, here the HA samples are significantly smaller ~ 10 mg when dehydrated and ~100 mg when swollen, therefore the parameters of the test required adapting to make them suitable to smaller scale samples. One parameter which requires adapting is the depth to which the probe penetrates into the sample, in original methodology the probe penetrates 12.5 mm into the sample however the HA

films have an average depth of 500-1500 µm. Therefore, the probe would need to indent significantly less to only indent part-way into the sample.

The average depth of the hyaluronic acid films can be measured by using profilometry software combined with a 3D optical microscope. This data can also be supported by using the texture analyser (used for the mechanical property measurements) to identify the height of a surface in comparison to the substrate below it, this gives film thickness. Knowing the average film thickness allowed for an experiment to be designed, in which the texture analyser would penetrate the sample at a series of known depths, helping identify an appropriate target depth of indentation.

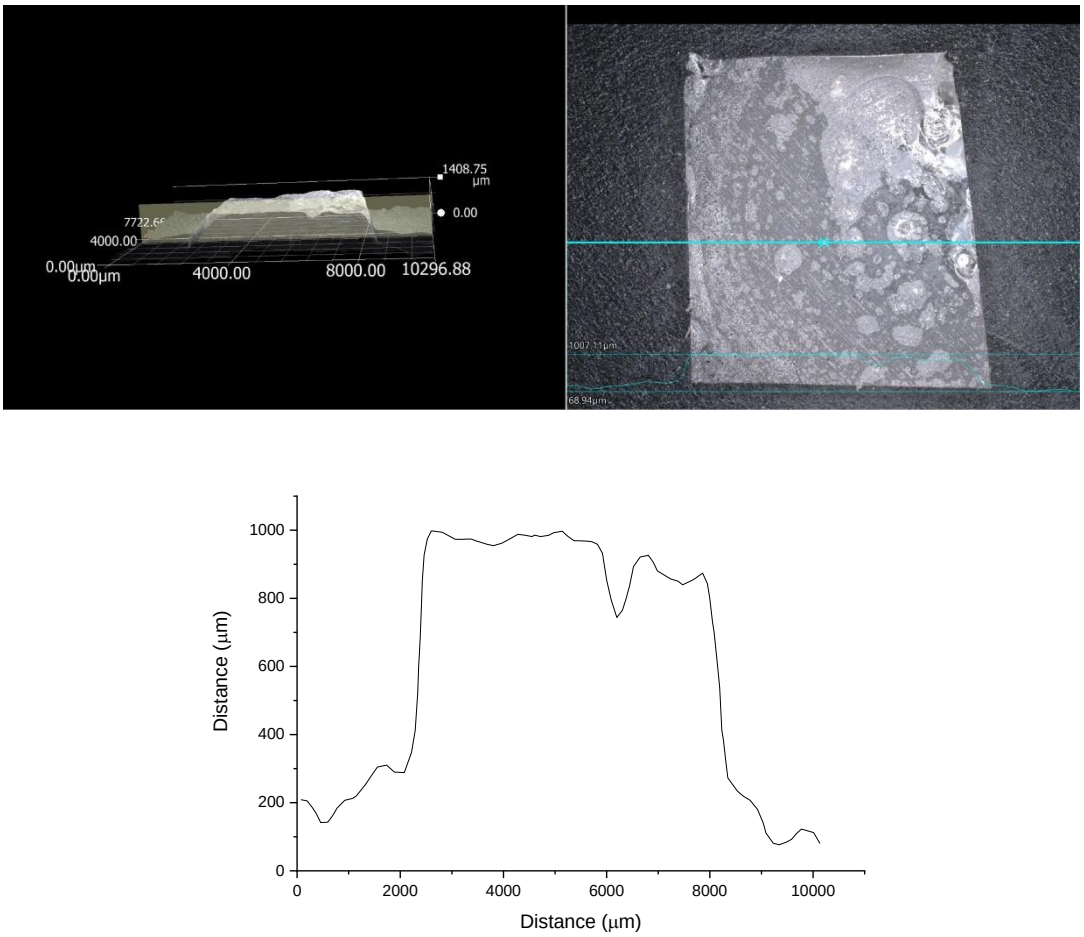

Figure 59. Optical microscope images. Top right detailing the 3D profile of the sample. Top left image shows the view of the sample from the top down. Bottom image is the generated profile of the sample.

Films of the HA scaffold were swollen in water, and the film thickness was measured by both the optical microscope (Figure 59) and by the texture analyser resulting in an average film thickness of ~0.55 mm (n=5). These samples were then compressed to a depth of 0.1 mm by the texture analyser, while measuring the force it takes to achieve such depths of indentation. The experiment was carried out using a trigger force of 0 N,

which means the first measurement occurs when the probe makes first contact with a surface.

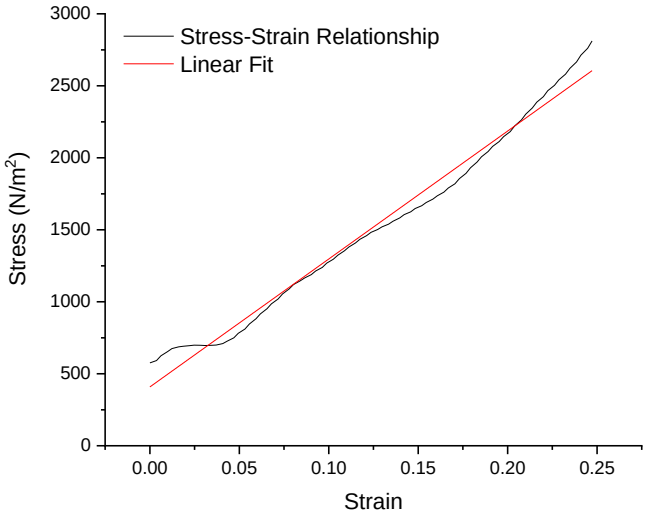

Figure 60. Stress-strain relationship of HA.

The stress-strain relationship is expected to be linear, without fluctuations, and there was concern that the water which is used to maintain a swollen state throughout the experiment may affect the measurements in the initial stages of the experiment, where probe first makes contact with a surface. The probe needs to push through any water which is over the surface of the hydrogel at a slow pace and at small amounts of force, this leads to fluctuations in the data as the surface tension changes when the probe moves through. The effect of this interaction is surmised to be the reason for the lack of linearity.

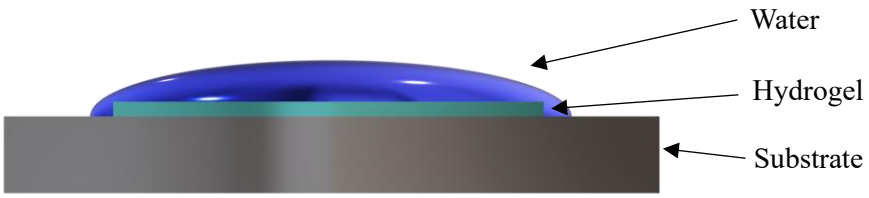

Figure 6461. Image showing the setup of the sample and the water used to keep it hydrated throughout the mechanical testing.

To ensure that probe penetrates through the surface water and begins to measure the sample below the target depth was increased to 0.2 and 0.3 mm. Also, to minimise any effects from the surface the trigger force was increase to 5 mN, this means the first measurement will start when the probe detects a force of 5 mN and should be enough

force to penetrate through any water before beginning to record data. The results of the changing target depth and changed trigger forces are compared in Figure 62.

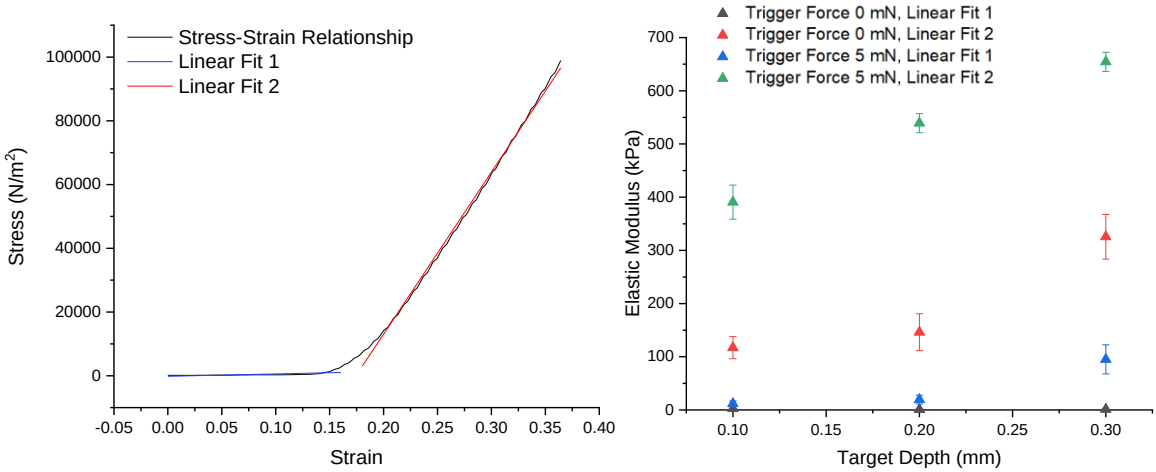

Figure 62. Stress-stain relationship analysed (left image). Graph on the right compares the effect of including a trigger force at 5 mN or at 0 mN.

Before explaining the results of this experiment, it is important to note how the stress-strain relationship looks quite different (to figure 60) following a change in either depth or trigger force. There are now two distinct regions. It is proposed that the first region, modelled by Linear Fit 1, is the elasticity of the sample but unlike the initial data in Figure 60 here there are no deviations away from a linear relationship. The second linear region on the graph (modelled by Linear Fit 2) is thought to be plastic deformation, with contributions from the glass substrate below.

By fitting a linear modelled in two places on the graph, Linear Fit 1 and 2, the difference in the obtained elastic modulus for the two regions can be quantitively. For an individual sample, such as figure 62, the elastic modulus for linear fit 1 is ~87 kPa whereas for linear fit 2 the elastic modulus is ~713 kPa. A value of >700 kPa is significantly harder than expected and is assumed to be a contribution from the glass substrate. Hence in this region it is assumed that the probe has travelled too far into the gel sample and is beginning to measure the glass substrate underneath. This observed is noticed across the data obtained using both 0 N and 5 mN trigger forces. The elastic moduli data for linear fit 1 is smaller than that of linear fit 2. It should also be noted that by increasing the trigger force to 5 mN the depth of indentation will therefore be smaller and may provide inflated elastic modulus values.

Indenting 0.3 mm into a relatively soft film of ~ 0.5 mm requires the probe to penetrate majority of the way through the sample and it is likely that some interference from the substrate below is included in the data, the glass substrate used below is harder and would have a significantly larger elastic modulus. If the probe travels to the point at

which the depth of indentation is affected by the substrate the moduli will be artificially larger. Instead, using contact mechanics proved to be a more appropriate means of examining the elastic modulus, where the depth of indentation is smaller. It is more likely the depth of indentation will be in the order of a hundredth to a tenth of a millimetre, which would be more suitable to gels of ~0.55 mm in thickness.

Summary of the elastic moduli:

Method	Elastic Modulus (kPa)	Standard Deviation (kPa)
Stress-Strain 0.1 mm 0 mN TF	7.03	1.17
Stress-Strain 0.2 mm 0 mN TF	55.53	17.42
Stress-Strain 0.3 mm 0 mN TF	46.32	12.02
Stress-Strain 0.1 mm 5 mN TF	14.21	2.40
Stress-Strain 0.2 mm 5 mN TF	28.41	11.11
Stress-Strain 0.3 mm 5 mN TF	94.32	22.35

Table 7. Summary of the elastic modulus values for the stress-strain relationship method with changing trigger forces.

In a contact mechanics approach a probe is lowered slowly to a surface and once it contacts the surface it begins to measure a load-force profile. Once a target force is achieved the probe continues to apply such as force for a known period before retracting. The point at which the force beings to measure the load-force relationship is known as the trigger force, this is set to 0 N so that it is the very first contact with a surface which triggers data recording. Whereas there is no equivalent value for when the probe retracts and hence data is recorded all the way to the position the probe rests at when it is not performing a measurement.

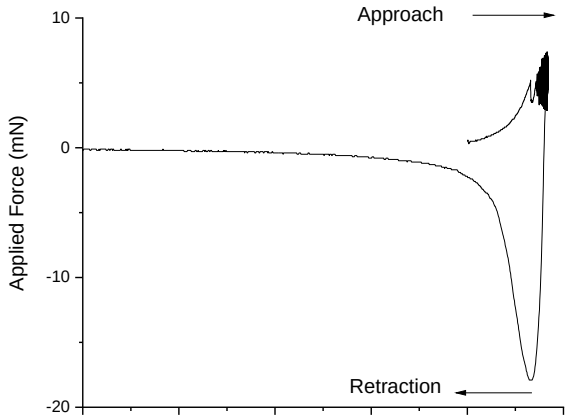

Figure 63. Force-distance graph as obtained from the mechanical tester. Showing the approach and retraction of the probe.

Initially three methods were proposed for extracting the depth of indentation from the load-force data these were:

1. Approach. This method looked at the data from the trigger force up until just before a period in which a target force has been achieved and is maintained for 30 s. The data in this section represent the probe making contact with a surface and beginning to indent, hence, being named approach.
2. Retraction. This method begins after the end of the 30 s period during which a known force is maintained. The retraction method begins from the point at which the probe begins to retract from the sample to the first point where the probe is no longer in contact with the sample.
3. Constant Force. Due to requiring some surface water to maintain a swollen state the exact point at which contact is made with the gel or when the probe leaves the gel can be hidden in the data by the interactions of the probe with the surrounding water. Therefore, the elastic modulus in this method is taken only from the 30 s period where the target force is maintained.

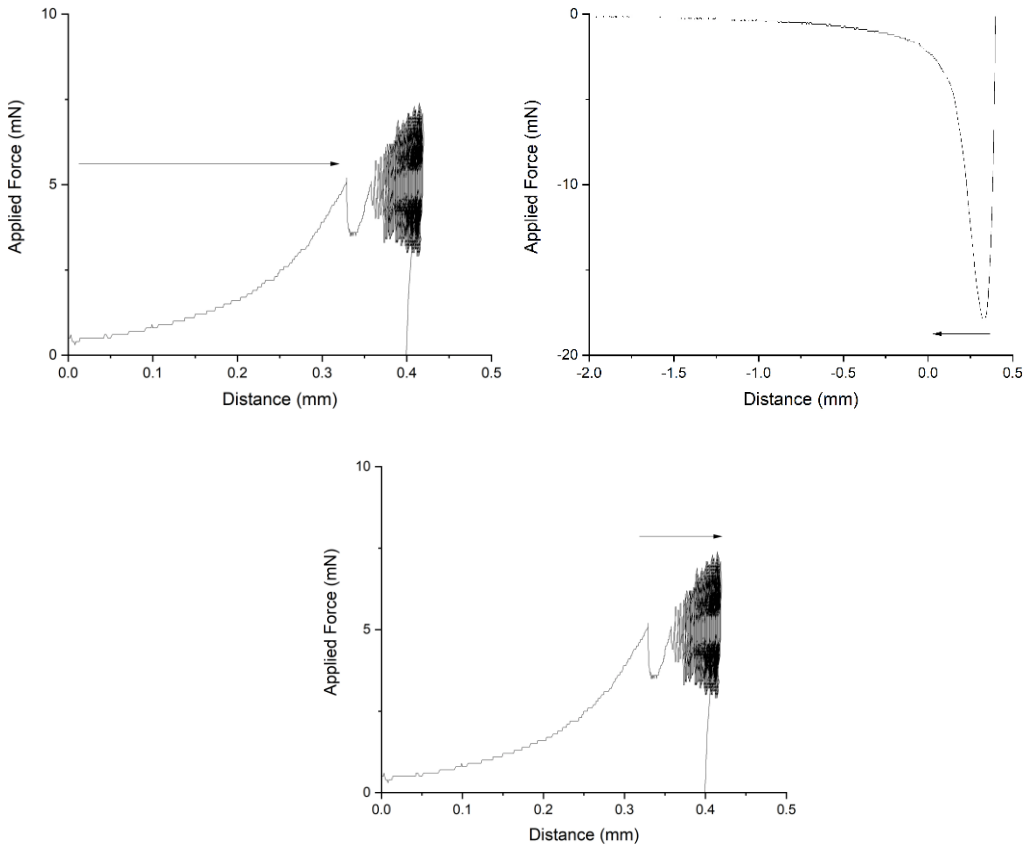

Figure 64. Showing the methods used for extracting where the contact with the scaffold may occur. Method 1 (top right) is the Approach method. Method 2 (top left) is the retraction method. Method 3 is the constant force method (bottom graph).

Before detailing the results of the methods, it is important to note that the methods use,

$$F_N(d) = 2E^* da, \qquad \text{Eq. 32}$$

in order calculate the elastic modulus. Eq 31 was derived from,

$$\frac{dF}{dh} = \frac{2}{\sqrt{\pi}} E^* \sqrt{2\pi r h + \pi r^2}, \qquad \text{Eq. 33}$$

a ratio of the change in force and depth of indentation. If the constant force model is applied here the change in force would become 0, meaning eq. 33 would no longer apply.

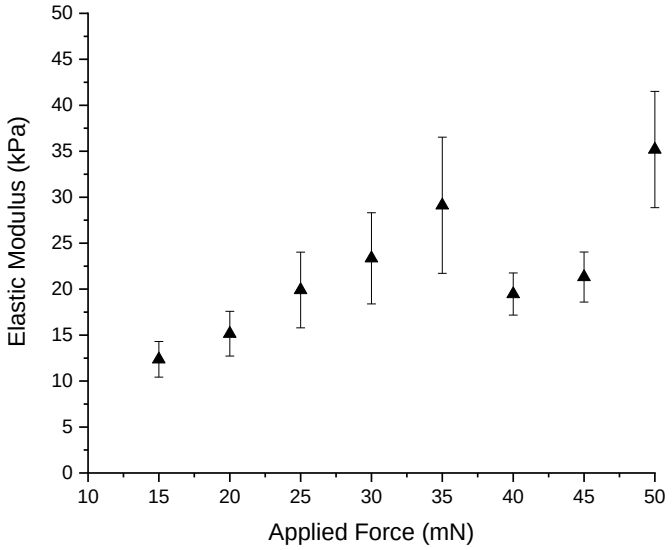

Figure 65. Elastic modulus using method 1 (approach).

The method for the elastic moduli calculated using the approach method are shown in figure 65. The elastic moduli here have been collected at a series of known applied forces, known as the target force, and the depth of indentation is measured between the trigger force and the point at which the target force is met. It is thought that the elastic modulus should not increase as the applied load is increased, because the depth of the indentation would increase accordingly. In the experimental data there is a slight increasing trend, where the average elastic moduli results increase with increasing applied force. However, there is no real difference between the data, with the error bars overlapping significantly, therefore the elastic moduli obtained under loads of 10-50 mN is constant.

In this method the point at which the probe makes first contact is clearly defined, however there is questions about what material the first contact is with. This data

measurement is triggered by contact with water or with contact with the sample. The sample was swollen, and any excess water was removed prior to the experiment to leave only a small amount of water to ensure the swollen state of the gel remains throughout the experiment. By removing as much excess water as possible without compromising the swollen state the likelihood of the data measurement being triggered by contact with the sample is increased.

Using method 1 (approach) the elastic modulus of the scaffold appears to be somewhere in the region of 10-30 kPa. For an applied load of 30 mN the elastic modulus is 23.36 ± 5 kPa. As mentioned in section 3.2.1 and section 7.1.4, the tissues which make up the spinal cord typically have elastic moduli in the range of 5-100 kPa, making this a good target range for the scaffold. Here, the scaffold has an elastic modulus of 10-30 kPa which puts it well into the target region.

Again, in the approach method the probe is lowered through any surface water into the sample, the surface tension of the water has enough force to tigger the data measurement and therefore it can be difficult to identify the exact point at which the probe begins to indent into the sample rather than pressing through the water prior to it. Method 2 (retraction) was proposed as a means of reducing this issue.

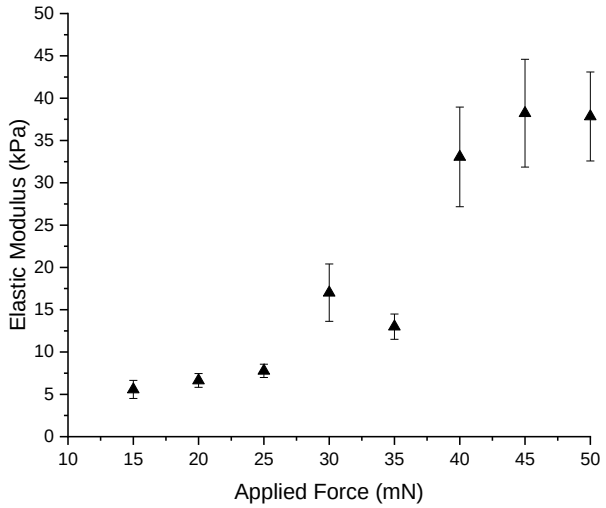

Figure 66. Elastic modulus using method 2 (retraction).

In the retraction method the depth of indentation is taken from the point at which the probe begins to retract (maximum distance travelled) to the point at which the probe lifts away from the hydrogel. Here, the elastic modulus appears to be relatively constant across loads of 15-35 mN. With the exception for the results at 30 mN the rest of the error bars within this range (15-35 mN) are relatively small, especially in comparison to

the approach method, suggesting the results are more precise. The elastic modulus in this range falls between 1-20 kPa, smaller than that of the elastic modulus obtained in the approach method. A smaller elastic modulus is typically the result of a larger indent, meaning the depth of indent identified over these loads is larger than the same indent identified in the approach method.

For loads of 40-55 mN the average elastic modulus is significantly increased, as are the error bars. The data in this region makes it hard to draw conclusive trends for the entire data set, the data for 15-35 mN can't be taken in isolation because the data in the latter half of the graph appear to disprove any proposed improvement in the preciseness of the data which may have been seen across 15-35 mN. Unfortunately, the data obtained in the retraction method do not appear to improve on the data which was obtained using the approach method. Although the point at which the probe begins to retract from the gel is clearly identifiable in the data, the point at which the probe leaves the gels surface is not as clear. This is because one the probe leaves the gel it still needs to travel through the small amount of water retained on the gels surface. The interaction between the water and probe still provides data measurements, and so the device is unable to distinguish between the gel and water. Therefore, the measurement continues until the probe returns to its starting point. The point at which the probe leaves the surface of the gel may be hidden in the data, becoming harder to identify and leading to similar issues with the approach method.

An advantage of the approach method is that the point at which the probe meets the surface of the gel is often easier to identify than the point at which the probe leaves the gels surface in the retraction method. This may account for a more constant average elastic modulus across all the loads tested. In the retraction method there are both small error bars and lager error bars, suggesting both large and small indentations have been interpreted from the data. If the retraction method was solely used the fluctuations in the size of the indentation may have been interpreted as fluctuations in the composition of the samples. Whereas when the approach, and the stress-strain methods, are included in the process it seems that the fluctuations are a matter of data interpretation, due to the apparent support the approach method and stress-stain method appear to provide each other.

The third method, constant force, was proposed because it looks only that the region where the probe is in contact with the sample, therefore no information is lost when the probe leaves or enters the samples surface via a small amount of water. Theoretically Eq

31 should not apply here because the force becomes constant, under constant force it is expected that the probe would cease to move. Given this information the left-hand-side of Eq 33 would become zero, hence Eq 32 would not be able to be derived.

However, experimentally there are small fluctuations in the force and the probe continues to move, therefore the equation was used. Although the equation was applied, the results should be taken with caution given the equation should not theoretically apply.

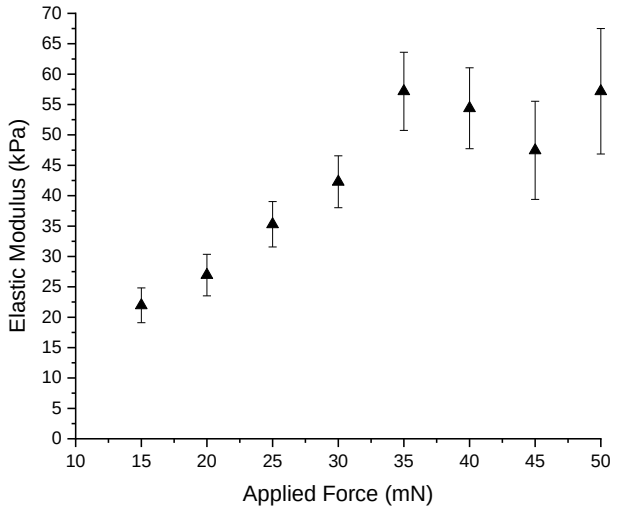

Figure 67. Elastic modulus by method 3 (constant force).

Although this method is affected by the inapplicability of Eq 32, it provides a means of comparison with the approach and retraction methods. What is particularly interesting in this method is there is no interaction of the probe with any surface water. The results of this method are like that of the approach and retraction method, particularly in the 15-30 mN region.

There is a slight increasing trend as applied force increases for the constant force method. This is suspected to be related to the substrate below the sample. In the constant force method, the gel is in its most compressed state and at this point there is an increased chance that the probe may begin to measure the substrate below the sample, hence the data includes a contribution from the substrate. This is most apparent at higher applied loads, where the sample has been compressed further. Such as at 50 mN where the large error bars include elastic moduli of >100 kPa due to contributions from the substrate. The data here are unaffected by the water which may affect the approach and retraction but since the data sets appear similar, particularly to the approach method, it suggests any adverse effects from the water are minimal.

A contact mechanics approach was compared with the stress-strain relationship, finding that there is some agreement about the elastic modulus of the sample using both approaches. However, each approach suffers its own issues. A stress-strain approach requires more of a significant indentation into a relatively soft material and therefore often includes significant contributions from the substrate. Whereas the approach and retraction methods both have contributions from the water (used to keep the sample swollen) and may have contributions from the substrate. Using a contact mechanics approach minimises such adverse contributions. Particularly in the case of the approach method where the measurement begins with includes first contact between the probe and ends with the probe reaching a target load, therefore this method has the smallest strain. A small strain is also key to minimising contributions from the substrate. This can also be achieved by using smaller loads, such as in the 15-30 mN range.

Table 8. Summary of the elastic modulus results.

Method	Elastic Modulus (kPa)	Standard Deviation (kPa)
Stress-Strain 0.1mm 0 mN TF	7.03	1.17
Stress-Strain 0.2mm 0 mN TF	100.38	35.85
Stress-Strain 0.3mm 0 mN TF	46.32	12.02
Stress-Strain 0.1mm 5 mN TF	14.21	2.40
Stress-Strain 0.2mm 5 mN TF	28.41	11.11
Stress-Strain 0.3mm 5 mN TF	94.32	22.35
Contact Mechanics: Approach 30 mN	23.36	24.80
Contact Mechanics: Retraction 30 mN	17.02	16.93

The elastic modulus of the scaffold using a contact mechanics approach is ~ 20 kPa at an applied force of 30 mN and ~ 46 kPa using the stress-strain relationship, which falls into the target region, mentioned earlier, of 5-100 kPa. This target region was proposed as a result of a literature study identifying the known elastic moduli of tissues in the spinal cord and of the elastic moduli of materials which are designed to be used as surrogate materials, summarised in Table 8.

Part. 3 Transducing PEDOT:GAG Films

Chapter 8. Bioelectronic Device Chemistry

8.1 Materials with Electronic Properties

Bioelectronic devices could provide a means of passing an electrical signal across an injury site where biological signals can no longer pass. These would bridge the gap in biological communication which result from injury to the local tissues. Such a device would be required to function in a similar means to the target tissue, which in this project is the spinal cord. Therefore, having an ability to mimic the action potential and signals which occur in the neural system is vital. A key parameter here is that the device must have an 'on' and 'off' state so that communications only occur, when necessary, similar to that which the action potential needs to reach a threshold value before transmission.[135, 152]

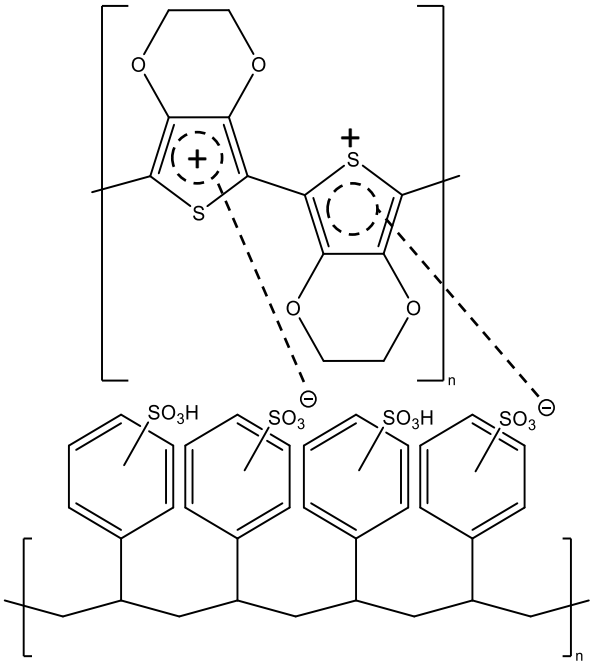

Figure 68. Interaction of PEDOT with PSS.

Organic electrochemical transistors (OECTs) display appropriate 'on' and 'off' states and are suitable for use in a liquid or wet environment, such is the body. OECTs comprise an electrolyte, organic electronic material or active layer and a substrate. The architecture of this device means that transduction can occur with both ionic and electronic currents, which makes it ideal for neurosynaptic transmission.[135, 146, 152, 282]

When a potential is applied to an OECT gate electrode, ions from the electrolyte diffuse into the active layer where they complex with the electronic material to change its doping state. Changing the doping state of the electronic polymer provides a means for controlling the conductivity of the device.[141, 146, 152, 282, 283]

8.1.1. PEDOT

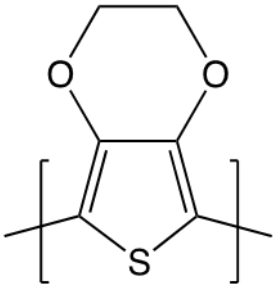

Figure 69. Chemical structure of PEDOT.

OECTs are frequently categorised as accumulation or depletion mode transistors.[284] The most common material used in a depletion mode transistor is poly(3,2-ethylenedioxythiophene) (PEDOT). PEDOT has conjugated π electrons in its backbone which provide its semiconductive ability. However, when PEDOT is synthesised from EDOT it is typically found in a doped state. In electrochemistry a doping agent is one which alters the oxidation state of PEDOT and similar conductive polymers. The doping agent is often found alongside another polymer or molecule which provides conductive enhancement.[285] The doping agent is commonly poly(styrene sulfonate) (PSS).[284, 286, 287] In its doped state PEDOT:PSS has a neutral net charge, where the anions from PSS are balanced by the positively charged holes in the backbone of PEDOT. When a positive potential is applied to the gate anions migrate towards the gate electrode and cations move into the active layer where they are attracted to the negatively charged PSS anions. The device would then be considered de-doped.[138, 283, 284, 286-288]

PEDOT has a relatively stable composition making it attractive for bioelectronic devices.[135, 286] Since 1995 different reports suggest that PEDOT shows promising properties when interfaced with neural tissue, although the long-term effects and tissue compatibility require further investigation.[289] The stability of PEDOT was examined as part of a PEDOT:PSS system; this system was polarised for 16 hours and electrochemical activity was compared to that of a polypyrrole:PSS system which had been treated the same way. It was found that 89% of the activity remained for a PEDOT

system compared to only 5% for the polypyrrole system. The stability of PEDOT makes it a useful material for implantable electrode devices.[289] It is this reason why PEDOT is considered as a better active layer material than polypyrrole.[290] There has been evidence of PEDOT:PSS systems stimulating cell growth on an implanted device, however the effects of PEDOT:PSS on the surrounding tissue are not known.[291]

Although a polymer like PEDOT provides fundamental chemistry to the device, the system is reliant on a doping charge from a secondary molecule. The properties of the polymer are somewhat reliant on the nature of the doping agent, and therefore this contributes to the overall performance of the material.

8.1.2. Poly(styrene sulfonate)

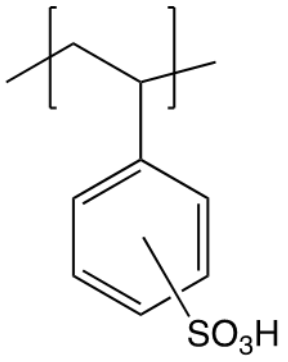

Figure 70. Chemical structure of poly(styrene sulfonate)

PSS was originally added to PEDOT to improve its ability to be handled in solution, PEDOT is insoluble in water and therefore by adding PSS, which is a surfactant, it can bridge the gap between the hydrophobic and hydrophilic states. Due to this commercial grade PEDOT:PSS became largely available as a suspension in water.[135, 285]

PEDOT:PSS is a flexible conductive material which can be used to from devices, suitable for many emerging technologies.[292] The systems have been found to have good conductivity, solution processability and the possibility to create devices with low cytotoxicity.[292-294] Therefore, they have been demonstrated in a number of different applications such as wearable devices, biosensors, drug delivery devices and as scaffolds for tissue engineering.[292, 295-297]

If prepared suitably PEDOT:PSS systems have been shown to have conductivities of up to 3000 S cm^{-1}. A common application of PEDOT:PSS is its use as a sensor, in these applications the system has been demonstrated with both OECT and electrolyte-gated organic field-effect transistor (EGOFET) architecture.[284, 298] An alcohol sensor was

developed by Bihar *et. al.* to be used as an alternative breathalyser. The PEDOT:PSS network was ink-jet printed to form electrodes on paper making a small and cheap device.[287] Here, PEDOT:PSS forms the electrodes rather than using metal electrodes such as in OECT or EGOFET architecture.[287, 298] The channel of this device consists of a collagen-based gel in which alcohol dehydrogenase and nicotinamide adenine dinucleotide are dispersed. In the presence of alcohol these compounds facilitate a reaction which forms acetaldehyde and electrons. The presence of these electrons changes the conductivity of the channel between source and drain, in this case the conductivity is decreased. By comparing the decrease in electrical activity to a calibration curve the extent of alcohol consumed can be extrapolated.[287]

More typically PEDOT:PSS is found in the channel itself rather than on the electrodes in transistor architecture. Another sensor application which involves the use of PEDOT:PSS in the channel is a glucose monitor. Here, glucose oxidase enzymes were used to convert glucose into gluconic acid and hydrogen peroxide. Hydrogen peroxide interacts with PEDOT:PSS changing its electrical activity, once again this can be compared with a calibration curve and the concentration of glucose determined.[299]

PEDOT:PSS has also been used in other applications, such as being used to record an electrocardiograph of a human heart. In this device a PEDOT:PSS channel is formed between gold contacts with OECT architecture and rests on a scaffold of poly(L-lactide-*co*-glycolic acid) (PLGA). This device is highly sensitive and is able to detect the small potential changes in the skin which occur when the heart beats. The introduction of PLGA provides a level of biocompatibility and biodegradability which wasn't accounted for in the previous two examples. A future application of this device could therefore look towards use in the body.[300]

The use of PEDOT:PSS in the body has raised questions about its long term biocompatibility and the potential effects it may have, especially on the brain. These concerns are raised due to the surfactant nature of PSS as well as polymer degradation into acidic products. In previous studies the ratio of PEDOT to PSS has been unequal, with more PSS than PEDOT, and due to excess SO_3H groups on the PSS backbone the environment of PEDOT:PSS tends to be acidic, with reported pH values of 3 or less. This pH is incompatible with physiological pH (7.4).[285, 286, 290, 301]

Although the *in vivo* and *in vitro* degradation of PEDOT:PSS is unknown, a study into the electrical activity following the degradation of PSS found that the acidic nature of

the derivative of PSS compromised the active layer and its ability to conduct.[302] To prevent deleterious effects on the performance of the device as it degrades, alternative doping agents have been suggested. A doping agent which has inherent biocompatibility would be ideal as it would enhance the ability of the device to be used for therapeutic applications.[303]

A literature study on the elastic properties of PEDOT:PSS reported elastic moduli in the gigapascal range, which fluctuated based on the humidity of the test environment. In the study thin films of PEDOT:PSS appear to become more brittle as the humidity increases. Tensile testing was used to measure the elastic modulus.[304] In this thesis compression testing was performed on the experimental samples (not on commercial PEDOT:PSS) which can yield different mechanical properties. The elastic modulus of a few different studies is reported in Table 9 for comparison.

Table 9. Summary of elastic modulus of PEDOT:PSS from literature.

Elastic Modulus (GPa)	Test Method	Comments
2.8 ± 0.50	Tensile	23% Humidity [304]
1.9 ± 0.02	Tensile	40% Humidity [304]
0.9 ± 0.20	Tensile	55% Humidity [304]
2.26 ± 0.05	Buckling	Theoretical Value 3.5 GPa [305]
1.10 ± 0.30	Tensile	Spun Microfibres [306]
2-3	AFM mapping	Higher regions of ~6 GPa [307]
2.6 ± 1.4	Tensile	Estimated [308]

The elastic moduli for the spinal cord is typically 5-100 kPa and therefore, the reported values for PEDOT:PSS are too firm for application to the spinal cord. Therefore, an alternative doping agent which can provide softer films would be more appropriate. A doping agent which can also function as a biocompatible scaffold would also be of use to provide mechanical properties similar to that of the spinal cord tissues.

PEDOT:PSS while flexible is typically too hard for use in a soft biological environment, it does not have desirable mechanical properties to be suitable to the spinal cord. Using a scaffold can minimise these properties. Recently, PEDOT has been doped with a number of different biomolecules, such as glycosaminoglycans (GAGs). This can be carried out via electro-polymerisation or by oxidative reactions.[309, 310]

8.2 Alternative Doping Agents

It has been proposed that there may be counter ions in the blood which may be capable of doping PEDOT.[290, 311] However, the conductivity of the PEDOT active layer is

partially reliant on the counter ion. It is important to consider the size of PEDOT and PSS, a small replacement ion would limit the conductive ability of the film and therefore a molecule of similar size to PSS would make the most appropriate counter ion.[135, 290, 311-313] Instead, the authors look towards larger molecules which are also present in the body such as GAGs. Heparin and hyaluronic acid are used as doping agents finding that they both result in films which are similar to PEDOT:PSS, and that a system of PEDOT:heparin displays similar electrical activity to that of PEDOT:PSS.[290, 311, 312] These systems have also been examined to understand their toxicity, finding that a PEDOT:GAG such as PEDOT:heparin showed no cytotoxicity when tested *in vitro* on both mice and human neuroblastoma cells. However, the *in vivo* effects of these compounds are not known.[290]

Various methods have been used to characterise PEDOT:GAG structures, such as FTIR and Raman spectroscopy. A network of PEDOT:HA in a scaffold composed of chitosan was successfully characterised using these methods, with the authors describing the device to have a 3D environment similar to the extracellular matrix rather than a planar geometry typically observed in a petri dish.[135, 226] Therefore, the possibility of the doping agent and the scaffold both being composed of material found naturally in the body was proposed.

Asplund *et. al.* electropolymerized PEDOT with different biomolecules, fibrinogen, hyaluronic acid and heparin. The three biomaterials are found naturally in the body and provide a good starting point to assess biocompatibility. The synthesis involves electropolymerising each of the three biomolecules on to platinum disks for known periods of time (100-2000 s) to provide films of different thickness. These films were then characterised using cyclic voltammetry (CV) and electrochemical impedance spectroscopy (EIS). PEDOT:fibrinogen was reported to be difficult to handled due to its adhesion to metal surfaces during polymerisation and led to films with poor electrical activity. However, PEDOT:HA and PEDOT:heparin had similar conductivities to that of PEDOT:PSS. Over the course of the experiment PEDOT:heparin was degrading but proved useful for producing a bioelectronic device with rapid biodegradability.[311, 314] The biocompatibility of the networks were also examined via standardised testing with cell lines, such as L929 fibroblast cells, and were coupled with the result from an *in vivo* study where PEDOT:heparin was implanted into the brain of rats. The results from both the studies showed similar results to that of a control (platinum was implanted into rat brains). Large immune responses were reported for both types of implants and these

were suspected to be due to disproportionate mechanical properties between the soft brain matter and hard implant. Therefore, there remain questions around the biocompatibility of the device, but the importance of appropriate mechanical properties is highlighted.[290, 311, 314]

Electrochemical polymerisation is a polymerisation process which results in the polymer being deposited onto a hard surface, such as a metal electrode. The mechanism itself occurs via oxidation of the monomer to form a positively charged radical species.[315] Films with a precise thickness can be applied using electrodeposition by controlling the potential at the electrode to which the film is applied.[135]

The properties of a film containing doped PEDOT are heavily reliant on the counterion and the arrangement of the polymer chains in the film itself. The polymerisation of PEDOT has been classified into three synthesis routes, one of which is electrochemical polymerisation, the other two are chemical polymerisation and transition metal-mediated coupling. Chemical polymerisation is the most popular route for polymerisation of PEDOT. There are many subgroups within the three main polymerisation categories, but within chemical polymerisation two methods are typically used: oxidative polymerisation and *in-situ* chemical polymerisation.[316] Oxidative polymerisation is the most promising route to synthesis on a large scale and therefore it is an essential starting point for small scale lab reactions.[317]

Oxidative polymerisation does not involve grafting a film onto hard electrodes, and also avoids carrying out *in-situ* reactions thereby allowing the development of a soft material in a laboratory environment.[316] The oxidant in the reaction is usually a metal ion which can easily be removed by common laboratory solvents such as ethanol. Iron-sulfonates were found to make ideal oxidants in the reaction, and it was this discovery, by Jonas *et. al.,* which lead to a breakthrough in the oxidative polymerisation of PEDOT.[316, 318-320] Dispersions of PEDOT and its doping agent could then be made by using the oxidant and EDOT in solvent. The reaction is also aided by the presence of an organic base, although the base acts as an inhibitor slowing the polymerisation of EDOT the altered pH results in PEDOT polymers which have better stability and conductivity. The conductivity of PEDOT is also linked to the temperature at which the polymerisation reaction is carried out.[316, 317]

Dispersions of PEDOT with a biomolecule doping agent have been created using various molecules such as DNA, cellulose, heparin, chondroitin sulfate and hyaluronic acid. The

synthesis of each is relatively similar, and involves dissolving the biomolecule and EDOT in water, followed by the addition of an oxidant, and a catalyst such as iron (III) sulfate. The exact parameters of each reaction vary, the temperature, pH and reaction time are largely affected by the chosen biomolecule.[317]

The overall aim for replacing PSS is to minimise the long-term negative health hazards posed by the acidic nature of PSS. Introducing PEDOT:biomolecule compounds are an important means of improving the biocompatibility. However, the long-term effects of these compounds remain unknown. In a 2017 study Mantione *et. al.* it was suggested that the longest known study on the biocompatibility of these compounds is a cytotoxicity test of PEDOT:dextran sulfate, lasting 96 hours with promising results.[317]

In another study by Mantione *et. al.*, PEDOT:GAGs were synthesised using an oxidative polymerisation method resulting in doped systems.[286, 317] These systems appeared to display no cytotoxicity and did not interfere with the normal functioning of the surrounding cells. Although there is a diversity of studies based around PEDOT:GAG complexes, such as PEDOT:HA and PEDOT:CS, there is very little on the use of these biomolecules as doping agents to PEDOT as part of a bioelectronic device.[286, 317]

While PEDOT and its doped forms have been extensively studied, finding that a system with PEDOT:CS or PEDOT:HA can display similar conductivities as PEDOT:PSS, there appears to be little research on designing a transistor like device out of them. Therefore, there is opportunity to explore their use in a bioelectronic device.

Chapter 9. PEDOT:Biomolecule Films

9.1 PEDOT:GAG Synthesis

Synthesising PEDOT:GAGs was carried out by D. Mantione *et. al.* reporting that compounds of PEDOT:CS and PEDOT:HA show no cytotoxic effects. They also carried biocompatibility assays on the compounds, testing them with cell lines SH-SY5Y and CCF-STTG1 finding the samples to be biocompatible and displaying signs of anti-inflammatory effects.[286]

The synthesis used by Mantione *et. al.* will form a basis for synthesising PEDOT:biomolecules in this thesis.[286]

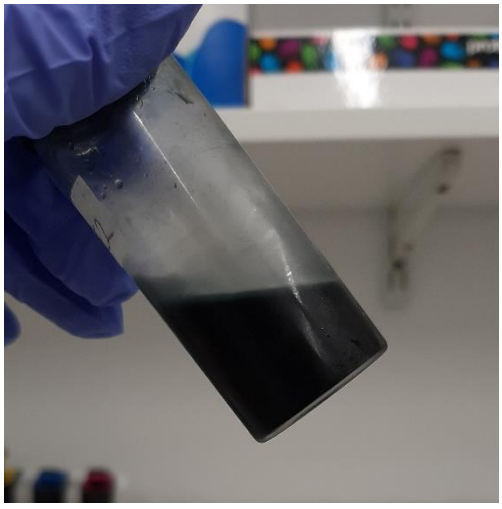

Figure 71. PEDOT:GAG suspension showing dark blue colour.

Mantione *et. al.* proposed that a solution containing 2% (wt/wt) of PEDOT:GAG was optimum and so this was used as a starting point for formulating the bioelectronic part of the device.[286] The polymerisation uses organic starting materials which are typically colourless, which is useful because the resulting complexes have a metallic nature and are often a dark blue colour, providing a distinctive colour change when the reaction is complete. Here, dispersions of PEDOT:CS were created using the methodology outlined by the authors. The reaction mixture starts off as a colourless solution, and has become a dark blue colour, almost black, by the end of the 48-hour reaction. The authors reported a similar colour change which occurred over 48 h, the same was observed here.[286]

A dispersion of PEDOT:HA was also created using the same methodology. This mixture also displayed the same observable colour change, suggesting the polymerisation had been successful. These solutions require application to an electrode to begin to

characterise their conductive abilities. The dispersions can be dropcast or spin coated. Some attempts were made to spin coat glass slides with films of PEDOT:HA however, the majority of the material is lost due to the centrifugal nature of the application. The samples should be dried under ambient or low temperatures to avoid forming pinholes in the film if the solvent is removed from the film too quickly by excessive heat. While this method is useful for producing films with a more consistent film thickness, the loss of material is not ideal. It means that PEDOT is lost and therefore reduces the chance that there are contact points between different PEDOT polymers, and when the number of contacts is reduced the chance that a current could be carried across the film is also reduced. The conductivity of the film relies on the proximity of PEDOT molecules.

PEDOT also needs to be applied to an electrode to carry out electrochemical analysis. Here, screen printed electrodes (SPEs) were used, which requires more precise application than can be achieved via spin coating. Therefore, dropcasting was used. Dropcasting also has some drawbacks due to are a lack of consistency in film thickness across different samples. This can be minimised by making sure the amount of material applied to each substrate is constant however the extent to which a drop spreads is not easily controlled and can result in films with differing thickness. Typically, a film cast by dropcasting is thicker than a film applied by spin coating and therefore the chance of a PEDOT network from one end of the film to the other is improved. There is evidence that dropcasting, does improve the conductivity ability of the films compared to spin coated ones.[321]

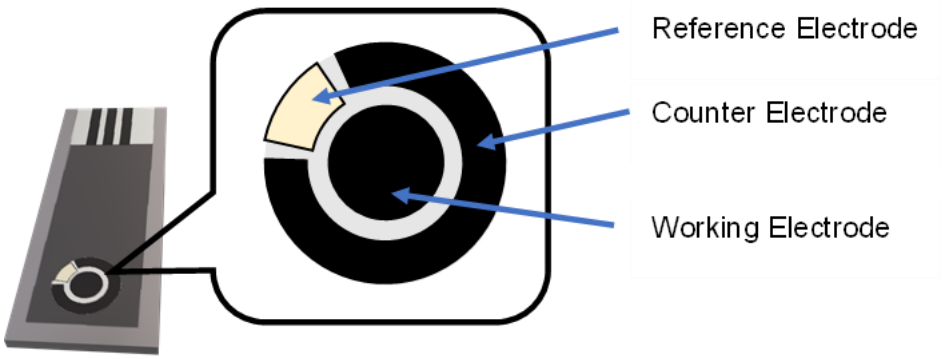

Figure 72. Image detailing the layer out of a screen printed electrode.

Figure 72 outlines where the working electrode can be found. This is the area which needs to be covered by the PEDOT dispersion. The dispersion can be applied here by dropcasting, ensuring that the sample does not touch the other electrodes, as this would interfere with the measurement. A drop of electrolyte is applied over all three electrodes,

this electrolyte is generally considered to be a salt which can maintain electrical conductivity throughout the system.

9.2 PEDOT:CS Characterisation

A means of characterising the dispersions was to carry out cyclic voltammetry (CV) on the samples to gain an idea of the conductivity and capacitance of the samples. CV monitors the redox chemistry occurring over a potential range. The working electrode is cycled through different potentials while the reference electrode is held at a constant potential, and this produces an excitation signal. A curve, typical of a CV, can be plotted based on the potential changes and the current at the working electrode.

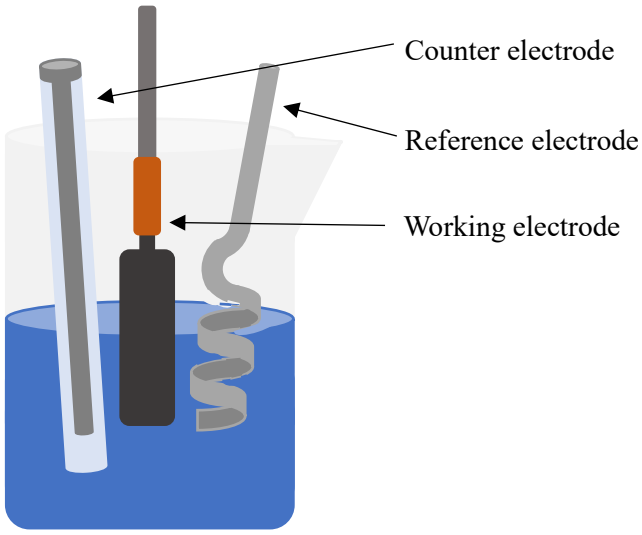

Figure 73. Image detailing the set-up of the electrodes for experiments such as CV and EIS.

The measurements are carried out by submerging each of the three electrodes in an electrolyte solution, ensuring that they don't touch each other. The sample is applied to an SPE and is lowered gently into the solution, making sure not to cause too much disruption to the SPE to prevent any loss of material into the solution.

In a CV experiment, the sample is submerged in an electrolyte. When a voltage is applied, an electrical double layer is expected to form om the sample. Double layer capacitance occurs at the interface of the electrolyte and the PEDOT:CS film. A layer of charged ions will form along the surface of the electrolyte where it meets the sample, and a layer of oppositely charged ions will form in the sample where it meets the electrolyte. The electrolyte has an important role in CV because it affects the peak position and its magnitude. Different electrolytes and differing concentrations of those

electrolytes can also affect the peaks. Therefore, an optimum electrolyte is required to produce reliable CV data from which further information can be drawn.

The initial CV tests were carried out using dispersions of PEDOT:CS, this was because the work of D. Mantione *et. al.* suggested that PEDOT:CS has better conductivity than dispersions of PEDOT:HA and it was therefore assumed it would be easier to adjust the CV to a sample which presents with a stronger signal.[286]

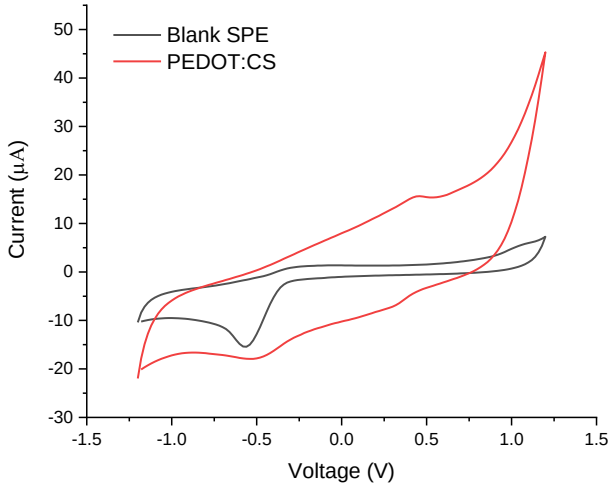

Figure 74. CV comparing a blank screen-printed electrode (SPE) with PEDOT:CS

To start off with the cyclic voltammetry experiments were carried out in an electrolyte solution of NaCl (0.1M) and an SPE was tested as a control which contained no experimental sample. The curve for this SPE is named 'blank SPE' in figure 74. Two of the most important features which can be learnt from a CV are the current and potential at which anodic and cathodic events occur. When the blank electrode is tested the redox activity of the electrolyte can be seen, showing that there is a reduction peak around -0.52 V which has an intensity of -15 µA. It is important to examine the CV of the electrolyte so that any peaks which occur can be assigned to either the electrolyte or the sample itself. When the dispersion is dropcast and dried to form a film on the working electrode, a CV can be measured of the sample and this is shown by the red line in figure 74. In this spectrum the reduction peak appears shifted to a slightly less negative voltage of -0.50 V suggesting this is due to events within the sample not only due to solvent and parasitic effects. A second small peak appears at 0.43 V, which is likely to be due to oxidation reactions occurring in the material. This second peak was not present in the spectrum for the blank electrode and therefore it is concluded that it is due to the PEDOT:CS sample. The reduction peak has a current of -17.9 µA and the

oxidation peak has a current of 15.6 µA, which are higher than the current observed for the blank SPE suggesting the sample is indeed conductive and aids current flow.

Another important feature in the CV is the breadth of the signal for the sample compared to the blank electrode. This can be identified by the distance between the forward and reverse sweeps. The breadth is seen by looking for a section of parallel lines for both sample and the blank electrode. The signal for the dispersion is significantly broader than it was for the blank SPE and suggests that when the PEDOT:CS sample is present, the system has increased capacitance, i.e., an increased capacity to store electrical charge. The ultimate aim of the work presented in this thesis is to produce an OECT, which transduces by potential changes at the gate electrode, hence changing its capacitance. Sensitivity to changes in capacitance is a measure of the performance of the device and so being able to characterise the capacitance of the device is important.[152]

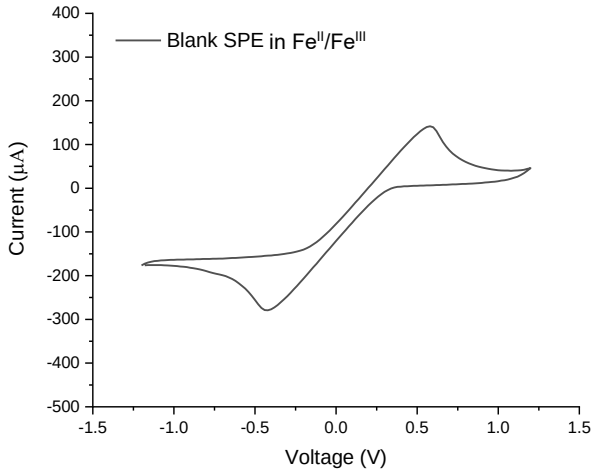

Figure 75. CV of a blank screen-printed electrode (SPE) after optimisation of the electrolyte. The electrolyte involves an Fe^{II}/Fe^{III} coupling.

The electrolyte in the first experiment was NaCl, this can be replaced by other solutions which contain a salt. Iron salt-based solutions make excellent electrolytes due to the redox capabilities of iron, where a solution containing both Fe^{2+} and Fe^{3+} acts as a reversible redox couple. A solution containing ferricyanide and ferrocyanide contains this redox couple and is often named ferri/ferrocyanide for short. This solution produces a CV which has a typical 'duck' shape. The CV of the blank SPE submerged in a ferri/ferrocyanide solution provides the graph in Figure 75, when the redox peaks can be seen at -0.42 V and at 0.59 V.

Using a ferri/ferrocyanide electrolyte enhances the redox peaks in the system therefore when the sample is added to the SPE the peaks should change either by shifting along the x-axis or by a larger flow of current through the sample. When the voltammogram for the sample is overlapped with the voltammogram for the blank SPE, any changes to the peaks can be seen, such is the case in Figure 76. The peaks have now shifted to -0.86 V and 0.90 V showing the redox ability of the sample itself differs from that of the electrolyte alone. The peaks are also at -437 and 291 µA, the breadth of the signal seen for the sample suggests the sample has a greater capacitance which suggests that the sample can store charges, typical of an electronic component alongside its ability to undergo redox reactions. However, the peaks are not well defined and appear broad. They are also very close to the voltage at which water is electrolysed and therefore this CV was not considered as optimised or considered for further study. It should be noted that the water here, (figure 76) is assumed to have a pH of 7 however this actual pH of water is dependent through the Nernst equation.

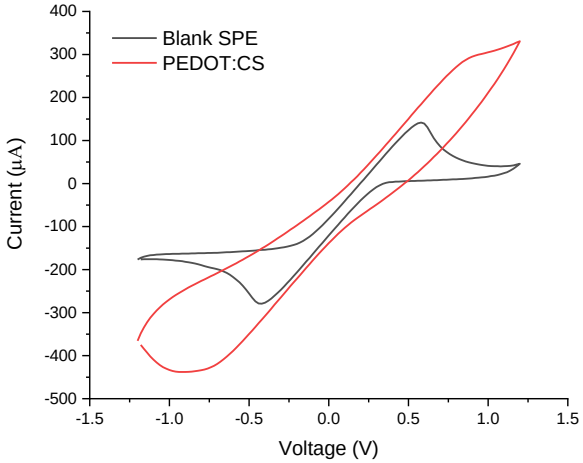

Figure 76. CV spectra for a blank SPE and PEDOT:CS carried out using a ferri/ferrocyanide electrolyte solution.

Before pursing with further characterisation to determine capacitance values, the CV need to be optimised to be reliable for further study. First, a relatively simple fix, the initial CV were carried out with a potential range of −1.25 to 1.25 V and at around 1 V water begins to undergo electrolysis therefore, any further CV should be carried out using a smaller voltage range which avoids the electrolysis of water occurring. The redox peaks are small, and the CV requires some tweaking in order to fully characterise the redox events occurring in the samples.

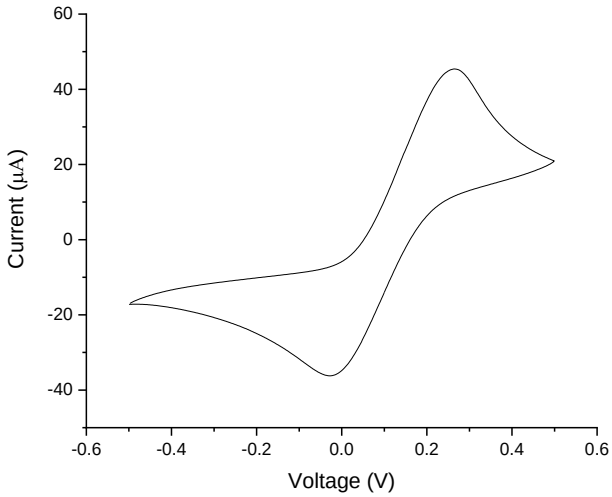

Figure 77. CV of a blank SPE after narrowing the voltage sweep window.

The parameters of the CV experiment were adjusted to stay within a region where the water in the electrolyte does not undergo electrolysis. The CV for the blank electrode was retested resulting in the spectra shown in Figure 77, here the voltage range was from −0.5 to 0.5 V. Following this the sample of PEDOT:CS was also tested.

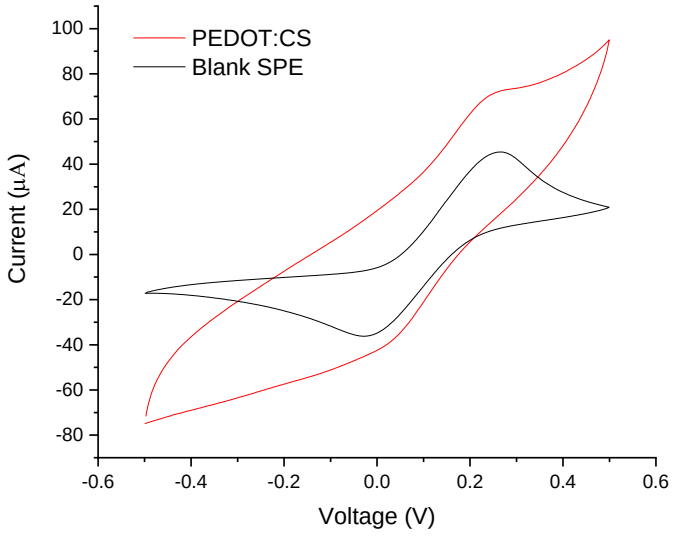

Figure 78. CV spectra for a blank SPE and PEDOT:CS following optimisation of the CV parameters.

The peaks present in the spectra for the CV of PEDOT:CS fall in almost the same place as they do in the spectra when only a blank SPE and the electrolyte are present. The peaks for the PEDOT:CS sample are at 0.03 and 0.25 V and for the control test the peaks are 0.02 and 0.26 V. The noticeable difference between the two spectra is the increased broadness of the sample of PEDOT:CS, suggesting the capacitance of the system has increased compared to the blank control SPE where no PEDOT:CS is present.

The capacitance of the double layer formed at the interface between the PEDOT:CS and electrolyte sample can be calculated from the CV data and provide a quantitative idea of the capacitance of the system. During CV the sample undergoes a voltage ramp, which leads to the generation of the double layer for a short time and therefore the capacitance is related by,

$$i_c = v \cdot C, \qquad \text{Eq. 34}$$

where, i_c is a steady-state capacitive current, v is the (potential) scan rate, and C is the capacitance of the system.[322, 323] The equation relies on the assumption that the system is an ideal capacitor and this must be considered when evaluating the reliability of capacitance calculated for the sample. Alternatively, an idea of the capacitance of the system can be determined from the relationship which relates the capacitance (C) to charge and mass,

$$C = \frac{Q}{V}.^{322, 323} \qquad \text{Eq. 35}$$

here, Q is the average charge occurring during redox or oxidation ramps, V is the potential across the sample. The charge can be obtained by integrating the peaks in the CV which results in a charge with units of coulombs. By carrying out the CV at multiple scan rates the capacitive current can also be identified by,

$$i_c = C \cdot \frac{dV}{dt} \qquad \text{Eq. 36}$$

relating the capacitance to the change in voltage per time (t). Multiple CV scans at different scan rates can be overlapped to obtain spectra which should how the direct relationship of the scan rate and conductive abilities of the film.[322, 323]

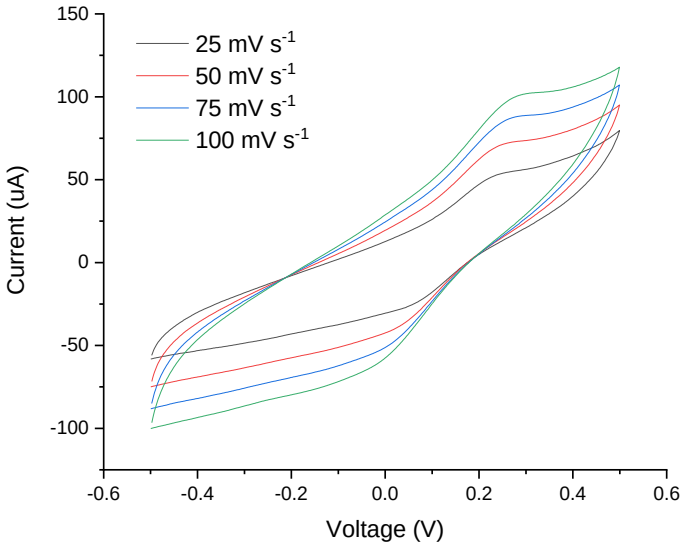

Figure 79. CV spectra for PEDOT:CS carried out over different scan rates.

This experiment can be repeated using multiple PEDOT:CS samples prepared using the same methodology and reaction conditions to obtain CV curves which can be integrated to find the average capacitance of the sample.

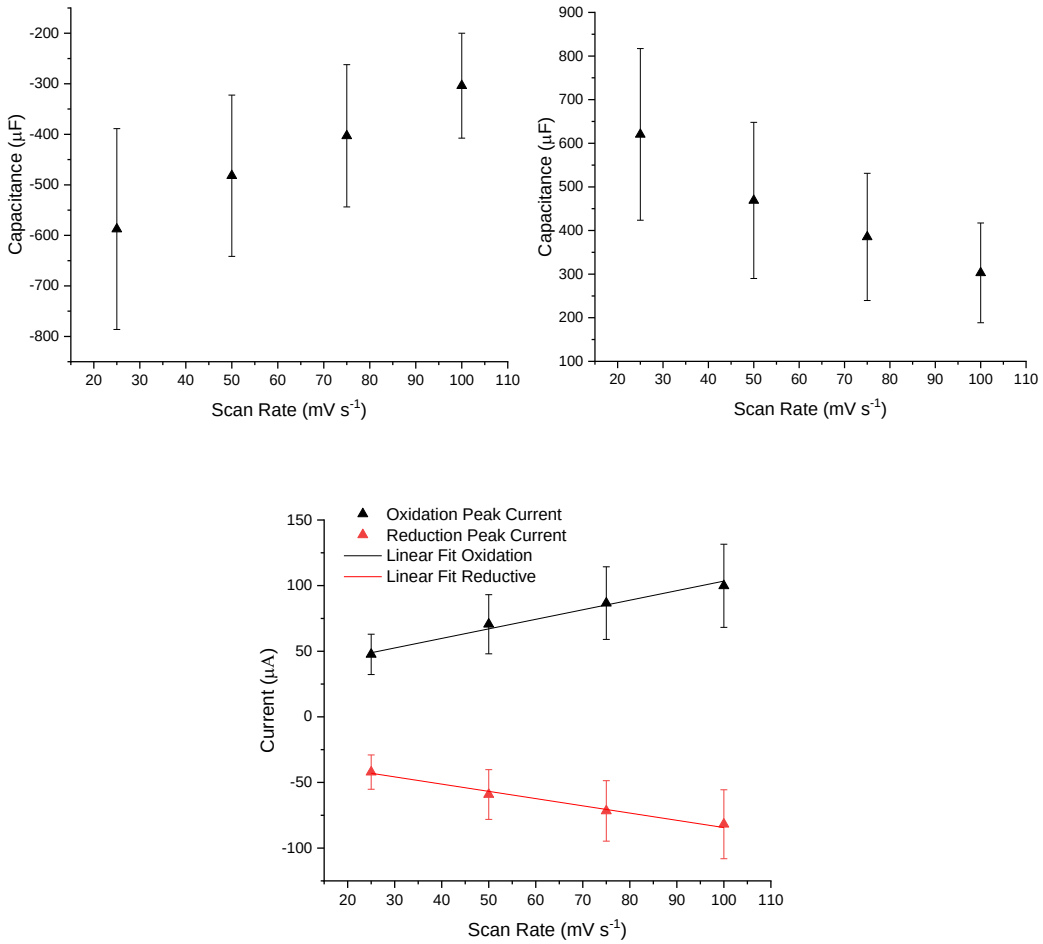

Figure 80. Top images detailing the relationship of the capacitance against scan rate dependent on the redox or oxidation peaks. Bottom image shows a summary of the upper two graphs.

As the scan rate increases the ability of the electrolyte to diffuse into the active material becomes inhibited and the capacitance of the system decreases.[324] Therefore, at lower scan rates the experimental capacitance could be considered to be the closer to the true value for the capacitance for the sample. At 25 mV/s the redox peak has a capacitance of 0.6 ± 0.2 mF. The error on the mean across this data set is large, suggesting a significant variation in capacitance across the samples. It should be noted that although the oxidation and reduction peak currents behave monotonically with scan rate the relationship is not proportional. A linear relationship implies proportionality, which in turn implies that not only are the redox events controlled by diffusion but would in fact confirm the presence of electroactivity in the film.

There are multiple possible explanations for the variation in the capacitance across multiple samples. The first of which could be related to the adhesion of the film to the electrode. Secondly, the arrangement of the polymers in the film may not form a clear conductive path from source to drain. There may also be an issue with the conductive ability of the film, and this needs to be addressed by changing the chemistry of the gel. To assess whether reformulation is required it was first necessary to optimise the CV, followed by further characterisation of the film by more informative characterisation methods, such as electrochemical impedance spectroscopy (EIS). The results from the two methods can be used to determine how the material should be changed.

Each of these reasons will be investigated in turn in the following sections.

9.2.1. CV Using Drop Sense Technology

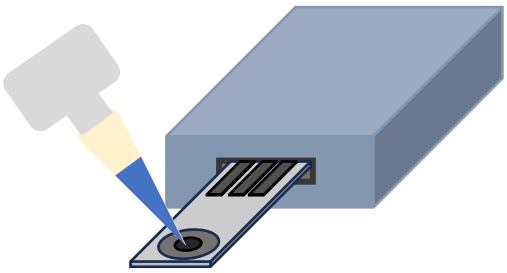

Figure 81. Image detailing where the experimental samples are applied to an SPE and how the SPE connects to the drop sense.

In the previous CV experiments, PEDOT:CS was dropcast to an SPE which is then submerged vertically into a solution of electrolyte. However, the PEDOT:CS film appears to have poor adhesion properties with the SPE and when it is submerged it begins to flake off into the electrolyte, where due to its density it sinks to the bottom. CV can be carried out before all the material is removed from the SPE, but the changing

mass over the cycles effects the reliability of the results. An alternative method was proposed for carrying out the CV which involves using drop sense technology. Here, the SPE is used horizontally as shown in Figure 81. Again, the sample is dropcast to the SPE and left to dry, once a dry film is formed the SPE is connected to the drop sensor and a drop of electrolyte is added to cover each of the three electrodes on the SPE, including the sample itself. Since the SPE is now used horizontally if the material delaminates from the electrode, it is unable to fall into the surrounding solution and will simply remain on the electrode however, with poorer contact.

The results from the dropcast sample had peaks at different potentials than those seen in the CV experiments carried out with a more traditional step-up. Here the peaks appear to occur around 0.05 and 0.50 V and shift with increasing scan rate. Whereas, in previous experiments the peaks occurred around 0.02 and 0.25 V.

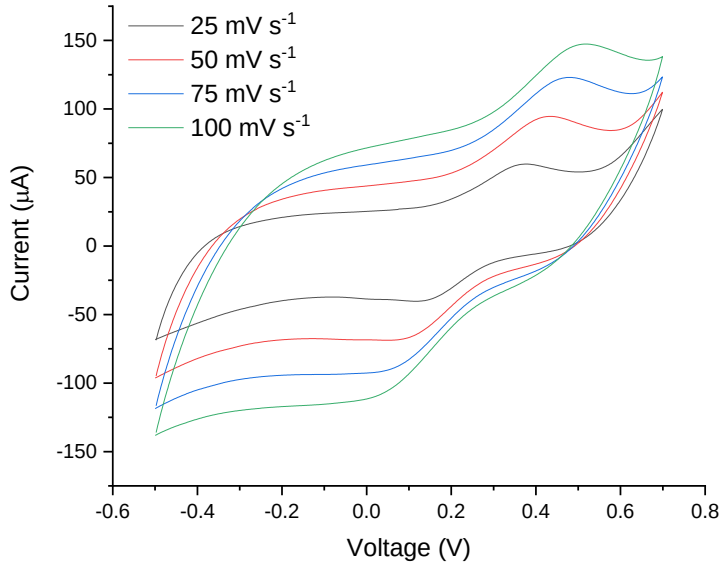

Figure 82. CV of PEDOT:CS after introducing the drop sense technology

9.3 Physical Properties of a PEDOT:GAG Film

A concern with the film of PEDOT:CS is that there is no continuous conductive path formed through the substrate. There may be cracks in the film which break the flow of electrons reducing the conductivity ability of some films more than others. There may also be a section in the material where there is no path formed between PEDOT chains, where the chains are further apart and the flow of electrons in inhibited. By applying more material to the electrodes, to form thicker films, the chances of forming continuous paths of PEDOT from source to drain are increased by increasing the amount of PEDOT which remains once the film dries. The thickness of the dry dropcast films was monitored by optical microscope. It should be noted that the increasing the concentration is also a route to improving the chances of a conducting path.

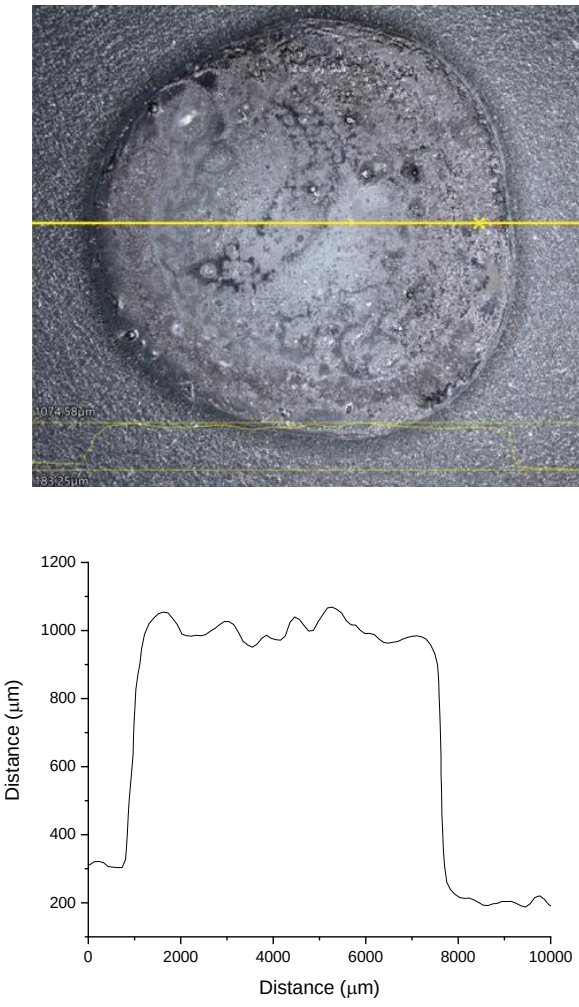

Figure 83. Upper image shows the microscope image of the dehydrated PEDOT:CS film. The lower image shows the depth profile of the same film.

The dropcast films have an average thickness of ~ 1 mm to maximise the conductive pathways through the sample. It should be noted that the samples examined under a microscope were applied to glass slides rather than SPEs. This was to ensure there was enough contrast between the dark coloured samples and the substrate below so that the software for the 3D scan can sufficiently distinguish between the substrate and the sample. Whereas the colour of the sample and the SPE are similar and do not provide enough distinction.

A second way to check that there are conductive paths between the samples was to dropcast the film onto a channel between a source and drain and test the potential.

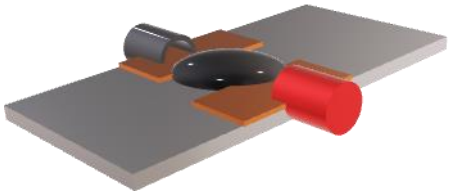

Figure 84. Image detailing how the suspension can be applied over two copper contacts. Crocodile clips can be attached to the contacts to connect a multimeter.

Using a multimeter, the resistance across the channel was measured giving an average of 0.35 ± 0.06 MΩ, which becomes 0.28 ± 0.09 MΩ when water is applied to the channel to swell the film of PEDOT:CS. Here, the error on the mean is small suggesting that there is little variation in the resistance of the film in each of the places it was measured. For a current to pass through the film there needs to be a continuous conductive path between the source and drain, and while this is not expected to be perfect the hope is that there are enough overlapping polymers for a pathway to be formed. Since the error on the mean is small it is believed that the film is fairly homogenous. If the error on the mean were large it would be concluded that there are areas in the film which are much more resistant and so the film would be more heterogenous and may not have as many occurrences of polymer crossover to form a continuous pathway.

A control was also carried out where the same set up was used with no sample applied to the channel. The same amount of water used to swell the samples was still applied over the channel to function as an electrolyte in a similar manner to the measurements of samples, giving a resistance of 2.42 ± 0.02 MΩ. The control sample also had a capacitance of 11.62 ± 0.55 nF, showing that ionic conductivity also occurs via the electrolyte itself.

When forming the hydrogel scaffold, crosslinks played a key role in the physical properties of the scaffold. With PEDOT:CS the physical properties of the film have been questioned, particularly when the sample was submerged vertically in solution, the film began disintegrating. Crosslinking could improve the properties of the PEDOT:GAG films in the same way which the improved the properties of the hyaluronic acid scaffold.

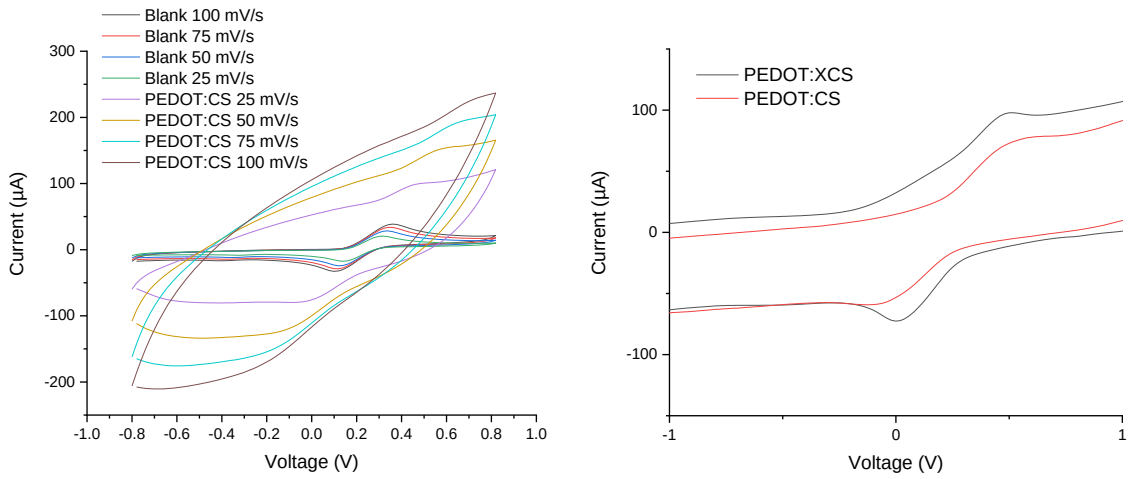

Figure 85. CV showing the effect of crosslinking. The image graph on left-hand-side shows CV of crosslinked PEDOT:CS and a blank SPE at different scan rates. The graph on the right-hand-side shows the impact crosslinking has on the redox and oxidation peaks looking only at the CV at 25 mV/s.

EDC was introduced to the reaction prior to the polymerisation of EDOT to form crosslinks between the CS chains. The results of adding the crosslinks to film provided promising results. The CV no longer had a typical 'duck' shape which it had for the blank electrode, but instead the CV curves were significantly broader and any peaks in the spectra much less well defined. Here, the CV would be considered to have more of the shape expected for a sample containing PEDOT with peaks around 0.40 and -0.05 V, which are better distinguished at slower scan rates. By comparing the CV curves of the crosslinked and uncrosslinked samples, any improvements made by crosslinking can be identified. The peak in the CV for the crosslinked sample is better defined and is at a higher current which would imply that the capacity in the crosslinked sample has improved. Therefore, it is proposed that the crosslinks improved the film properties and should be included in each sample. However, the sample continued to disintegrate with time and so PEDOT:HA was proposed as an alternative material since HA demonstrated superior performance than CS when crosslinked with EDC/NHS.

When CS was used to form scaffolds there were persistent issues due to the poor physical properties of the film. It was difficult to form a film of CS with and without crosslinks

due to the solubility of the film. However, crosslinks provide limited improvement in a system with PEDOT. Changing to hyaluronic acid (HA) provided scaffolds with improved physical properties, especially when the polymer was crosslinked in the presence of EDC and NHS. Therefore, the first step to improving the physical properties of the PEDOT:GAG film was to look into changing PEDOT:CS to PEDOT:HA. The methodology used to form PEDOT:CS was repeated but exchanged CS for HA.

9.4 PEDOT:HA as a Conductive Material

First the CV for a film of uncrosslinked PEDOT:HA was compared with the uncrosslinked PEDOT:CS.

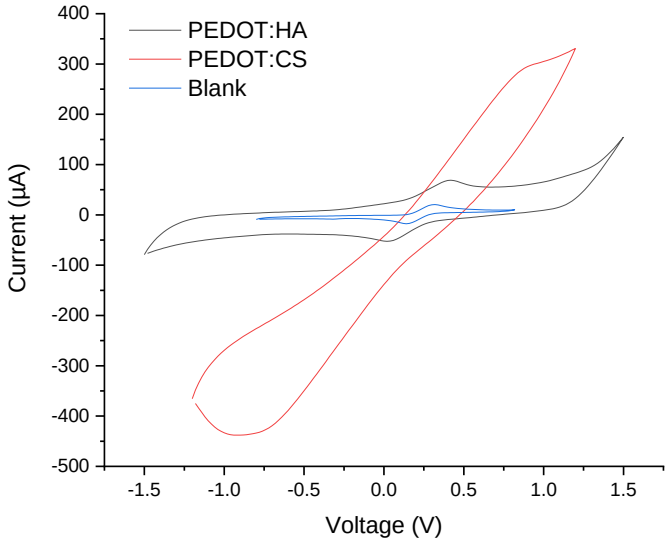

Figure 86. CV comparing a blank SPE, PEDOT:CS and crosslinked PEDOT:CS.

The CV curves for PEDOT:HA are less broad than they are for PEDOT:CS suggesting the capacitance of the PEDOT:HA films is smaller. The oval shape which begins to from in the spectra for PEDOT:CS is often referred to as having rectangular shape when this shape at is at its most extreme. The more rectangular the CV curve the stronger the double layer capacitance is assumed to be. Therefore, the different shape in PEDOT:HA suggests a reduction in the double layer. The shape of the PEDOT:HA curve is similar to that of the blank electrode, but while it is less broad than the PEDOT:CS plot, it continues to be broader than the blank electrode suggesting that the PEDOT:HA does in fact improve the conductivity of the device.

Since PEDOT:HA appears to demonstrate conductive abilities the films were crosslinked using the same methodology as was used for crosslinked PEDOT:CS. The dispersion was then dropcast onto SPEs to be characterised via CV using the drop sense method.

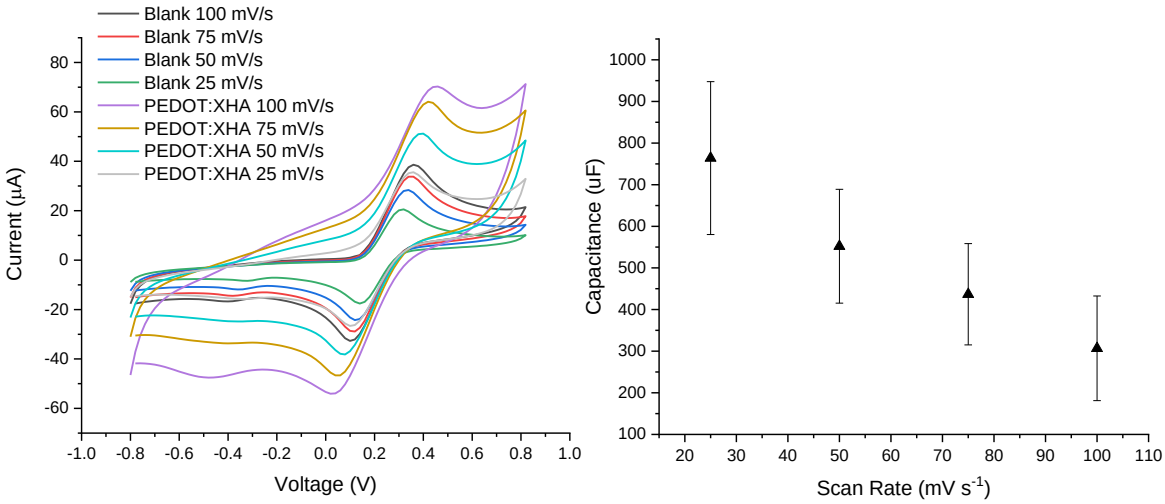

Figure 87. The graph on the left shows the CV of a blank SPE and crosslinked PEDOT:HA. The graph on the left shows the relationship between capacitance and scan rate for the crosslinked PEDOT:HA sample

The crosslinked PEDOT:HA films appear to have better capacitive properties than the blank electrodes due to the apparent broadening of the CV curves, although, the spectra for the crosslinked PEDOT:HA at 25 mV/s overlapped with the blank electrode at 100 mV/s. This overlap can be attributed to the speed at which the CV was carried out, as the scan rate increases the CV curves are expected to broaden because the diffusion of ions into the active material becomes poorer. This effect is demonstrated by the decreasing capacitive trend, shown in Figure 87 as scan rate increases.

Rather than compare between the original experiment and the drop sense experiments all subsequent experiments were carried out using the drop sense technology as it limits potential disruption to the sample during testing. PEDOT:PSS can be considered a gold standard here, because it has been widely applied in various studies and therefore it was used to gain an understanding of the performance and conductivity characteristics that the samples in described in this project should display. A dispersion of PEDOT:PSS was created by agitating a solid of PEDOT:PSS in water, where PEDOT:PSS was bought and is readily available. A comparison of PEDOT:HA and PEDOT:PSS will be used as a means of determining how alternative doping agents perform.

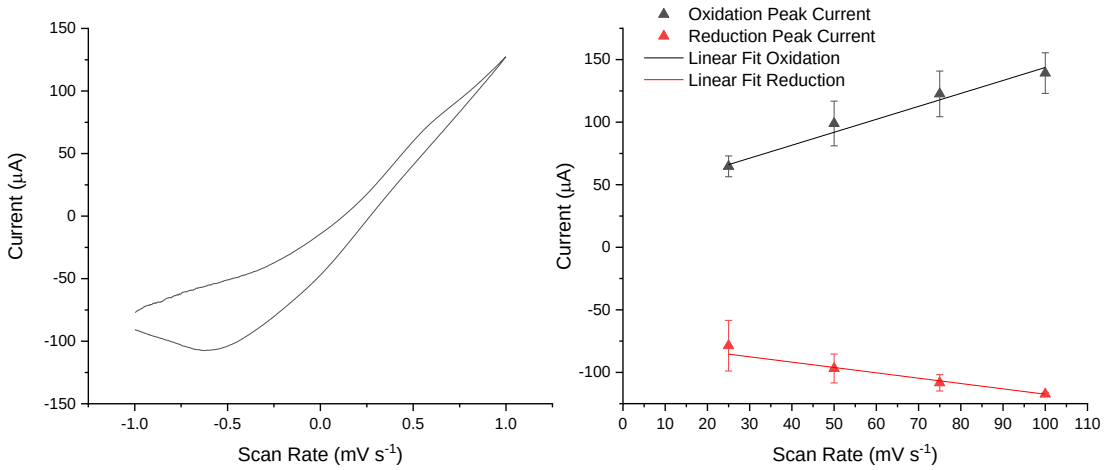

Figure 88. The CV on the left is of PEDOT:PSS and the graph on the right compares the redox and oxidation peak currents against scan rate.

The CV for PEDOT:PSS has a shape which would be expected of a capacitive material, where the redox peaks are much less definable. The Randles-Sevcik equation provides a means of quantifying the diffusion coefficient (D) and can provide information about how the film conducts. The Randles-Sevcik related the scan rate (v) to the peak current (i_p),

$$i_p = 0.4463nFAC\,(\frac{nFvD}{RT})^{1/2}, \qquad \text{Eq. 37}$$

where F is the Faraday constant, A is the area of the electrode, C is the concentration of the electrolyte, R is the gas constant and T is the absolute temperature.[322, 325] However, when the experiment is carried out in solution at 25 °C the equation becomes,

$$i_p = 2.69 \times 10^5 \cdot n^{3/2} \cdot AC\sqrt{Dv}. \qquad \text{Eq. 38}$$

The equation can then be rearranged to find the diffusion coefficient,

$$D = \sqrt{\frac{i_p}{(2.69 \times 10^5) \cdot ACn^{-3/2}v^{1/2}}}.^{322, 323} \qquad \text{Eq. 39}$$

An increasing diffusion coefficient suggests that one material can more rapidly diffuse through another, therefore in terms of the CV here, this would suggest increased diffusion in the analyte.

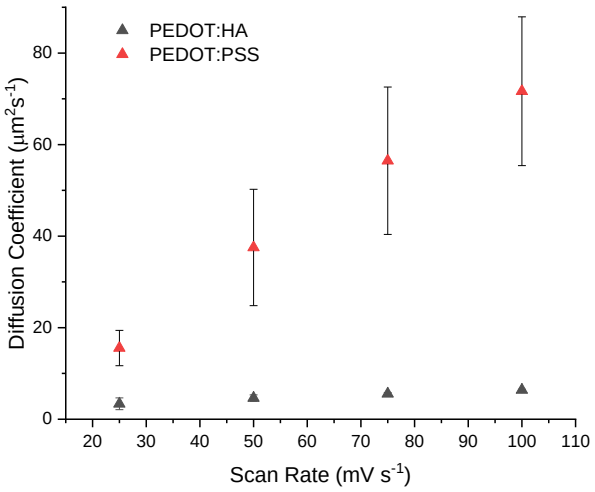

Figure 89. A graph comparing the diffusion coefficients of PEDOT:HA and PEDOT:PSS

At a scan rate of 25 mV/s the diffusion coefficient for crosslinked PEDOT:HA films was 3.37 $\mu m^2 s^{-1}$ whereas for PEDOT:PSS the coefficient was 15.56 $\mu m^2 s^{-1}$. The higher the diffusion coefficient the faster diffusion occurs through the analyte, therefore in the case of PEDOT:PSS diffusion is occurring more rapidly through the film than it does in PEDOT:HA. Therefore, according to CV, PEDOT:HA does not conduct as well as PEDOT:PSS. However, to confirm this, EIS, which can be considered a 'gold standard' when it comes to modelling capacitance, was performed.

Electrochemical impedance spectroscopy (EIS) involves using an electrochemical cell to which an excitation is applied. If this signal is sinusoidal, an AC current signal results, which can be analysed as a Fourier series. EIS data are most frequently represented in a Nyquist plot. The equation which represents the impedance is represented,

$$Z_{(\omega)} = \frac{E}{I} = Z_0 e^{j\phi} = Z_0(\cos\phi + \mathrm{j}\sin\phi).^{326} \qquad \text{Eq. 40}$$

Equation 39 involves both real and imaginary components, plotting the imaginary part on the y-axis and the real part on the x-axis results in a Nyquist plot. Theoretically Nyquist plots form a shape which comprise several semicircles; experimentally, however, the data are often limited to one semicircle. The data from the Nyquist plot can be fitted to an appropriate circuit model to draw quantitative conclusions from it.

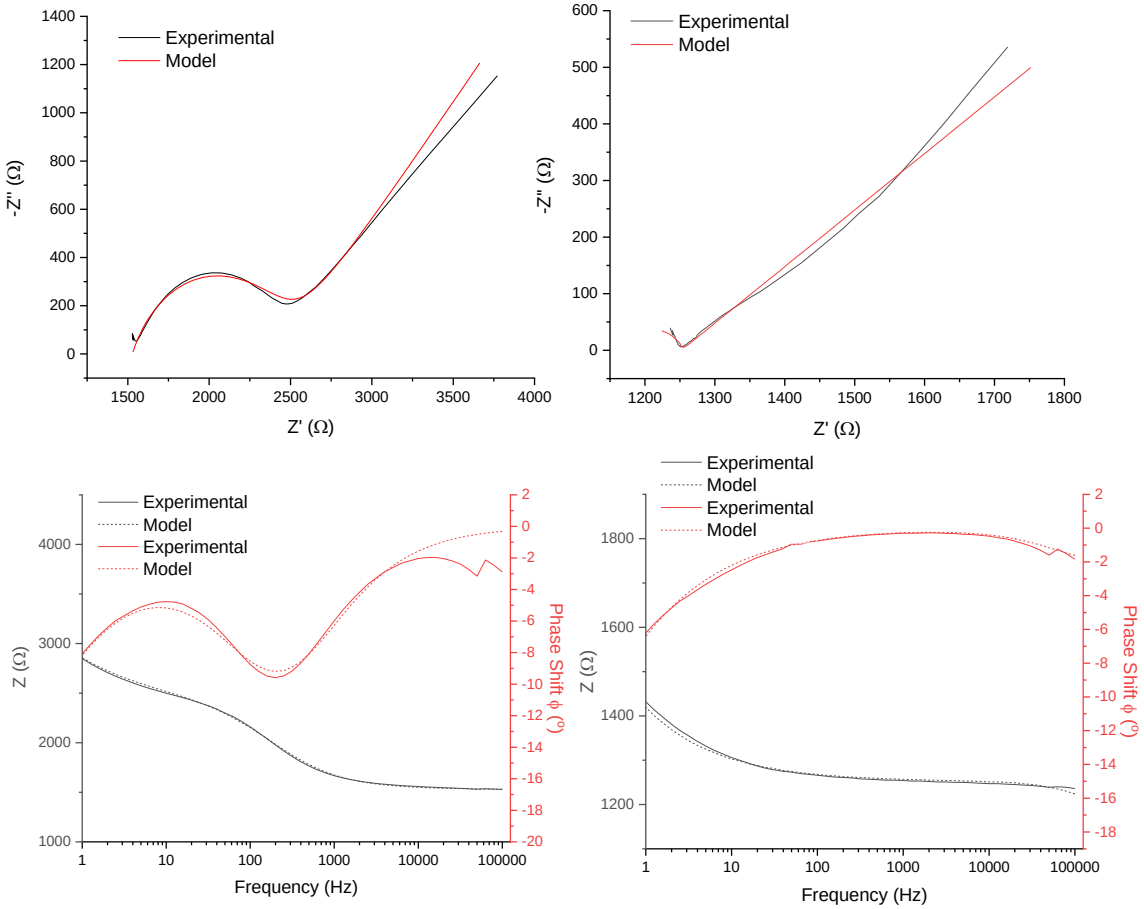

Figure 90. Nyquist (top) and Bode (bottom) plots for PEDOT:HA (left) and PEDOT:PSS (right)

Samples of PEDOT:HA were dropcast on to SPE in the same way as they were for the CV experiments, and the dropsense device was also used to be able to perform horizontal EIS measurements in electrolyte. The resultant EIS can be seen in figure 90. The shape of the EIS was almost as expected. Typically, a perfect capacitor has a Nyquist plot which is linear and at 90° to the x-axis. For non-perfect capacitors, such as PEDOT, this line is often angled, capacitive materials have an EIS which extends to low frequencies and this can be seen for the PEDOT:HA sample shown in Figure 90.[327, 328] The blank electrode has a similar EIS shape to what would be expected when the material is not a capacitor, however this semi-circle shape is a familiar sight in impedance spectroscopy and may initial come across as an 'ideal' shape therefore care must be taken to make sure not to confuse the characteristics of a capacitive material with another. When compared to the EIS of capacitive materials such as PEDOT:PSS the required shape of the curve can be identified. Although the Nyquist plot for PEDOT:HA here, demonstrates the target shape, it also displays redox events. The exact capacitive nature

of the film can be quantitatively examined by modelling with a circuit. These circuits are based on a Randles equation and can be adapted to suit the shape of the curve, the model which fits the experimental data best it a circuit which contains a CPE and a Warburg element both of which will be explained in the following section. However, since it is important to use a model which has a good fit to the experimental data it is necessary to examine the extent to which other models fit the data too.

A Randles circuit is based on an example where an electrode is submerged in an electrolyte forming an ionic resistance (R_u) and a double layer capacitance (C_{dl}). The Randles circuit also involves a second resistor, this occurs in parallel when a faradaic reaction also occurs in the film, resulting in charge transfer resistance (R_p).[326]

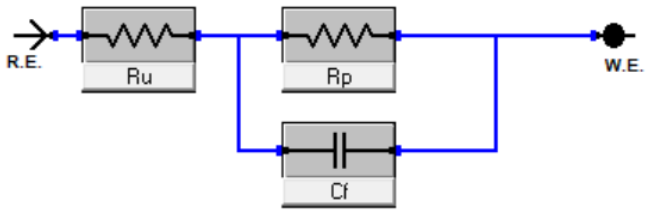

Figure 91. Detailing the components of a Randles circuit.

The model to fit the Nyquist plot comprises different circuit elements such as a capacitor or a resistor. The most basic circuit which can be applied to the EIS data is a Randles circuit which is made up of a resistor and capacitor in parallel, as shown in Figure 91.

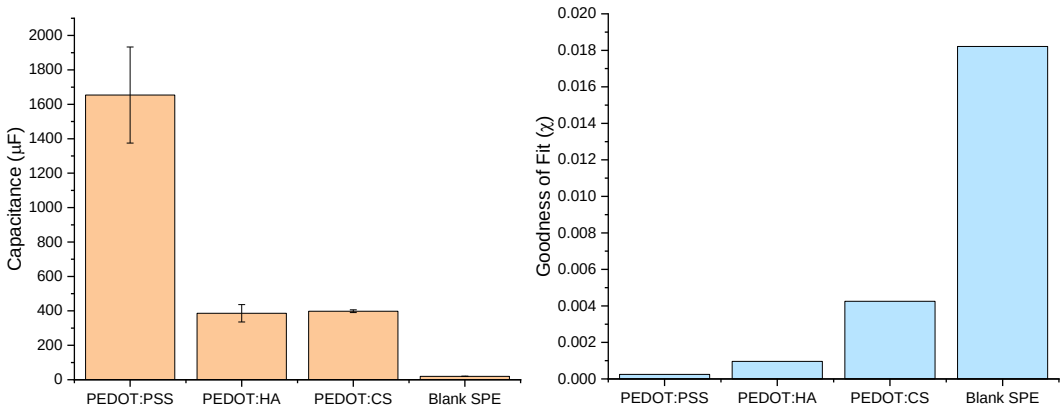

Figure 92. Graphs comparing samples of PEDOT:PSS, PEDOT:HA, PEDOT:CS and a blank SPE in terms of their capacitance and the goodness of fit of the model to the EIS data using a Randles circuit.

Using a Randles circuit to fit the data shows that the commercially available PEDOT:PSS has a larger capacitance than the experimental PEDOT:HA and PEDOT:CS samples which have been mentioned so far in this project. The capacitance of

PEDOT:PSS was ~1650 μF whereas the samples of PEDOT:HA and PEDOT:CS both have a capacitance ~385 μF. Once again there was issues with adhesion of the film to the SPE and therefore it is believed that improving the physical properties of the samples could improve the capacitance results by nature of providing better EIS. It is important that the model fits the experimental data well, and this can be monitored quantitatively by looking at the χ^2 value denoted when the model is applied to the data, this value is a measure of fit, it details the goodness of fit of the model to the raw data. A model with is deemed to be a good fit should have a χ value in the order of 1^{-4}. The only sample which had a goodness of fit in this order is the PEODT:PSS sample, which has a goodness of fit of ~2×10^{-4}. The PEDOT:HA and PEDOT:CS samples have goodness' of fit in the order of ~9×10^{-3}, which suggests other models could be more appropriate. Lastly, the blank SPE has a very poor goodness of fit ~ 0.02 and therefore this model is not suitable to this experiment. Therefore, other circuits should be applied to these samples.

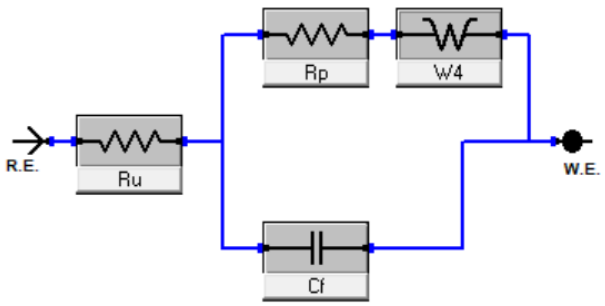

Figure 93. Randles circuit including a Warburg element.

As seen in Figure 90, the EIS for the PEDOT:HA samples form a more linear shape than the curve which appears for the blank SPE. This linear shape is often linked to a component known as the Warburg element, known for its distinguishable 45° linear slope which appears in the Nyquist plot. The Warburg element is a diffusion resistant element and, in this circuit, it is placed in with R_p. It is important to note that assumptions are made about concerning the faradaic reactions being controlled by reactants diffusing to the electrode.[326] Knowing whether the Warburg element is appropriate can be almost self-identifiable in the EIS spectra, applicable here due to the linear slope in the Nyquist plot.[326]

$$Z_w = \sigma(\omega)^{-\frac{1}{2}}(1-j)\ ,^{329} \qquad \text{Eq. 40}$$

where Z_w is the infinite impedance, ω is angular frequency and j is the imaginary unit.[330] The Warburg coefficient (σ) which can be defined,

$$\sigma = \frac{RT}{An^2F^2\sqrt{2}}\left(\frac{1}{C_O^b\sqrt{D_O}} + \frac{1}{C_R^b\sqrt{D_R}}\right), \qquad \text{Eq. 41}$$

where R is the ideal gas constant, T is the temperature, A is the area of the electrode, n is the valency, F is the Faraday constant, D is the diffusion of either the oxidised species (O) or the reduced species (R).[326] The remaining terms related to the concentration (C) of the oxidised or reduced species in the bulk (b). This term relates to the infinite diffusion impedance, and so it applies when the when the diffusion layer has an infinite thickness, and so required modification to apply to dropcast films.[329]

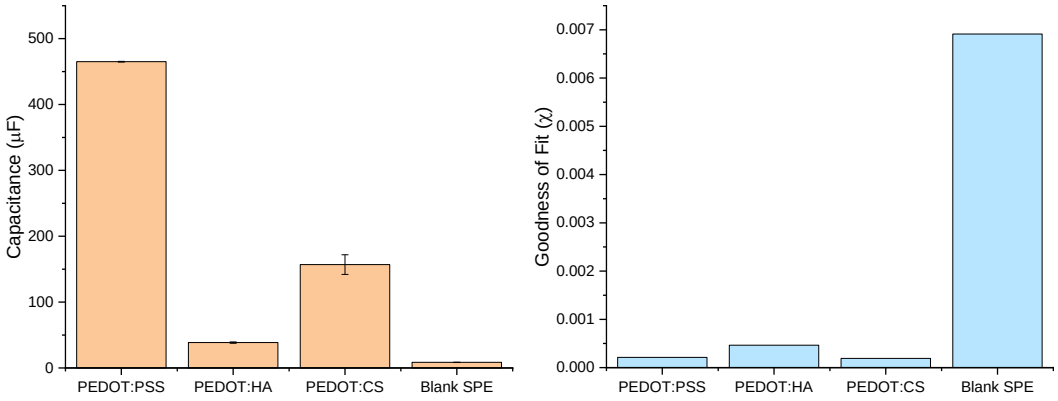

Figure 94. Figures comparing samples of PEDOT:PSS, PEDOT:HA, PEDOT:CS and a blank SPE for their capactiance and goodness of fit. The model used to calculate this data is a Randles circuit with a Warbugh element.

A similar trend can be seen when the data is modelled with this circuit as when it was modelled with the traditional Randles circuit, PEDOT:PSS displays the largest capacitance (~465 μF) and the experimental samples had smaller capacitance. When modelled using a Warburg element in the circuit, the capacitance for PEDOT:CS was greater than it was for PEDOT:HA which appears with this model to have a capacitance closer to that of the blank SPE than to PEDOT:CS. Here, PEDOT:HA has a capacitance of ~ 38 μF and the blank SPE has a capacitance of ~ 8 μF. This apparent drop in could be attributed once again adhesion issues with the film which effect the samples for both PEDOT:HA and PEDOT:CS during the measurement or could be due to the fit of the model. The goodness of fit, shown in the right-hand graph in Figure 94, appears larger for PEDOT:HA than it does PEDOT:CS although both are on an order would be deemed as an acceptable fit, the increase in χ for PEDOT:HA would suggest it is not as good as the fit the mode is for PEDOT:CS. Once again, the model is not a good fit for the data

obtained for the blank SPE. The model was again adapted in an attempt to find a model which would be suitable for each of the samples.

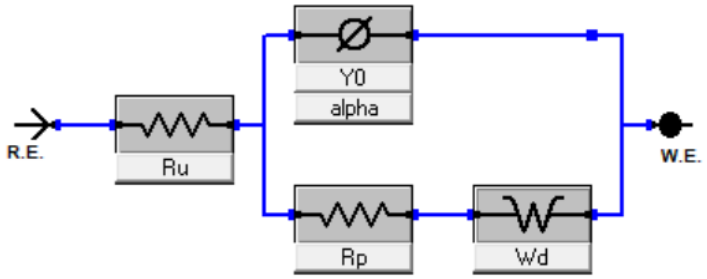

Figure 95. Randles circuit with a Warburg element, where a capacitor has been replaced with a constant phase element.

This final model, in Figure 95, is based on a simple Randles circuit and includes a Warburg element however, the double layer capacitance has been replaced with a constant phase element. This element is suitable for modelling the double layer of an imperfect capacitor and its inclusion in the circuit provides a better goodness of fit (χ) to the experimental data than can be achieved using a traditional double layer capacitor (C_{dl}). A traditional capacitor is defined,

$$Z = \frac{1}{j\omega C} \qquad \text{Eq. 43}$$

where the non-faradaic components in the device behave as ideal capacitors.[326, 329] During an experiment, samples do not often function as ideal capacitors and so the equation is frequently adapted to model a non-ideal capacitor. For an ideal capacitor the signal shifts by a phase of $\pi/2$ whereas, in non-deal capacitors this shift is better represented by $\alpha\pi/2$ where α is a characteristic of the constant phase element. Therefore, the impedance of the constant phase element (CPE) can be defined,

$$Z_{CPE} = \frac{1}{Y_O(i\omega)^{\alpha}} \qquad \text{Eq. 44}$$

where Y_O is another characteristic of the CPE.[331, 332] Y_O does not have a clear physical meaning but there have been attempts made to generate a formula which could convert between Y_O and capacitance,

$$C = \frac{Y_O(\omega)^{\alpha-1}}{\sin(\frac{\alpha\pi}{2})}.^{332, 333} \qquad \text{Eq. 45}$$

A second conversion which was published by Hsu and Mansfeld which can be applied to find the capacitance of the device from the maximum point in the imaginary part of the impedance, defined,

$$C = Y_O(\omega''_{max})^{\alpha-1}.^{332,\,334} \qquad \text{Eq. 46}$$

The parameter ω''_{max} is the maximum point in the imaginary impedance, often referred to as the angular frequency and can be identified in the Bode plot. The capacitance can be calculated from the EIS data and models for each of the samples, PEDOT:CS, PEDOT:HA and, PEDOT:PSS providing a quantitate means of comparison.

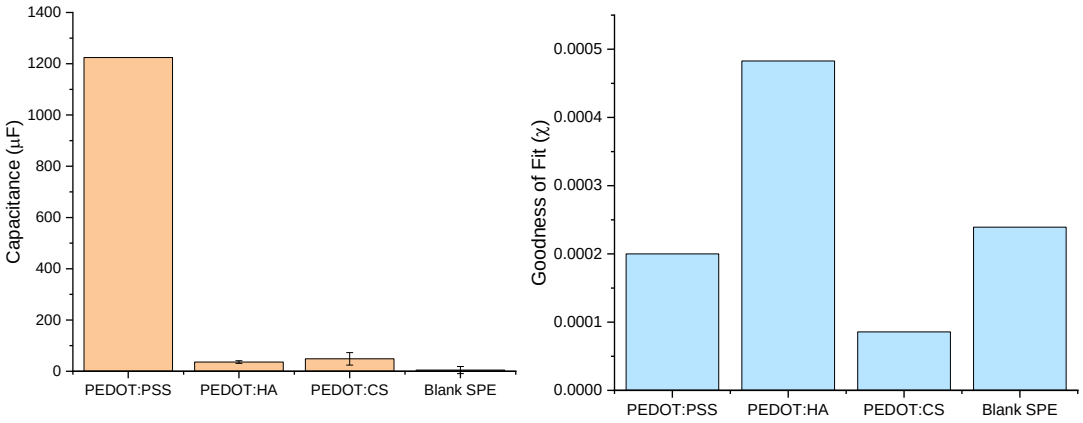

Figure 96. Graphs comparing samples of PEDOT:PSS, PEDOT:HA, PEDOT:CS and a blank SPE in terms of their capacitance and the goodness of fit of the model to the EIS data using a Randles circuit with a Warburg and constant phase element.

Using this model the capacitance measured for PEDOT:PSS is significantly higher than it is for both the experimental samples. However, the goodness of fit for all the models is in the order of magnitude which would be deemed as an acceptable fit for the data and so it can be determined that the samples do not have the same capacity that which the commercial PEDOT:PSS displays. The sample of PEDOT:CS displays a greater uncertainty in the capacitance, which may be explained by the film breaking apart when submerged in electrolyte. This issue was improved when using PEDOT:HA with the addition of EDC/NHS however the film does not adhere well to SPEs and this may account for some of the apparent reduction in the capacitive abilities of the material.

9.5 Characterisation of PEDOT:HA Films as Devices

Capacitance alone is not a sufficient means of understanding the capabilities of a device. The measurements which characterise the abilities of a transistor are the output and transfer characteristics of the device. This can be achieved in a three-electrode set-up where the current flow between a source and drain can be assessed and subjected to changes in the potential at a gate electrode when all three are in contact with the electrolyte. To assess a film's ability to modulate a current, PEDOT:HA and HA itself were applied to an electrode which was coated with PEDOT:PSS.

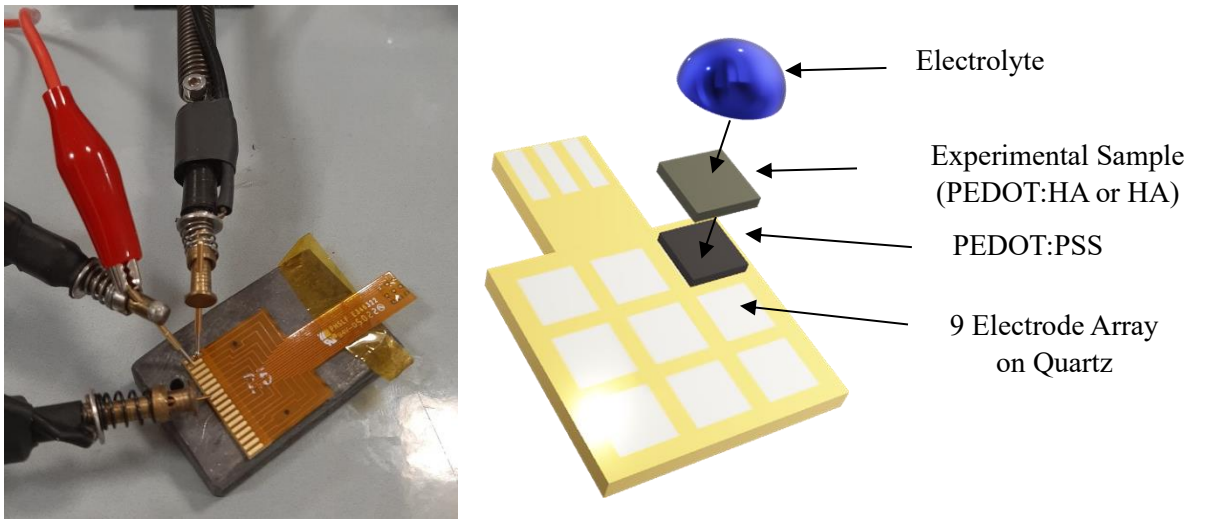

Figure 97. Image detailing how the suspension is applied to an array of electrodes and how the electrodes are connected to the rest of the circuit.

PEDOT:PSS was included as a base layer on the electrode in order to provide an improved surface on which the experimental films could adhere. This again was related to adhesion issues between the electrode and the experimental samples once the electrolyte was applied. The PEDOT:PSS film was applied in the same manner and under the same conditions for every sample and repeat, ensuring it had minimal effect on the characterisation of the experimental samples.

The first sample tested in this set up was PEDOT:HA, which was applied between the channel and gate onto a layer of PEDOT:PSS. Both layers were dried using heat and no electrolyte was applied to the system. The films have an average thickness of ~1 μm. The linear shape formed on the I_{GS} vs V_{GS} implies that the film here does not conduct, in fact there is no ionic conductivity happening in this measurement. This is as expected because the film is in its dry state and as an OECT an electrolyte is required to complete

the system in to transduce. Therefore, an electrolyte was applied over the film and the experiment was repeated.

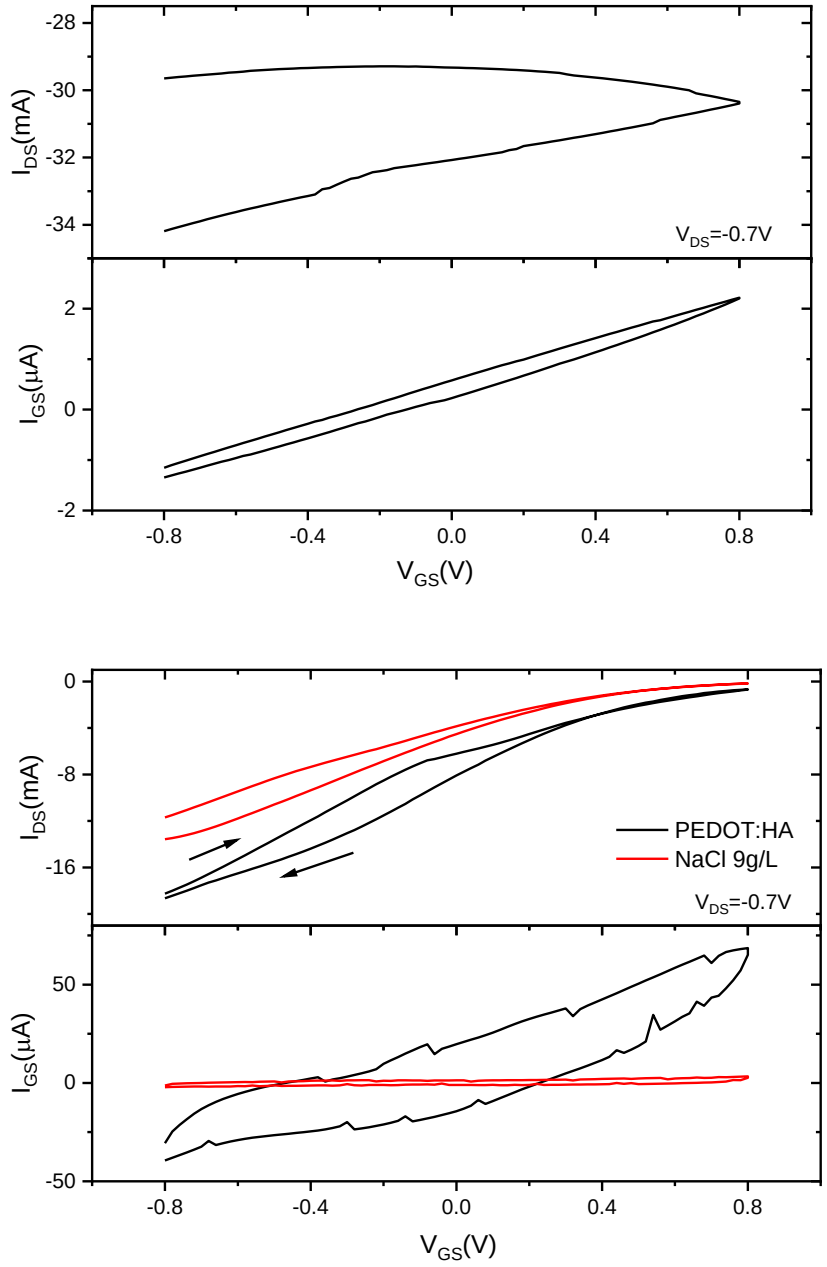

Figure 98. Showing the electronic characterisation of PEDOT:HA and NaCl electrolyte. The top image details a transfer curve of dehydrated PEDOT:HA and the bottom image shows the transfer curve of the samples following swelling.

After the film was hydrated using an electrolyte solution approximating physiological conditions (NaCl 9 g/L), the results of the experiment are more promising. The curve in the top of Figure 98 is a transfer curve which details the current between the drain to source as the gate voltage changes. The transfer curve for a control is also present and

provides a means of comparison with the experimental sample. The control is the same set up, i.e. an electrode coated with PEDOT:PSS and electrolyte but without PEDOT:HA applied between the channel and gate. The control sample does not achieve the same currents as PEDOT:HA so it can be assumed that PEDOT:HA is conductive. The device containing PEDOT:HA exhibits higher current between the drain and source - as well as between gate and source - than the control and therefore this improved conductive ability can be associated to the experimental film. However, high current values between the gate and source and are not appropriate for this device. Such transfer curves are important in the characterisation of an electronic device because they describe the device's ability to respond to an input signal. Gaining a fundamental understanding of the device's ability to respond to stimuli is essential for the application of the device to the spinal cord where it will be required to respond to action potentials which arise as a result of a stimulus elsewhere in the reflex arc.

Transfer curves are important for determining a number of properties which relate to the functioning of a transistor, such as threshold voltage (V_T), on/off ratio and maximum transconductance (g_m). The threshold voltage can be determined by plotting the square root of the drain-source current against the gate voltage.[335] It should be noted this method makes assumptions about the regime in which the transistor is tested. A system of PEDOT:HA should be in depletion mode, however this function appears to be OFF when there is no voltage at the gate and therefore this method of relating the drain-source current and gate voltage should be used with caution.

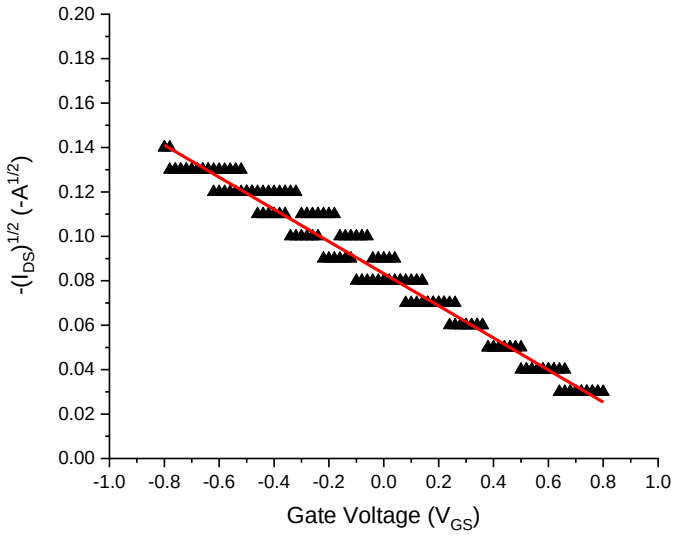

Figure 99. Graph detailing the threshold voltage obtained from the square root of the drain-source current plotted against gate voltage.

The threshold voltage of a transistor is governed by the material which forms the channel, in this case the material is PEDOT:HA and results in a V_T of ~ -1.18 V. Threshold voltage is typically used to determine the voltage at which any potential limitation in the flow of a current is overcome, sometimes referred to as the voltage at which a trap state may be overcome. A trap state is a point in the material where the movement of either the holes or electrons has been restricted.[335, 336] In an OECT the threshold voltage relies of the activity of the channel material, providing insights about the materials performance, and how well ions penetrate through it.[335]

Threshold voltage is an essential parameter in the passing of an action potential along a neuron, it is the value at which the membrane depolarises initiating an action potential. In the human body the threshold potential is around 0.05-0.055 V to achieve an action potential in neurons the threshold (t_h) which an action potential passes is significantly smaller than the threshold value in PEDOT:HA samples, therefore the conductivity of the device would need to be more selective and so requires improvement. Without improvement the threshold for transconductance may not be met due to weaker biological signals in the body. Although the method for finding V_T provides details about the device's overall conductivity, the method is affected by parasitic resistance and is limited by dopant concentrations and so it cannot be used as a sole measurement for the conductivity of the device.

The transfer curve can be used to estimate the ON/OFF ratio of the device, taken from the point at which the current is at a maximum while the device is turned on, and the current while the device is turned off. For PEDOT:HA this ratio of ~ -0.7 mA. For a neuromorphic device the larger and more stable the ON/OFF ratio the more effective the device will be due to improving output signals. Higher ON/OFF ratios provide better detection between signal and background noise, providing improved detection of lower limit signals, a key properties required of a sensor in the spinal cord.[335]

One of the most important quantitative parameters which help define a devices performance is its maximum transconductance (g_m). The maximum transconductance of the device indicated the devices amplification factor. This parameter is largely dependent on film thickness and the width of the channel and therefore it is crucial to use a standardised way of reporting $g_{m.}$ The device geometry and g_m can be normalised by,

$$g_m(\mathrm{NR}) = \frac{g_m \cdot L}{W \cdot d}, \qquad \text{Eq. 47}$$

where the width (W), length (L) and thickness (d) of the sample are included in the measurement.[335] An equation to predict g_m was first developed by Bernards and Malliaras and can be defined,

$$g_m = \frac{\Delta I_D}{\Delta V_G}.^{335, 337} \qquad \text{Eq. 48}$$

For the PEDOT:HA sample the maximum transconductance, according to the Bernards and Malliaras equation, was ~ 1.12×10^{-2} S. When this is corrected to account for the geometry of the device the transconductance becomes ~28.1×10^2 S m^{-1}.

Transfer curves are not the only parameters of a device which should be considered, output characteristics are also important. Again, these characteristics are vital to the understanding of the device's ability to respond to a stimulus.

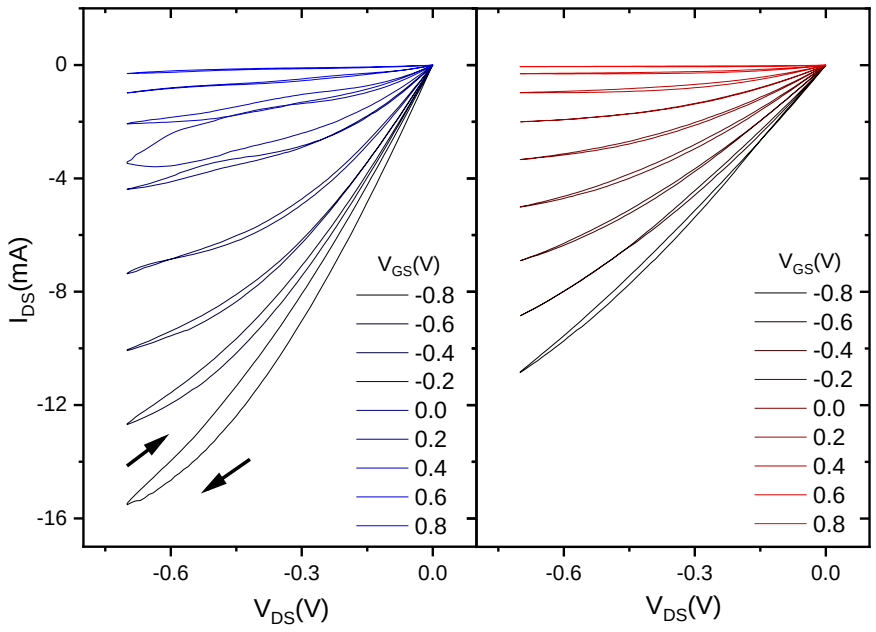

Figure 100. Output characteristics of PEDOT:HA (left) and a control sample (right) which contains only electrolyte.

The output characteristics of a device show how current, as a function of drain voltage, responds to changes in the gate voltage. If the shape of the output curve is lost on repeat cycles, it would imply that irreversible redox events are occurring in the sample. In Figure 100. the output characteristics for the PEDOT:HA sample and a control sample are shown, the sample with the experimental material has a better output signal than those of the control test, showing the experimental material improves the performance of the device and is indeed for conductivity.

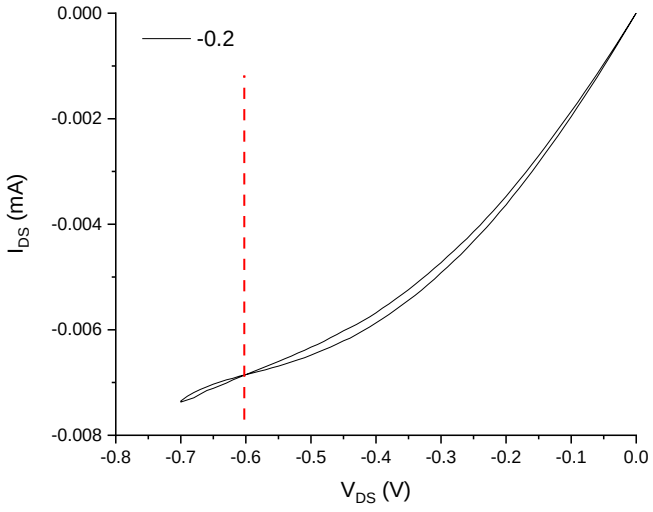

Figure 101. Graph of the output characteristics for PEDOT:HA with an attempt at marking the point at which a plateau may occur.

Typically, the output characteristics of an OECT exhibit a curve which plateaus beyond a certain drain voltage. However, in the output characteristics of PEDOT:HA it is difficult to tell whether the point at which this plateau begins has been reached. Figure 101 takes a closer look at the one of the individual curves which make up the overall output characteristics shown in Figure 100. The red line has been added to indicate the point at which the plateau may occur however more data beyond -0.7 V_{DS} is required to be able to tell if this is a true trend. Being able to reliably identify where the relationship forms a plateau is important because it indicates the point at which the relationship between V_D and V_G becomes saturated. At this point the transistor would be considered to have a saturation regime, which occurs when the transistor reaches its threshold value. It is also possible that an ideal curve may not be seen because at high drain voltages some devices have been found to deviate from the ideal saturation behaviour and instead begin to decrease at this point. It should be noted that this may also occur for PEDOT:HA but more data beyond -0.7 V_{DS} would be needed to test any relationship. Extending the experiment beyond -0.7 V_{DS} would need to be done with care as to prevent electrolysis of the electrolyte which occurs around $\pm$ 1 V.

The application of PEDOT:HA over a base layer of PEDOT:PSS was to provide a better surface onto which PEDOT:HA can adhere. However, when the electrolyte is applied it could be argued that the swollen film of PEDOT:HA could be considered a solid electrolyte. This concept lead to the idea that the scaffold from section 2.7 could be considered as a solid electrode for commercially available semiconductors such as PEDOT:PSS.

9.6 Characterisation of the HA Scaffold in a Device

To be applied to the spinal cord the device must be 3D rather than a flat planar film, therefore a hydrogel scaffold is important because it can be crosslinked to provide a 3D structure through which a film of PEDOT:PSS can be held. Therefore, the HA scaffold created in section 2.7 could be used as an electrolyte to the electronic component.

Since the conductive abilities of the PEDOT:HA film are inferior to those displayed by PEDOT:PSS, PEDOT:PSS was used as the channel material so that the nature of the electrolyte can be evaluated. The OECT uses the same set up as in the previous tests, however this time instead of applying PEDOT:HA, a sample of HA was applied and swollen using the physiological solution used as an electrolyte in the previous tests.

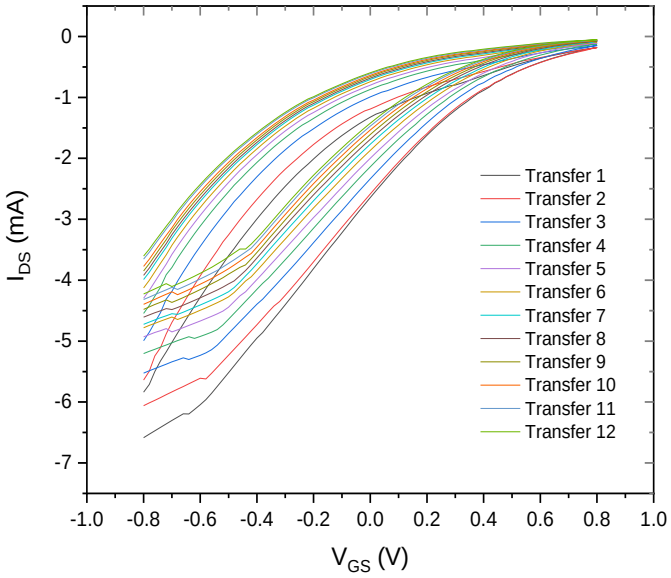

Figure 102. PEDOT:HA transfer characteristics using OFET architecture.

Again, the transfer and output characteristics of the device created using HA as a solid electrolyte were created. Here, the device has an OFET geometry which displays a similar hysteresis as seen in the previous transfer curve (CS). The key difference being that the sample here has a much smaller maximum current at the drain and therefore it can be assumed that in previous tests the presence of PEDOT:HA was aiding the conductivity of the device even with PEDOT:PSS present. In this test, it appears as though HA acts as an appropriate electrolyte, although it may be argued that an electrolyte of swollen PEDOT:HA has better conductive abilities.

The threshold value of the device was ~ 1 V, which is a slight improvement on the threshold value obtained from the system which uses PEDOT:HA as a solid electrolyte however this value is still quite far removed from the action potentials threshold value and again this device would have too high a threshold to be suitable for use in the body. The device also has a maximum transconductance of 9.5×10^2 S m^{-1} which is reduced in comparison to the system which has PEDOT:HA as a solid electrolyte. This transconductance reduction is expected since the HA scaffold is not conductive.

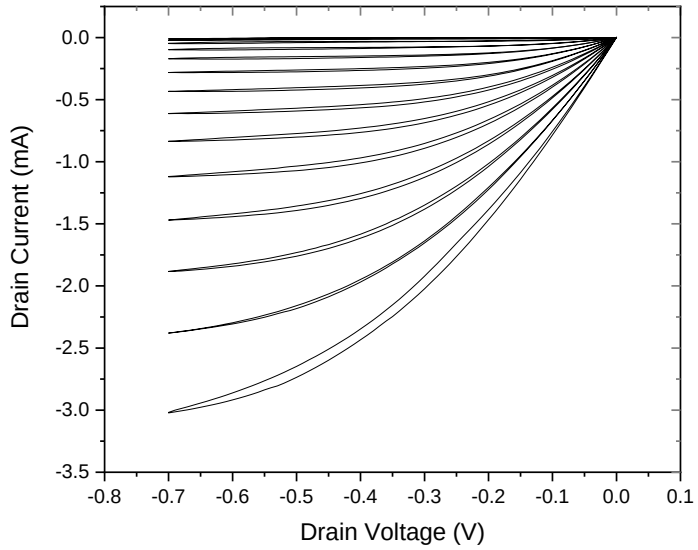

Figure 103. Output characteristics of PEDOT:HA with updated architecture.

The output characteristics of the device also have a good shape, similar to that seen of the system containing PEDOT:HA. However, there is an important difference in the amount of output current. The output characteristics for the device with PEDOT:HA reached a maximum current output of ~ 16 mA whereas the device here has a maximum output of ~3 mA. This current output is smaller than the current output achieved for the control device where the system was only a layer of PEDOT:PSS and a physiological solution electrolyte, the output of the control sample was ~11 mA. This would imply that the output of the system with a solid electrolyte of HA conducts poorly and a typical liquid electrolyte would be better. The advantage of the solid electrolyte, however, is that it provides the right physical properties for the body whereas a film and liquid electrolyte (such as in the control) do not.

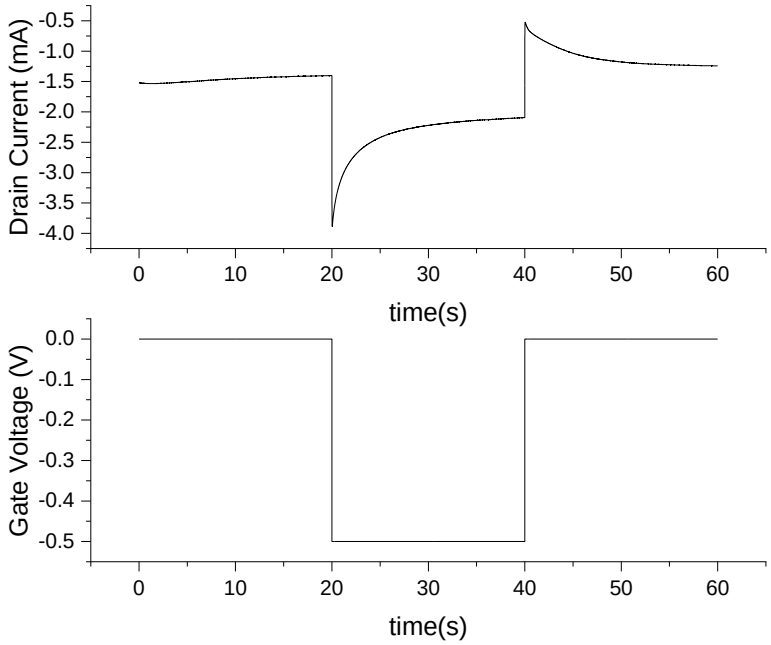

Figure 104. Square pulse characterisation of PEDOT:HA

Another way of characterising the electronic properties of the device is by applying square pulses of voltage to the gate electrode and monitoring the effect it has on the current at the drain. This is a means of characterising the devices' ability to perform with in a set-up which more closely models the spinal cord. The set up uses three electrodes, a gate, a drain and source. However, the drain and source are instead considered to be the presynaptic electrode and the postsynaptic electrode.

The HA scaffold does not contain PEDOT of which the long-term effects on the body are unknown. Therefore, the HA scaffold is used to surround a film containing PEDOT in order to minimise any possible long-term effects from PEDOT. Being able to use the scaffold as an electrolyte on a system of PEDOT:PSS is important as it has been designed in a way to have appropriate physical and chemical properties to be exposed to the extracellular matrix, whereas PEDOT:PSS has not. PSS is toxic and PEDOT:PSS does not have appropriate physical properties to make direct contact with the ECM therefore a scaffold is a means of bridging the interface of the tissue and electronic component. Even though when HA is used as an electrolyte the device has weaker conductive properties than PEDOT:HA alone, it is still important because of its biological application. PEDOT:HA as a film cannot be used as a scaffold to PEDOT:PSS because it does not have the right physical properties.

9.7 Summary

While the results for the PEDOT:HA sample are promising, showing good transfer and output characteristics necessary for a device which would function as an OECT, the device must be characterised on its own without the aid of a primer of PEDOT:PSS. While PEDOT:PSS provides a surface to which the PEDOT:HA sample can be adhered the effect from a second conductive substrate is unknown and therefore the tests require repeating without the presence of PEDOT:PSS. Attempts were made to complete this characterisation but the tests failed due to the lack of adhesion between the electrode and PEDOT:HA film once an electrolyte was applied. These attempts included capping the film with insoluble polymers but the electrolyte, which is essential for the functioning of the device, was unable to penetrate the capping layer so was excluded from the system. Capping the film in a material which electrolyte cannot penetrate through was unsuccessful, partially soluble capping resulted in loss of adhesion as the fault lies between PEDOT:HA and the electrode rather than between PEDOT:HA and a capping layer.

Another issue with the device created here is that it is a film with 2D properties, but to be applied to a SCI, a 3D device is required to fill in the cavity formed by the initial injury. Due to the devices' relatively poor conductivity when compared to commercial PEDOT:PSS, the poor adhesion properties of the films and their lack of 3D structure resulted in the decision to go back to the formulation of the device and the scaffold and attempt to find a material which would solve these issues.

The HA scaffold was found to be a good electrolyte of a system of PEDOT:PSS. Therefore, the next step in designing a device was to improve the merger of the HA scaffold and the electronic component by building a 3D structure of HA through which PEDOT could be dispersed and HA would function as the scaffold, electrolyte and the doping agent.

Part. 4 Transducing Scaffolds

Chapter 10. Materials for 3D Transducing Hydrogels

10.1 Alternative Materials with Electronic Properties

Conducting films can be applied to a wide range of different applications, however their application to SCI is limited by the fact that they are flat films which require a substrate on which they can adhere. An individual with an SCI is likely to have a cavity from the initial injury and so over time all or some of this cavity will need to be replaced by the extracellular matrix and other tissues. Therefore, to speed up the healing process 3D scaffolds have been used to fill the cavity and encourage quicker proliferation on the ECM.[168] These scaffolds have been functionalised with different materials, such as medicinal drugs to perform a variety of additional functions alongside aiding in the healing of the cavity and wound. These functions have included pain management, minimising infection, application of grafts or for inserting transducing cells. Therefore, the stable 3D shape provided by the scaffold is ideal for dispersing conductive material throughout it.

Traditional bioelectronic devices are constructed by assembling the electronic matrix and then grafting this to a material which can support it. However, recent studies have been looking into integrating the electronic component and the scaffold at an earlier stage, or alternatively looking at the interfacing the tissue directly with the electronic component.[338] This concept was first performed by Richardson-Burn *et. al.* who were able to successfully deposit PEDOT onto a mouse brain by the electropolymerisation of EDOT.[338, 339] However, for the polymerisation to take place *in vivo* a trigger to initiate the reaction is necessary.[338]

A hyaluronic acid scaffold swells in the presence of water to form a stable and robust hydrogel. The mechanism by which the hydrogel swells can be exploited to cause the hydrogel to host a conductive polymer. PEDOT is such a polymer, and it can be incorporated in the gel network in the hope of producing a transducing hydrogel. PEDOT is not soluble in water and therefore has risks of phase separating from the water swollen hyaluronic acid over time. Therefore, other conductive polymers which have varying degrees of miscibility with water should be considered.

In the initial stages of crosslinking hyaluronic acid, the starting materials for the polymerisation of a conductive polymer can be added to the mixture so that as the

crosslinks form in the gel the polymer also begins to from and forms a network where the two polymers become inseparable.

10.1.1. Trimers Based on PEDOT

Since the hydrogel structure is mostly water and therefore a conductive polymer which is soluble in water would appear to the most suitable for remaining in phase with the hydrogel. Alternatives to PEDOT should have minimal risks associated with them, ideally, they will be biocompatible. The biocompatibility of PEDOT and any alternative compound is largely unknown, and when choosing new materials, a good starting point is to choose from polymers which have no known hazards and/or have been used in an organism before.

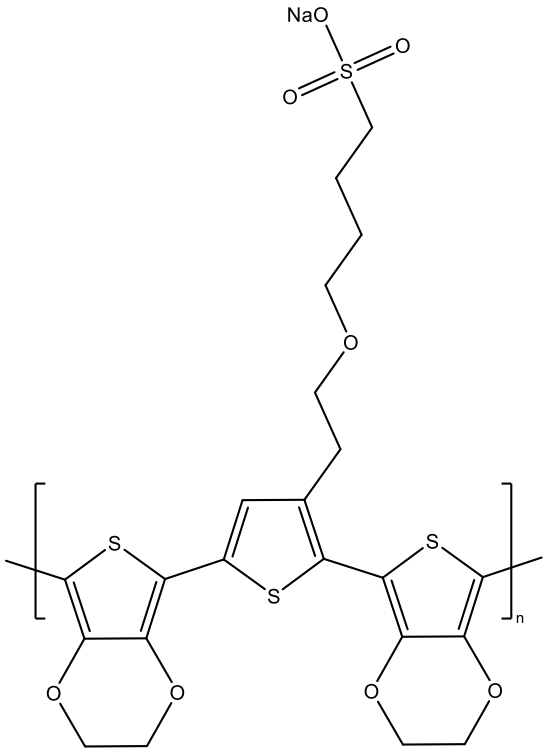

Figure 105. Chemical structure of PETE-S

D. Mantione *et. al.* identified a means of polymerising bis[3,4-ethylenedioxythiophene]-3-thiophene butyric acid, sodium salt (ETE-S), which can be carried out *in vivo* within a plant using the natural concentration of hydrogen peroxide to undergo an enzymatic polymerisation forming PETE-S.[338] The reaction has also been performed *in vitro* finding that the limiting rate of the reaction related to the hydrogen peroxide concentration.[340] In plants the presence of the monomer overrides a biological process and leads to the polymers of ETE-S being deposited in the plant cell walls and hence forming conducting materials in the shape of the plants vein like structure.[338, 340]

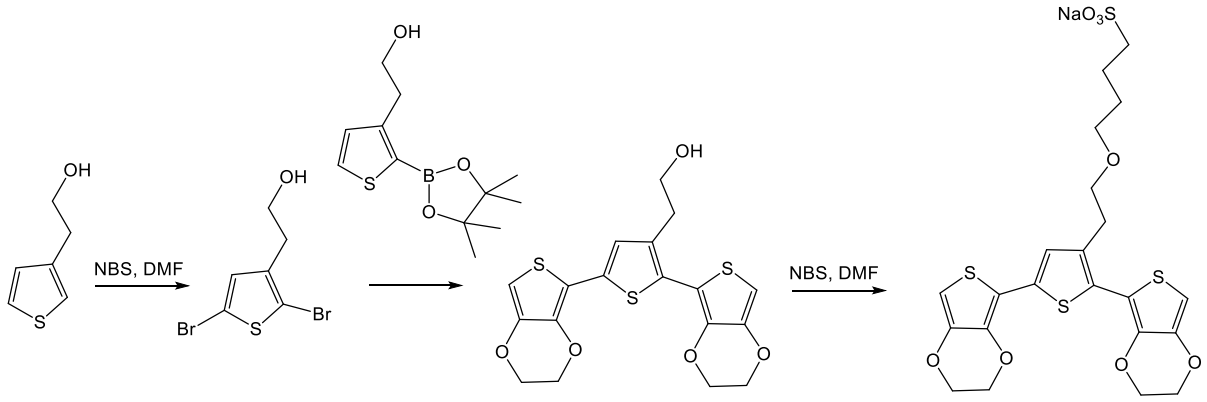

Figure 106. Formation of ETE-S from starting materials.

ETE-S is believed to be the first example of a conjugated molecule which can undergo enzymatic polymerisation at physiological pH. Therefore, it is very interesting to the field of bioelectronics which typically focuses on other polymers such as PEDOT and aniline, both of which were also enzymatically polymerised but at low pH, *in vitro*. Another key feature of ETE-S is that it is water soluble and provides solutions of the polymer rather than dispersions as is the case with PEDOT, and therefore the PETE-S solutions are more stable. This improved stability also offers more biological applications than PEDOT and similar derivatives. PETE-S is a polymerised trimer, where the central unit which makes up the trimer of ETE-S is a thiophene group which has been designed in a way to offer an anchor point for functionalisation of the polymer. The remaining two units, to each side of the thiophene, have a lower oxidation potential and provide ETE-S with increased reactivity.[338]

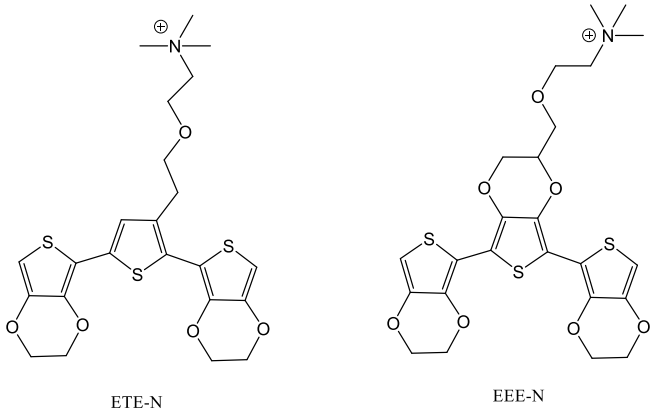

Figure 107. Other trimers which can be formed using a similar reaction to the one which forms ETE-S.

There are two further trimers which can be formed from the functionalisation of the central unit in the trimer. The first of which (ETE-N) can be achieved in the synthesis of ETE-S by leaving the hydroxyl group on the thiophene ring active. The second trimer

(EEE-N) is formed from a similar reaction however a different monomer was introduced into an earlier step in the synthesis to generate a central unit with more of a tradition PEDOT structure.

10.1.2. Poly(thiopheneethanol)

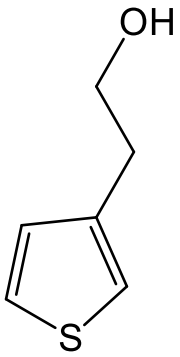

Figure 108. Chemical structure of poly(thiopheneethanol)

Poly(thiophene)s have been shown to display some conductivity and therefore thiophene derivatives like PEDOT could also be considered as alternative polymers. The starting material in the synthesis of ETE-S is 2-thiopheneethanol (TE) which is also a starting material in the synthesis of EDOT. It is current classified as a non-hazardous material and, while its use in bioelectronics is relatively unknown, its low toxicity makes it a candidate for use in a device, subject to appropriate conductive properties.

2-thiopheneethanol is slightly soluble in water and therefore has a solubility which could be considered in between that of EDOT and ETE-S, where EDOT is insoluble, and ETE-S is soluble in water. Therefore, a broader study on the how the solubility of the monomer affects the resulting device can be carried out.

Chapter 11. Conductive HA Scaffolds

11.1 Producing 3D scaffolds with PEDOT

In the previous chapter the polymerisation of PEDOT doped with HA resulted in suspensions of PEDOT:HA which required agitating and dropcasting as films in order to be characterised. The application of the device as a film is limited and would be improved by having a shape which could be tailored to fit a cavity which resulted from an SCI. There are a series of variabilities with must be considered when designing such a device, the first of which addresses the conductivity of the device. Films of PEDOT:HA had relatively poor conductivity which could be improved by crosslinking the HA, which both improves the physical properties of the film but also forces PEDOT strands to be in closer proximity and therefore more likely to form conductive paths through the film. The proximity of PEDOT molecules needs to be maintained in any change made to the device to maintain conductivity. However, moving to a 3D gel will likely decrease the number of conductive pathways and this must be addressed. Secondly, the methodology used to polymerise PEDOT required adapting to be able to yield gels rather than suspensions. The gels will then need to be handled and sliced to be suitable for electronic characterisation.

The physical properties of the HA scaffold have been specifically tailored to provide a scaffold with an elastic modulus which would be compatible with the spinal cord. These scaffolds also have good stability in solution. Therefore, any changes made to the crosslinking reaction of HA should have minimal effect on the physical properties of the gel. Any gel formed will again need to be characterised in a similar means to that of the HA scaffold.

The polymerisation of PEDOT was based on the method proposed by D. Mantione *et. al.* where HA is dissolved in water before EDOT is added and polymerised in solution.[286] The first method attempted to produce gels rather than suspensions was to merge the method proposed by Mantione which the methodology developed in Part 3 for the formation of the HA scaffold. Therefore, rather than dissolving HA in water, EDC and NHS were added to ethanol at 0 °C and given time to react. Following this HA was added and left to begin to react with the crosslinking agents. HCl was then added to lower the pH to ~4 followed by water which was added dropwise. This resulted in a gel like that of Part 3. Rather than ending the process here to form a scaffold EDOT, APS (ammonium

persulfate) and a catalytic amount of iron sulfate were added and allowed to react for 48 h.

The resulting mixture was gelatinous but did not form a specific shape; the gel could be poured from one container to another with the gel taking the shape of the new container. However, these gels were difficult to handle and therefore they were not characterised. It was decided to change the polymerisation reaction again to improve upon these gels.

New mixtures were created in the same way, linking the approach from D. Mantione with the HA scaffold synthesis. However, before adding EDOT the pH of the mixture was increased to ~6. This was determined regarding the tunability of the conductivity of PEDOT and how this can be influenced by factors such as pH and temperature. The temperature was lowered to 0 °C inhibit the self-polymerisation of EDC and therefore this was not changed in this reaction. K. I. Ritzau-Reid *et. al.* proposed that changing the pH to 6 allowed them to produce homogeneity of OligoEDOT crosslinked hydrogels and therefore this pH was chosen as a starting point.[341]

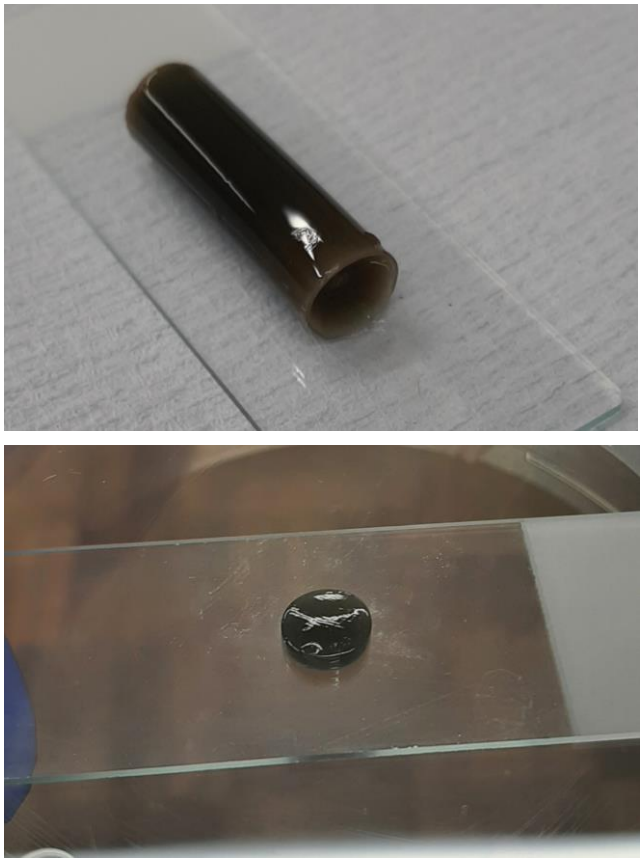

Figure 109. Images of the 3D transducing scaffold before and after slicing.

Changing the pH produced a remarkable difference to the resulting material, gels were now produced which could be handled and cut up into smaller pieces. These gels were rinsed in a 70 % ethanol in water solution for 48 hours to remove any impurities or remaining starting materials. The gels were then sliced into disks to have their mechanical properties examined.

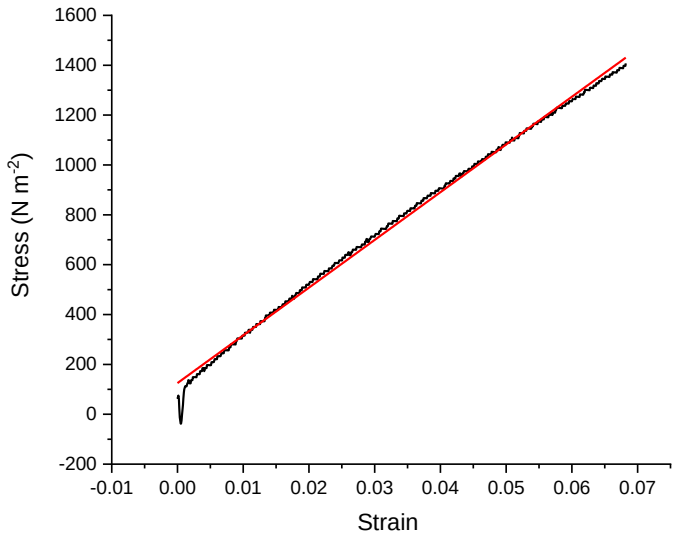

Figure 110. Stress-strain relationship of the PEDOT:HA 3D scaffold

The mechanical properties were examined using a stress-strain relationship and with contact mechanics the same way that the HA scaffold was tested. Although both test methods are used to check the reliability of the results, the stress-strain method is a more commonly implemented for calculating the elastic modulus. In this work, however contact mechanics proved to be more useful for measuring the thin film of HA scaffold. Here, the slices of PEDOT:HA gel are thicker and so either method could be reliably implemented. The stress-strain relationship gave an elastic modulus of 15 ± 1 kPa.

Sliced gels cut from the larger piece of the material were examined under the optical microscope to build up an image of the of the profile of the cut slice.

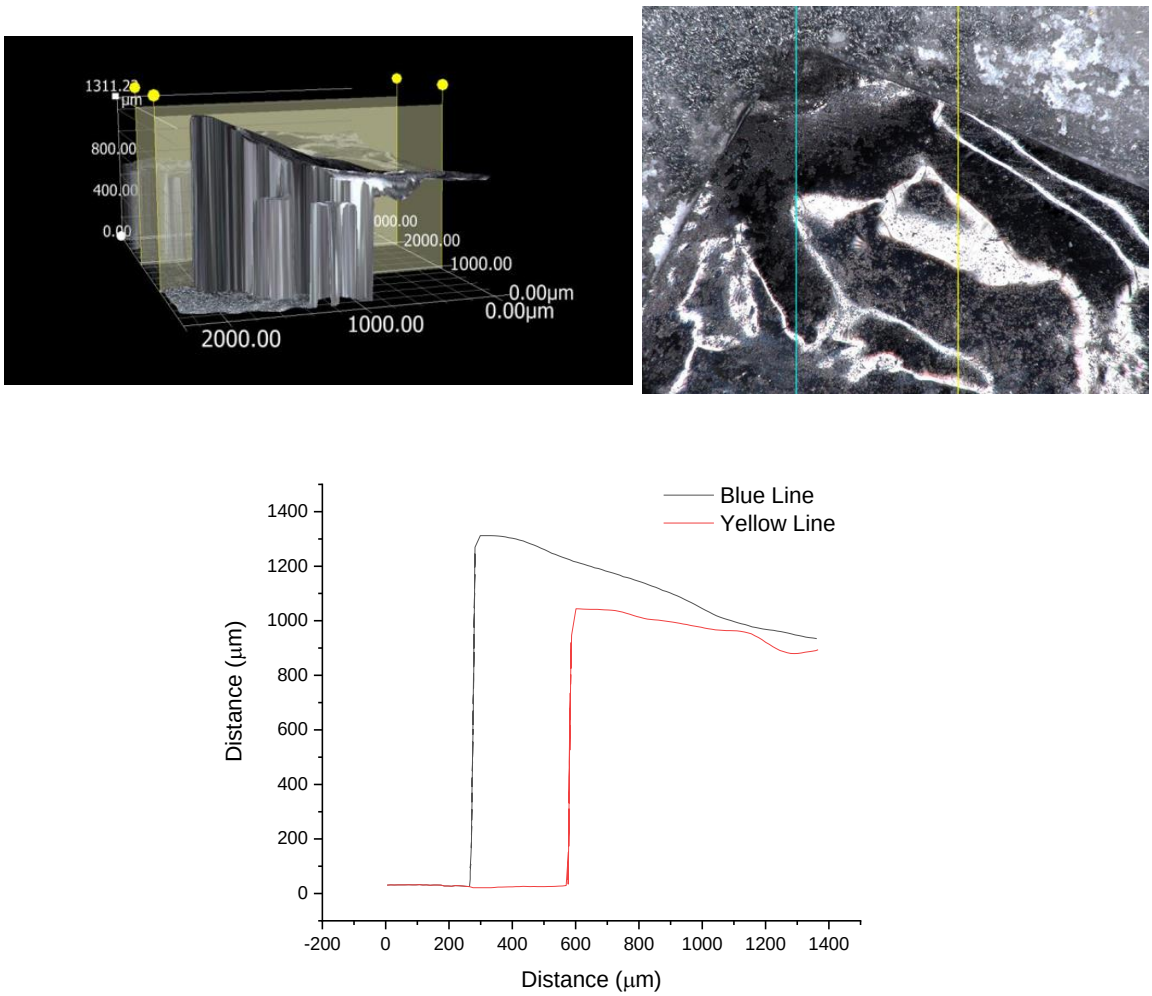

Figure 111. Graphs showing the cross section used to measure the depth profile of the scaffold. The upper images show the position of the measurement visible on the microscope image, the graph at the bottom is the depth profile.

Because the thickness of the gel varies with each slice cut, care was taken to make sure the gels are cut to a size which is visibly similar. Nevertheless, the slices will differ, and each were be measured using either the mechanical tester or the optical microscope. Some 10 µm slices of the gel were made using a microtome however it was necessary that the gel was filled with paraffin wax to replace the water in the gel so that it could be sliced. This dramatically changes the properties of the gel and was not considered further.

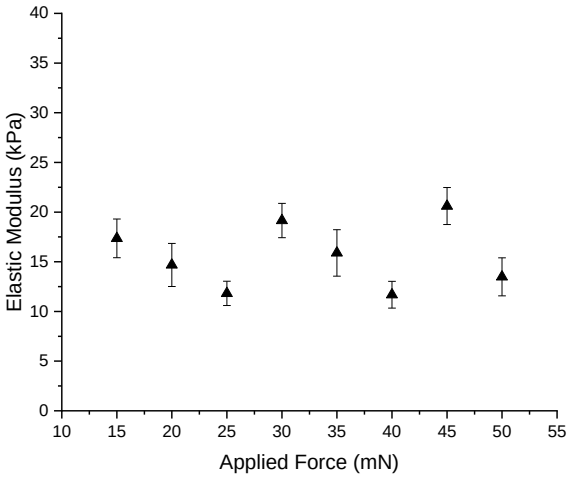

Figure 112. The elastic modulus of the PEDOT:HA scaffold over different applied forces.

The elastic modulus obtained from a contact mechanics approach is in the region of 10-20 kPa, when the applied force is 30 mN the respective elastic modulus is 19.2 ± 1.7 kPa. The two methods provide very similar elastic moduli suggesting the results are reliable. The comparison with the elastic modulus of the HA scaffold is detailed in Table 10.

Table 10. Summary of the elastic modulus values obtained for the hydrogel scaffold and the PEDOT:HA scaffold.

Material	Method	Elastic Modulus	Error on the Mean
HA Scaffold	Stress-Strain depth of 0.3 mm	46.32	2.69
	Contact Mechanics at 30 mN	23.36	4.96
PEDOT:HA Scaffold	Stress-Strain depth of 0.3 mm	15.12	1.09
	Contact Mechanics at 30 mN	19.16	1.73

Using a contact mechanics approach the elastic modulus of the PEDOT:HA and HA scaffold are relatively similar and therefore it could considered that PEDOT has not caused a dramatic effect to the physical properties of the gel and the scaffold continues to be compatible with the spinal cord. However, using the stress-strain method the PEDOT:HA scaffold appears to be somewhat softer, which was unexpected due to the addition of a relatively inflexible polymer, PEDOT, into the gel. The result here may be due to the thinness of the HA film because the method requires the probe to penetrate the scaffold to a fixed depth, when the film is thin the probe can penetrate to the point when it begins to be influenced by the substrate underneath the film and therefore provide inflated elastic modulus results. Thin films also contain fewer crosslinks, and a

lack of appropriate crosslinking has been demonstrated to yield a scaffold with softer physical properties.

The elastic modulus obtained for the PEDOT:HA scaffold is similar to the elastic modulus of the HA scaffold itself, which was considered to have a modulus appropriate for the spinal cord. A range of 5-100 kPa was the target for the scaffold, with an aim to ensure that the material is softer than the spinal cord so that it does not cause abnormal mechanical fiction on the tissues which in turn leads to wear and damage to the tissues, while still being firm enough to be able to be handled. The PEDOT:HA scaffold also fits into this range and is therefore also considered to be appropriate for the spinal cord. The result was supported by the similarity of the results from the two test methods.

11.2 Producing scaffolds with PETE-S

PETE-S is proposed as an alternative conducting agent to PEDOT due to its lower toxicity and therefore the potential to develop more biologically compatible devices. PETE-S is also considered to be self-doped, so by incorporating it into a scaffold of HA should provide improved conductive properties when compared to PEDOT:HA which relies on the formation of conductive pathways between PEDOT and the doping agent HA.

Figure 113. Image depicting the colour of PETE-S during the polymerisation reaction.

The first step towards developing PETE-S scaffolds is the polymerisation of ETE-S. Previously, the monomer was polymerised in plants using the enzymes which occur naturally within it. However, here a more ideal synthesis would be one which can be carried out in a one-pot synthesis where the polymer can be incorporated directly into a hydrogel without the need for an additional step to extract the polymer from the plant.

The methodology used to polymerise EDOT was repeated, swapping EDOT for ETE-S. This methodology was based on that proposed by D. Mantione *et. al*.[338]

Figure 114. PETE-S formed by polymerisation of the trimer ETE-S showing characteristic dark blue colour. PETE-S has undergone further crosslinking to form stable gels.

The polymerisation of ETE-S appears to be significantly quicker than that of EDOT. This again can be seen visually changing from a yellow colour to a dark reddish brown almost black. This colour change occurs within hours (~2 h) of mixing the monomer with APS in the presence of HA and a catalytic amount of iron sulfate, whereas the colour change when EDOT is present instead of ETE-S happens slowly 48 h. The resulting mixture was in a gel phase but could not be handled, when tweezers were taken to the gel they go through the material in a similar way as they would to a liquid. When the pH was altered according to section 4.2.1 the resulting mixture again remained to be a very soft gel. Therefore, to be able to handle this material further crosslinking was required. Rather than change the initial formula the crosslinking agent was added after the polymerisation in a method like that described by K. Tomihata *et. al.*[57] The authors describe a multi-step crosslinking approach where the material is submerged into a solution containing an increased amount of crosslinking agent for a fixed amount of time. This allows for further crosslinks to form near and on the surface of the material to improve its stability. A solution of 5% EDC in ethanol was carefully added to the container were the PETE-S was held and left for 24 h. Following this extra crosslinking step 3D gels were formed which could be handled.

There was concern that by increasing the amount of crosslinker in the gel the conductive ability of the film would be reduced. Therefore, the PETE-S:HA sample which was initially made and the samples which underwent further crosslinking to form a gel were compared by CV.

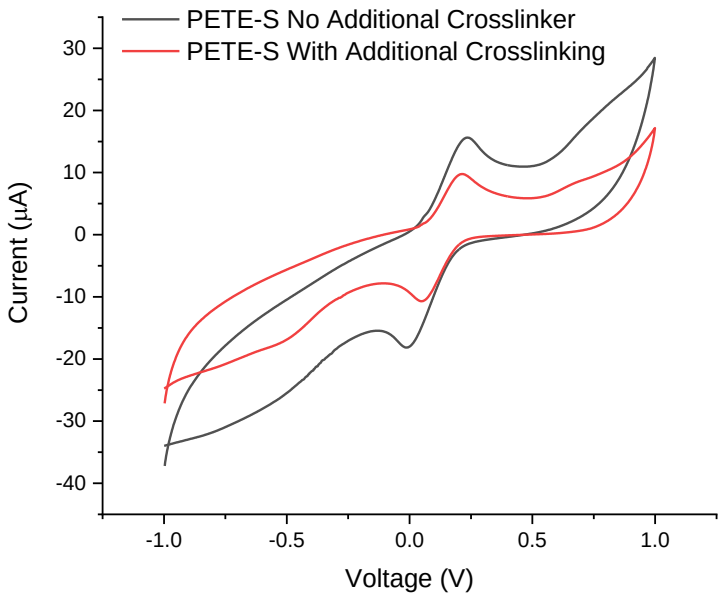

Figure 115. CV for PETE-S before and after the additional crosslinking step.

There is some apparent reduction in the conductive ability of the film once the additional crosslinking has been achieved, however this effect is minimal and in CV appears to cause a reduction of ~10 µA. However, the sample which had no additional crosslinking step was drop cast and dried onto the SPE before the electrolyte was added. However, the sample with additional crosslinking formed a gel which was cut into a smaller section and placed onto the SPE. When the electrolyte was added to the SPE the gel moves and the contact between the gel and the electrode is poorer than it is between an adhered film and the electrode, which could also account for a reduction in capacity. The results from the CV are similar and the changes could be attributed to a number of factors, as well as the additional crosslinking. It was however decided that the crosslinking did not cause a significant effect and the benefits of forming a gel outweigh any issues arising from the additional crosslinking and so the extra crosslinking step will be retained through the result of the project.

11.3 Producing scaffolds from Thiopheneethanol

A synthesis of PETE-s was proposed to be carried out in Newcastle however the use of sodium hydride requires a Schlenk line and other measures which could not be safely achieved in the university lab available over the course of this project. Other facilities would be able to routinely carry out this synthesis. While studying the synthesis it was noted that the starting material thiopheneethanol is currently considered to be not a hazardous material and the nature of the thiophene aromatic ring makes it a potentially conductive material. The combination of these properties makes this chemical a candidate for application to this project.

Figure 116. Image showing a slice of poly(thiopheneethanol) which is an orange gel strucutre.

Again the same synthesis was implemented to form poly(thiopheneethanol) (PTE) gels which had a similar consistency to the PEDOT:HA gels which formed gels which can be handled. However, a key difference with the gels formed from TE is that the resulting gel is an orange colour. This colour change was unexpected and since it is not a dark metallic colour it is assumed the conductive properties of the gel will be limited.

11.4 Combinations of Polymers

A mixture of conductive polymers may offer the most suitable properties by offering a wider range achievable properties without the need for compromise. These combinations can be compared against the individual polymers to provide an idea of the range of properties which can be targeted. A small number of polymer combinations were tested to find out their mechanical properties and the possible conductive abilities alongside PEDOT, PETE-S and PTE. The scaffolds which perform the best in the initial tests will be carried forward into more detailed OECT characterisation.

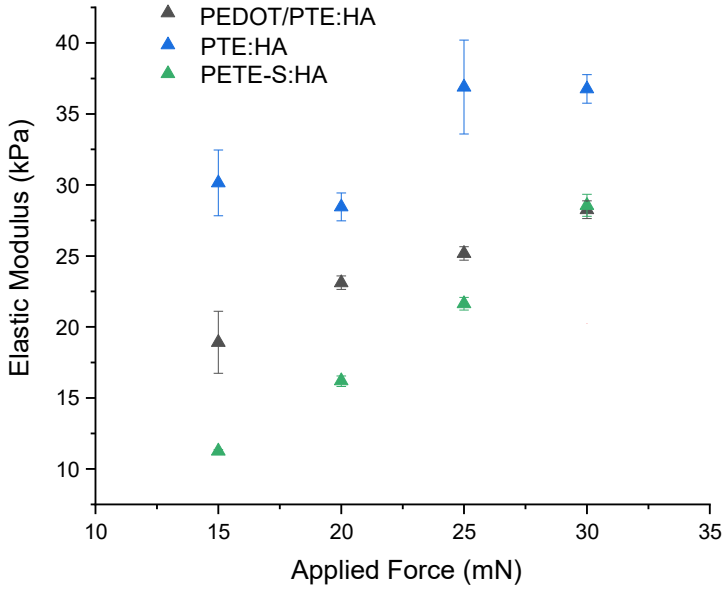

Figure 117. Elastic modulus for each of the gels containing conducting polymers.

The mechanical properties of the gels were examined using the same contact mechanics approach which was established earlier in project. The results all fall into the range outlined as suitable for spinal cord application (5-100 kPa). The results for PETE-S can be compared to that of PEDOT:HA (figure 112) and appear to fall into a similar range, while the elastic modulus of PTE is slightly higher than that of PEDOT:HA and PETE-S. The presence of PTE appears to increase the mechanical properties of a scaffold containing PEDOT, probably because the PTE itself has an increased modulus, suggesting that the PTE is a slightly harder polymer than the others. The sample containing a mixture of PEDOT and PTE was made using a 1:1 ratio of the two polymers, the sum weight of the two polymers was then matched in a 1:1 ratio with HA. The four mixtures tested here would all be considered appropriate for spinal cord application based on the aims and outlines set earlier on.

Due to the relatively good mechanical properties, of each of these samples will have their electronic properties characterised through CV and EIS. Small sections of roughly 4.5 mm^3 were cut from the larger sample and placed onto the SPEs ready to undergo cyclic voltammetry and impedance spectroscopy. Electrolyte was carefully added to the SPE over the gel ensuring the maximum contact between the gel and the SPE was retained.

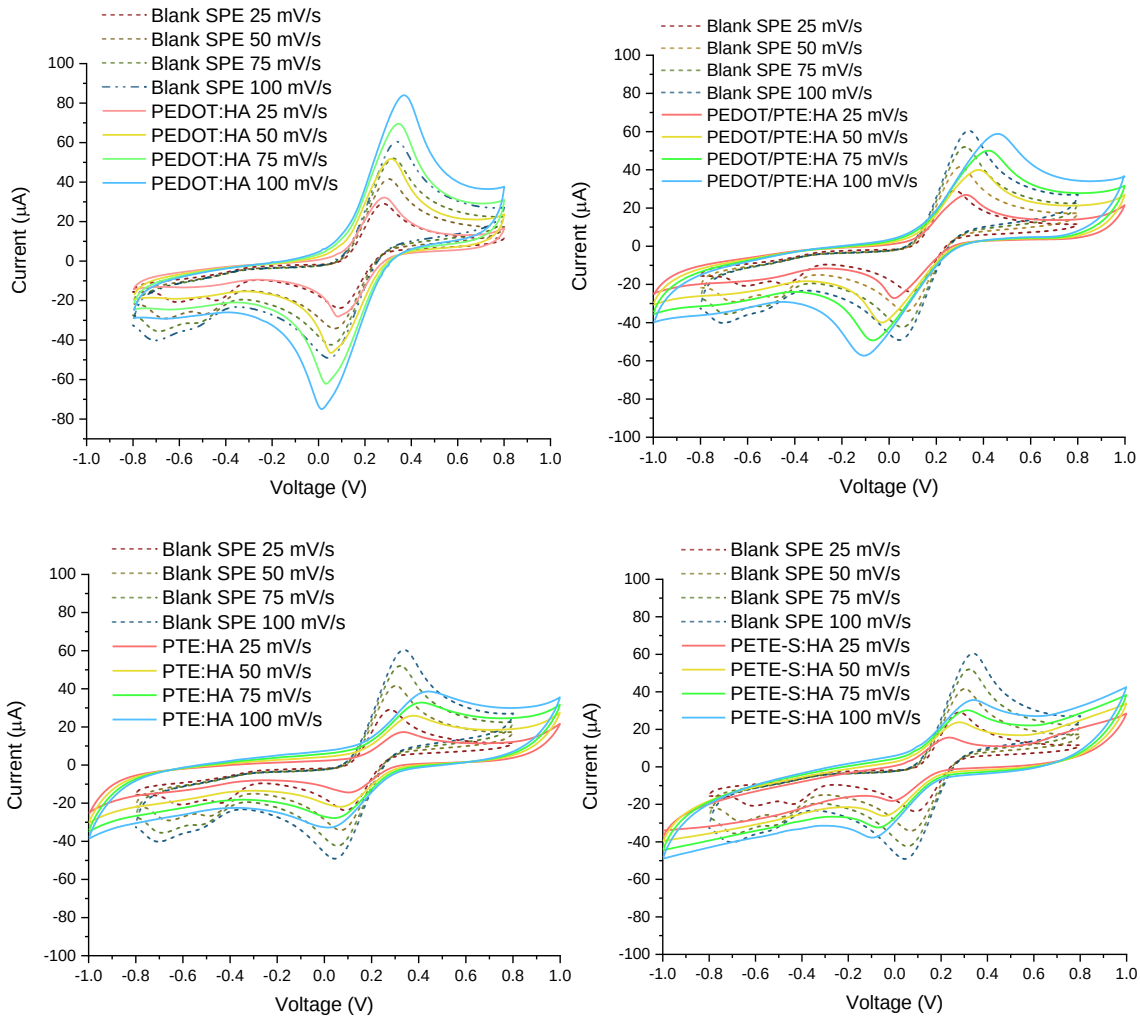

Figure 118. CV spectra for each of the gels containing a conductive polymer, each gel was also examined over four different scan rates. These gel are PEDOT:HA (top left), PEDOT/PTE:HA (top right), PTE:HA (bottom left) and PETE-S:HA (bottom right).

PEDOT:HA appears to have the best conductive performance from the CV, seen by the increased current recorded when compared to the blank electrode. In the spectra for PEDOT:HA the sample appears to have a larger current than the blank SPE whereas in the other materials the current appears reduced when compared to the blank electrode. An increase in current and a broadening of the forward and reverse sweeps indicates an increase in the capacitive nature of the material. An increased capacitance would suggest an improved conductive ability and when the capacitance is reduced the conductive ability is also reduced.

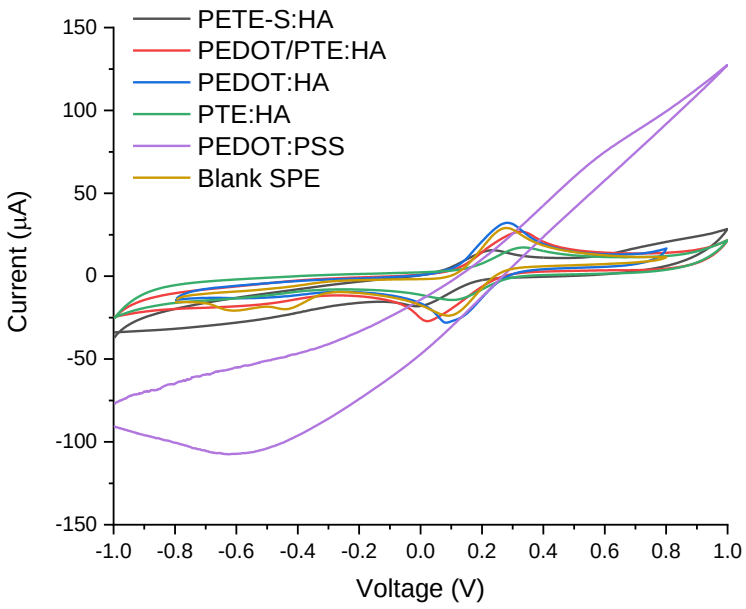

Figure 119. CV spectra of each of the experimental scaffolds containing PEDOT, PTE, PETE-S, PEDOT and PTE, and a comparison spectra of commercial PEDOT:PSS.

Although PEDOT:HA appears to perform better than the other experimental materials in the CV, the results are relatively poor in comparison to that for PEDOT:PSS. The PEDOT:PSS spectra is significantly more broad and the shape which would be expected of a capacitive material. However, the shape of the spectra observed for the each of other materials is more typical of a material undergoing redox reactions than a material which conducts by electron transport. It should be noted that the PEDOT:PSS used here is a commercial sample and forms a dispersion which is applied as a film rather than a gel. Some of the apparent reduction in conductivity of the experimental materials could be due to the nature of the gel and a lack of adhesion between the SPE and the sample. Some reduction in conductivity was expected due to the gel being swollen with water and therefore the proximity of the conductive polymers is somewhat reduced and therefore reduces the conductive ability of the film. The gel is also placed onto the SPE and then electrolyte is added. The electrolyte can move the gel around and it may be that there is poor contact between the electrode and the material. This could be seen by the fact that the experimental materials have a very similar looking CV to that of the blank electrode. Some peak shifts were observed and can also be attributed to redox reactions occurring in the CV.

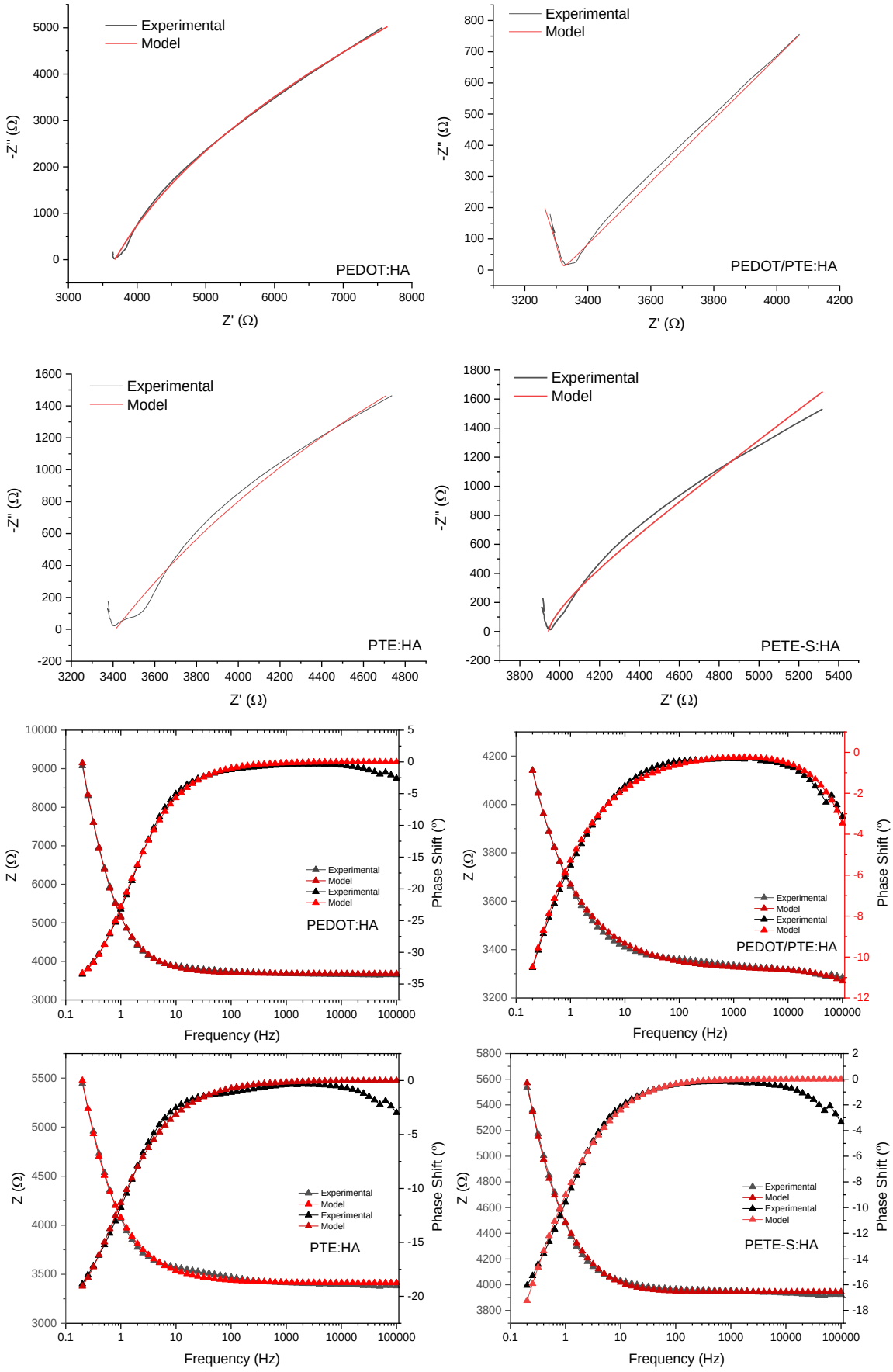

Figure 120. Nyquist and bode plots for PEDOT:HA, PTE:HA, PETE-S, and PEDOT/PTE:HA.

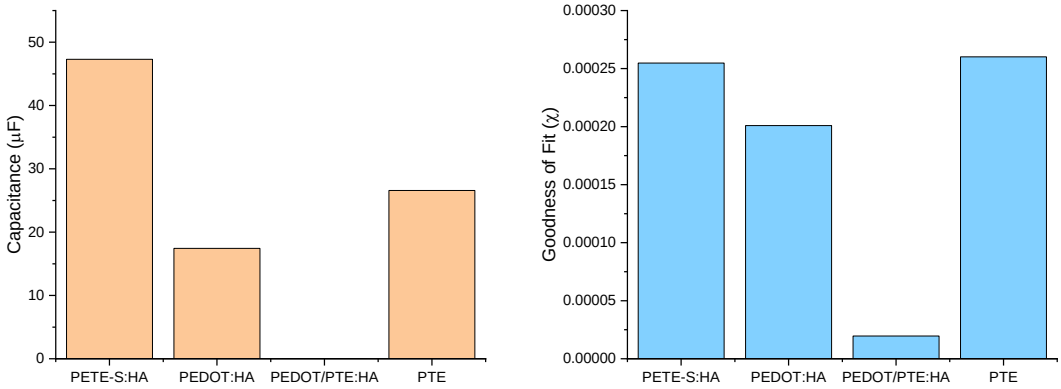

Figure 121. Summary of the capacitance calculated for each sample using a model circuit (right hand side). The graph on the left-hand-side shows the goodness of fit of this model to the raw data of each sample.

The materials were then characterised by electrochemical impedance spectroscopy (EIS) using the same architecture with SPEs as it has throughout the electrochemical experimental tests. The Nyquist plots obtained for each material have shapes characteristic of a capacitive material. However, the Nyquist plots each have different scales and by fitting these curves to a model a capacitance can be calculated which provides a better means of comparing the samples. The capacitance for each of the materials was calculated. PETE-S exhibits the largest capacitance suggesting it is the more conductive material, this is followed by PTE then PEDOT:HA, with a combination of PEDOT and PTE performing the poorest. The model used to calculate these capacitive values were again based on a Randles circuit with an additional Warburg element and the use of a constant phase element in the place of the capacitor in parallel. The models all appear to have a relatively good fit to the experimental data, each recording χ values in the scale of 10^{-4}.

To gain more of an understanding of how these devices perform, a drop cast sample of PEDOT:PSS modelled with the same circuit provides a capacitance of 1224 μF. This is significantly larger than the capacitance of the experimental materials. However, the doping agent believed to be weaker than PSS and so a reduction in the ability of the material was to be expected. S. Carli *et. al.* electrodeposited different PEDOT:doping agent films onto electrodes at two known deposition charges with one of the doping agents tested being HA. This device was characterised using EIS and modelled with a circuit containing a Warburg element to obtain a capacitance of 19.0 ± 0.3 μF. This value is similar to the 17.44 μF value obtained for PEDOT:HA in the experiments. This suggests the conductive performance of the materials is reasonable for the proposed application.

The results from the EIS are not in agreement with the results from the CV. According to the CV PEDOT:HA appears to be the most conductive of the materials, with PETE-S performing relatively poorly. However, the CV results largely overlap and therefore the variations in the results are small and may be attributed to poor contact between the sample and the electrode. Two solutions were proposed to combat the loss of data resulting from the poor connection between the two. The first of which is to use a flat paddle gate electrode, where the gate would approach the system from the top and would press the gel onto the source and drain electrodes to ensure the gel remains in good contact. The second solution was to use more sensitive electrodes, such as gold or chromium plated electrodes, which would improve the detection of weaker signals which rise from weakly conductive material with poor connection to the electrodes.

When the experiment is repeated the results for the materials appear to constant, with the exception of PTE. The results for this polymer appear to vary and may account for the reason why the PEDOT:PTE sample had a very small capacitance in shown in Figure 121. This variation in the performance of the material can may be attributed to the polymerisation reaction, where some of the resultant gels form an orange colour and others becoming a pinker colour. This suggests that something is changing in the reactions between the samples and the materials tested are not constant.

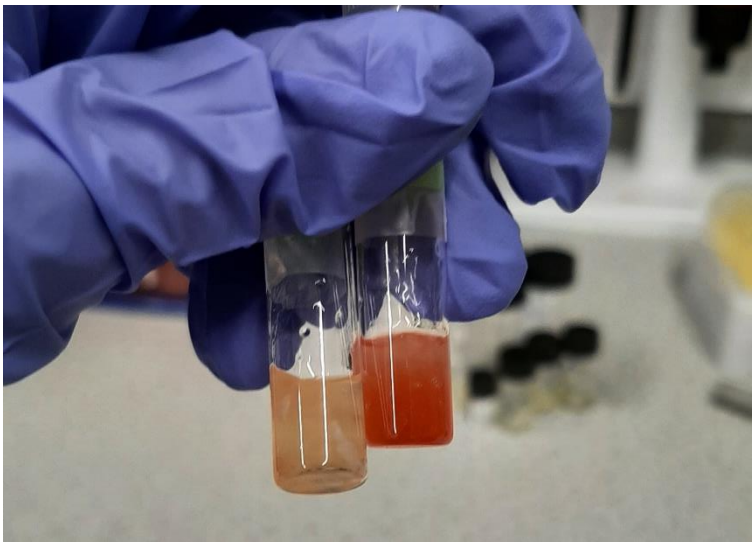

Figure 122. Image showing the colour changes observed during the synthesis of poly(thiopheneethanol) under the same conditions.

It is believed that PTE:HA has the potential to make a promising material for a biologically compatible OECT, however it would require more consistent materials. This is something which could be achieved by optimising the polymerisation reaction,

although this was not considered any further here. Therefore, the material which could be constantly reproduced, PEDOT:HA and PETE-S:HA were chosen for further OECT characterisation. PEDOT/PTE:HA was also discounted at this point due to the reproducibility issues with PTE.

11.5 Biocompatibility of the Devices

PEDOT:HA and PETE-S:HA were chosen as candidates for further characterisation, and so, as potential candidates for biological application they need to be biocompatible. Therefore, they require *in vitro* biocompatibility characterisation.

A cell line can be used to see the effect the material has on the normal function of the cells. The cell viability gives an indication of the devices ability to be used *in vivo.* Cell line biocompatibility studies of these materials were carried out by S. Garg using an Alamar Blue cytotoxicity assay with a 3T3 fibroblast cell line. Typically, there are three cell lines which are used for such a study, of which the 3T3 (a mouse fibroblast cell line) is the most commonly used.

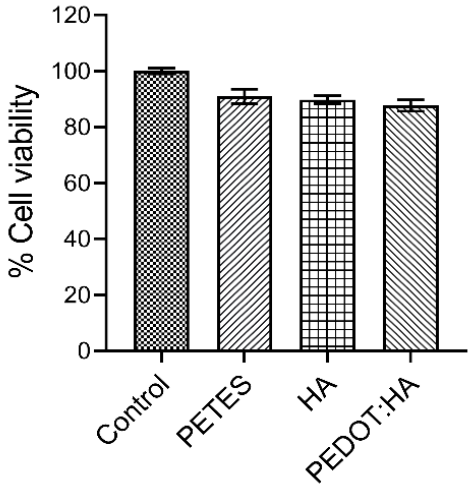

Figure 123. Biocompatibility results for PETE-S:HA, PEDOT:HA and a scaffold of crosslinking HA where no conductive polymer is present.

The biocompatibility studied *in vitro* were carried out at the University of Manchester by S. Garg. Samples of PEDOT:HA, PETE-S:HA and the HA scaffold itself were tested to gain asses their biocompatibility, the scaffold itself was included as a way of identifying whether the conductive polymers are responsible for a reduction in the biocompatibility of the device. However, the results indicate that this is not the case. All three of the materials would be considered biocompatible based on the results shown in

Figure 123. Where the three materials have cytotoxicity of ~9%, 10% and 12% for HA, PETE-S:HA and PEDOT:HA. These values correspond to those found in previous literature reports.[301, 342] According the standard ISO 10933-5 the tolerable limits for biocompatibility are at 30% and therefore, even with PEDOT:HA samples reportable ~12% cytotoxicity, all three samples remain well within the limits and can be considered biocompatible.[343, 344]

11.6 Transistor Behaviour of the Devices

The device will be characterised in terms of its transfer and output characteristics. These properties define the device's ability to function as a transistor and therefore they are crucial for understanding how the device would function if applied to the spinal cord. As mentioned in Chapter 9 the initial CV and EIS testing were affected by the contact between the electrode and the sample, and it was proposed that a more sensitive electrode and altered architecture could help combat any signal loss between the sample and electrode.

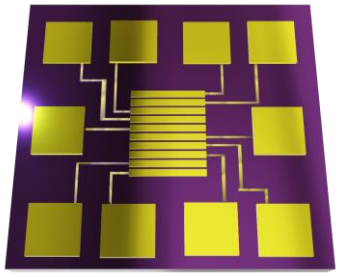

Figure 124. Image demonstrating the electrode array used for electronic characterisation tests

A more sensitive electrode was chosen for the transfer and output characteristic tests. These electrodes consisted of a gold electrode coated in chromium plating. The sample would be applied to the central electrodes with one of the larger square electrodes being used as the gate electrode. Alternatively, a square paddle electrode could be placed above the sample as a gate electrode which can also hold the sample in place. The electrodes are then checked to see if there is any leakage current. Each electrode was examined before use, finding that the leakage current was commonly in the picoamps region.

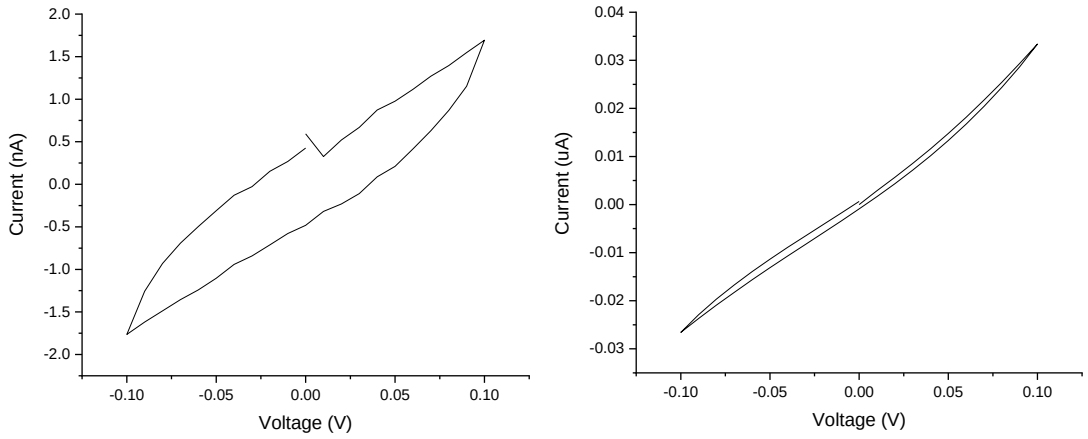

Figure 125. IV sweeps of PEDOT:HA and PETE-S:HA

Before carrying out any transfer or output characterisation, a current/voltage sweep (IV) is taken of the device to determine whether the materials are conductive. These IV tests are carried out without electrolyte. A linear IV would suggest that the material is electronically conductive, as seen for PETE-S:HA in Figure 125. The sample for PEDOT:HA is more broad IV suggesting that there is some faradaic reactions occurring which mask whether there is electronic conductivity occurring at the same time. However, these IV are taken for a very narrow voltage sweep and this requires extending to assess fully the conductive nature of the samples.

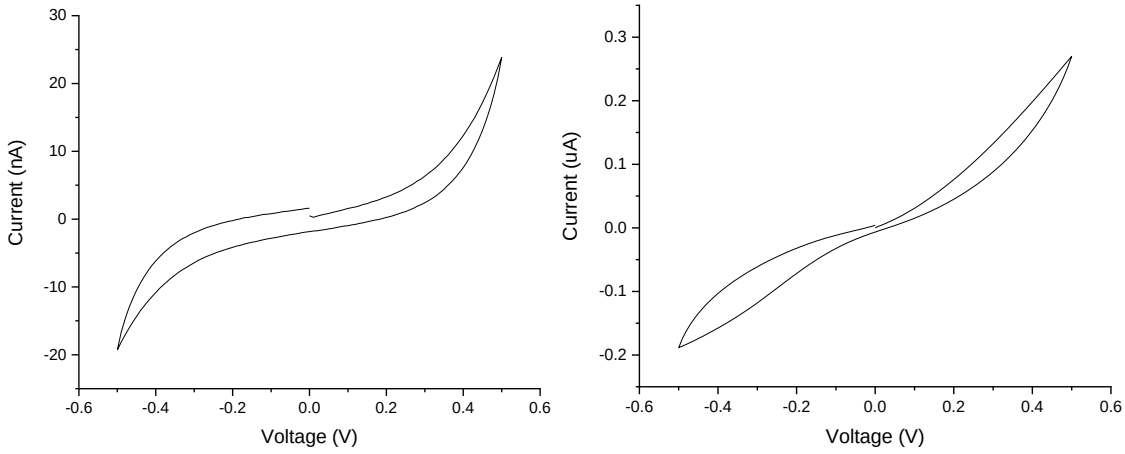

Figure 126. IV sweeps of PEDOT:HA and PETE-S:HA performed over a larger voltage range.

When the voltage sweep is extended, the PETE-S:HA sample begins to move away from having a linear relationship. The IV curves of both samples have more of a 'duck' shape typical from a CV of a material which undergoes redox behaviour. The PEDOT:HA sample having a very small current with a small amount of broadening between the forward and reverse sweep. The PETE-S:HA has some broadening which suggests the material has a capacitive nature. It also has more of a linear shape than seen in the

PEDOT:HA sample, although redox reactions are likely to be happening within these samples too.

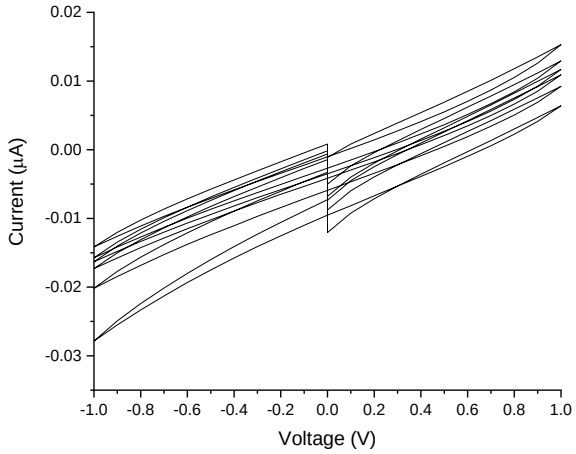

Figure 127. Cycling through the voltage range to produce multiple IV traces to see how the current migrates throughout.

To understand more about what was happening in the PETE-S samples, a continuous IV was taken where at each sweep a small step is input. With time, the IV settles to around 14 nA, which occurs without any electrolyte present and indicates that the material appears to provide a better measurement when a slight delay is used to measure the data. The IV were then repeated using a short and longer delay to compare the effect of this delay.

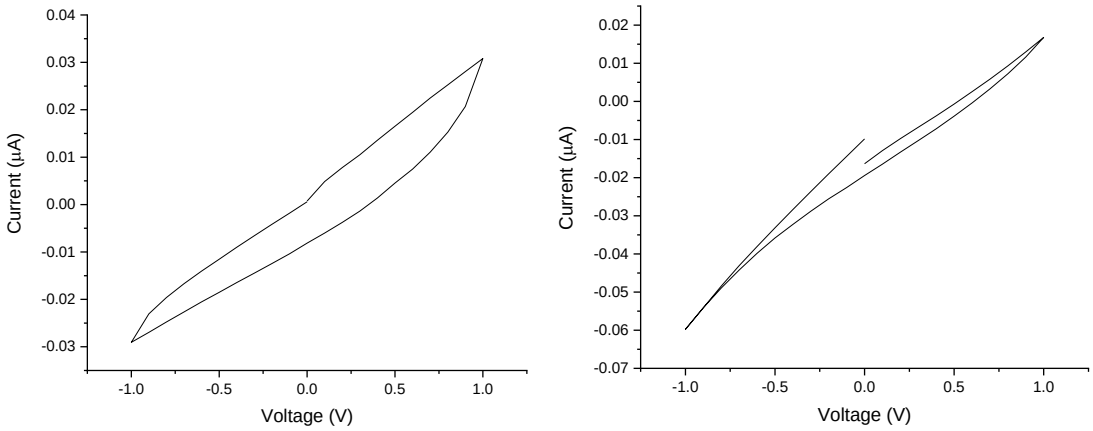

Figure 128. IV sweep after increasing the delay between measuring each data point.

With a longer delay, the gap between the forward and reverse signal can be minimised, suggesting that the material is undergoing a redox reaction which requires more time before the maximum electronic conduction between source and drain can be achieved.

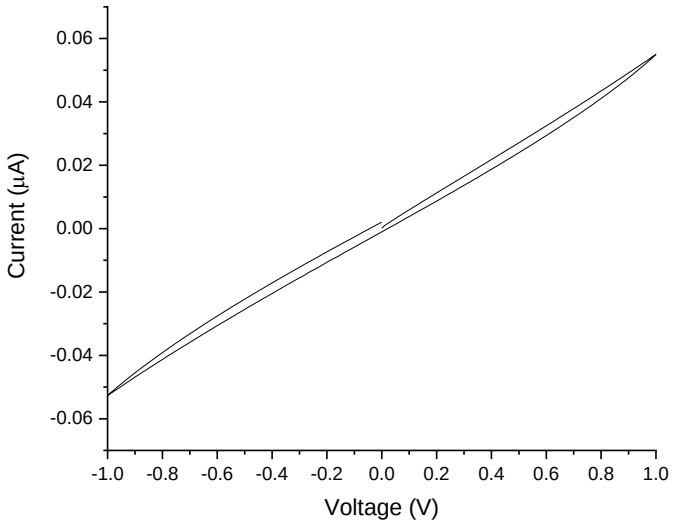

Figure 129. PETE-S IV after optimising the experiment parameters.

When the delay in the measurement is optimised, the IV is linear and has minimal noise. Here, the PETE-S sample looks much more like a capacitive material which was the aim of this project. This optimisation from the control set up can then be applied to the transfer and output characteristics, by including a delay between each datum point.

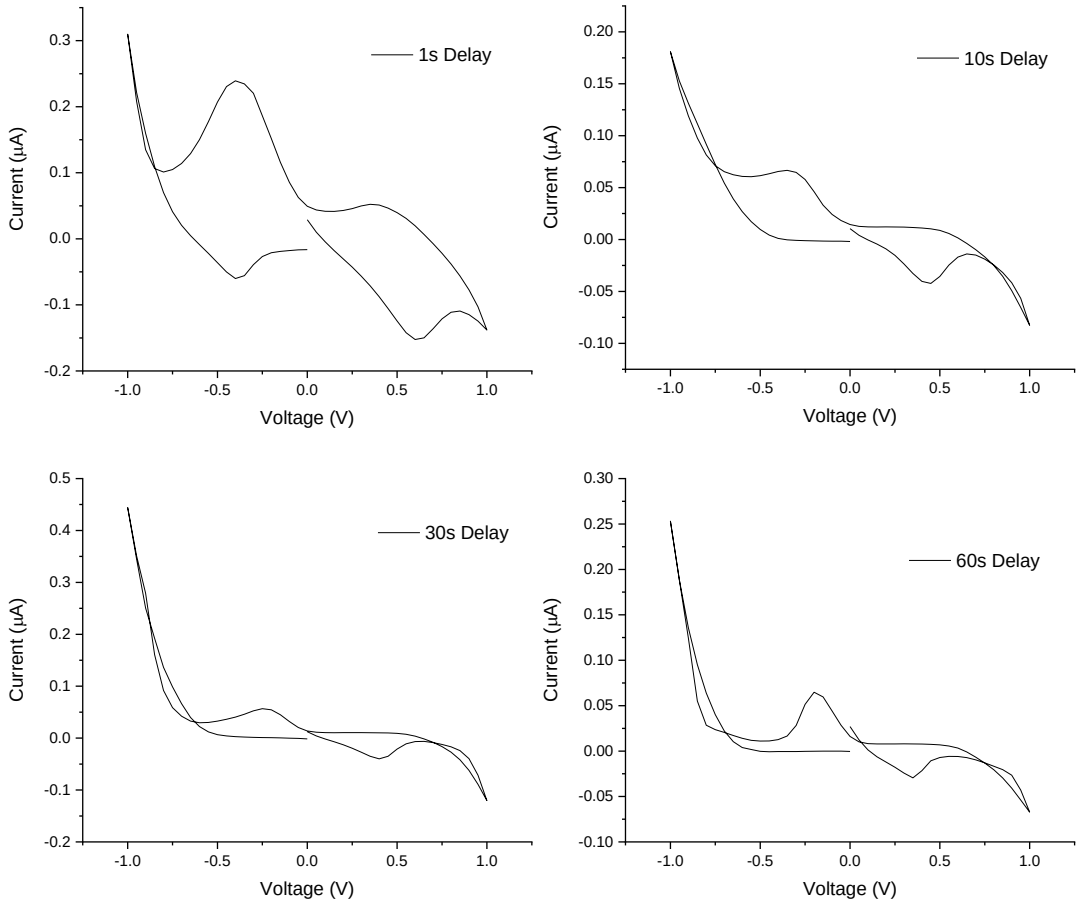

Figure 130. Transfer characteristics of PETE-S:HA using different length delays between each measurement..

The effect of adding a delay between the measurement of each datum point across the voltage sweep can been seen in Figure 130, where several different delay periods were used. With increasing delay, the peaks which are associated with redox events occurring in the material become smaller. Therefore, by using a long enough delay between each measurement, the redox events can complete. The signal which is detected after this is therefore associated with electronic currents rather than redox events. The delay can be used to separate the signals which arise from both electronic and redox events, which are often inseparable in characterisation methods such as EIS. When the sample is in a dehydrated state, the resistance appears to be in the order of 20 MΩ whereas when the sample is hydrated the resistance appears to increase. This appears to be tied to the delay between the measurements and so it is assumed the nature of the material is capacitive.

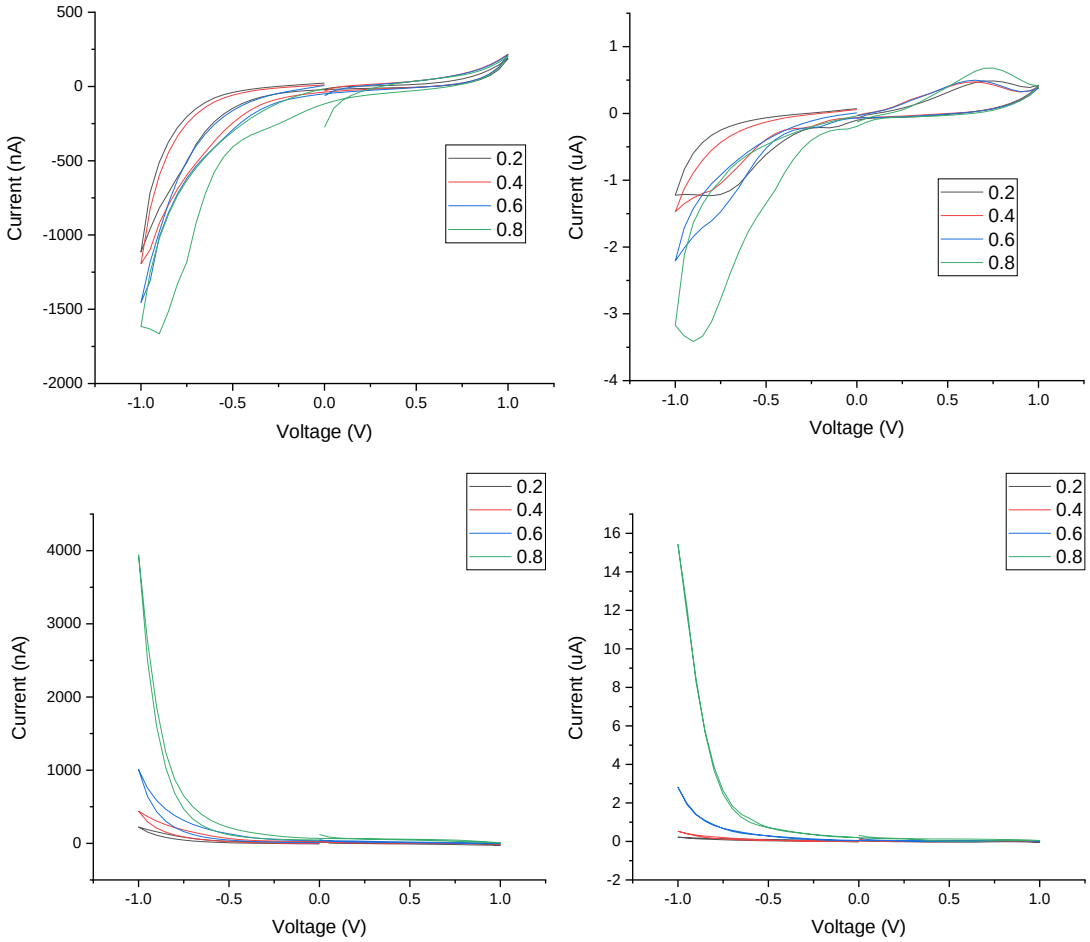

Figure 131. Transfer (bottom) and output (top) characteristics of PEDOT:HA (left-hand side) and PETE-S:HA (right-hand side).

The results from both the output and transfer characterisation of PEDOT:HA and PETE-S:HA scaffolds have the form expected from a functioning OECT, where there is a clearly definable 'on' state and an 'off' state. This may be slightly more apparent in the transfer properties where the current increases exponentially when the voltage is in the range of -0.5 to -1 V. Although the overall shape of the curve displays the transistor characteristics which were hoped for, there is concern that some of the observed current arises from a parasitic contribution and therefore results in the broadening of the output curves. The results of the IV appear to suggest that the sample undergoes a capacitive conduction. However, when the experiment is changed to characterise the sample with transistor architecture, the results appear to suggest an opposite effect. Here, the samples appear to be affected by faradaic currents at the gate and drain which seem to be because the experiment involves sweeping the gate-source voltage without controlling the gate-drain voltage in a system where the drain is immersed in electrolyte. The same tests were

repeated using a different piece of equipment (KEITHLEY 4200A parameter analyser) which gathers data for each of the electrodes simultaneously. Being able to define each electrode would help to identify any channel transport which is masked by larger ionic contributions.

The KEITHLEY 4200A parameter analyser provides data from the source, drain, and gate electrodes so the source current can be plotted against the voltage. By doing this, the total current across the system can be monitored and should be equal to the current observed in the other graphs. This is a good way of determining if there are any parasitic contributions which occur when ions in the electrolyte are displaced or whether there are real hopping charges present.

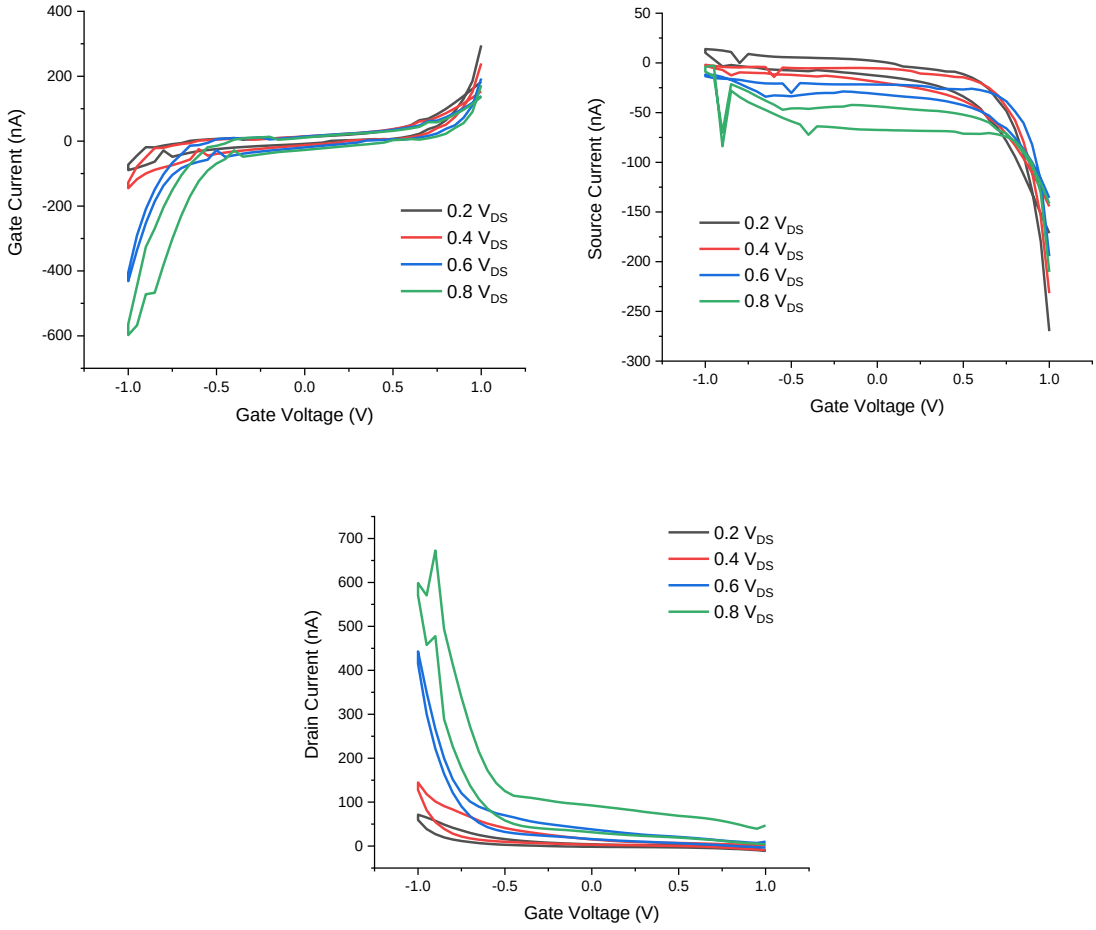

Figure 132. PEDOT:HA transfer characteristics carried out on a more sensitive device.

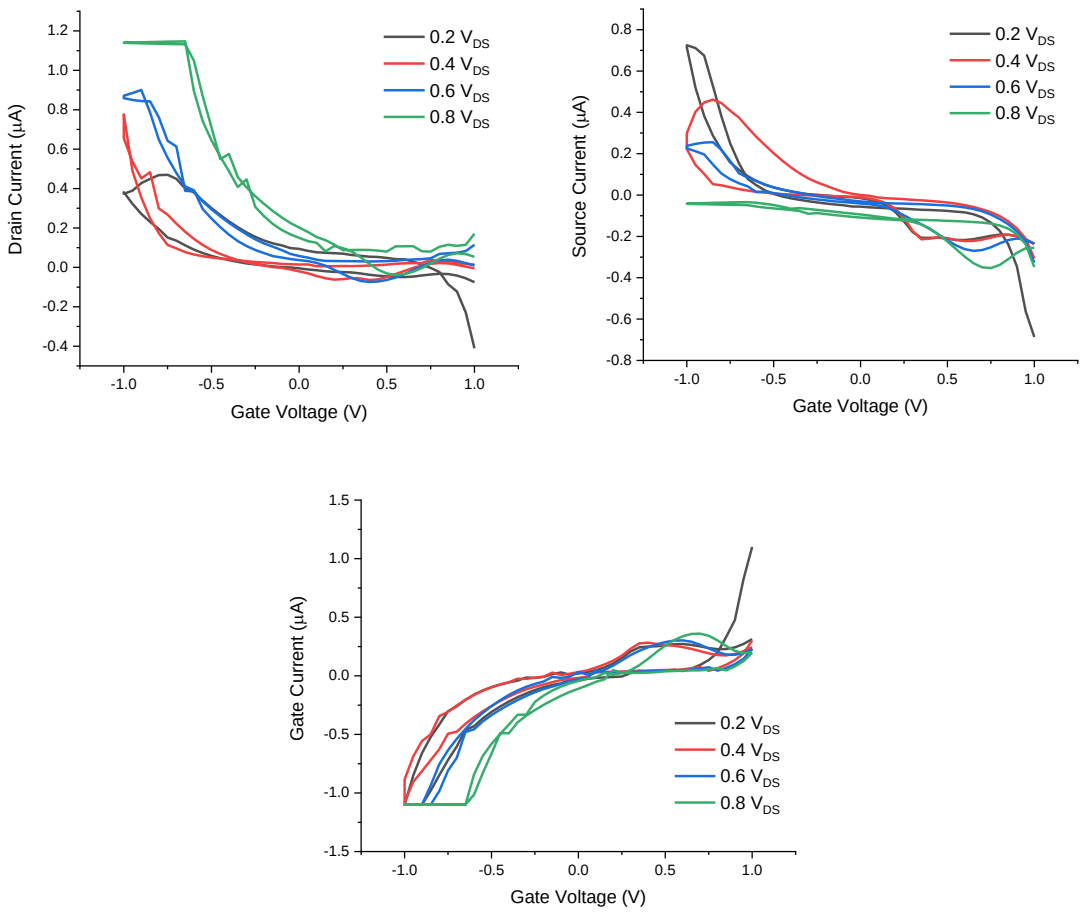

Figure 133. PETE-S:HA transfer characteristics carried out on a more sensitive device.

When a voltage is applied between the source and the drain, a current is expected to occur when the transistor is in an 'on' state. A similar current is also seen from the gate and this is considered to be a leakage current. When a dielectric material is being tested, there should in theory be no current at the gate electrode since the applied current occurs across a capacitor. If the architecture was an OFET the gate would be responsible for the distribution of charges in the channel. When the transistor is 'on', the charges migrate to the interface with the conductor and current flows. However, the only current flow through the dielectric is to charge it, whereas in the architecture used in this experiment (an OECT) the current flow is not quite as straightforward. The electrolyte used in the OECT is largely water which has a very high dielectric constant and so there are free charges which can flow. This is considered to be simple leakage current rather than parasitic. Parasitic currents should flow when the device is also in an 'off' state and would be considered a major problem if they affected the transistor's switching ability. When a current is applied to the source, the charges should flow to the drain. Here, there

is some flow of current to the gate and so the current at the source is equal to the sum of the current at the gate and drain electrode. Ideally, the current at the gate would be negligible, if not zero, otherwise this current is leakage. It should be noted that although there is leakage occurring in the on state, it was not observed in the off state. Therefore, the leakage seen here was assumed to be a simple leakage, relating to the fact that the conductive polymer (PEDOT) is not continuous and so the current flow is not necessarily directed from source to drain. It is believed that if PEDOT was intact between the source and drain the charge would leave and no gate leakage would be detected.

To ensure that leakage was not caused because of poor contacts between the sample and the electrode, it was beneficial to repeat the experiments using a delay and by comparing how a flat paddle gate which is kept in contact with the sample compares to experiments where the gate electrode was only in contact with the electrolyte. The results from the experiment provide an idea of the conductive performance of the samples however they are largely affected by noise and require repeating to produce more precise results.

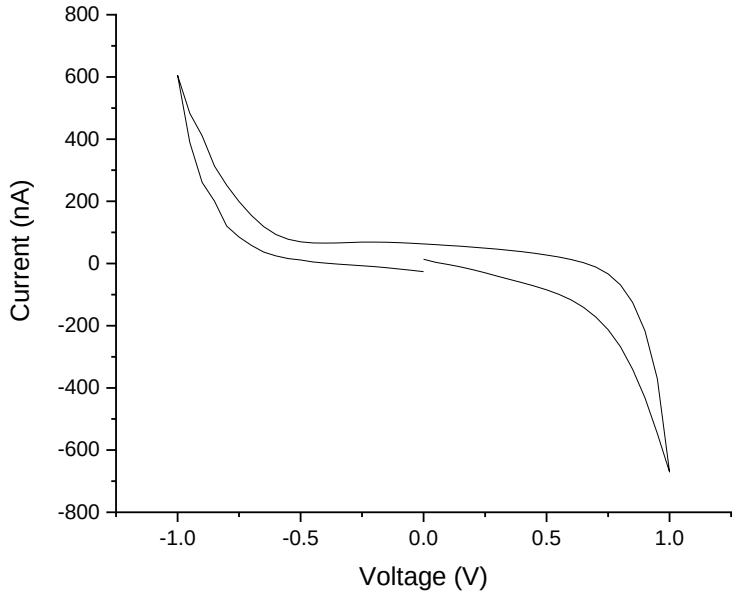

Figure 134. Transfer curve of PETE-S:HA using a flat paddle electrode as the gate electrode.

It should be noted that the experiments which attempted to use a flat paddle-shaped gate to compress the hydrogel samples onto the source and drain resulted in small observed currents and larger leakage currents. Therefore, the paddle gate idea was discontinued.

11.6.1. PETE-S:HA as a Transducing Scaffold

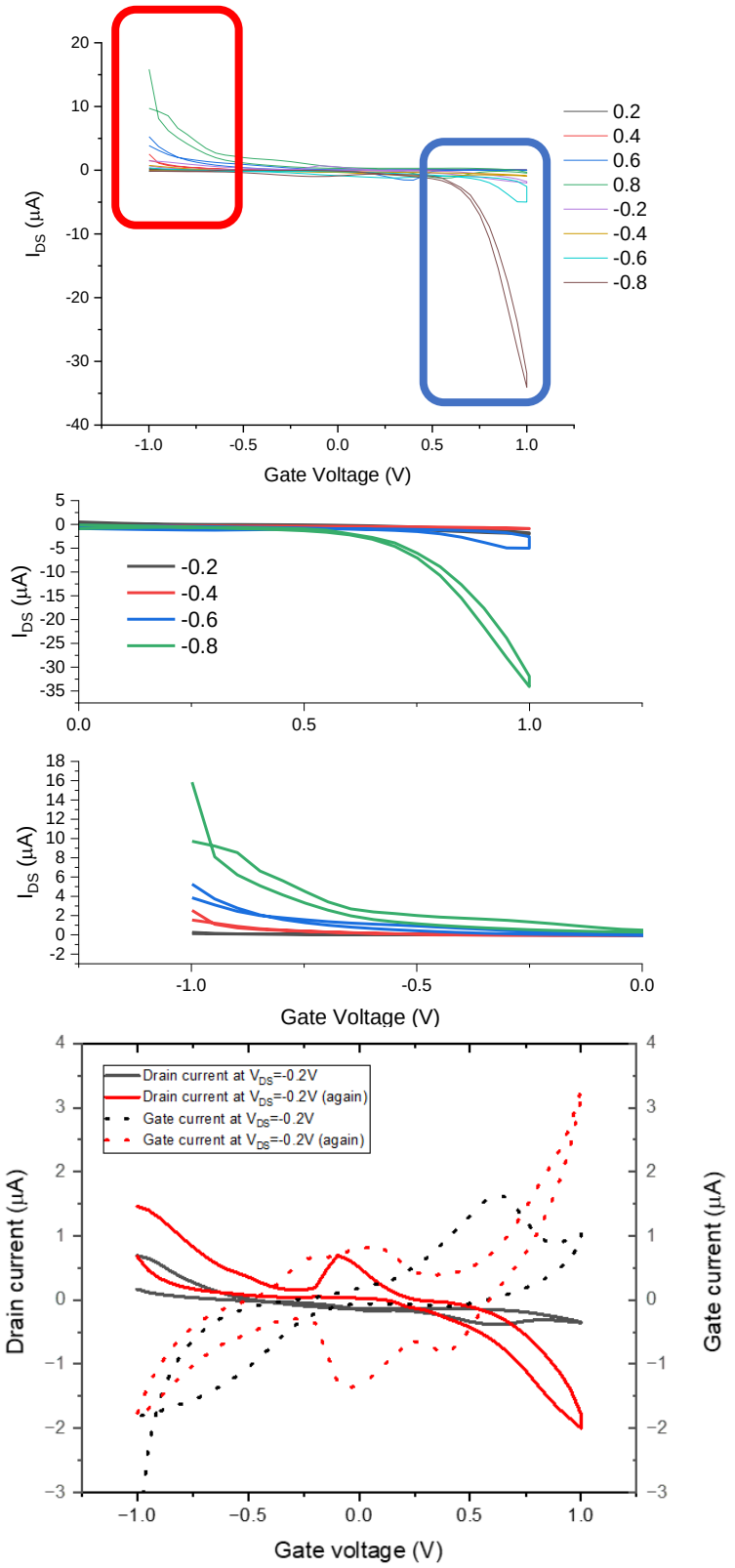

Figure 135. Image showing the electronic characteristics of PETE-S:HA. Top graph shows the transfer curves of PETE-S:HA taken over different $V_{drain\text{-}source}$ values. The middle image shows the zoomed in sections highlighted in the top graph. The bottom image compares the current at the gate and at the drain.

The ON/OFF ratio for the PETE-S:HA device can be identified in the transfer characteristics of the device once the experiment parameters have been fully optimised. The device current increases as the voltage sweeps to both positive and negative extreme voltages where it would be in the 'on' state. Around zero volts, the voltage plateaus around zero amps where it would then be considered 'off'.

The ON/OFF ratio can be taken from either of the sweeps where the device appears to have transistor switching. Ideally, the sweep at each extreme of the gate voltage would result in the same ON/OFF ratio, however experimentally that is not always the case. When the gate voltage is swept in a negative voltage, the ON/OFF ratio is ~5 when the V_{DS} is 0.6 V. Whereas when the voltage is swept in a positive direction, the ON/OFF ratio for the same V_{DS} is also ~5.

The transfer sweeps were repeated for V_{DS} values of 0 to -0.8 V at increments of 0.2V starting from -0.2 V_{DS} then working down to -0.8 V_{DS} before repeating -0.2 V_{DS}. The hope was that the trace seen for the initial -0.2 V_{DS} would be repeatable after taking the device to -0.8 V_{DS}. The trace is largely repeatable, however the repeated trace appears to have a larger faradaic contribution. This trace was taken to determine whether the electrolyte was undergoing hydrolysis when it approaches -1 V.

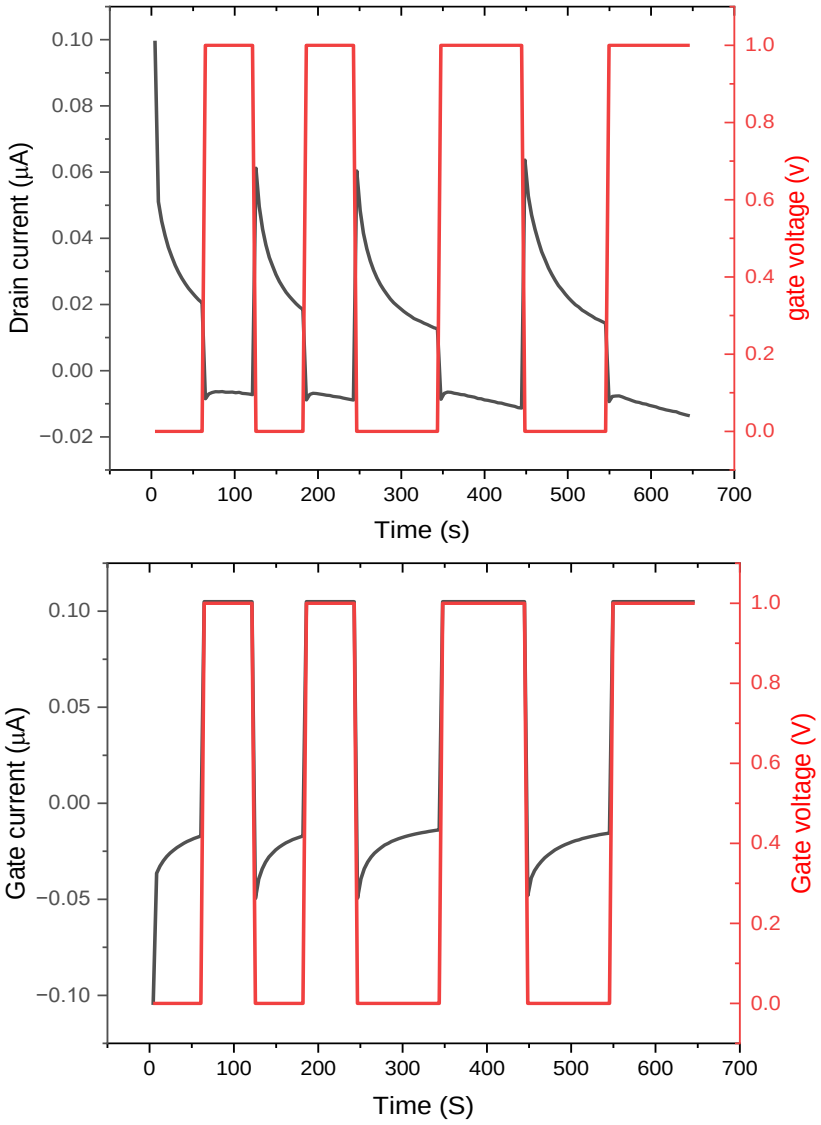

Figure 136. Square pulse response curves of PETE-S:HA for positive and negative currents.

By plotting a square pulse response, the conductive nature of the device can be explored further, figure 136. Here, the current is measured at the source with a pulse between 0 and 1V. The symmetry of the data appears to imply no observed ON/OFF functionality, which does not help to characterise the device, however this data can provide a means of establishing if leakage is occurring and what that leakage may be. If the leakage occurring was ion migration, this would be seen throughout the experiment, regardless of if the device is ‘on’ or ‘off’. However, in the figure 136 the off-state decays rapidly to zero. It can be assumed that a small, limited leakage is occurring, but it is likely that electronic transport occurs only along the PETE-S backbone. The exact current contributions would need to be understood before this device could undergo *in vivo* testing.

11.6.2. PEDOT:HA as a Transducing Scaffold

The same experiments were repeated this time using PEDOT:HA.

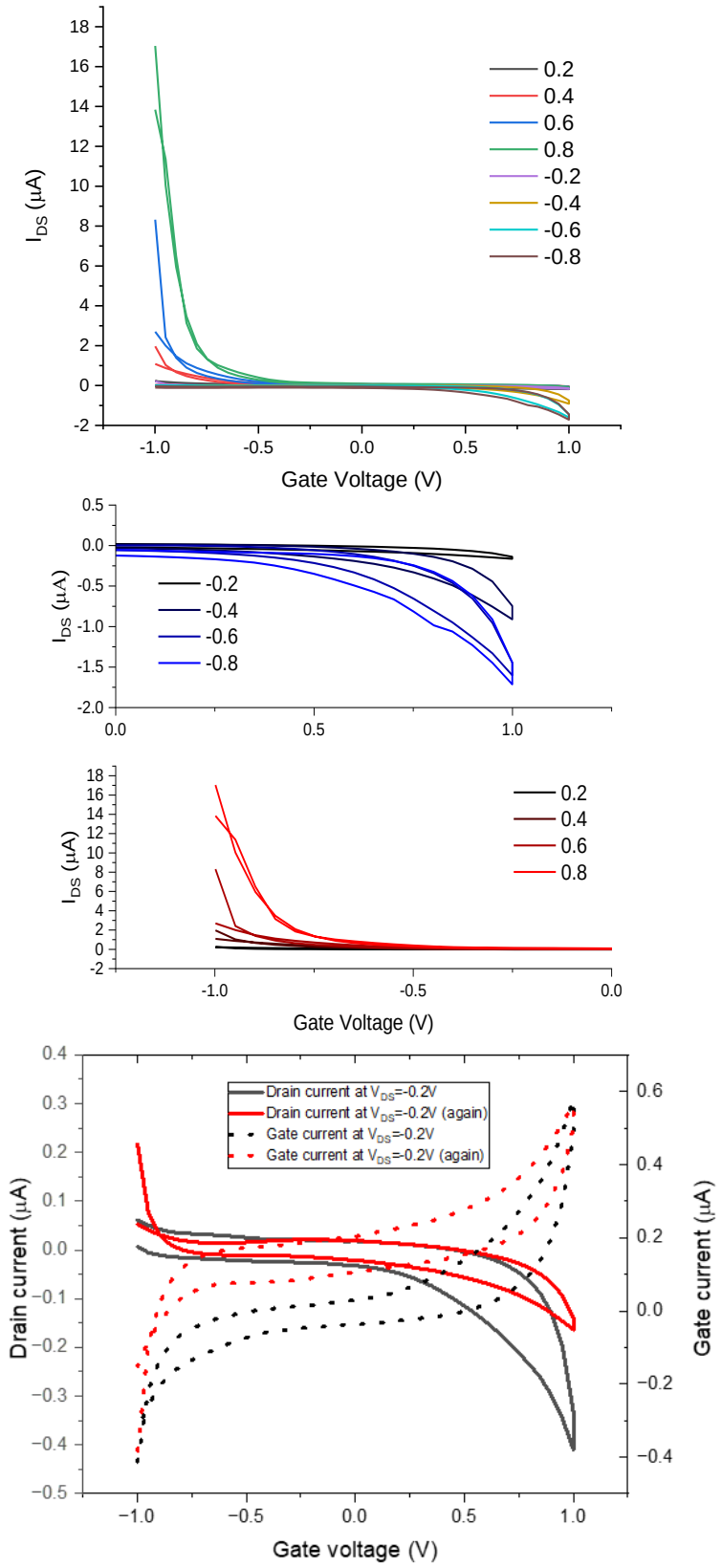

Figure 137. Image showing the electronic characteristics of PEDOT:HA. Top graph shows the transfer curves of PETE-S:HA taken over different $V_{drain\text{-}source}$ values. The middle image shows the zoomed in sections highlighted in the top graph. The bottom image compares the current at the gate and at the drain.

The results from the transfer curves of the PEDOT:HA a favourable in terms of their transistor switching behaviour. Similar concerns are raised about the channel current and whether or not the conduction occurring is by ion migration.

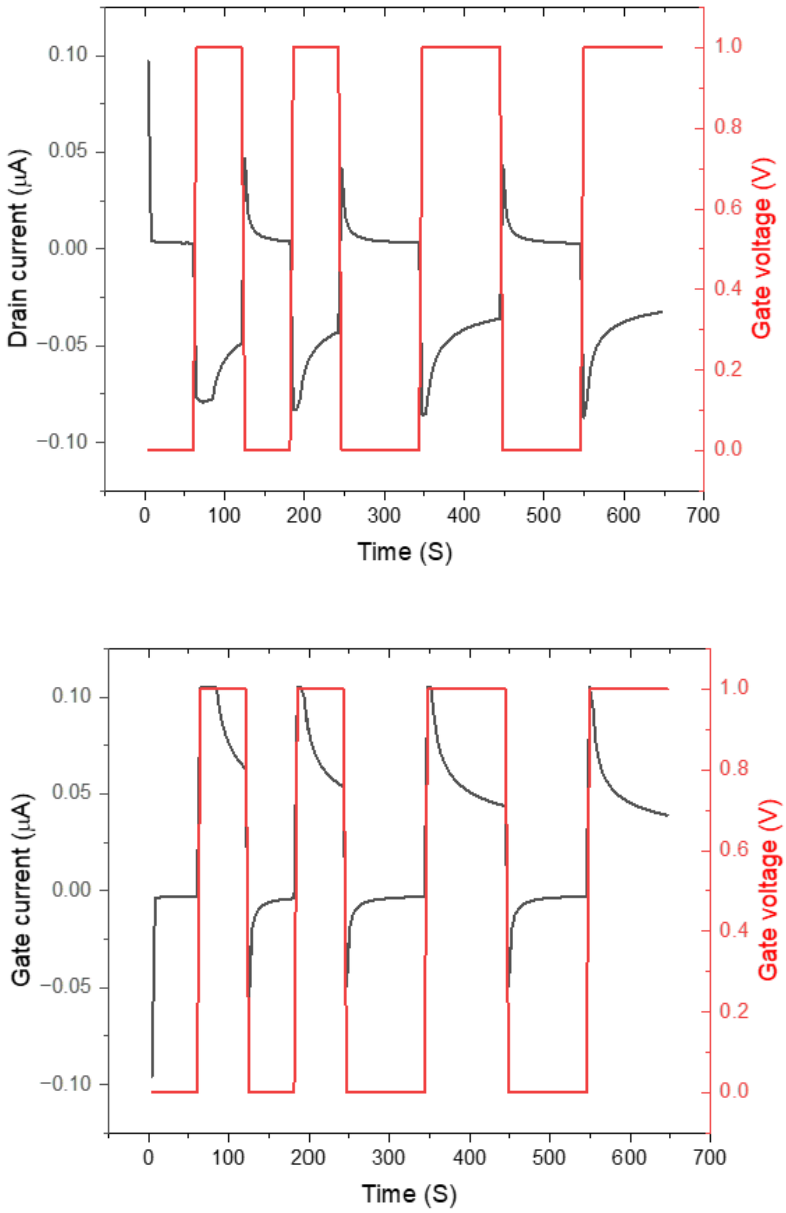

Figure 138. Square pulse response curves of PEDOT:HA for positive and negative currents

Again, a square pulse is applied to the device, measuring currents between 0 and 1V at the source. As it was for PETE-S:HA the datum appears to have some symmetry, implying no ON/OFF functionality, although this is not ideal the data here help to identify whether there is a leakage occurring. Ion migration, which occurs as leakage, should be observed in both the 'on' and 'off' states, however here the off-state decays to zero rapidly, suggesting there is only a small leakage. Here, transport only occurs along the PEDOT polymer.

The transconductance of the PEDOT transistor is roughly 0.1 mS which appears to be a positive result despite being subject to leakage current and a relatively poor ON/OFF current (the reason for which is subject to further study).[345] The threshold voltage appears to be roughly 0.75 V which would be considered poor for a device which targets the spinal cord.

11.7 Summary

While the electronic characterisation of the 3D gels provides a promising look at the potential these samples have, they are limited by the fact that their conductive nature cannot quite be characterised by transfer, output and square pulse response experiments. More knowledge about the ability of HA to undergo faradaic processes and ion transport is required to be able to determine where the injection of 'extra' current, seen in the square pulse response, comes from. The nature of the 3D gel means each sample is a slightly different size, therefore more uniform cuttings would need to be taken to delve deeper into its electronic properties such as maximum transconductance.

Although the nature of the transfer curves cannot be exactly explained in terms of the physics of the device, the shape of the curve indicates transistor switching. It is this switching which is essential for a device where the aim is to form a biocompatible OECT. So, while there are many questions raised by the electronic characterisation of the 3D transducers there are also promising results in terms of the devices ability to function as a biocompatible transistor.

Part. 5 Summary and Future Work

Chapter 12. Summary

Crosslinking using EDC and NHS as an initiator provides a means of producing hydrogels with improved mechanical properties while having a minimal effect on the biocompatibility of the original starting material. Such hydrogels have been created from gelatin and hyaluronic acid. No success was observed forming hydrogels of chondroitin sulfate. There was however much success when it came to gelatin and hyaluronic acid, both of which produced robust gels at room temperature which can be tailored to have desirable mechanical properties by tweaking the crosslinker density in the samples. These mechanical properties can be determined using indentation testing using a mechanical probe. Hyaluronic acid was more robust than gelatin over a wider spread of temperatures, including around body temperature which is key for a device which would be used in the body. Gelatin undergoes a transition to a liquid state around 40 ^{o}C, although crosslinking can help to raise the temperature at which this occurs. Unfortunately, the stability of the material was affected, with it breaking down quicker than hyaluronic acid does at an elevated temperature and therefore hyaluronic acid was favoured.

Hyaluronic acid gels were stable after being submerged in water for 25 days, and so the tests were extended to 60 days. Over this time degradation began to occur with some samples beginning to degrade and others remaining constant. Again, on extension to 5 months, many more samples had begun to degrade which indicates the life-time these material may have in the body. However, some samples did not degrade and provided an average mass of 91% after 5 months of submersion in water.

The main mode of degradation which would occur in the body is enzymatic and therefore solutions of various enzymes were made up to determine which has the most effect on HA. Lysozyme was the first enzyme examined and was found to have little to no effect on the hydrogel, which was the result of a 25-day exposure to lysozyme coming out very similar to the results observed when the solution was only water. Therefore, it was determined that lysozyme was not complementary to HA and no enzymatic degradation was occurring. If any degradation was occurring, it was hydrolytic. Two different hyaluronidase enzymes were tested, type 2 and type 1. Both of which are the most common hyaluronidase enzymes found in the body and therefore it is essential to

understand how they interact with HA. After 25 days of submersion in hyaluronidase, around 30% of the mass was lost from the original HA for type 2. Therefore, enzymatic degradation was confirmed to occur. Similar results were observed when the enzyme was changed to hyaluronidase type 1. Although the enzyme had begun to break down the sample more quickly than would be ideal for application to the spinal cord, it is important to know that the device is capable of biodegradation as this would be essential to the biocompatibility of the device.

To be compatible with the spinal cord the device needs to be a similar softness to that of the tissues which it would be surrounded by, to minimise the amount of adverse mechanical friction or wear that the device may cause on such tissues. The elastic modulus provides a means of quantifying these mechanical properties. The elastic modulus can be measured by determining the stress-strain relationship or by contact mechanics. For a thin, soft film such as the hyaluronic acid ones, contact mechanics appears to be a more appropriate method due to the stress-strain relationship requiring samples with a greater film thickness. Two methods were proposed to help to identify the sample amongst noise created by the water in which the sample is dispersed. These methods were named approach and retraction methods, when an applied load of 30 mN is used, the elastic modulus for the HA gels via the approach method is ~23 kPa and ~17 kPa using the retraction method. Both results are in the region identified as ideal for the spinal cord. According to moduli values available in the literature for both spinal cord tissues and for surrogate materials, an appropriate elastic modulus would be one which falls in a region of 5-100 kPa.

The HA gels which were stable in water, degraded with hyaluronidase enzymes and displayed good mechanical properties were considered to have optimal crosslinking densities and therefore the quantities of the materials were kept as semiconductive polymers began to be integrated into the formulation.

To function as a bioelectronic device there must be an element of the device which can carry a current, and so it was essential to incorporate semiconductive properties to provide the device with desirable transistor characteristics.

Dispersions containing HA and PEDOT can be created via the oxidative polymerisation of EDOT and are quickly characterised by a distinguishable colour change from colourless to a dark blue/almost black. These dispersions can be applied by either spin coating or by drop casting. Drop casting was found to be more efficient at creating films

without too much loss of material. Similar dispersions can also be created using chondroitin sulfate, however they have poor stability when cast and rehydrated. PEDOT:HA was initially characterised by CV finding that most samples provided spectra with broad traces when compared to a control of only the electrolyte. This broadening was assumed to be of a capacitive nature since the sample provided a broader spectrum than the control and so this broadening was thought to be an increase in the capacitive nature of the device when the sample was present. It was also discovered that the crosslinking did not hinder the conductive performance of the dispersion, with the crosslinked samples performing somewhat better than the uncrosslinked ones. This was believed to be related to the crosslinks forcing PEDOT chains closer together.

The dispersions have poor adhesion to the SPE on which the CV was carried out. Therefore, to minimise the amount of sample lost to the electrolyte, the CV was carried out horizontally where gravity would keep the samples on the correct electrode rather than vertically where, once detached, the sample sinks into the surrounding electrolyte. Changing to this method helped to optimise the CV experiments and allowed the sample to remain in place long enough to carry out EIS. A series of circuits were used to model the EIS data finding that a Randles circuit with the addition of a Warburg element and a constant phase element in the place of the capacitor provides the closest fit for the experimental data. Dispersions of both PEDOT:HA and PEDOT:CS were examined using EIS and compared to commercial PEDOT:PSS. PEDOT:PSS outperformed both of the experimental samples in terms of its capacitance and therefore ability to store charge.

Throughout the CV and EIS experiments the drop cast films were observed to be falling apart in solution. This was important to avoid when formulating the hydrogel, and therefore going back to the original formulation and methodology was essential to recover some of the stability found in the HA hydrogels themselves.

The polymerisation of EDOT was modified to maximise the successful crosslinking of HA, resulting in 3D gels which could be sliced with a knife and manipulated without falling apart. These gels could be cut to thicknesses which were appropriate for measuring the stress-strain profile via indentation testing. This provides an elastic modulus which can be compared to the elastic moduli obtained from a contact mechanics approach. Both methods provided moduli which fall into the 5-100 kPa range set as the target moduli for this project.

Two other polymers were proposed as alternatives to PEDOT. These were PETE-S and poly(thiopheneethanol), both of which have low hazards associated with them. PETE-S was ultimately favoured due to its self-doping ability. Both polymers could be synthesised using the same method as PEDOT however further crosslinking was required to form robust gels of PETE-S:HA. The gels of both of these polymers with HA displayed good mechanical properties which would fall into the range deemed acceptable for this project. The CV and EIS for the different gels had mixed results, with PETE-S:HA and PTE:HA appearing to have the poorest capacitive properties in the CV results. These two polymers had nevertheless better apparent capacitive properties when examined by EIS. The PTE:HA samples appeared to be slightly different colours to each other and therefore the samples were not investigated further. The PTE:HA samples have promising electronic properties, especially when used in a system which also contains PEDOT, but the polymerisation of thiopheneethanol requires optimisation to produce constant samples before further characterisation can be carried out.

Both the PEDOT:HA and PETE-S:HA samples as well as the HA scaffold itself displayed good biocompatibility when tested *in vivo* with a cell line. All three materials had low cytotoxicity values of 9%, 10% and 12% for HA, PETE-S:HA and PEDOT:HA respectively. Tolerable limits of biocompatibility are roughly 30% and so each of these samples would be considered biocompatible.

The gel samples of PEDOT:HA and PETE-S:HA display good biocompatibility, stability, and mechanical properties. Lastly, the samples needed to be characterised in terms of their ability to function as transistors. An IV was taken of each sample to determine whether the samples are indeed conductive. For PETE-S:HA an almost linear relationship between the current and voltage was found and therefore showed some electronic ability. However, the PEDOT:HA sample provided broader IV traces, suggesting that there are faradaic process going on, but this does not rule out the presence of electronic conductivity also occurring. When the IV was measured over a wider voltage, the linear relationship for both samples was lost, suggesting it is not only PEDOT:HA which undergoes faradaic reactions. A delay between each measurement was included which aimed to take data measurements after any faradaic processes had occurred. This improved the IV traces, providing a linear result for PETE-S:HA. By optimising the delay between the measurements, the effect of the faradaic processes can be minimised providing a means of distinguishing the electronic signal which also occurs in the samples.

Once the presence of electronic conductivity was confirmed, the samples could be characterised in terms of their transfer and output characteristics. The transfer characteristics for both samples display a clearly definable ‘on’ and ‘off’ state however there appears to be a leakage occurring. This leakage current does not occur during the ‘off’ state and therefore it is not determinantal to proving that the samples can function as a transistor. Its origin, however, is unclear. When a square pulse is applied to these samples, there is an injection of current from the gate which requires identifying. It was suspected that this current is related to both electronic and faradaic processes.

Robust, biocompatible, transducing gels of PETE-HA and PEDOT:HA have been produced. These samples can be created to the shape of a mould, sliced, and manipulated without interfering with the conductive nature of the device. These novel gels provide a foundation of knowledge that can be built upon for producing a 3D transducing hydrogel which can mimic the spinal cord.

12.1 Future Work

In the short term, PETE-S:HA and PEDOT:HA require further electronic characterisation to try and pin down the exact nature of the current transport which occurs, whether this is faradaic, electronic, or both. To do this, further transfer and output experiments are needed, particularly to understand the nature of the leakage which occurs.

Some initial characterisation was carried out on PEDOT:Gelatin samples. While they display good and versatile mechanical properties and have initial CV which appear promising, the chemistry of gelatin is unknown, making it hard to fully characterise the materials. However, there is promise for devices with a larger range of mechanical properties to be created from a co-system of gelatin and PEDOT. Similarly, CS has been proven to function as a good doping agent for PEDOT. Therefore, if an improvement can be made into the stability of CS in a gel, then there is potential to produce 3D gels with better conductive abilities than PEDOT:HA. Alternative crosslinking agents could also be considered which could help aid the stability of CS. Some initial work was carried out with (3-glycidoxypropyl)trimethoxysilane (GOPS) which is an adhesion promotor but also provides a means of forming an interpenetrating network. This work was abandoned due to silane having poor biocompatibility and no routes to natural biodegradation. However, there may be other crosslinking agents which could be considered and may improve the physical properties of the gels, something which would be essential for any work which would be carried out with CS.

Alternative architectures could also be considered for PETE-S:HA and PEDOT:HA such as a synapstor. Synapstors are largely of interest due to their ability to replicate the synapses in the spinal cord and therefore this would make the function of the device specifically relevant to the spinal cord and to SCIs.

Lastly, the device does not have to be limited to the spinal cord. The physical properties of the device can be tailored by changing the crosslinker density and therefore there are a number of biological and nonbiological applications which can benefit from a tuneable, responsive device.

Part. 6 Experimental Methods

Chapter 13. Materials

Gelatin, hyaluronic acid (sodium salt from streptococcus *equi*), chondroitin sulfate (sodium salt from bovine trachea), 1-ethyl-3-(3-dimethylaminopropyl)carbodiimide hydrochloride, (EDC.HCl), (3-glycidoxypropyl)trimethoxysilane, ethanol, and phosphate buffered saline tablets, were all purchased from Merck and used as received. Iron sulfate, ammonium persulfate and thiopheneethanol were purchased from Fisher Scientific and used as received.

Chapter 14. Experimental Methodology

14.1.1. Initial Gelatin Gels

Solution of gelatin in DI water were made by dissolving varying weights of gelatin in water (10g) which was warmed to 40 °C. The percentage amounts of gelatin were 0.5, 1.0, 1.5, 2.0, 2.5, 3.0, 5.0, 10.0% by mass. The mixture was stirred until the gelatin was completely dissolved. Once dissolved, the mixture was transferred to the fridge and left for 24 hours to set into a gel.

14.1.2. FTIR of Gelatin

A solution of 10% gelatin in DI water was prepared by dissolving gelatin powder in water (10 g) at 40 °C and stirring until it was fully dissolveed. The solution was then poured into a 80x15 mm petri dish and left for 72 h at room temperature to completely dry out. The sample must be dry before carrying out FTIR experiments to prevent water dominating the spectra. To get good compression of the solid gelatin to the crystal, the film needs to be divided into smaller fragments and the force gauge on the spectrometer should be applied to minimise noise. A Perkin Elmer UATR Spectrum Two FTIR spectrometer was used, with the settings 500-4000 cm^{-1}, 32 scans in transmission mode.

14.1.3. Identifying the Load-Force Relationship for Gelatin Gels

A solution of 10% gelatin in DI water was prepared by dissolving gelatin powder in water (10 g) at 40 °C and stirring until it was fully dissolved. The solution was then stored in the fridge for 24 h for it to set into a gel. This gel was then tested using a compression test on a Stable Micro Systems TA.XTPlusC Texture Analyser, Surrey, UK. First the thickness of the gel must be identified, this can be carried out by calibrating the device and then measuring the height of the sample by setting the probe to move until it makes contact with the surface of the gel. To measure the load-force relationship,

a cylindrical Delrin probe with a radius of 5 mm was used and the test to indent to specified depth was chosen.

14.1.4. Swelling Unmodified Gelatin Gels

A solution of 10% gelatin in DI water were prepared by dissolving gelatin powder in water (10 g) at 40 °C and stirring until it fully dissolved. The solution was then poured into a 80 × 15 mm petri dish and left for 72 hours at room temperature to completely dry out. The dehydrated hydrogel films were then cut into 1 cm^2 pieces which were weighed. The samples were then swollen by adding DI water at various temperatures dropwise (20, 25, 30, 35, 40 °C). The samples were again weighed before being submerged in 2 mL of DI water at their respective temperatures for 5 minutes. Following this, the samples were separated from the water solution and were again weighed. The samples were then left to dry at room temperature before being weighed again.

14.1.5. Recovering A Gel after Heating

The method for producing gels outlined in 2.2.2 was again used to produce gels with the following percentage gelatin contents by weight, see Table 11. These gels were then heated to 90 °C until they became liquids. Following heating, the gels were moved to the fridge and stored for 72 h to see if gelation occurred.

Table 11. Gelatin samples and observations about the mixture.

Gelatin (%wt)	Gelatin (g)	Water (g)	Comment
0.0100	0.0005	4.9995	Solid gelatin dissolved during heating. Gelation did not occur on storage in fridge
0.1000	0.0050	4.9950	Solid gelatin dissolved during heating. Gel set in fridge after 1+ hours
0.5000	0.0250	4.9750	Solid gelatin dissolved during heating. Gel set in fridge after 1+ hours
1.0000	0.0500	4.9500	Solid gelatin dissolved during heating. Gel set in fridge after 1+ hours
1.5000	0.0750	4.9250	Solid gelatin dissolved during heating. Gel set in fridge after 1+ hours
2.0000	0.1000	4.9000	Solid gelatin dissolved during heating. Gel set in fridge after 1+ hours
2.5000	0.1250	4.8750	Solid gelatin dissolved during heating. Gel set in fridge after 1+ hours
3.0000	0.1500	4.8500	Solid gelatin dissolved during heating. Gel set in fridge after 1+ hours
5.0000	0.2500	4.7500	Solid gelatin dissolved during heating. Gel set in fridge after 1+ hours
10.0000	0.5000	4.5000	Solid gelatin dissolved during heating. Gel set in fridge after 1+ hours

14.1.6. Initial Gelatin Crosslinking Trial

Gelatin was added to DI water at various concentrations (See Table 12) and heated to 40 °C until the powder had dissolved. Solutions of EDC in ethanol were made up and combined with the gelatin solution. The mixtures were stirred for 15 minutes and moved to the fridge for 24 h to allow gelation to occur.

Table 12. Initial crosslinked Gelatin gel formulations

% EDC	Gelatin Mass (g)	Water (g)	Ethanol (g)	Comment
5	0.0943	0.8592	0.0443	Gel set on cooling after 12+ hours
10	0.0939	0.8021	0.1052	Some solid crashing out.
20	0.0882	0.7302	0.2106	Some solid crashing out.
30	0.0793	0.6507	0.3191	Gel layer and liquid layer.
40	0.0258	0.272	0.1942	Gel layer and liquid layer.
50	0.0244	0.2181	0.2448	Gel layer and liquid layer.

14.1.7. Crosslinking Gelatin Hydrogels

A mixture of gelatin (400 mg) in DI water (2.7 mL) was heated to 40 °C until the gelatin powder was dissolved. A second solution consisting of EDC (0.4 mg) and ethanol (1.14 mL) was stirred until all the solid was dissolved. This sample is considered as a 0.01% EDC sample. The gelatin solution was removed from the heat and combined with the ethanol solution. The mixture was stirred for 15 minutes and was then moved into the fridge for 24 h for gelation to occur. Other crosslinker densities were made using the same methodology but according to the quantities in Table 13.

Table 13. Crosslinked Gelatin gel formulations

% EDC	EDC (mg)	Gelatin (mg)	Water (uL)	Ethanol (mL)
0.01	0.40	400.00	2699.70	1140.56
0.05	2.00	400.00	2698.50	1140.05
0.10	4.00	400.00	2697.00	1139.42

14.1.8. Swelling Gelatin Hydrogels

The procedure detailed in 2.2.7 was repeated, however, instead of placing the gels into the fridge for 24 h, the gels were poured into a 80×15 mm petri dish and were left to dry at room temperature for 72 hours. The dehydrated hydrogel films were then cut into 1 cm^2 pieces which were weighed. The samples were then swollen by adding DI water at various temperatures dropwise (20, 25, 30, 35, 40 °C). The samples were again weighed before being submerged in DI water (2 mL) at their respective temperatures for a specified time. Following this, the samples were separated from the water solution and were again weighed.

14.1.9. Swelling Methods

Three methods were used to find the best methodology for measuring the maximum swelling of the gels. The first is using a Buchner funnel. The gels were prepared and swollen according to section 2.2.8. However, when the gel requires weighing the method changes. During the Buchner funnel method, the solution containing the gel is poured

into the funnel containing filter paper and is filtered under vacuum before the gel is freed from the paper and weighed.

Two further methods are employed to compare with the Buchner funnel approach, these are a tweezer approach and blotting approach - both used to determine the maximum swelling of the gels. The first method involves using tweezers to simply lift the gel from the solution before blotting and weighing it. In the second method, filter paper is used so that the solution can be separated from the gel. Here, the solution is tipped into a funnel containing filter paper and is allowed to drip through unaided. Once all the solution has passed, the gel is removed from the paper and is weighed.

14.1.10. FTIR of Crosslinked Gelatin Samples

The samples were prepared according to the procedure detailed in 2.2.7, however rather than placing the sample in the fridge, the samples were poured into 80×15 mm petri dishes and left at room temperature for 72 h to dehydrate. The samples were then removed whole from the dishes using a scalpel and transferred onto the crystal of the Perkin Elmer UATR Spectrum Two FTIR spectrometer. Ten separate spectra were recorded at different positions of the film using a wavenumber range of 500-4000 cm^{-1}, 32 scans and in transmission mode.

14.1.11. Molecular Mass of Gelatin

A Malvern Zetasizer ZS DLS with a red laser (633 nm) was used for the molar mass measurements of the gelatin samples. A series of samples containing various concentrations of gelatin in water were made up (1.0, 2.5, 5.0, 7.5, 10%) ensuring no visible particulate matter remained in the vial before testing. The samples were then transferred to a cuvette and placed in position for the laser. Each sample is measured in turn according to a standard operating procedure (SOP) for molecular weight, this includes using the solvent refractive index (1.330) and a standard Rayleigh ratio of 1.15×10^{-6}.[239] A Debye plot is then automatically generated by the software from which the average molecular weight is estimated.

14.1.12. Examining the Flory Huggins Swelling Parameter of Gelatin

The samples used in this section were prepared according to section 2.2.9.

14.1.13. Swelling Gelatin Samples at various pH

The procedure detailed in 2.2.7 was repeated, however instead of placing the gels into the fridge for 24 hours the gels were instead poured into an 80×15 mm petri dish and were left to dry at room temperature for 72 h. The dehydrated hydrogel films were then

cut into 1 cm^2 pieces which were weighted. The samples were then swollen by adding DI water at various temperatures dropwise (20, 25, 30, 35, 40 °C). The samples were again weighed before being submerged in 2 mL of solution at a specified pH (1-14 respectively). The samples were weighed every 10 minutes to monitor how their mass changed. Following this, the samples were separated from the water solution and were again weighed. Solutions with a pH of 1-6 were made by adding HCl to DI water. Samples tested in pH's 8-14 used a solution of KOH in DI water and adjusted to a necessary pH. The sample tested at pH 7 used a solution of deionised water.

14.1.14. Hydrolytic Degradation Studies of Gelatin Samples

Again, the procedure to produce dehydrated films was carried out by following section 14.1.7 however instead of placing the samples into the fridge, the gels were left to dehydrate for 72 h in a petri dish (80 x 15 mm) at room temperature. The samples were then cut into 1 cm^2 pieces and were weighed. Each section was then swollen using DI water and placed into a 2 mL solution at 37 °C. Each sample was weighed each hour for 4 h to see how the mass changed during the experiment.

14.1.15. Mechanical Properties

Samples were prepared according to section 2.2.9. Once gelation had occurred, the samples were placed onto the platform of the Stable Micro Systems TA.XTPlusC Texture Analyser. A compression test was carried out where the probe was lowered to the surface of the gel at a speed of 30 mm/min. Once in contact with the sample, the measurement began. The tester was set to indent to a specified force (0.01-0.08N) at a speed of 15 mm/min and then the indenter would retract from the sample at 30 mm/min. A cylindrical Delrin probe was used with a radius of 5 mm, an elastic modulus of 3600 MPa and a Poisson's ratio of 0.35. The hold time once the target force is reached is 0.5 min, and the trigger force is set to 0 N.

14.1.16. Creating Chondroitin Sulfate Films

EDC (4.1 mg), NHS (1.6 mg) and ethanol (0.98 mL) were mixed together until the EDC and NHS were dissolved. Chondroitin sulfate (20 mg) was then added to the mixture. Water (3 mL) was then slowly added to the mixture dropwise and then the mixture was left to stir for 30 minutes. The mixture was then poured into a petri dish (80 x 15 mm) and left to dry at room temperature for 24 hours.

14.1.17. Creating Chondroitin Sulfate/Gelatin Films

A mixture of gelatin (400 mg) in DI water (2.7 mL) was heated to 40 °C until the gelatin powder was dissolved. A second solution consisting of EDC (0.4 mg) and ethanol (1.14 mL) was stirred until all the solid was dissolved, and to this CS was added in the amounts listed in Table 14. The gelatin solution was removed from the heat and combined with the ethanol/crosslinker/CS solution. The mixture was stirred for 15 minutes and was then moved into the fridge for 24 hours for gelation to occur.

Table 14. Mixtures of Gelatin and chondroitin sulfate

Sample Name	Gelatin (mg)	CS (mg)
1:1 Gelatin:CS	200	200
1:2 Gelatin:CS	133	267
1:5 Gelatin:CS	67	333
1:10 Gelatin:CS	36	364
1:1 CS:Gelatin	200	200
1:2 CS:Gelatin	133	267
1:5 CS:Gelatin	67	333
1:10 CS:Gelatin	36	364

14.1.18. Creating Hyaluronic acid Gels

A vial was set up on a magnetic stirring plate and surrounded by ice to maintain a cool environment. EDC, NHS and ethanol (0.98 mL) were mixed together according to the amounts in Table 15 until the EDC and NHS were dissolved. Hyaluronic acid (20 mg) was then added to the mixture. HCl (pH 4, 0.4 mL) was added and allowed to stir in the mixture for 15 minutes. Water (2.6 mL) was then slowly added to the mixture dropwise, following this the mixture was left to stir for 30 minutes. The mixture was then poured into a petri dish (80x15 mm) and left to dry at room temperature for 24 h.

Table 1586. Crosslinked hyaluronic acid. Formulations showing different crosslinker densities.

Material	Material by Mass (mg)						
	Formulation 1	Formulation 2	Formulation 3	Formulation 4	Formulation 5	Formulation 6	Formulation 7
HA	2.00	2.00	2.00	2.00	2.00	2.00	2.00
EDC	0.02	0.04	0.08	0.16	0.20	0.40	0.80
NHS	0.08	0.16	0.32	0.64	1.28	2.56	5.12
Ethanol	48.95	48.90	48.79	48.60	48.26	47.52	46.04
Water	148.95	148.90	148.79	148.60	148.26	147.52	146.04

14.1.19. Swelling Hyaluronic Acid Gels

The dehydrated hydrogel films were cut into 1 cm^2 pieces which were weighed. The samples were then swollen by adding DI water before being submerged in water for a

known amount of time. After the designated time interval, the samples were removed from the water, blotted, and weighed.

14.1.20. FTIR of HA Gels

Dehydrated samples were cut into small pieces and placed onto the test plate on the FTIR device itself. The foot of the FTIR was lowered onto the sample and 32 scans were ran and overlayed into one spectrum.

14.1.21. Creating Hyaluronic acid Gels with alternative Solvents

EDC (2 mg), NHS (12.8 mg) and ethanol (0.39 mL) were mixed together until the EDC and NHS were dissolved. Hyaluronic acid (20 mg) was then added to the mixture. Water (1.48 mL) was then slowly added to the mixture dropwise, and following this the mixture was left to stir for 30 minutes. The solutions were PBS, MES, Water, and HCl respectively. The mixture was then poured into a petri dish (80 x 15 mm) and left to dry at room temperature for 24 h.

14.1.22. Creating Hyaluronic acid Gels with Varying Ethanol Content

Three different samples were made up with different ethanol contents (0.39, 0.78 and 1.17 mL respectively) to which EDC (2 mg) and NHS (12.8 mg) were added and mixed together until the EDC and NHS were dissolved. Hyaluronic acid (20 mg) was then added to the mixture. Water (0.49, 0.99 and 1.48 mL) was then slowly added to the mixture dropwise, after which the mixture was left to stir for 30 minutes. The mixture was then poured into a petri dish (80 x 15 mm) and left to dry at room temperature for 24 h.

14.1.23. Degradation of Hyaluronic Acid Gels in Water or PBS

The dehydrated hydrogel films were then cut into 1 cm^2 pieces which were weighed. The samples were then swollen by adding DI water before being submerged in water or PBS for a known amount of time. After the designated time interval, the samples were removed from the water, blotted, and weighed. These samples were then dried in an oven for at least 4 hours at 50 ^{O}C and the samples were weighed again to find out the mass of their dehydrated state.

14.1.24. Particle Size Measurements of Hydrolytic Degradation

The solution in which the gels were contained for their degradation experiments was kept and poured into a cuvette to undergo dynamic light scattering analysis. An SOP was created which contains the reflective index of the sample to which the blank is compared.

2.2.1 Enzymatic Degradation of Hyaluronic Acid Gels

Three enzymatic solutions were created: one containing lysozyme (100 mg per L), the second containing hyaluronidase type 2 (80 U/mL), and the third solution containing hyaluronidase type 1 (80 U/mL). The dehydrated hydrogel films were then cut into 1 cm^2 pieces which were weighed. The samples were then swollen by adding DI water before being submerged into small quantities of the solutions for a known amount of time. After the designated time interval, the samples were removed from the water, blotted, and weighed. These samples were then dried in an oven for at least 4 h at 50 °C and the samples were weighed again to find out the mass of their dehydrated state.

14.1.25. Optical Microscope Images

The dehydrated hydrogel films were then cut into 1 cm^2 pieces and placed onto a glass slide. This slide was then examined using a 3D optical profilometer to build and image of the depth of the film.

14.1.26. Measuring the Stress-strain Relationship

The dehydrated hydrogel films were cut into 1 cm^2 pieces and placed onto a glass slide underneath the probe of the Stable Micro Systems TA.XTPlusC Texture Analyser. The probe was then set to indent into the sample to a known depth using 30 mm/min. The probe used was a cylindrical Delrin probe with a radius of 5 mm, an elastic modulus of 3600 MPa and a Poisson's ratio of 0.35. The test uses a pre-test speed, a test speed and a post-test speed of 0.5 mm/s in each case.

14.1.27. PEDOT:GAG Synthesis

The synthesis used by D. Mantione *et. al.* will form the basis for synthesising PEDOT:biomolecules in this thesis.[286]

A 2% wt solution of PEDOT:GAG was produced in this synthesis where PEDOT and GAG were in a 1:1 ratio. The GAGs used are hyaluronic acid and chondroitin sulfate. GAG (20 mg) was added to water (1.48 mL) and left until fully dissolved. Ethanol (0.39 mL) was added and left to stir for 15 minutes. EDOT was then added to the solution and left for a further 15 minutes to dissolve. APS (in 1.5 mol ratio with EDOT) and a catalytic amount of iron sulfate were then added. The mixture was then left to stir for 48 h.

14.1.28. Cyclic Voltammetry

A series of 0.1 M solutions were to be used as electrolytes, these were NaCl, KOH, ferri/ferrocyanide in PBS. Roughly 15 mL of solution was used for CV measurements. 20 µL of sample PEDOT:GAG was drop cast to the SPE and dried for 30 minutes using a hot plate set to 60 ºC. Following this the SPE is connected to the electrodes and lowered so that the test area is submerged. CV are then run between known voltages, at specified scan rates according to each experiment.

14.1.29. CV and EIS with Drop Sense Technology

Roughly 15 mL of solution was used for CV measurements. 20 µL of sample PEDOT:GAG was drop cast to the SPE and dried for 30 minutes using a hot plate set to 60 °C. Following this 60 µL of solution was added carefully to the top of the test area making sure it covers the other electrodes too.

14.1.30. Crosslinked PEDOT:GAG Synthesis

A 2% wt solution of PEDOT:GAG was produced in this synthesis where PEDOT and GAG were in a 1:1 ratio. GAG (20 mg) was added to water (1.48 mL) and left until fully dissolved. EDC (2 mg), NHS (12.8 mg) and ethanol (0.39 mL) were then added and left to stir for 15 minutes. EDOT was then added to the solution and left for a further 15 minutes to dissolve. APS (in 1.5 mol ratio with EDOT) and a catalytic amount of iron sulfate were then added. The mixture was then left to stir for 48 h.

14.1.31. Transfer and Output characterisation

5 µL of PEDOT:GAG was added carefully to each electrode in the 9 electrode array, and dried in a thermostatic oven at 120 °C for 30 minutes. The source, drain and gate are then lined up and a sweep of changing gate voltage between -0.8 and 0.8 V can be applied to the system monitoring the drain-source current throughout. The transistor experiments can be carried out with or electrolyte according to the experiment. The electrolyte used was 1 mL of NaCl (9 g/L) applied over the nine-electrode array.

14.1.32. Square Pulse Characterisation

Carried out using the same experimental procedure as in 2.2.33 however the software was amended to only apply a voltage for a known amount of time (20 seconds) while monitoring the three electrodes.

14.1.33. Synthesising Transducing PEDOT Hydrogels

A vial was set up on a magnetic stirring plate and surrounded by ice to maintain a cool environment. EDC (2 mg), NHS (12.8 mg) and ethanol (0.39 mL) were mixed together

until the EDC and NHS were dissolved. Hyaluronic acid (20 mg) was then added to the mixture. HCl (pH 4, 0.4 mL) was added and left to stir for 15 minutes. Water (1.48 mL) was then slowly added to the mixture dropwise, following this the mixture was left to stir for 30 minutes. The pH was then raised to ~6 using KOH. EDOT (20 mg) was then added to the solution and left for a further 15 minutes to dissolve. APS (in 1.5 mol ratio with EDOT) and a catalytic amount of iron sulfate were then added. The mixture was then transferred to a shaking plate and left on it for 48 h to react. From here the resulting gel was transferred to a solution of ethanol (70% v/v) in water and left for 24 hours to remove and impurities. The sample was then rinse with further ethanol (70% v/v) in water.

14.1.34. Synthesising Transducing PETE-S or Poly(thiopheneethanol) Hydrogels

A vial was set up on a magnetic stirring plate and surrounded by ice to maintain a cool environment. EDC (2 mg), NHS (12.8 mg) and ethanol (0.39 mL) were mixed together until the EDC and NHS were dissolved. Hyaluronic acid (20 mg) was then added to the mixture. HCl (pH 4, 0.4 mL) was added and left to stir for 15 minutes. Water (1.48 mL) was then slowly added to the mixture dropwise, following this the mixture was left to stir for 30 minutes. The pH was then raised to ~6 using KOH. ETE-S (20 mg) or thiopheneethanol (20 mg) was then added to the solution and left for a further 15 minutes to dissolve. APS (in 1.5 mol ratio with ETE-S or thiopheneethanol) and a catalytic amount of iron sulfate were then added. The mixture was then transferred to a shaking plate and left on there for 48 hours to react. From here the resulting gel was transferred to a solution of ethanol (70%) in water and left there for 24 hours to remove and impurities. The sample was then rinsed with further ethanol (70%) in water.

14.1.35. Crosslinking PETE-S Hydrogels

The methodology outlined in 14.1.34 was followed to polymerise ETE-S within hyaluronic acid. This gel is then placed into a 5% EDC in ethanol and water (70:30) mixture for 24 hours where it is left to further crosslink. From here the resulting gel was transferred to a solution of ethanol (70% v/v) in water and left there for 24 h to remove and impurities. The sample was then rinsed with further ethanol (70% v/v) in water.

14.1.36. Synthesising PEDOT/Poly(thiopheneethanol) Hydrogels

PEDOT and poly(thiopheneethanol) were in a 1:1 ratio by volume in this experiment. A vial was set up on a magnetic stirring plate and surrounded by ice to maintain a cool environment. EDC (2 mg), NHS (12.8 mg) and ethanol (0.39 mL) were mixed together until the EDC and NHS were dissolved. Hyaluronic acid (20 mg) was then added to the

mixture. HCl (pH 4, 0.4 mL) was added and left to stir for 15 minutes. Water (1.48 mL) was then slowly added to the mixture dropwise, following this the mixture was left to stir for 30 minutes. The pH was then raised to ~6 using KOH. EDOT (10 mg) and thiopheneethanol (10 mg) was then added to the solution and left for a further 15 minutes to dissolve. APS (in 1.5 mol ratio with EDOT) and a catalytic amount of iron sulfate were then added. The mixture was then transferred to a shaking plate and left on there for 48 hours to react. From here the resulting gel was transferred to a solution of ethanol (70% v/v) in water and left for 24 hours to remove and impurities. The sample was then rinsed again with ethanol (70% v/v) in water.

14.1.37. IV, Transfer and Output Characterisation of 3D Gels

A slice of gel roughly 5 x 5 x 5 mm in dimension of PEDOT:HA or PETE-S:HA was added carefully to each electrode in the electrode array. PBS electrolyte was then gently added over the sample ensuring to include the gate in the electrolyte. The source, drain and gate connections were then lined up and a sweep of changing gate voltage between -1 and 1 V can be applied to the system monitoring the drain-source current throughout. For transfer characteristics the drain-source voltage is changed at known intervals. For the output characteristics the gate voltage is changed. The initial experiments were carried out using a Keithley 2450 and 2000 analyser. For the later experiments where data was required for each individual electrode the device used was a Cascade station with Keithley 3200A parameter analyser.

14.1.38. Square Pulse Characterisation with 3D gels

Square pulse characterisation was carried out using the same experimental procedure as in 14.1.32 using the Cascade station with a Keithley 3200A parameter analyser. However, the software was amended to only apply a voltage for a set amount of time while monitoring the three electrodes.

Part. 7 Bibliography

1. C. R. Noback, N. L. Strominger, R. J. Demarest and D. A. Ruggiero, in *The Human Nervous System: Structure and Function*, Humana Press, Totowa, NJ, 2005, DOI: 10.1007/978-1-59259-730-7_2, pp. 11-39.
2. C. R. Noback, N. L. Strominger, R. J. Demarest and D. A. Ruggiero, in *The Human Nervous System: Structure and Function*, Humana Press, Totowa, NJ, 2005, DOI: 10.1007/978-1-59259-730-7_1, pp. 1-10.
3. B. P. Daly, D. M. Eichen, B. Bailer, R. T. Brown and C. L. Buchanan, in *Encyclopedia of Human Behavior (Second Edition)*, ed. V. S. Ramachandran, Academic Press, San Diego, 2012, DOI: https://doi.org/10.1016/B978-0-12-375000-6.00084-7, pp. 454-459.
4. A. Tuladhar, N. Mitrousis, T. Führmann and M. S. Shoichet, in *Translational Regenerative Medicine*, eds. A. Atala and J. G. Allickson, Academic Press, Boston, 2015, DOI: https://doi.org/10.1016/B978-0-12-410396-2.00030-X, pp. 415-435.
5. J. Ross, *Nervous system*, Mosby Ltd., 4th ed.. edn., 2015.
6. C. G. Smith, in *Basic Neuroanatomy*, University of Toronto Press, 1961, pp. 1-12.
7. R. D. Fields, A. Araque, H. Johansen-Berg, S.-S. Lim, G. Lynch, K.-A. Nave, M. Nedergaard, R. Perez, T. Sejnowski and H. Wake, *The Neuroscientist*, 2013, **20**, 426-431.
8. D. Debanne, E. Campanac, A. Bialowas, E. Carlier and G. Alcaraz, *Physiological Reviews*, 2011, **91**, 555-602.
9. J. M. Williamson and D. A. Lyons, *Frontiers in Cellular Neuroscience*, 2018, **12**.
10. E. Mtui, *Fitzgerald's clinical neuroanatomy and neuroscience*, Philadelphia : Elsevier, Eighth edition.. edn., 2021.
11. M. H. Grider, R. Jessu and R. Kabir, in *StatPearls*, StatPearls Publishing, Treasure Island (FL), 2022.
12. B. P. Bean, *Nature Reviews Neuroscience*, 2007, **8**, 451-465.
13. Q. R. Morell P, *The Myelin Sheath. In: . Basic Neurochemistry: Molecular, Cellular and Medical Aspects.*, Lippincott-Raven, Philadelphia, 6th edn., 1999.
14. A. E. Wilkinson, A. M. McCormick and N. D. Leipzig, in *Central Nervous System Tissue Engineering: Current Considerations and Strategies*, eds. A. E. Wilkinson, A. M. McCormick and N. D. Leipzig, Springer International Publishing, Cham, 2012, DOI: 10.1007/978-3-031-02582-2_2, pp. 3-16.
15. J. Gruchot, V. Weyers, P. Göttle, M. Förster, H. P. Hartung, P. Küry and D. Kremer, *Cells*, 2019, **8**.
16. A. D. Gaudet, P. G. Popovich and M. S. Ramer, *Journal of Neuroinflammation*, 2011, **8**, 110.
17. C. S. Ahuja, J. R. Wilson, S. Nori, M. R. N. Kotter, C. Druschel, A. Curt and M. G. Fehlings, *Nature Reviews Disease Primers*, 2017, **3**, 17018.
18. A. Alizadeh, S. M. Dyck and S. Karimi-Abdolrezaee, *Frontiers in Neurology*, 2019, **10**, 282.
19. D. McDaid, A. L. Park, A. Gall, M. Purcell and M. Bacon, *Spinal Cord*, 2019, **57**, 778-788.
20. L. D. Hachem, C. S. Ahuja and M. G. Fehlings, *Journal of Spinal Cord Medicine*, 2017, **40**, 665-675.
21. Y. Chen, Y. He and M. J. DeVivo, *Archives of Physical Medicine and Rehabilitation*, 2016, **97**, 1610-1619.
22. J. W. McDonald and C. Sadowsky, *The Lancet*, 2002, **359**, 417-425.
23. D. Sandean, *World J Orthop*, 2020, **11**, 573-583.
24. J. McRae, C. Smith, A. Emmanuel and S. Beeke, *BMC Health Services Research*, 2020, **20**, 783.
25. N. MacBean, E. Ward, B. Murdoch, L. Cahill, M. Solley and T. Geraghty, *Journal of Medical Speech - Language Pathology*, 2006, **14**, 167+.
26. S. Brady, R. Miserendino, D. Statkus, T. Springer, M. Hakel and V. Stambolis, *Journal of Applied Research in Clinical and Experimental Therapeutics*, 2004, **4**, 1-11.
27. P. W. New, F. Simmonds and T. Stevermuer, *Spinal Cord*, 2011, **49**, 909-916.
28. Spinal Injuries Association. A Paralysed System?, https://www.spinal.co.uk/wp-content/uploads/2015/11/SIA-APP-Paralysed-System-Report-FINAL-lo-res.pdf, (accessed 23rd September, 2022).

29. P. Kennedy and L. Hasson, *Spinal Cord*, 2016, **54**, 141-144.
30. D. H. Hwang, H. Y. Shin, M. J. Kwon, J. Y. Choi, B.-Y. Ryu and B. G. Kim, *The Journal of Neuroscience*, 2014, **34**, 12788-12800.
31. H. Barbeau and S. Rossignol, *Brain Research*, 1987, **412**, 84-95.
32. R. G. Lovely, R. J. Gregor, R. R. Roy and V. R. Edgerton, *Experimental Neurology*, 1986, **92**, 421-435.
33. R. D. d. Leon, J. A. Hodgson, R. R. Roy and V. R. Edgerton, *Journal of Neurophysiology*, 1998, **79**, 1329-1340.
34. R. de Leon, J. A. Hodgson, R. R. Roy and V. R. Edgerton, *Brain Research*, 1994, **654**, 241-250.
35. C. A. Giuliani and J. L. Smith, *Journal of Neuroscience*, 1985, **5**, 1276-1282.
36. M. E. Goldberger, *Experimental Brain Research*, 1988, **73**, 329-342.
37. R. D. D. Leon, J. A. Hodgson, R. R. Roy and V. R. Edgerton, *Journal of Neurophysiology*, 1998, **80**, 83-91.
38. R. P. Bunge, W. R. Puckett, J. L. Becerra, A. Marcillo and R. M. Quencer, *Advanced Neurology*, 1993, **59**, 75-89.
39. J. Kjell and L. Olson, *Disease Models & Mechanics*, 2016, **9**, 1125-1137.
40. M. Fraidakis, T. Klason, H. Cheng, L. Olson and C. Spenger, *Experimental Neurology*, 1998, **153**, 299-312.
41. R. D. Nandoe Tewarie, J. Yu, J. Seidel, S. T. Rahiem, A. Hurtado, B. M. Tsui, J. A. Grotenhuis, M. G. Pomper and M. Oudega, *Molecular Imaging*, 2010, **9**, 108-116.
42. C. H. Tator, *Neurosurgery*, 2006, **59**, 957-982.
43. N. Zhang, M. Fang, H. Chen, F. Gou and M. Ding, *Neural Regenation Research*, 2014, **9**, 2008-2012.
44. B. K. Kwon, F. Streijger, C. E. Hill, A. J. Anderson, M. Bacon, M. S. Beattie, A. Blesch, E. J. Bradbury, A. Brown, J. C. Bresnahan, C. C. Case, R. W. Colburn, S. David, J. W. Fawcett, A. R. Ferguson, I. Fischer, C. L. Floyd, J. C. Gensel, J. D. Houle, L. B. Jakeman, N. D. Jeffery, L. A. Jones, N. Kleitman, J. Kocsis, P. Lu, D. S. Magnuson, M. Marsala, S. W. Moore, A. J. Mothe, M. Oudega, G. W. Plant, A. S. Rabchevsky, J. M. Schwab, J. Silver, O. Steward, X. M. Xu, J. D. Guest and W. Tetzlaff, *Experimental Neurology*, 2015, **269**, 154-168.
45. D. M. Basso, M. S. Beattie and J. C. Bresnahan, *Journal of Neurotrauma*, 1995, **12**, 1-21.
46. H.-J. K. Nureddin Ashammakhi, Arshia Ehsanipour, Rebecca D. Bierman, Outi Kaarela, Chengbin Xue, Ali Khademhosseini, and Stephanie K. Seidlits, *Tissue Engineering Part B: Reviews*, 2019, **25**, 471-491.
47. C. S. Ahuja, S. Nori, L. Tetreault, J. Wilson, B. Kwon, J. Harrop, D. Choi and M. G. Fehlings, *Neurosurgery*, 2017, **80**.
48. R. P. Salewski, R. A. Mitchell, L. Li, C. Shen, M. Milekovskaia, A. Nagy and M. G. Fehlings, *Stem Cells Translational Medicine*, 2015, **4**, 743-754.
49. S. J. Buwalda, K. W. M. Boere, P. J. Dijkstra, J. Feijen, T. Vermonden and W. E. Hennink, *Journal of Controlled Release*, 2014, **190**, 254-273.
50. A. Bhardwaj and L. M. Pandey, in *Nanoscale Engineering of Biomaterials: Properties and Applications*, eds. L. M. Pandey and A. Hasan, Springer Nature Singapore, Singapore, 2022, DOI: 10.1007/978-981-16-3667-7_4, pp. 89-114.
51. L. Jiang, B. Woodington, A. Carnicer-Lombarte, G. Malliaras and D. G. Barone, *Journal of Neural Engineering*, 2022, **19**.
52. K. Výborný, J. Vallová, Z. Kočí, K. Kekulová, K. Jiráková, P. Jendelová, J. Hodan and Š. Kubinová, *Scientific Reports*, 2019, **9**, 10674.
53. R. F. Rivera-Santiago, S. Sriswasdi, S. L. Harper and D. W. Speicher, *Methods*, 2015, **89**, 99-111.
54. P. F. Gratzer and J. M. Lee, *Journal of Biomedical Materials Research*, 2001, **58**, 172-179.
55. J. W. Kuo, D. A. Swann and G. D. Prestwich, *Bioconjug Chem*, 1991, **2**, 232-241.
56. J. S. Pieper, A. Oosterhof, P. J. Dijkstra, J. H. Veerkamp and T. H. van Kuppevelt, *Biomaterials*, 1999, **20**, 847-858.
57. K. Tomihata and Y. Ikada, *Journal of Biomedical Materials Research*, 1997, **37**, 243-251.
58. M. N. Collins and C. Birkinshaw, *Journal of Applied Polymer Science*, 2007, **104**, 3183-3191.
59. M. Hanthamrongwit, W. H. Reid and M. H. Grant, *Biomaterials*, 1996, **17**, 775-780.

60. F. Li, M. Ducker, B. Sun, F. G. Szele and J. T. Czernuszka, *Acta Biomaterialia*, 2020, **112**, 122-135.
61. M. Gottlieb, in *Biological and Synthetic Polymer Networks*, ed. O. Kramer, Springer Netherlands, Dordrecht, 1988, DOI: 10.1007/978-94-009-1343-1_27, pp. 403-414.
62. M. Geoghegan, G. Hadziioannou, M. Geoghegan and G. Hadziioannou, in *Polymer Electronics*, Oxford University Press, 2013, DOI: 10.1093/acprof:oso/9780199533824.003.0007, pp. 131-167.
63. M. Geoghegan, in *Advances in Solid State Physics*, ed. B. Kramer, Springer Berlin Heidelberg, Berlin, Heidelberg, 2006, DOI: 10.1007/11423256_3, pp. 29-44.
64. Y. Lan, M. G. Corradini, X. Liu, T. E. May, F. Borondics, R. G. Weiss and M. A. Rogers, *Langmuir : the ACS journal of surfaces and colloids*, 2014, **30**, 14128-14142.
65. E. Nagy, Basic Equations of Mass Transport through a Membrane Layer, Hungary, Elsevier. 2nd edition, 2019
66. D. J. Kozuch, W. Zhang and S. T. Milner, *Polymers*, 2016, **8**, 241.
67. U. Akalp, S. Chu, S. C. Skaalure, S. J. Bryant, A. Doostan and F. J. Vernerey, *Polymer (Guildf)*, 2015, **66**, 135-147.
68. K. S. Oh, J. S. Oh, H. S. Choi and Y. C. Bae, *Macromolecules*, 1998, **31**, 7328-7335.
69. M. Vert, Y. Doi, K.-H. Hellwich, M. Hess, P. Hodge, P. Kubisa, M. Rinaudo and F. Schué, *Pure and Applied Chemistry*, 2012, **84**, 377-410.
70. H. Jung, *Archives of Plastic Surgery*, 2020, **47**, 297-300.
71. A. B. Csóka, S. W. Scherer and R. Stern, *Genomics*, 1999, **60**, 356-361.
72. G. C. Gurtner, S. Werner, Y. Barrandon and M. T. Longaker, *Nature*, 2008, **453**, 314-321.
73. R. Grose and S. Werner, *Molecular Biotechnology*, 2004, **28**, 147-166.
74. P. Martin and S. J. Leibovich, *Trends in Cell Biology*, 2005, **15**, 599-607.
75. P. Martin, D. D'Souza, J. Martin, R. Grose, L. Cooper, R. Maki and S. R. McKercher, *Current Biology*, 2003, **13**, 1122-1128.
76. S. Werner and R. Grose, *Physiological Reviews*, 2003, **83**, 835-870.
77. S. R. Opalenik and J. M. Davidson, *Faseb journal*, 2005, **19**, 1561-1563.
78. S. Werner, T. Krieg and H. Smola, *Journal of Investigative Dermatology*, 2007, **127**, 998-1008.
79. A. Szabowski, N. Maas-Szabowski, S. Andrecht, A. Kolbus, M. Schorpp-Kistner, N. E. Fusenig and P. Angel, *Cell*, 2000, **103**, 745-755.
80. J. Pelleg, in *Mechanical Properties of Materials*, ed. J. Pelleg, Springer Netherlands, Dordrecht, 2013, DOI: 10.1007/978-94-007-4342-7_1, pp. 1-84.
81. T. Young, *A course of lectures on natural philosophy and the mechanical arts*, London : Printed for Taylor and Walton, London, A new / with references and notes, by the Rev. P. Kelland.. edn., 1845.
82. A. A. Griffith, *Philosophical Transactions of the Royal Society of London Series A*, 1921, **221**, 163-198.
83. C. Lee, X. Wei, J. W. Kysar and J. Hone, *Science*, 2008, **321**, 385-388.
84. N. L. Ramo, K. L. Troyer and C. M. Puttlitz, *Acta Biomaterialia*, 2018, **75**, 253-262.
85. T. L. E. Mazuchowski E. L., presented in part at the Summer Bioengineering Conference, Sonesta Beach Resort in Key Biscayne, Florida, 2003, 2003.
86. A. Karimi, A. Shojaei and P. Tehrani, *Journal of Chemical Neuroanatomy*, 2017, **86**, 15-18.
87. L. E. Bilston and L. E. Thibault, *Annals of Biomedical Engineering*, 1995, **24**, 67-74.
88. R. J. Oakland, R. M. Hall, R. K. Wilcox and D. C. Barton, *Proceedings of the Institution of Mechanical Engineers, Part H: Journal of Engineering in Medicine*, 2006, **220**, 489-492.
89. H. Zhang, P. Falkner and C. Cai, Cham, 2016.
90. H. Ozawa, T. Matsumoto, T. Ohashi, M. Sato and S. Kokubun, *Journal of of Neurosurg-spine*, 2004, **1**, 122-127.
91. C. Cheng, J. Kmech, V. K. Mushahwar and A. L. Elias, *IEEE Transactions on Biomedical Engineering* 2013, **60**, 1667-1676.
92. H. Ozawa, T. Matsumoto, T. Ohashi, M. Sato and S. Kokubun, *Journal of Neurosurgery*, 2001, **95**, 221-224.
93. A. R. Tunturi, *Journal of Neurosurgery*, 1977, **47**, 391-396.
94. K. Miller, K. Chinzei, G. Orssengo and P. Bednarz, *Journal of Biomechanics*, 2000, **33**, 1369-1376.

95. T.-K. Hung and G.-L. Chang, *Journal of Biomechanical Engineering*, 1981, **103**, 43-47.
96. T.-K. Hung, G.-L. Chang, J.-L. Chang and M. S. Albin, *Surgical Neurology*, 1981, **15**, 471-476.
97. S. Cheng, E. C. Clarke and L. E. Bilston, *Medical Engineering & Physics*, 2008, **30**, 1318-1337.
98. M. A. Howard, III, M. Utz, T. J. Brennan, B. D. Dalm, S. Viljoen, J. K. Kanwal and G. T. Gillies, *Journal of Applied Physics*, 2011, **110**, 074701.
99. S. G. Kroeker, P. L. Morley, C. F. Jones, L. E. Bilston and P. A. Cripton, *Journal of Biomechanics*, 2009, **42**, 878-883.
100. J. H. McElhaney, J. W. Melvin, V. L. Roberts and H. D. Portnoy, in *Perspectives in Biomedical Engineering: Proceedings of a Symposium organised in association with the Biological Engineering Society and held in the University of Strathclyde, Glasgow, June 1972*, ed. R. M. Kenedi, Palgrave Macmillan UK, London, 1973, DOI: 10.1007/978-1-349-01604-4_34, pp. 215-222.
101. W. C. Oliver and G. M. Pharr, *Journal of Materials Research*, 1992, **7**, 1564-1583.
102. B. Riccardi and R. Montanari, *Materials Science and Engineering: A*, 2004, **381**, 281-291.
103. V. Cerruti, *Accademia dei Lincei, Roma*, 1882.
104. J. Ochshorn, in *Structural Elements for Architects and Builders*, ed. J. Ochshorn, Butterworth-Heinemann, Boston, 2010, DOI: https://doi.org/10.1016/B978-1-85617-771-9.00003-9, pp. 61-71.
105. R. Hooke, *Lectures de Potentia Restitutiva, Or of Spring Explaining the Power of Springing Bodies*, John Martyn, 1678.
106. W. D. Pilkey, *Formulas for stress, strain, and structural matrices*, Hoboken, NJ : Wiley, Hoboken, NJ, 2nd . edn., 2005.
107. D. Gross, W. Ehlers, P. Wriggers, J. Schröder and R. Müller, in *Mechanics of Materials – Formulas and Problems: Engineering Mechanics 2*, Springer Berlin Heidelberg, Berlin, Heidelberg, 2017, DOI: 10.1007/978-3-662-53880-7_1, pp. 1-28.
108. E. Stavrinidou and C. M. Proctor, *Proceedings of the National Academcy of Science of the United States of America*, U.S.A, 114 (11) 2807-2812 DOI: 10.1063/9780735424470_001, 0.
109. S. S. Stevens, *The Journal of the Acoustical Society of America*, 1937, **8**, 191-195.
110. A. L. Hodgkin, A. F. Huxley and B. Katz, *The Journal of Physiology*, 1952, **116**, 424-448.
111. A. L. Hodgkin and A. F. Huxley, *The Journal of Physiology*, 1952, **117**, 500-544.
112. V. A. Sironi, *Frontiers in Integrative Neuroscience*, 2011, **5**.
113. A. L. Benabid, *Expert Review of Medical Devices*, 2007, **4**, 895-903.
114. M. Parastarfeizabadi and A. Z. Kouzani, *Journal of NeuroEngineering and Rehabilitation*, 2017, **14**, 79.
115. E. Bloch, Y. Luo and L. da Cruz, *Therapeutic Advances in Ophthalmology*, 2019, **11**, 2515841418817501.
116. L. S. Eisenberg, *Hearing Research*, 2015, **322**, 52-56.
117. S. Raspopovic, G. Valle and F. M. Petrini, *Nature Materials*, 2021, **20**, 925-939.
118. R. Sutton, J. D. Fisher, C. Linde and D. G. Benditt, *European Heart Journal Supplements*, 2007, **9**, I3-I10.
119. J. A. McWilliam, *British Medical J*ournal 1889, **1**, 348-350.
120. S. J. Moon, I. Jung and C. Y. Park, *Diabetes & Metabolism Journal*, 2021, **45**, 813-839.
121. A. Rowald, S. Komi, R. Demesmaeker, E. Baaklini, S. D. Hernandez-Charpak, E. Paoles, H. Montanaro, A. Cassara, F. Becce, B. Lloyd, T. Newton, J. Ravier, N. Kinany, M. D'Ercole, A. Paley, N. Hankov, C. Varescon, L. McCracken, M. Vat, M. Caban, A. Watrin, C. Jacquet, L. Bole-Feysot, C. Harte, H. Lorach, A. Galvez, M. Tschopp, N. Herrmann, M. Wacker, L. Geernaert, I. Fodor, V. Radevich, K. Van Den Keybus, G. Eberle, E. Pralong, M. Roulet, J.-B. Ledoux, E. Fornari, S. Mandija, L. Mattera, R. Martuzzi, B. Nazarian, S. Benkler, S. Callegari, N. Greiner, B. Fuhrer, M. Froeling, N. Buse, T. Denison, R. Buschman, C. Wende, D. Ganty, J. Bakker, V. Delattre, H. Lambert, K. Minassian, C. A. T. van den Berg, A. Kavounoudias, S. Micera, D. Van De Ville, Q. Barraud, E. Kurt, N. Kuster, E. Neufeld, M. Capogrosso, L. Asboth, F. B. Wagner, J. Bloch and G. Courtine, *Nature Medicine*, 2022, **28**, 260-271.

122. M. AlGhatrif and J. Lindsay, *Journal of Community Hospital Internal Medicine Perspectives*, 2012, **2**.
123. C. Pitsalidis, A.-M. Pappa, A. J. Boys, Y. Fu, C.-M. Moysidou, D. van Niekerk, J. Saez, A. Savva, D. Iandolo and R. M. Owens, *Chemical Reviews*, 2022, **122**, 4700-4790.
124. E. Neher and B. Sakmann, *Journal of Physiology*, 1976, **258**, 705-729.
125. E. Neher, B. Sakmann and J. H. Steinbach, *Pflugers Arch*, 1978, **375**, 219-228.
126. C. L. Hill and G. J. Stephens, in *Patch Clamp Electrophysiology: Methods and Protocols*, eds. M. Dallas and D. Bell, Springer US, New York, NY, 2021, DOI: 10.1007/978-1-0716-0818-0_1, pp. 1-19.
127. M. D. Lauro, PhD Program in Molecular and Regenerative Medicine, Unimore - University of Modena and Reggio Emilia, 2017.
128. T. J. Biden, M. Prentki, R. F. Irvine, M. J. Berridge and C. B. Wollheim, *Biochemical Journal*, 1984, **223**, 467-473.
129. M. E. Ortiz and D. Endy, *Journal of Biological Engineering*, 2012, **6**, 16.
130. S. R. Forrest and S. R. Forrest, in *Organic Electronics: Foundations to Applications*, Oxford University Press, 2020, DOI: 10.1093/oso/9780198529729.003.0001, p. 0.
131. G. Inzelt, in *Conducting Polymers: A New Era in Electrochemistry*, ed. G. Inzelt, Springer Berlin Heidelberg, Berlin, Heidelberg, 2012, DOI: 10.1007/978-3-642-27621-7_1, pp. 1-6.
132. B. D. Ratner, A. S. Hoffman, F. J. Schoen and J. E. Lemons, in *Biomaterials Science - An Introduction to Materials in Medicine (2nd Edition)*, Elsevier, 2nd Edition edn., 2004, pp. 10-19.
133. M. Y. Mulla, L. Torsi and K. Manoli, in *Methods in Enzymology*, eds. P. Pelosi and W. Knoll, Academic Press, 2020, vol. 642, pp. 403-433.
134. J. Rivnay, S. Inal, A. Salleo, R. M. Owens, M. Berggren and G. G. Malliaras, *Nature Reviews Materials*, 2018, **3**, 17086.
135. D. T. Simon, E. O. Gabrielsson, K. Tybrandt and M. Berggren, *Chemical Reviews*, 2016, **116**, 13009-13041.
136. T. Someya, *IEEE Spectrum*, 2013, **50**, 50-56.
137. J. Xu, S. Wang, G.-J. N. Wang, C. Zhu, S. Luo, L. Jin, X. Gu, S. Chen, V. R. Feig, J. W. F. To, S. Rondeau-Gagné, J. Park, B. C. Schroeder, C. Lu, J. Y. Oh, Y. Wang, Y.-H. Kim, H. Yan, R. Sinclair, D. Zhou, G. Xue, B. Murmann, C. Linder, W. Cai, J. B. H. Tok, J. W. Chung and Z. Bao, *Science*, 2017, **355**, 59-64.
138. L. Torsi, M. Magliulo, K. Manoli and G. Palazzo, *Chemical Society Reviews*, 2013, **42**, 8612-8628.
139. A. Tibaldi, L. Fillaud, G. Anquetin, M. Woytasik, S. Zrig, B. Piro, G. Mattana and V. Noël, *Electrochemistry Communications*, 2019, **98**, 43-46.
140. S. A. El-Khodary, Y. Cui, Y. Bu and J. Lian, *Electrochemical Capacitors*, *IOP Publishing*, 1-60 2023, DOI: 10.1088/978-0-7503-5042-6ch1.
141. L. Kergoat, B. Piro, M. Berggren, G. Horowitz and M. C. Pham, *Analytical Bioanalytical Chemistry*, 2012, **402**, 1813-1826.
142. S. Casalini, F. Leonardi, T. Cramer and F. Biscarini, *Organic Electronics*, 2013, **14**, 156-163.
143. V. Parkula, M. Berto, C. Diacci, B. Patrahau, M. Di Lauro, A. Kovtun, A. Liscio, M. Sensi, P. Samorì, P. Greco, C. A. Bortolotti and F. Biscarini, *Analytical Chemistry*, 2020, **92**, 9330-9337.
144. F. Buth, A. Donner, M. Sachsenhauser, M. Stutzmann and J. A. Garrido, *Advanced Materials*, 2012, **24**, 4511-4517.
145. D. Wang, V. Noël and B. Piro, *Electronics*, 2016, **5**, 9.
146. H. S. White, G. P. Kittlesen and M. S. Wrighton, *Journal of the American Chemical Society*, 1984, **106**, 5375-5377.
147. S. Zhang, E. Hubis, C. Girard, P. Kumar, J. DeFranco and F. Cicoira, *Journal of Materials Chemistry C*, 2016, **4**, 1382-1385.
148. D. Nilsson, T. Kugler, P.-O. Svensson and M. Berggren, *Sensors and Actuators B: Chemical*, 2002, **86**, 193-197.
149. M. Hamedi, R. Forchheimer and O. Inganäs, *Nature Materials*, 2007, **6**, 357-362.
150. S. Zhang and F. Cicoira, *Nature*, 2018, **561**, 466-467.
151. J. Rivnay, P. Leleux, M. Sessolo, D. Khodagholy, T. Hervé, M. Fiocchi and G. G. Malliaras, *Advanced Materials*, 2013, **25**, 7010-7014.

152. D. L. Pulfrey, *Understanding Modern Transistors and Diodes*, Cambridge University Press, Cambridge, 2010.
153. J. Ristein, *Science*, 2006, **313**, 1057-1058.
154. D. Khodagholy, J. Rivnay, M. Sessolo, M. Gurfinkel, P. Leleux, L. H. Jimison, E. Stavrinidou, T. Herve, S. Sanaur, R. M. Owens and G. G. Malliaras, *Nature Communications*, 2013, **4**, 2133.
155. I. Gualandi, M. Marzocchi, E. Scavetta, M. Calienni, A. Bonfiglio and B. Fraboni, *Journal of Materials Chemistry B*, 2015, **3**, 6753-6762.
156. B. D. Ratner, A. S. Hoffman, F. J. Schoen and J. E. Lemons, in *Biomaterials Science - An Introduction to Materials in Medicine (2nd Edition)*, Elsevier, 2nd Edition edn., 2004, pp. 1-19.
157. C. M. Abraham, *Open Dentistry Journal*, 2014, **8**, 50-55.
158. A. Bobbio, *Revista da Associacao Paulista de Cirurgioes Dentistas*, 1973, **27**, 27-36.
159. L. H. Cohn, *Circulation*, 2003, **107**, 2168-2170.
160. W. J. Kolff, The Invention of the Artificial Heart. The International Journal of Artificial Organs. 1990;13(7):396-403. doi:10.1177/039139889001300702
161. Pillay R, Hansraj R, Rampersad N. Historical Development, Applications and Advances in Materials Used in Spectacle Lenses and Contact Lenses. Clin Optom (Auckl). 2020 Sep 29;12:157-167. doi: 10.2147/OPTO.S257081.
162. L. L. Hench and I. Thompson, *Journal of the Royal Society Interface*, 2010, **7 Suppl 4**, S379-391.
163. L. L. Hench, *Science*, 1980, **208**, 826-831.
164. N. Eliaz, *Materials (Basel)*, 2019, **12**.
165. S. Rea and W. Bonfield, *Journal of the Australasian Ceramic Society*, 2004, **40**, 43-57.
166. E. S. Thian, J. Huang, S. M. Best, Z. H. Barber, R. A. Brooks, N. Rushton and W. Bonfield, *Biomaterials*, 2006, **27**, 2692-2698.
167. T. C. Ho, C. C. Chang, H. P. Chan, T. W. Chung, C. W. Shu, K. P. Chuang, T. H. Duh, M. H. Yang and Y. C. Tyan, *Molecules*, 2022, **27**.
168. E. M. Ahmed, *Journal of Advanced Research*, 2015, **6**, 105-121.
169. H. Tan and K. G. Marra, *Materials (Basel)*, 2010, **3**, 1746-1767.
170. O. Wichterle and D. LÍM, *Nature*, 1960, **185**, 117-118.
171. N. A. Peppas and R. E. Berner, *Biomaterials*, 1980, **1**, 158-162.
172. R. W. Korsmeyer and N. A. Peppas, *Journal of Membrane Science*, 1981, **9**, 211-227.
173. P. A. King and J. A. Ward, *Journal of Polymer Science Part A-1: Polymer Chemistry*, 1970, **8**, 253-262.
174. A. Metters and J. Hubbell, *Biomacromolecules*, 2005, **6**, 290-301.
175. M. Malkoch, R. Vestberg, N. Gupta, L. Mespouille, P. Dubois, A. F. Mason, J. L. Hedrick, Q. Liao, C. W. Frank, K. Kingsbury and C. J. Hawker, *Chemical Communications*, 2006, DOI: 10.1039/B603438A, 2774-2776.
176. B.-H. Hu, J. Su and P. B. Messersmith, *Biomacromolecules*, 2009, **10**, 2194-2200.
177. M. Ehrbar, S. C. Rizzi, R. Hlushchuk, V. Djonov, A. H. Zisch, J. A. Hubbell, F. E. Weber and M. P. Lutolf, *Biomaterials*, 2007, **28**, 3856-3866.
178. R. W. Korsmeyer, R. Gurny, E. Doelker, P. Buri and N. A. Peppas, *International Journal of Pharmaceutics*, 1983, **15**, 25-35.
179. M. F. A. Goosen, M. V. Sefton and M. W. C. Hatton, *Thrombosis Research*, 1980, **20**, 543-554.
180. M. I. Neves, M. Araújo, L. Moroni, R. M. P. da Silva and C. C. Barrias, *Molecules*, 2020, **25**, 978.
181. V. H. Pomin and B. Mulloy, *Pharmaceuticals (Basel)*, 2018, **11**.
182. A. Ialenti and M. Di Rosa, *Agents Actions*, 1994, **43**, 44-47.
183. Y. Gao, Y. Sun, H. Yang, P. Qiu, Z. Cong, Y. Zou, L. Song, J. Guo and T. P. Anastassiades, *International Journal of Molecular Science*, 2019, **20**.
184. N. Broguiere, L. Isenmann and M. Zenobi-Wong, *Biomaterials*, 2016, **99**, 47-55.
185. J. Karvinen, T. Joki, L. Ylä-Outinen, J. T. Koivisto, S. Narkilahti and M. Kellomäki, *Reactive and Functional Polymers*, 2018, **124**, 29-39.
186. E. Caló and V. V. Khutoryanskiy, *European Polymer Journal*, 2015, **65**, 252-267.

187. Q. Li, C. G. Williams, D. D. Sun, J. Wang, K. Leong and J. H. Elisseeff, *Journal of Biomedical Material Research A*, 2004, **68**, 28-33.
188. J. W. Wassenaar, R. L. Braden, K. G. Osborn and K. L. Christman, *Journal of Materials Chemistry B*, 2016, **4**, 2794-2802.
189. Y. Wang, J. Bao, X. Wu, Q. Wu, Y. Li, Y. Zhou, L. Li and H. Bu, *Scientific Reports*, 2016, **6**, 24779.
190. T. Jiang, X. J. Ren, J. L. Tang, H. Yin, K. J. Wang and C. L. Zhou, *Materials Science and Engineering C Materials for Biological Applications*, 2013, **33**, 3514-3521.
191. Y. Li, L. Li and C. Hölscher, *CNS Drugs*, 2016, **30**, 889-897.
192. L. L. Hench and J. Wilson, in *Clinical Performance of Skeletal Prostheses*, eds. L. L. Hench and J. Wilson, Springer Netherlands, Dordrecht, 1996, DOI: 10.1007/978-94-011-0541-5_1, pp. 1-10.
193. F. J. Schoen, R. J. Levy and H. R. Piehler, *Cardiovascular Pathology*, 1992, **1**, 29-52.
194. B. D. Ratner, A. S. Hoffman, F. J. Schoen and J. E. Lemons, in *Biomaterials Science (Third Edition)*, eds. B. D. Ratner, A. S. Hoffman, F. J. Schoen and J. E. Lemons, Academic Press, 2013, DOI: https://doi.org/10.1016/B978-0-08-087780-8.00153-4, pp. xxv-xxxix.
195. O. V. Mikhailov, *International Journal of Molecular Sciences*, 2023, **24**.
196. P. Jaipan, A. Nguyen and R. J. Narayan, *MRS Communications*, 2017, **7**, 416-426.
197. V. Crescenzi, A. Francescangeli and A. Taglienti, *Biomacromolecules*, 2002, **3**, 1384-1391.
198. J. Ratanavaraporn, R. Rangkupan, H. Jeeratawatchai, S. Kanokpanont and S. Damrongsakkul, *International Journal of Biological Macromolecules*, 2010, **47**, 431-438.
199. R. Naomi, H. Bahari, P. M. Ridzuan and F. Othman, *Polymers (Basel)*, 2021, **13**.
200. B. Balakrishnan, M. Mohanty, P. Umashankar and A. Jayakrishnan, *Biomaterials*, 2005, **26**, 6335-6342.
201. B. F. Pierce, E. Pittermann, N. Ma, T. Gebauer, A. T. Neffe, M. Hölscher, F. Jung and A. Lendlein, *Macromolecular Bioscience*, 2012, **12**, 312-321.
202. P. Angele, R. Müller, D. Schumann, C. Englert, J. Zellner, B. Johnstone, J. Yoo, J. Hammer, J. Fierlbeck and M. K. Angele, *Journal of Biomedical Materials Research Part A: An Official Journal of The Society for Biomaterials, The Japanese Society for Biomaterials, and The Australian Society for Biomaterials and the Korean Society for Biomaterials*, 2009, **91**, 416-427.
203. X. Li, Q. Xu, M. Johnson, X. Wang, J. Lyu, Y. Li, S. McMahon, U. Greiser, S. A and W. Wang, *Biomaterials Science*, 2021, **9**, 4139-4148.
204. S. R. Caliari and B. A. C. Harley, *Biomaterials*, 2011, **32**, 5330-5340.
205. K. C. Kavya, R. Dixit, R. Jayakumar, S. V. Nair and K. P. Chennazhi, *Journal of Biomedical Nanotechnology*, 2012, **8**, 149-160.
206. G. P. Raeber, M. P. Lutolf and J. A. Hubbell, *Biophysical Journal*, 2005, **89**, 1374-1388.
207. M. J. Mahoney and K. S. Anseth, *Biomaterials*, 2006, **27**, 2265-2274.
208. J. Shin, E. H. Kang, S. Choi, E. J. Jeon, J. H. Cho, D. Kang, H. Lee, I. S. Yun and S.-W. Cho, *ACS Biomaterials Science & Engineering*, 2021, **7**, 4230-4243.
209. X. Hu, D. Li, F. Zhou and C. Gao, *Acta Biomaterialia*, 2011, **7**, 1618-1626.
210. H. C. Kolb and K. B. Sharpless, *Drug Discovery Today*, 2003, **8**, 1128-1137.
211. A. Conovaloff and A. Panitch, *Journal of Neural Engineering*, 2011, **8**, 056003.
212. X. Xu, A. K. Jha, D. A. Harrington, M. C. Farach-Carson and X. Jia, *Soft Matter*, 2012, **8**, 3280-3294.
213. H. G. Garg and C. A. Hales, *Chemistry and biology of hyaluronan*, Elsevier, 2004.
214. E. Papakonstantinou, M. Roth and G. Karakiulakis, *Dermatoendocrinology*, 2012, **4**, 253-258.
215. T. Laurent, *Chemistry, biology and medical applications of hyaluronan and its derivatives*, 1998, **72**, 1-2.
216. T. Segura, B. C. Anderson, P. H. Chung, R. E. Webber, K. R. Shull and L. D. Shea, *Biomaterials*, 2005, **26**, 359-371.
217. K. Tomihata and Y. Ikada, *Journal of Polymer Science Part A: Polymer Chemistry*, 1997, **35**, 3553-3559.
218. B. D. Ratner, A. S. Hoffman, F. J. Schoen and J. E. Lemons, in *Biomaterials Science - An Introduction to Materials in Medicine (2nd Edition)*, Elsevier, 2nd Edition edn., 2004, pp. 1-9.

219. W. R. Wagner, S. E. Sakiyama-Elbert, G. Zhang and M. J. Yaszemski, *Biomaterials Science : An Introduction to Materials in Medicine*, Elsevier Science & Technology, San Diego, UNITED STATES, 2020.
220. B. D. Ratner and A. S. Hoffman, in *Hydrogels for Medical and Related Applications*, AMERICAN CHEMICAL SOCIETY, 1976, vol. 31, ch. 1, pp. 1-36.
221. J. A. Hunt, R. Chen, T. van Veen and N. Bryan, *Journal of Materials Chemistry B*, 2014, **2**, 5319-5338.
222. M. Dornish, D. Kaplan and O. Skaugrud, *Ann N Y Acad Sci*, 2001, **944**, 388-397.
223. S. N. Pawar and K. J. Edgar, *Biomaterials*, 2012, **33**, 3279-3305.
224. Y.-J. Hwang, J. Granelli and J. G. Lyubovitsky, *Analytical Chemistry*, 2011, **83**, 200-206.
225. N. N. Fathima, B. Madhan, J. R. Rao, B. U. Nair and T. Ramasami, *International Journal of Biological Macromolecules*, 2004, **34**, 241-247.
226. S. Wang, S. Guan, Z. Zhu, W. Li, T. Liu and X. Ma, *Materials Science and Engineering C Materials for Biological Applications*, 2017, **71**, 308-316.
227. G. Kogan, L. Šoltés, R. Stern, J. Schiller and R. Mendichi, in *Studies in Natural Products Chemistry*, ed. R. Atta ur, Elsevier, 2008, vol. 34, pp. 789-882.
228. V. B. Lokeshwar and M. G. Selzer, *Seminars in Cancer Biologyl*, 2008, **18**, 281-287.
229. S. Bowman, M. E. Awad, M. W. Hamrick, M. Hunter and S. Fulzele, *Clinical and Translational Medicine*, 2018, **7**, 6.
230. F. J. O'Brien, *Materials Today.*, 2011, **14**, 88-95.
231. Y. Zhong and R. V. Bellamkonda, *Journal of The Royal Society Interface*, 2008, **5**, 957-975.
232. D. A. Prystupa and A. M. Donald, *Polymer Gels and Networks*, 1996, **4**, 87-110.
233. J. H. Muyonga, C. G. B. Cole and K. G. Duodu, *Food Chemistry*, 2004, **86**, 325-332.
234. V. Renugopalakrishnan, G. Chandrakasan, S. Moore, T. Hutson, C. Berney and R. S. Bhatnagar, *Macromolecules*, 1989, **22**, 4121-4124.
235. Y. Chen, Q. Duan, L. Yu and F. Xie, *Carbohydrate Polymers*, 2021, **272**, 118522.
236. C. D'Agostino, R. Liuzzi, L. F. Gladden and S. Guido, *Soft Matter*, 2017, **13**, 2952-2961.
237. *United States of America Pat.*, 1540979, 1925.
238. F. A. Osorio, E. Bilbao, R. Bustos and F. Alvarez, *International Journal of Food Properties*, 2007, **10**, 841-851.
239. British Standards Institution, Methods for sampling and testing gelatine (physical and chemical methods), London, pp. 1-34, 1975.
240. R. H. Pritchard and E. M. Terentjev, *Polymer*, 2013, **54**, 6954-6960.
241. P. V. Kozlov and G. I. Burdygina, *Polymer*, 1983, **24**, 651-666.
242. C. M. Stultz, *Protein Sci*, 2006, **15**, 2166-2177.
243. A. Hayashi and S.-C. Oh, *Agricultural and Biological Chemistry*, 1983, **47**, 1711-1716.
244. P. J. Flory and J. Rehner, Jr., *Journal of Chemical Physics*, 1943, **11**, 521-526.
245. P. J. Flory and J. Rehner, Jr., *The Journal of Chemical Physics*, 2004, **11**, 521-526.
246. Y. Tian, K. Qian, E. Jacobs, E. Amstad, D. S. Jones, L. Stella and G. P. Andrews, *Pharmaceutics*, 2019, **11**.
247. S. Aldrich, Gelatin Product Information, https://www.sigmaaldrich.com/deepweb/assets/sigmaaldrich/product/documents/333/625/g9382pis.pdf, 2023).
248. J. R. Vyvyan, *Introduction to spectroscopy*, Australia : Cengage Learning, Fifth edition.. edn., 2015.
249. J. Carneiro, P. M. Döll-Boscardin, B. C. Fiorin, J. M. Nadal, P. V. Farago and J. P. d. Paula, *Brazilian Journal of Pharmaceutical Sciences*, 2016, **52**, 645-651.
250. Q. Yan, H.-N. Zheng, C. Jiang, K. Li and S.-J. Xiao, *RSC Advances*, 2015, **5**, 69939-69947.
251. E. Hall, 2020.
252. G. K. Schwalfenberg, *Journal of Environmental Public Health*, 2012, **2012**, 727630.
253. M. J. Mitchell, O. E. Jensen, K. A. Cliffe and M. M. Maroto-Valer, *Proceedings of the Royal Society A: Mathematical, Physical and Engineering Sciences*, 2010, **466**, 1265-1290.
254. M. Xue and C. J. Jackson, *Advances in Wound Care (New Rochelle)*, 2015, **4**, 119-136.
255. R. N. Gomes, F. Manuel and D. S. Nascimento, *npj Regenerative Medicine*, 2021, **6**, 43.
256. P. Ferraboschi, S. Ciceri and P. Grisenti, *Antibiotics (Basel)*, 2021, **10**(12):1534. doi: 10.3390/antibiotics10121534.

257. J. J. Water, M. M. Schack, A. Velazquez-Campoy, M. J. Maltesen, M. van de Weert and L. Jorgensen, *European Journal of Pharmaceutics and Biopharmaceutics*, 2014, **88**, 325-331.
258. J. Kim, J.-Y. Chang, Y.-Y. Kim, M.-J. Kim and H.-S. Kho, *Archives of Oral Biology*, 2018, **89**, 55-64.
259. J. Newman, A. Cacatian, A. Josephson and A. Tsang, *The Lancet*, 1974, **304**, 756-757.
260. T. Chanmee, P. Ontong and N. Itano, *Cancer Letters*, 2016, **375**, 20-30.
261. P. K. Robinson, *Essays Biochemistry*, 2015, **59**, 1-41.
262. G. E. Briggs and J. B. Haldane, *Biochemical Journal*, 1925, **19**, 338-339.
263. K. A. Johnson and R. S. Goody, *Biochemistry*, 2011, **50**, 8264-8269.
264. K. Schmith and V. Faber, *Scandinavian Journal of Clinical and Laboratory Investigation*, 1950, **2**, 292-297.
265. H. Lineweaver and D. Burk, *Journal of the American Chemical Society*, 1934, **56**, 658-666.
266. K. A. Johnson, *FEBS Letters*, 2013, **587**, 2753-2766.
267. M. R. Natowicz and Y. Wang, *Clinica Chimica Acta*, 1996, **245**, 1-6.
268. S. Fang, A. M. Hays Putnam and M. J. LaBarre, *Analytical Biochemistry*, 2015, **480**, 74-81.
269. A. Kaul, W. D. Short, X. Wang and S. G. Keswani, *International Journal of Molecular Science*, 2021, **22**.
270. T. Segura, B. C. Anderson, P. H. Chung, R. E. Webber, K. R. Shull and L. D. Shea, *Biomaterials*, 2005, **26**, 359-371.
271. S. A. Unterman, M. Gibson, J. H. Lee, J. Crist, T. Chansakul, E. C. Yang and J. H. Elisseeff, *Tissue Engineering Part A*, 2012, **18**, 2497-2506.
272. J. A. Burdick, C. Chung, X. Jia, M. A. Randolph and R. Langer, *Biomacromolecules*, 2005, **6**, 386-391.
273. B. A. Buhren, H. Schrumpf, E. Bölke, K. Kammers and P. A. Gerber, *European Journal of Medical Research*, 2018, **23**, 37.
274. W. Lee, W. Oh, S. M. Oh and E. J. Yang, *Plastic and Reconstructive Surgery*, 2020, **145**, 957-964.
275. Merck, Enzymatic Assay of Hyaluronidase (3.2.1.35), https://www.sigmaaldrich.com/GB/en/technical-documents/protocol/protein-biology/enzyme-activity-assays/enzymatic-assay-of-hyaluronidase, (accessed February, 2024).
276. T. K. Hung and G. L. Chang, *Journal of Biomechanical Engineering*, 1981, **103**, 43-47.
277. R. J. Fiford and L. E. Bilston, *Journal of Biomechanics*, 2005, **38**, 1509-1515.
278. S. Cheng and L. E. Bilston, *Journal of Biomechanics*, 2007, **40**, 117-124.
279. H. Ozawa, T. Matsumoto, T. Ohashi, M. Sato and S. Kokubun, *J Neurosurgery: Spine*, 2004, **1**, 122-127.
280. K. Ichihara, T. Taguchi, Y. Shimada, I. Sakuramoto, S. Kawano and S. Kawai, *Journal of Neurotrauma*, 2001, **18**, 361-367.
281. H. Ozawa, T. Matsumoto, T. Ohashi, M. Sato and S. Kokubun, *Journal of Neurosurgery: Spine*, 2001, **95**, 221-224.
282. E. Garcia-Breijo, B. Gomez-Lor Perez, P. Cosseddu. Organic Sensors: Materials and Applications. Institution of Engineering and Technology, 2016
283. K. Feron, R. Lim, C. Sherwood, A. Keynes, A. Brichta and P. C. Dastoor, *International Journal of Molecular Sciences*, 2018, **19**, 2382.
284. M. Moser, J. F. Ponder Jr., A. Wadsworth, A. Giovannitti and I. McCulloch, *Advanced Functional Materials*, 2019, **29**, 1807033.
285. A. Elschner, Kirchmeyer, S., Lovenich, W., Merker, U., & Reuter, K., *PEDOT: Principles and Applications of an Intrinsically Conductive Polymer* CRC Press, 1st edn., 2010.
286. D. Mantione, I. Del Agua, W. Schaafsma, J. Diez-Garcia, B. Castro, H. Sardon and D. Mecerreyes, *Macromolecular Bioscience*, 2016, **16**, 1227-1238.
287. E. Bihar, Y. Deng, T. Miyake, M. Saadaoui, G. G. Malliaras and M. Rolandi, *Scientific Reports*, 2016, **6**, 27582.
288. M. D. Ferro and N. A. Melosh, *Advanced Functional Materials*, 2018, **28**, 1704335.
289. H. Yamato, M. Ohwa and W. Wernet, *Journal of Electroanalytical Chemistry*, 1995, **397**, 163-170.
290. M. Asplund, E. Thaning, J. Lundberg, A. C. Sandberg-Nordqvist, B. Kostyszyn, O. Inganäs and H. von Holst, *Biomedical Materials*, 2009, **4**, 045009.

291. J. Isaksson, P. Kjäll, D. Nilsson, N. D. Robinson, M. Berggren and A. Richter-Dahlfors, *Nature Materials*, 2007, **6**, 673-679.
292. Y. Lu, R. Liu, X.-C. Hang and D. J. Young, *Polymer Chemistry*, 2021, **12**, 2115-2121.
293. S. C. Luo, E. Mohamed Ali, N. C. Tansil, H. H. Yu, S. Gao, E. A. Kantchev and J. Y. Ying, *Langmuir*, 2008, **24**, 8071-8077.
294. S. Khan, M. Ul-Islam, M. W. Ullah, M. Israr, J. H. Jang and J. K. Park, *International Journal of Biological Macromolecules*, 2018, **107**, 865-873.
295. A. Nozariasbmarz, H. Collins, K. Dsouza, M. H. Polash, M. Hosseini, M. Hyland, J. Liu, A. Malhotra, F. M. Ortiz, F. Mohaddes, V. P. Ramesh, Y. Sargolzaeiaval, N. Snouwaert, M. C. Özturk and D. Vashaee, *Applied Energy*, 2020, **258**, 114069.
296. J. A. Arter, D. K. Taggart, T. M. McIntire, R. M. Penner and G. A. Weiss, *Nano Letters*, 2010, **10**, 4858-4862.
297. R. S. Ambekar and B. Kandasubramanian, *Industrial & Engineering Chemistry Research*, 2019, **58**, 6163-6194.
298. M. ElMahmoudy, S. Inal, A. Charrier, I. Uguz, G. G. Malliaras and S. Sanaur, *Macromolecular Materials and Engineering*, 2017, **302**, 1600497.
299. J. Liu, M. Agarwal and K. Varahramyan, *Sensors and Actuators B: Chemical*, 2008, **135**, 195-199.
300. A. Campana, T. Cramer, D. T. Simon, M. Berggren and F. Biscarini, *Advanced Materials*, 2014, **26**, 3874-3878.
301. R. M. Miriani, M. R. Abidian, D. R. Kipke, Cytotoxic analysis of the conducting polymer PEDOT using myocytes. Annu Int Conf IEEE Eng Med Biol Soc. 2008;2008:1841-4. doi: 10.1109/IEMBS.2008.4649538.
302. V. R. Feig, H. Tran and Z. Bao, *ACS Central Science*, 2018, **4**, 337-348.
303. J. Cameron and P. J. Skabara, *Materials Horizons*, 2020, **7**, 1759-1772.
304. U. Lang, N. Naujoks and J. Dual, *Synthetic Metals*, 2009, **159**, 473-479.
305. D. Tahk, H. H. Lee and D.-Y. Khang, *Macromolecules*, 2009, **42**, 7079-7083.
306. H. Okuzaki and M. Ishihara, *Macromolecular Rapid Communications*, 2003, **24**, 261-264.
307. S. Benaglia, S. Drakopoulou, F. Biscarini and R. Garcia, *Nanoscale*, 2022, **14**, 14146-14154.
308. J. Qu, L. Ouyang, C.-c. Kuo and D. C. Martin, *Acta Biomaterialia*, 2016, **31**, 114-121.
309. A. R. Harris, P. J. Molino, A. G. Paolini and G. G. Wallace, *Synthetic Metals*, 2016, **222**, 338-343.
310. Y. Ner, M. Invernale, J. Grote, J. Stuart and G. Sotzing, *Synthetic Metals*, 2010, **160**, 351-353.
311. M. Asplund, H. von Holst and O. Inganäs, *Biointerphases*, 2008, **3**, 83-93.
312. J. Patterson, R. Siew, S. W. Herring, A. S. Lin, R. Guldberg and P. S. Stayton, *Biomaterials*, 2010, **31**, 6772-6781.
313. H. von Holst, *Biochimica et Biophysica Acta (BBA) - General Subjects*, 2013, **1830**, 4345-4352.
314. E. M. Thaning, M. L. Asplund, T. A. Nyberg, O. W. Inganäs and H. von Holst, *Journal of Biomedical Materials Research Part B Applied Biomaterials*, 2010, **93**, 407-415.
315. T. A. Saleh, in *Polymer Hybrid Materials and Nanocomposites*, ed. T. A. Saleh, William Andrew Publishing, 2021, DOI: https://doi.org/10.1016/B978-0-12-813294-4.00002-9, pp. 177-212.
316. S. Nie, Z. Li, Y. Yao and Y. Jin, *Frontiers in Chemistry*, 2021, **9**.
317. D. Mantione, I. Del Agua, A. Sanchez-Sanchez and D. Mecerreyes, *Polymers*, 2017, **9**, 354.
318. F. Jonas and J. T. Morrison, *Synthetic Metals*, 1997, **85**, 1397-1398.
319. Heywang, G. and Jonas, F. (1992), Poly(alkylenedioxythiophene)s—new, very stable conducting polymers. Adv. Mater., 4: 116-118.
320. Goktas H, Wang X, Ugur A, Gleason KK. Water-Assisted Vapor Deposition of PEDOT Thin Film. Macromol Rapid Commun. 2015 Jul;36(13):1283-9. doi: 10.1002/marc.201500069.
321. D. Valtakari, J. Liu, V. Kumar, C. Xu, M. Toivakka and J. J. Saarinen, *Nanoscale Research Letters*, 2015, **10**, 386.
322. N. Elgrishi, K. J. Rountree, B. D. McCarthy, E. S. Rountree, T. T. Eisenhart and J. L. Dempsey, *Journal of Chemical Education*, 2018, **95**, 197-206.
323. PalmSens, Capacitive Current, https://www.palmsens.com/knowledgebase-article/capacitive-current/, 2023).

324. O. Gharbi, M. T. T. Tran, B. Tribollet, M. Turmine and V. Vivier, *Electrochimica Acta*, 2020, **343**, 136109.
325. LibreTexts, Cyclic Voltammetry, https://chem.libretexts.org/Bookshelves/Analytical_Chemistry/Instrumental_Analysis_(LibreTexts)/25%3A_Voltammetry/25.04%3A_Cyclic_Voltammetry, 2024).
326. A. C. Lazanas and M. I. Prodromidis, *ACS Measurement Science Au*, 2023, **3**, 162-193.
327. J. Bobacka, A. Lewenstam and A. Ivaska, *Journal of Electroanalytical Chemistry*, 2000, **489**, 17-27.
328. J. Bobacka, *Analytical Chemistry*, 1999, **71**, 4932-4937.
329. R. Vedalakshmi, V. Saraswathy, H.-W. Song and N. Palaniswamy, *Corrosion Science*, 2009, **51**, 1299-1307.
330. T. Q. Nguyen and C. Breitkopf, *Journal of The Electrochemical Society*, 2018, **165**, E826.
331. S. Holm, T. Holm and G. Martinsen Ø, *PLoS One*, 2021, **16**, e0248786.
332. B.-Y. Chang, *Journal of Electrochemical Science and Technology*, 2020, **11**, 318-321.
333. E. P. M. van Westing, G. M. Ferrari and J. H. W. de Wit, *Corrosion Science*, 1993, **34**, 1511-1530.
334. C. H. Hsu and F. Mansfeld, *Corrosion*, 2001, **57**, 747-748.
335. D. Ohayon, V. Druet and S. Inal, *Chemical Society Reviews*, 2023, **52**, 1001-1023.
336. J. Zaumseil and H. Sirringhaus, *Chemical Reviews*, 2007, **107**, 1296-1323.
337. D. A. Bernards and G. G. Malliaras, *Advanced Functional Materials*, 2007, **17**, 3538-3544.
338. D. Mantione, E. Istif, G. Dufil, L. Vallan, D. Parker, C. Brochon, E. Cloutet, G. Hadziioannou, M. Berggren, E. Stavrinidou and E. Pavlopoulou, *ACS Applied Electronic Materials*, 2020, **2**, 4065-4071.
339. S. M. Richardson-Burns, J. L. Hendricks and D. C. Martin, *Journal of Neural Engineering*, 2007, **4**, L6.
340. G. Dufil, D. Parker, J. Y. Gerasimov, T.-Q. Nguyen, M. Berggren and E. Stavrinidou, *Journal of Materials Chemistry B*, 2020, **8**, 4221-4227.
341. K. I. Ritzau-Reid, C. D. Spicer, A. Gelmi, C. L. Grigsby, J. F. Ponder, Jr., V. Bemmer, A. Creamer, R. Vilar, A. Serio and M. M. Stevens, *Advanced Functional Materials*, 2020, **30**, 2003710.
342. J.-T. Kim, D. Y. Lee, T.-H. Kim, Y.-S. Song and N.-I. Cho, *Metals and Materials International*, 2014, **20**, 555-563.
343. S. Gruber and A. Nickel, *Frontiers in Medical Technology*, **5,** 2023. doi: 10.3389/fmedt.2023.1195529
344. efor, Biocompatibility assessment of MD (ISO/TR 10993-55:2023), https://efor-group.com/en/biocompatibility-assessment-of-md-iso-tr-10993-552023/#:~:text=The%20threshold%20value%20for%20cell,50%2C%2075%20and%20100%25). 2024).
345. D. Khodagholy, J. Rivnay, M. Sessolo, M. Gurfinkel, P. Leleux, L. H. Jimison, E. Stavrinidou, T. Herve, S. Sanaur, R. M. Owens and G. G. Malliaras, *Nature Communications*, 2013, **4**, 2133.